Cardiff University
School of Psychology

Functional and Structural Properties of Spatial Processing Networks in the Brain

A thesis submitted to Cardiff University for the degree of Doctor of Philosophy

Marie-Lucie Read

Supervisors: Katja Umla Runge, Kim Graham, Krish D. Singh

June 2021

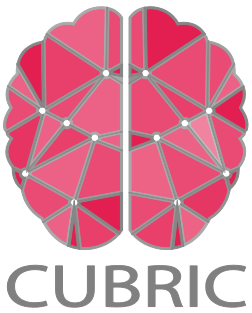

Summary

The Perceptual-Mnemonic (PM) view of the Medial Temporal Lobe (MTL) suggests it processes representations for both perception and memory and that functional separation in its regions echoes differing modality specialisation of two widespread networks. This thesis investigated a Posteromedial Network (PMN) facilitating spatiotemporal navigation, contrasting it with an Anteroinferior Network (AIN) facilitating aggregate object/face processing.

Supporting the PM-view, previous work reported correlations between network tract microstructure, functional magnetic resonance imaging-measured MTL signals and perceptual performance. However: the microstructure measures were biologically non-specific; no studies used magnetoencephalography (more temporally precise); the relative importance in MTL-reliant behaviours of PMN tracts that connect different MTL areas were uninvestigated; and studies relating PMN network structure to temporal processing produced conflicting results.

This project investigated relationships between inter-individual differences in behaviour and these networks' structures and functions using perceptual and mnemonic tasks probing perception of scenes and faces, and memory of objects-in-sequences. Microstructure measures were reduced into biologically interpretable components. Those of the fornix – a proxy of hippocampal-PMN communication – correlated with scene perception and object-in-sequence memory performance. Those of the parahippocampal cingulum, which connects other PMN areas, did not, indicating the specific role of the hippocampus in spatiotemporal representation. Those of the inferior longitudinal fasciculus, part of the AIN, correlated with face perception performance. PMN theta/gamma power modulation occurred more during scene perception than face perception. In-task MTL theta power modulation (reflecting hippocampal/parahippocampal processing), and PMN - posterior cingulate cortex resting-state connectivity correlated with scene perception performance. Conversely, AIN theta/gamma power modulations occurred during face perception. These imply that MTL regions are important for both perception and memory and that two dissociable networks cater for the different modalities. An implication of the findings is that MTL damage (e.g., as occurs in Alzheimer's Disease) may not produce purely memory disorders but impair representations for use across behaviours.

Acknowledgments

I would like to thank the following people for their kind and helpful guidance, without which I would not have been able to complete this thesis. First, my supervisors, Katja Umla-runge, Kim Graham and Krish Singh have been wonderfully supportive, insightful and enthusiastic throughout my studies, making my early years in academia very enjoyable. Katja has been a thoughtful educator at every stage, particularly by supporting the projects and helping me develop well-rounded research skills. Krish has provided valuable education into the use of magnetoencephalography and discussion on relevant topics. Kim's advice in shaping the over-all project and supporting collaborations with researchers outside of the university have been essential to my career development. I would also like to thank Andrew Lawrence who has provided suggestions for analysis techniques, valuable discussions, and advice and invaluable support on future career steps.

A delightful aspect of CUBRIC life is that researchers do not work alone, and there are many others who have provided help to my studies. I would like to thank John Evans, Allison Cooper and Greg Parker for their help in setting up MRI protocols, training me in MRI operations and sharing analyses protocols. Similarly, thank you to Gavin Perry for his help in setting-up the MEG study and for providing support during data collection. I am also grateful to all those members of the computing department, Kim Graham's laboratory group, and the MEG laboratory group.

Thank you also to my husband who has provided unparallel support, and to my Cardiff friend-group who are fun, kind and caring people. Lastly, I am very grateful to my parents who have always been encouraging and loving.

Data collection

All analyses in this thesis were performed by me.

The experiment design and collection of pilot data, described in Chapter 3, were carried out by me. The behavioural, MEG and MRI data presented in Chapters 4 to 6 were collected by me. The majority of the scene stimuli used for the studies described in Chapters 2 to 5 were made by the authors of Lee et al. (2013) and were adapted to be reused in this project, with permission. The remaining stimuli used in the studies described in these chapters were created by me.

Chapter 7 describes the analysis of a previously collected dataset in a study led by Katja Umla-Runge and Kim Graham, in collaboration with Charan Ranganath and Frank Hsieh. The behavioural and MRI data were collected by Katja Umla-Runge and Alison Costigan, with help from Ashvanti Valji and Vera Dehmelt. The behavioural data were collated and organised by Matthew Jones and Angharad Williams.

Contents

List of Figures

List of Tables

Glossary

The following abbreviations are used within this thesis and defined with their first usage:

AAL – Automated Anatomical Labelling

AD – Alzheimer's Disease

AIN – Anteroinferior Network

AMICO - Accelerated Microstructure Imaging via Convex Optimization

ANOVA – Analysis of Variance

AxD – Axial Diffusivity

BET – Brain Extraction Tool

BIC – Binding of Items and Context

BOLD – Blood Oxygen Level Dependent

CHARMED – Composite Hindered And Restricted Model of Diffusion

CSF – Cerebrospinal Fluid

DMN – Default Mode Network

dODF – diffusion Orientation Density Function

dRL – damped Richardson–Lucy

DTI – Diffusion Tensor Imaging

DWI – Diffusion Weighted Imaging

FA – Fractional Anisotropy

FFA – Fusiform Face Area

FG – Fusiform Gyrus

fMRI – Functional Magnetic Resonance Imaging

fODF – fibre Orientation Density Function

FOV – Field of View

HPC – Hippocampal Complex

ICA – Independent Components Analysis

ILF – Inferior Longitudinal Fasciculus

IOC – Inferior Occipital Cortex

IPL – Inferior Parietal Lobule

KMO – Kaiser-Meyer-Olkin

LCMV – Linearly Constrained Maximum Variance

LTM – Long Term Memory

MD – Mean Diffusivity

MEG – Magnetoencephalography

MPF – Molecular Proton Fraction

mPFC – medial Prefrontal Cortex

MRI – Magnetic Resonance Imaging

MT – Magnetization Transfer

MTL – Medial Temporal Lobe

NODDI – Neurite Orientation Dispersion Density Imaging

OD – Orientation Dispersion

OFA – Occipital Face Area

OPA – Occipital Place Area

PAC – Phase Amplitude Coupling

PCA – Principal Components Analysis

PCC – Posterior Cingulate Cortex

PHC – Parahippocampal Cingulum

PMAT – Posterior Medial Anterior Temporal

PMC – Posteromedial Cortex

PMN – Posteromedial Network

PrC – Perirhinal Cortex

qMT – quantitative Magnetization Transfer

RESDORE – Robust Estimation in Spherical Deconvolution by Outlier Rejection

RESTORE – Robust Diffusion Tensor Estimation by Outlier Rejection

RM ANOVA – Repeated Measures Analysis of Variance

ROI – Region of Interest

RS – Resting State

RSC – Retrosplenial Cortex

RT – Reaction Time

SD – Standard Deviation

SNR – Signal to Noise Ratio

SQUIDS – Super Conducting Quantum Interference Devices

SSIM – Structural Similarity Index Measure

TE – Echo Time

TR – Time to Repetition

VS – Virtual Sensor

Chapter 1. Introduction to the topic.

1.1 Network models of brain function dissociate modality-specific processes.

This thesis examined functional and structural properties of spatial processing networks in the brain to evaluate the Perceptual-Mnemonic (PM) View (Lee, Bussey, et al., 2005; Murray & Bussey, 1999; Murray et al., 2007). This view challenges the commonly-held belief that perceptual and mnemonic processes occur exclusively in separate areas of the brain, a dichotic view of memory and perception. It is encompassed by two representational models, the 'Evolutionary Accretion Model' (EAM) (Murray et al., 2017, 2018) and the Posterior-Medial and Anterior-Temporal (PMAT) framework (Ranganath & Ritchey, 2012; Ritchey et al., 2015). Both models state: that Medial Temporal Lobe (MTL) regions conduct processes that aid both perception and memory; that MTL regions function as key regions in two widespread cortical networks; and that the functional separation seen in MTL regions echoes the differing modality preferences of the two widespread networks. Despite some differences, the two networks they describe are largely similar. This thesis focused on a Posteromedial Network (PMN), contrasting it with an Anteroinferior Network (AIN). The PMN is thought to conduct sequencing and separation to create models for spatiotemporal navigation. It incorporates network areas associated with spatial processing (Hodgetts et al., 2016; Nasr et al., 2013) and recollection memory (Rugg and Vilberg, 2013) such as: posterior portions of the hippocampus; parahippocampal cortex; retrosplenial cortex (RSC); posterior cingulate cortex (PCC); inferior parietal cortex and medial prefrontal cortex (mPFC). The AIN is thought to conduct aggregate processing to create models for identification and meaning. It incorporates areas associated with semantic memory (Jefferies, 2013), object processing (Ishai et al., 2000) and face processing (Haxby et al., 2000) such as: the perirhinal cortex (PrC); inferior temporal cortex, inferior occipital cortex (IOC); orbitofrontal cortex; amygdala; and temporal pole.

This introductory chapter describes the background of the PM-view, to assess the evidence for it, and to expand upon the proposed PMN and AIN areas and functions. The chapter starts by describing the two memory models upon which the thesis is predicated. Then, functional separations of the MTL memory system and the roles of the PMN and AIN in mnemonic processes are described, highlighting how similar underlying mechanisms may support the multiple roles these networks have been associated with - such that they can

be considered as two generalizable toolboxes. It is then argued that dissociable roles of these networks, and their generalizable functionality, also extend to processes outside of Long-Term Memory (LTM). Lastly, the aim of the thesis, to further investigate the role of the PMN in spatiotemporal processing by examining individual differences in network structure, network function and task performance, is outlined.

1.1.1 Complementary and differing ideas of the EAM and the PMAT framework.

The ideas described here, including the meeting of two wide-spread cortical networks in the MTL that act as generalizable toolboxes processing different modalities across different cognitive contexts, are encompassed by the EAM (Murray et al., 2017) and the PMAT framework (Ranganath & Ritchey, 2012). The core premise of the EAM is that representational brain systems evolved from more primitive memory systems, including: a Navigation system which evolved in early vertebrates and utilizes visual and olfactory information for mobile foraging; a Feature system which evolved in anthropoids and supports visual representations to aid foraging; and a Goal system which also evolved in anthropoids and provides abstract thinking and attributed context to memories, to enhance foraging strategies. Eventually, a Social-subjective System evolved in hominins, developed from these older systems, and comprises a medial component for mental simulation of events that encompasses an extended hippocampus-based Navigation system, and a lateral component for concept comprehension that encompasses Feature and Goal systems (Murray et al., 2017). Therefore, it is proposed that our current brain networks, and our human experience of memory, arose through interactions between older brain systems. The EAM's 'Medial network' includes the mPFC, PCC, precuneus, anterior cingulate cortex, medial parietal cortex, RSC, parahippocampal cortex and the hippocampus. The EAM's 'Lateral network' includes higher order areas of the ventral visual stream and various frontal regions (including the orbitofrontal region), inferior occipital gyrus, Fusiform Face Area (FFA), superior temporal cortex and an anterior-temporal lobe 'semantic hub' (Murray et al., 2017).

The networks of the PMAT framework are based upon brain areas' anatomical connectivities and common functions (Ranganath & Ritchey, 2012; Ritchey et al., 2015). The PMAT framework's 'Posterior Medial system' includes a 'core recollection network' comprising parahippocampal cortex, RSC, angular gyrus, PCC, precuneus, anterior thalamus and mPFC. Its 'Anterior Temporal system' includes PrC, anterior temporal cortex, lateral orbitofrontal cortex, and amygdala.

These models differ in two important ways. The first concerns the view of hippocampal function within the two networks. The EAM views an extended hippocampal system, connected via the fornix, as an integral component of the 'medial network', while the PMAT framework views the hippocampus as a convergence point for both networks (Ritchey et al., 2015). Therefore, the EAM predicts that the hippocampus is also important for online spatiotemporal processes (such as complex scene perception) whereas the PMAT does not. However, the EAM agrees that hippocampal areas, termed the 'amygdaloid-hippocampus', are important for semantic memory (Murray et al., 2017), thus acknowledging that the hippocampus's heterogenous structure means it provides processing to multiple network systems. Secondly, there are differences in the general network structures. The PMAT framework's 'Anterior Temporal system' does not include inferior ventral visual stream areas whereas the 'Lateral network' of the EAM does, and the PMAT framework places more importance on parietal areas such as the angular gyrus, as part of the 'Posterior Medial system' than does the EAM in its 'Medial Network'. An outcome of these inconsistencies is the difference in the importance each model places in connecting white matter. In the EAM, the fornix should connect PMN areas and the Inferior Longitudinal Fasciculus (ILF) should connect AIN areas, whereas descriptions of the PMAT framework do not discuss these tracts and predicts only the importance of the Parahippocampal Cingulum (PHC) and the uncinate fasciculus for these functions (Ranganath & Ritchey, 2012; Ritchey et al., 2015).

Of course, neither model suggests that brain networks work in isolation and the differences between the networks described could be ascribed to differences in emphasis of network functions and terminology. The PMAT framework does not discuss the findings that support a role of the hippocampus in scene perceptual tasks requiring online creations of internal view-invariant scene representations, but not in tasks requiring face representations (Hodgetts et al., 2015; Lee, Buckley, et al., 2005; Lee et al., 2008) (see section 1.3.3.). These findings support the claim of the EAM that the hippocampus is part of a 'medial network', rather than sitting between two networks. However, the hippocampus likely uses object information fed from 'Lateral network' or 'Anterior Temporal system' areas to fill its spatiotemporal maps (i.e., joining objects in scenes) and, with this view, the hippocampus *is* acting as a convergence site of two systems, aligning with the PMAT framework. In part, this thesis aims to address these differences by directly comparing the importance of the fornix and the PHC in spatiotemporal processing in young healthy adults,

thereby testing the importance of hippocampal communication, relative to communication between other PMN areas, in PMN-related functions.

1.2 The MTL as a meeting point of two wide-spread memory networks.

The MTL contains heavily connected areas including the hippocampal complex (HPC), the amygdaloid complex and the cortical tissue surrounding these structures (Van Hoesen, 1995). The HPC comprises the hippocampus itself and the immediately adjacent entorhinal, PrC and parahippocampal cortices[1].

Animal studies indicate unequal connectivity patterns between MTL areas that closely match the functional segregation within the system. The parahippocampal cortex is strongly connected to the dorsal visual stream (Lavenex et al., 2002; Suzuki & Amaral, 1994a) and the PrC is strongly connected with the inferior temporal regions of the ventral visual processing stream (Suzuki & Amaral, 1994). The subiculum (an area of the hippocampus), the mamillary bodies and thalamus (strongly connected to the hippocampus through the fornix) show stronger connections with the parahippocampal cortex and RSC than the PrC; and the amygdala is more strongly connected to the PrC than the PHC or the RSC (Aggleton, 2012; Stefanacci et al., 1996). Resting state (RS) functional magnetic resonance imaging (fMRI) analysis in humans has confirmed and extended this pattern of two networks (Kahn et al., 2008). Activity of a network that included the anterior lateral temporal lobe correlated with activity of the PrC and the head of the hippocampus. Activity of another, which included the inferior parietal lobule (IPL), the RSC and the PCC, correlated with activity of the posterior parahippocampal cortex and the body of the hippocampus (Kahn et al., 2008).

Traditional mnemonic views of functional separation in the MTL system closely follows this pattern. Recognition memory is thought to have two components: recollection, which is context-bound memory and reliant on the hippocampus and parahippocampal cortex; and familiarity, which is contextless and reliant on the PrC (Aminoff et al., 2013; Brown & Aggleton, 2001). 'Context' in this case, refers to the positioning of a percept or concept in time and/or space or relative to other percepts or concepts. For example, recollection can be the understanding that object A was encountered before object B when navigating a route, or understanding the location relationship between block A and block B in a scene.

[1]Definition used: Hippocampal Complex. (2009). In M. D. Binder, N. Hirokawa, & U. Windhorst (Eds.), *Encyclopedia of Neuroscience* (pp. 1840-1840). Springer Berlin Heidelberg. https://doi.org/10.1007/978-3-540-29678-2_2211

Conversely, familiarity is the phenomenon of knowing something, for example knowing that object A has been encountered before, but not being able to link this knowledge with details about the learning event. This dichotomy is referred to as the Dual Process Model (Brown & Aggleton, 2001), and it has gained support from several experimental mediums including: response time experiments, showing that familiarity arises more quickly than recollection (Gronlund et al., 1997); analysis of receiver operating characteristics curves constructed of hits (correctly identified reoccurrences) and false alarms (incorrectly identifying a new occurrence as old), which show differing shapes for answers labelled as familiar and recollective (Yonelinas, 1994); and through the study of event-related potentials, which indicate electrophysiological differences between familiarity and recollection responses (Rugg & Curran, 2007).

Similarly, the BIC (Binding of Items and Context) model suggests that functional separation is based on modality (Diana et al., 2007; Eichenbaum et al., 2007). In this model, the PrC processes object information, the parahippocampal cortex processes context information, and the hippocampus binds these representations, creating sequences and scenes of objects.

These mnemonic models can be unified by considering MTL regions as key aspects of two networks with generalizable toolboxes, possessing different processing qualities that make them applicable to differing modalities. For example, the hippocampus is sensitive to representations of conjoined items in a spatiotemporal context and the PrC is sensitive to aggregate, but contextless, representations of items.

1.2.1 The hippocampus and the creation of context-bound memory.

The hippocampus has been shown to have a role in declarative memory generally (Scoville & Milner, 1957), and to have specific roles in spatial (O'Keefe & Dostrovsky, 1971), temporal (Hsieh et al., 2014) and abstract associative (Zeithamova et al., 2012) memory. For example, presentation of novel scenes created by spatial rearrangement of familiar objects gives an increase in immediate early gene expression (an indirect marker of neuronal activity) in the rat hippocampus but not the PrC (Aggleton & Brown, 2005). The involvement of the hippocampus in both recollection and spatial memory implicates it as a builder of cognitive maps that are not constrained to portraying a geographical world, but can be built by either relating conceptual elements such as events in episodic memory, or physical objects that may be encountered when navigating a space (Schiller et al., 2015).

Supporting this idea is evidence of involvement of the hippocampus in binding items in temporal orders. Hsieh et al. (2014) used multivariate pattern analysis on fMRI signals during the retrieval of object sequences. Before scanning, participants learned several different object sequences. There was one unique, fixed sequence, another two pairs of sequences that shared common objects in particular positions, and a random sequence. During fMRI, the participants were tested on their memory of the sequences through answering semantic questions. The creation of various similarity matrices showed that: hippocampus response patterns are sensitive to object-in-sequence information; hippocampus activity patterns for overlapping sequences are different; and that individual differences in participant sequence learning correlated with hippocampus pattern similarity differences for learned, relative to random, sequences. The results indicate that the hippocampus can support object-temporal-position binding and, by comparing different combinations of the sequences, that these patterns could not be explained by object or by temporal position alone.

Moreover, there is evidence of hippocampal processing of conjoined items in abstract space. Using fMRI and multivariate pattern analysis, Zeithamova et al. (2012), found a relationship between participants' abilities to learn overlapping associations and infer novel relationships (learn AB then BC and infer AC), and patterns of hippocampal online reactivation of old experiences (AB) during the encoding of related events (BC). Importantly, these associations are not bound by time or space, further supporting the idea that the hippocampus can form manipulable conceptual cognitive maps.

The underlying processes of the hippocampus, thought to result in its sensitivity to conjoined items in conceptual cognitive maps, might be those of pattern separation and pattern completion (Rolls, 2016). The hippocampus appears to store multiple memories in the same neuronal circuits by an unknown mechanism, perhaps explaining why a partial cue of a memory can lead to recollection of the whole memory (Horner et al., 2015; Rolls, 2016).

1.2.2 A posteromedial network for spatiotemporal navigation in memory.

The hippocampus and parahippocampal cortex connect to other cortical areas as part of spatial processing and recollection networks that mostly reside in posteromedial locations. The scene network is thought to include the RSC, occipital place area (OPA; or transverse occipital sulcus), parahippocampal cortex, posterior parietal cortex (Ciaramelli et al., 2010; Cukur et al., 2016; Nasr et al., 2013), angular gyrus, lateral prefrontal cortex (Summerfield

et al., 2010) and hippocampus (Hodgetts et al., 2016). Different regions of a spatial network may interact to produce spatial processing behaviour and memory. The hippocampus is thought to support the creation of allocentric (based upon stable locations and relative positions of landmarks) cognitive maps, as opposed to egocentric maps (based upon one's own personal movement and location), which are thought to be created in posterior parietal areas (Gramann et al., 2006). Measurement using fMRI has shown that the OPA, but not the parahippocampal cortex or RSC, responds similarly to images of complete rooms and to rooms that have been altered so that they no longer fit together to produce a coherent scene, suggesting that the OPA processes the component parts individually, rather than the global arrangement (Kamps et al., 2016). The RSC is thought to aid allocentric processing (Vann & Aggleton, 2002) and navigation, perhaps by coding permanent landmarks in an environment (Auger et al., 2012; Auger et al., 2017) and supporting orientation within a broader spatial environment (Epstein, 2008). The parahippocampal cortex is associated with the perception of local scenes (Epstein et al., 2007), responding to coherent scenes only (Kamps et al., 2016) and this processing has been shown to be viewpoint-specific (Epstein et al., 2003).

Similarly, an episodic recollection network has been proposed to include the hippocampus, parahippocampal cortex, the RSC, posterior parietal cortex and the angular gyrus (Rugg & Vilberg, 2013). The parahippocampal cortex has been shown to be involved in contextual aspects of memory and associative memories (Aminoff et al., 2013). Importantly, this function extends beyond the spatial domain, as the parahippocampal cortex can associate abstract concepts (Wagner et al., 1998) and odours (Alvarez et al., 2001).

These areas have also been implicated in temporal sequencing, an aspect of episodic recollection. Hsieh & Ranganath (2015) reanalysed the data of Hsieh et al., (2014) (described in section 1.2.1.). They found that activation patterns of the mPFC, RSC, and angular gyrus represented information about the position of each object in a sequence, regardless of whether those positions were associated with particular objects. Conversely, the PrC activation patterns represented information about objects only, regardless of sequence position. These results further support the role of the PMN areas in spatiotemporal navigation, and highlight the differences between their processes and those of the PrC.

These networks and roles are unified by a PMN, which conducts sequencing, patterning and separation to create generalised models for spatiotemporal processing, regardless of

the precise nature of the cognitive process. Context can be thought of as arranged objects/concepts/events with spatial or non-spatial (such as temporal) associations (Aminoff et al., 2013), so it is understandable that similar mechanisms support both spatial processing and episodic memory.

1.2.3 Associations and similarities between the PMN and the Default Mode Network.

PMN areas overlap with the areas of the Default Mode Network (DMN), which includes the mPFC, lateral parietal cortex, inferior parietal lobe and posteromedial cortex (PMC) – containing the PCC and the precuneus (Bellana et al., 2017; Raichle, 2015). The DMN is notable for displaying reduced fMRI-measured Blood Oxygen Level Dependant (BOLD) signal during a task condition compared with a baseline rest condition, suggesting reduced activity during task engagement (Raichle, 2015). This has also been demonstrated as a reduction in broadband gamma power through electrophysiological recording (Li et al., 2019) and as power suppression associated with increasing task difficulty (Ossandón et al., 2011). Conversely, there is increased gamma power in the DMN during tasks involving internal processing such as memory retrieval (Foster et al., 2012) and imagining (Benoit & Schacter, 2015), indicating that DMN areas disengage during tasks requiring processing of predominantly external stimuli but engage during internally-generated processes.

The parahippocampal cortex and the RSC show higher connectivity with the DMN than does the PrC, indicating greater commonality between the DMN and PMN, than between the DMN and AIN (Kahn et al., 2008; Ranganath & Ritchey, 2012). RS fMRI has shown increased functional connectivity between the DMN and MTL during memory retrieval and future imagining than at rest, while core DMN structures, such as the mPFC and the PCC, showed increased connectivity during rest than during retrieval and imagining (Bellana et al., 2017). These results suggest that the PMN and DMN overlap when the current cognitive state requires spatiotemporal processing of internally stored/generated information and that connectivity patterns within and between them dynamically adjust during a range of processes.

1.2.4 An anteroinferior network for aggregate processing.

The PrC, part of the AIN, has been shown to provide complementary processing to face and object processing networks, which reside mostly in anteroinferior locations (Kivisaari et al., 2012; O'Neil et al., 2013). Memory research has provided evidence that the PrC has a role

in memory, separate to that of the hippocampus, involving recognition for items, without context. For example, the presentation of novel rather than familiar visual objects is associated with increased levels of immediate early gene expression in the PrC but not the hippocampus of the rat (Aggleton & Brown, 2005). The association between the PrC and recognition memory is also supported by fMRI studies in humans, which have shown modulated PrC BOLD in response to repeated objects (Gonsalves et al., 2005; Kafkas & Montaldi, 2012; Martin et al., 2016). Furthermore, PrC BOLD activity has also been shown to be associated with cumulative lifetime familiarity of object concepts as well as recent object concept (names of objects) exposure (Duke et al., 2017).

The PrC may also play a role in semantic memory. Category-specific responses from the PrC, using intracranial electroencephalography (EEG), have been seen as early as 130 ms after the onset of the presentation of a written word (Chan et al., 2011). Areas of the ventral anterior temporal lobe, including the PrC, are thought to encode semantic categories and interact with upstream visual processing areas, such as the occipitotemporal cortex, during visual processing, to aid object identification. Furthermore, through multivariate pattern analysis of fMRI, it has been found that activity patterns in the PrC reflect semantic similarities between individual objects (Clarke & Tyler, 2014). In this study, the PrC also showed increased activation when recognizing highly confusable objects, indicating that these objects placed a higher demand on the PrC, with its integrative function. The authors suggested that the PrC creates semantic whole-object representations through complex aggregation of information fed from connecting areas.

The PrC is proposed to be at the apex of the ventral visual pathway, a hierarchical stream that supports visual object processing (Ishai et al., 2000; Magazzini & Singh, 2018), and that includes early visual areas as well as the inferior temporal cortex and the PrC (Bussey & Saksida, 2007; Rottschy et al., 2007). fMRI data from participants who underwent an object-naming task were used to test the idea of a deep neural network model of vision combined with an “attractor network” model of semantics. Posterior ventral temporal cortex activity best represented early layers of the semantic network model, whereas PrC activity best represented late layers of the semantic network model, showing the passage of information in a hierarchical fashion (Devereux et al., 2018).

The face processing network is thought to comprise two parts, core and extended subnetworks (Haxby et al., 2000). The core subnetwork comprises the Occipital Face Area (OFA), superior temporal sulcus and Fusiform Gyrus (FG), and the extended subnetwork

includes the intraparietal sulcus, amygdala, anterior temporal cortex and the orbitofrontal cortex (Haxby et al., 2000; Musch et al., 2014). The extended subnetwork is thought to be involved in the extraction of meaning from faces and the recognition of faces (Musch et al., 2014), and the PrC is thought to contribute to this network when a task demands face-based person-memory or discrimination between faces with overlapping features (Collins & Olson, 2014). Collins and Olsen (2014) suggested that the PrC achieves this by integrating features into viewpoint-invariant representations designed to give identity and face individuation. Relatedly, O'Neill et al. (2014) examined RS fMRI connectivity across regions in a face-processing network and found resting connectivity patterns between the PrC and the FFA and the PrC and the amygdala. The former connectivity patterns correlated with inter-individual differences in the extent to which inverting the orientation of a face disrupted subsequent recognition, indicating that individual differences in communication between the PrC and members of the face network affect face memory performance. Faces can also be considered as aggregated whole-object items. Isolated face or object items can exist without context, highlighting a similarity between object/face processing and familiarity memory.

1.2.5 Neurodegenerative diseases may target distinct neural networks.

The 'network degeneration hypothesis' suggests that some neurodegenerative diseases are the results of network dysfunction. Although, abnormalities on the small scale (molecular neuropathology/deficits in neuronal firing behaviour or synaptic communication) contribute to larger circuits and, ultimately, to network dysfunction (Palop et al., 2006), this hypothesis highlights that symptom-complexes can relate more closely to dysfunction of affected networks than to underlying neuropathologies (Drzezga, 2018). Two degenerative diseases, Alzheimer's Disease (AD) and semantic dementia unequally target PMN and AIN areas (Ranganath & Ritchey, 2012). AD is associated with hippocampal atrophy (Lee et al., 2019), abnormal DMN activity (Greicius et al., 2004) and abnormal RS-connectivity between MTL and DMN regions (Grajski & Bressler, 2019). Semantic dementia is associated with atrophy of AIN areas such as the amygdala, anterior temporal lobe and temporal pole (Boxer et al., 2003), and semantic memory impairment relates to PrC volume in semantic dementia patients (Davies et al., 2004). (However, it should be noted that the brain areas affected in these diseases are not entirely separable).

The PM-view and representational models have implications for how we view diseases such as AD and semantic dementia, which affect the MTL. They are often seen as purely

memory disorders, which may not be the case (Hutchings et al., 2017; Quental et al., 2013) and furthering our understanding of the functional roles of brain network may allow us to better characterize network diseases, and potentially provide earlier diagnoses by including non-mnemonic based tests (Gaynor et al., 2019; Wu et al., 2020).

1.2.6 Dissociable reliance on white-matter tracts between the two networks.

The fornix and the PHC connect PMN areas. The fornix is the major carrier of hippocampal input/output tracts, and contains afferents from the diencephalon (Saunders & Aggleton, 2007). Through the fornix, the hippocampus, mamillary bodies and anterior thalamic nuclei are considered to form an extended hippocampal system for episodic memory and spatial processing (Aggleton & Brown, 1999; Dumont et al., 2015). The fornix also connects this formation with the prefrontal cortex (Metzler-Baddeley et al., 2011). Fornix transection causes amnesia, showing that it is crucial in supporting episodic memory (Gaffan & Gaffan, 1991). Its microstructure properties correlate with free recall performance (Metzler-Baddeley et al., 2012) and episodic content of autobiographical recall (Hodgetts, Postans, et al., 2017). Moreover, microstructure properties of the fornix that may reflect fibre damage are reported in AD patients, and in the precursor condition, mild cognitive impairment (MCI) (Bozoki et al., 2012; Mielke et al., 2009).

The PHC is part of the cingulum, which is comprised of long and short association fibres, and connects the temporal lobe to the frontal lobe, running along the dorsal surface of the corpus callosum (Bubb et al., 2018). It has segments with differing connection patterns or properties according to the connections they support (Bubb et al., 2017). The PHC is the most lateral region extending into the temporal lobe (Jones, Christiansen, et al., 2013), and is associated with episodic memory functioning (Metzler-Baddeley et al., 2012). It connects the MTL, mostly the parahippocampal cortex, with the occipital lobe and posterior parietal cortex (Bubb et al., 2017; Jones, Christiansen, et al., 2013; Wu et al., 2016). Microstructure properties of the PHC also differ between healthy adults and AD patients (Bozoki et al., 2012), and have been found to correlate with recognition memory performance in MCI patients (Metzler-Baddeley et al., 2012).

The ILF and uncinate fasciculus connect AIN areas. The ILF is a major occipital-temporal association pathway and connects the ventral visual stream (Herbet et al., 2018), emanating from the occipital lobe and concluding in the ventro-anterior temporal lobe (including connections to the PrC) (Catani et al., 2003). It may be important in several areas of cognition, including object, face and semantic memory, and socio-emotional processing

(Herbet et al., 2018). The range of processes associated with ILF can be explained through the breadth of areas connected through this tract. Based on connections within the occipital lobe, it has dorsolateral-occipital, fusiform, cuneal and lingual segments, each with differing proportions terminating in five temporal cortical regions (Latini, 2015). Microstructure properties of the ILF are different in children with impaired object recognition (Ortibus et al., 2012), in progressive prosopagnosia (Grossi et al., 2014) and in semantic dementia patients (Agosta et al., 2010; Sundqvist et al., 2020), compared with healthy controls.

The uncinate fasciculus is a curved tract that connects the medial and anterior temporal lobe to the medial and orbital prefrontal cortex (Hau et al., 2017). It is associated with the semantic retrieval aspect of language (Papagno, 2011), socio-emotional behaviour (Coad et al., 2017), and reward/value-based associative learning (Thomas et al., 2012). Its microstructure also differs in semantic dementia patients (Agosta et al., 2010; Sundqvist et al., 2020) compared with healthy controls. An illustration of the proposed structures of the PMN and AIN are shown in Figure 1.

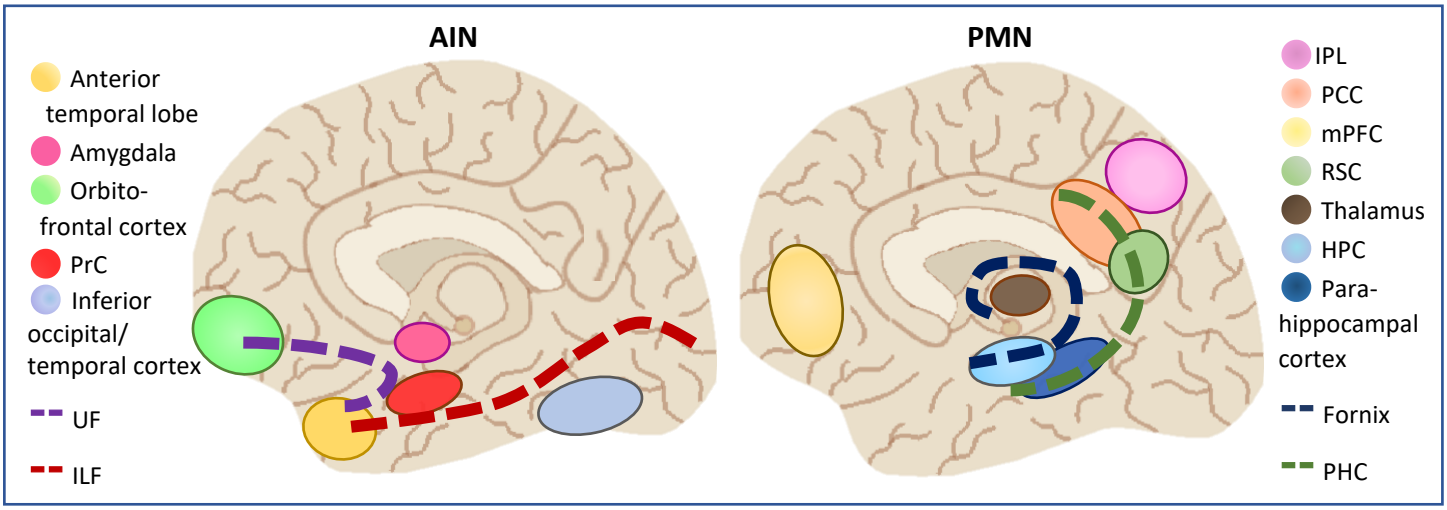

Figure 1. The proposed anatomy for the AIN and PMN.

AIN and PMN areas are shown with tracts that connect them, coloured according to the keys.

AIN: Anterior Inferior Network. PMN: Posteromedial Network. HPC: Hippocampal Complex. ILF: Inferior Longitudinal Fasciculus. IPL: Inferior Parietal Lobule. mPFC: medial Prefrontal Cortex. PCC: Posterior Cingulate Cortex. PHC: Parahippocampal Cingulum. PrC: Perirhinal Cortex. RSC: Retrosplenial Cortex. UF: Uncinate Fasciculus.

1.3 The roles of AIN and PMN areas outside LTM.

Contrary to a pure-mnemonic view of the MTL, the PM-view suggests roles of the PMN and AIN that extend beyond mnemonic processes. However, the roles of the hippocampus and PrC in perceptual processes are highly contested (Suzuki, 2009; Urgolites et al., 2018). There are reports of intact performance in complex perceptual tasks in MTL-damaged patients (Stark & Squire, 2000; Urgolites et al., 2018), suggestions that impairments in memory display as apparent impairments in perception (Knutson et al., 2013), and reports of intact scene construction and perspective shifts in hippocampal-lesioned patients (Rungratsameetaweemana & Squire, 2018). The following evaluates the evidence that the hippocampus and PrC contribute to processes outside of memory and discusses their contributions to PMN and AIN networks, respectively.

1.3.1 The Hippocampus and the PMN support spatiotemporal representations over short timescales.

The hippocampus is implicated in roles outside of memory, including online spatial processing (Voss & Cohen, 2017; Warren et al., 2012; Yee, 2014), imagining fictitious space (Barry et al., 2019; Hassabis et al., 2007) and online temporal encoding (Banquet et al., 2021).

Regarding online spatial processing, a focus of animal research on the hippocampus is how cognitive maps are formed, and how they affect subsequent behaviour. The well-known ‘place cells’ alter their activity depending on the location of the animal in its environment (O'Keefe & Dostrovsky, 1971). Changes to the pattern of place cell activation during exploration and the re-run of this pattern during consolidation, have evidenced the hippocampus in encoding during exploration (Sosa et al., 2018). However, hippocampal processes may not be passive recipients of sensory information, but may guide on-going behaviour to manipulate information sampling. For example, vicarious trial and error behaviour is a trait observed in rodents and involves back-and-forth movements of the head during movement decisions. Animals with intact hippocampi display more vicarious trial and error behaviour in trials prior to locating the reward, than on subsequent trials whereas hippocampus-lesioned rodents do not show this pattern (Bett et al., 2012), indicating that internal model building or model retrieval by the hippocampus affects online spatial decisions. Similarly, supporting the role of the hippocampus in online visual processing, saccadic eye-movements can align with the phase of the hippocampal theta rhythm in both humans and macaques, during visual exploration (Hoffman et al., 2013).

Exploratory behaviour in humans can be measured through eye-movements rather than head movements, and humans with hippocampal damage show impaired exploration (Yee, 2014). In this study participants were required to find a goal in novel scenes, but their exploration behaviour was made measurable by restricting the view of the scene through a 'viewing window' that could be moved by the participant using a joystick, emulating visual searching. Patients showed a less organised search strategy during the first attempt, than did healthy subjects, by revisiting areas more and covering lower percentages of the images.

In healthy humans, vicarious trial and error behaviour (expressed through eye-movements) has been associated with improved performance on a visual pick-the-odd-one-out task, in which multiple similar objects were shown simultaneously, with one differing slightly (Voss & Cohen, 2017). In this task, vicarious trial and error behaviour also correlated with BOLD in PMN areas such as the hippocampus, PFC and lateral parietal cortex.

Several studies have evidenced a role for PMN areas in mental simulation or future imaginings (Addis et al., 2007; Andelman et al., 2010). In an fMRI study comparing activation during periods of past and future imaginings, the posterior hippocampus, mPFC, parahippocampal cortex, RSC, PCC and precuneus were found to be active in both states and the IPL was more active during future imaginings (Addis et al., 2007). Supporting the role of the hippocampus specifically, MEG recording during mental simulation has shown that the mPFC drives hippocampal activity during novel scene imagery (Barry et al., 2019), and patients with hippocampal damage render poorly detailed mental simulations which can lack spatial coherence (Hassabis et al., 2007). This deficit may also extend to mind-wandering, as patients with hippocampal damage have also been shown to have more semantic-based (rather than episode-based), and more abstract (rather than scene-based) thoughts, than controls, when asked to freely describe their thoughts (McCormick et al., 2018). Furthermore, in an fMRI study in healthy individuals, functional connectivity strength between the hippocampus and areas of the mPFC correlated positively with individual differences in the propensity to engage in future- and past-focused thoughts in mind wandering (Karapanagiotidis et al., 2017).

Strong evidence for the involvement of the hippocampus in creating mental representations of scenes comes from research investigating boundary extension. This is the phenomenon in which a memory erroneously includes more scene than was originally viewed (Intraub & Richardson, 1989). It can be measured either by asking participants to

draw previously-viewed scenes by memory or by asking them to choose the previously-viewed image from a choice which includes wider-angled images. It is evident after only 42 ms, the duration of a saccade, of the studied item being absent from view (Dickinson & Intraub, 2008; Intraub & Dickinson, 2008), which strongly supports the idea that scene representations are formed within a perceptual timeframe. It has been argued that boundary errors occurring during visual scanning would be useful for scene perception because it would aid the perception of a continuous landscape and that without such gap-filling the world would comprise disjointed fragments given from individual views (Intraub & Dickinson, 2008).

Patients with bilateral hippocampal or ventro-mPFC damage show attenuated boundary effects (De Luca et al., 2018; Mullally et al., 2012), and fMRI scanning of healthy individuals found a boundary-effect-related hippocampal BOLD response that manifested during, or shortly after, the first presentation of the scenes and before the second (Chadwick et al., 2013), suggesting that the hippocampus's role in the boundary effect relates more to the construction of internal spatial representations rather than to a recollection error.

Monitoring of time also appears to be a process that the hippocampus conducts during an event (Banquet et al., 2021). Like place cells, 'time cells' have been recorded in the hippocampus, mPFC and striatum during time-delays within memory tasks or at specific moments in temporally structured tasks (Akhlaghpour et al., 2016; Eichenbaum, 2017a; Salz et al., 2016; Tiganj et al., 2017). Experimentation in rats has shown that hippocampal time cells can monitor absolute time in a delay and update their firing patterns when delay periods change to allow monitoring of bridging of temporally discontinuous but related events (MacDonald et al., 2011).

This research, along with episodic memory research, demonstrates that the hippocampus, in conjunction with other PMN areas, supports spatiotemporal processing across behaviours (Eichenbaum, 2017a). Indeed, episodic memory, exploration, imagining fictitious scenes and temporal processing all require grouping of sequentially encountered information. For example, to comprehend a route, an animal must hold information and places that were just revisited, and visual search involves scanning by swiftly moving the foveal portion of the visual field. The space or the visual scene can only be understood when the discrete pockets of information are joined.

The mechanism by which the hippocampus performs real-time sequencing is unclear (Banquet et al., 2021). A major form of temporal organisation seen across the brain is the

synchronisation of population neuronal excitation and inhibition, displayed as oscillatory activity. Oscillations in the theta (4-8 Hz) and gamma (>30 Hz) bands may play particularly important roles in hippocampal processing (Colgin, 2016), and firing patterns of time and place cells are known to interact with temporal properties of theta waves (Dragoi & Buzsaki, 2006; Drieu & Zugaro, 2019; Pastalkova et al., 2008). On a larger scale, Elfman et al. (2014) designed a computer model simulating three input/output layers of the hippocampus (CA1, CA3, and dentate gyrus) and inputs and outputs running through an entorhinal cortex layer, emulating on-going pattern completion and separation for comparisons in memory and perception. They successfully demonstrated that their model could simulate previous human results from memory and perception tasks. Importantly, they did not adjust model parameters between perception and memory tasks. Instead, they found that differing signal patterns for each emerged as a result of the different task demands. The results suggest that the hippocampus contributes similar representations in aid of both mnemonic and online processing.

1.3.2 The PrC and AIN support aggregate item representations over short timescales.

The EAM and PMAT framework both suggest that the PrC is optimally placed, at the apex of the ventral visual processing stream, to play a major role in aggregate item processing across perception and memory (Murray et al., 2017; Ranganath & Ritchey, 2012).

As described above, the PrC along with classic face processing areas, has been implicated in face processing through neuroimaging and neuropsychology studies (Collins & Olson, 2014; O'Neil et al., 2013). During perception, the PrC appears to be important in the identification aspect of face processing. It has been shown to have increased activity in response to face memory and perceptual discrimination tasks that require whole face processing, over tasks that require isolated face feature processing (O'Neil et al., 2013). Correspondingly, patients with ventral anterior temporal lobe damage (including the PrC) have been shown to be impaired in a face identity judgment task but not a face age judgment task (Olson et al., 2015), which is thought to be because face-age judgments can be performed by comparing individual features, but identity judgment requires comparisons of the whole object.

It is thought that the same underlying mechanism supports aggregate item representations in the PrC across perception as well as memory (Sadil & Cowell, 2017). A model network was designed containing a layer corresponding to areas of the posterior ventral visual

stream, which were assumed to hold 'features' (simple conjunctions of two visual dimensions), and a top PrC layer, upon which features converged, and it was assumed to represent whole objects. The model emulated a phenomenon named 'representational tuned-ness'. The authors hypothesized that a familiarity or online discrimination decision requires an individual to scan back and forth, either between a memory and an encountered object, or between two simultaneously encountered objects, and if the representation of the second item appears less tuned, then this provides a mismatch signal. By comparing results with and without a PrC layer, they successfully simulated impairments shown by PrC lesioned patients: worse performance on discrimination tasks between highly ambiguous objects (sharing many features) than less ambiguous objects (which could be distinguished by their features by lower levels); and poorer object familiarity memory than controls (Sadil & Cowell, 2017). Together, this research shows that the PrC, in conjunction with the AIN, is important for online processing of aggregate items.

1.3.3 The 'oddity task' has provided evidence of MTL involvement in perceptual processes.

Results of studies using the perceptual oddity task have provided further support for the roles of the hippocampus and PrC in perceptual spatiotemporal and aggregate processing, respectively. In a study by Buckley et al. (2001), the perceptual oddity task was first introduced, with the aim of being able to modulate perceptual difficulty while keeping memory demands constant. In this study, monkeys were trained to identify the odd image out of six presented images. Task types included: face oddity; object oddity; colour oddity; degraded object oddity; shape oddity; scene oddity and size oddity (control task in which the subjects were required to identify the 2D shape of a different size). Face and object oddity tasks showed images taken from different viewpoints, and monkeys with PrC lesions were impaired when making perceptual discriminations in these tasks. They were unimpaired in face trials when the images were presented from one viewpoint, or on tasks that required simple feature discrimination, such as those in the size and shape oddity tasks, even when these were difficult. These data support the idea that the PrC is required to create representations of complex conjunctions as part of perceptual processes because only performance on oddity tasks that required perceptual discrimination at an abstract level was impaired.

The oddity task has also been used to demonstrate MTL involvement in perception in humans. Lee, et al. (2005) aimed to provide evidence for, and differentiate between, the roles of the hippocampus and the PrC in spatial and object perception, respectively, in

humans. They investigated visual discrimination performance patterns in two groups of patients, one with MTL damage including hippocampus and PrC, and one with MTL damage including hippocampus but not PrC. Both groups were found to be unimpaired on tasks that could be solved on the basis of simple features and also complex scene and face tasks that did not demand viewpoint-independent perception. For tasks involving differing viewpoints, both groups were impaired on scene tasks, and the group with PrC damage were also impaired on face and object tasks. Moreover, when examining the results from repeated trials, lesioned patients performed worse than controls on the first trials of the blocks, thus making it unlikely that differences between lesion and control groups were entirely due to differences in memory encoding.

The dissociable roles of the hippocampus and PrC in scene and face complex visual perception is further supported by the results of fMRI studies in healthy humans (Hodgetts et al., 2015; Lee et al., 2008). In these, participants were asked to complete differing-view face and scene oddity tasks and size oddity tasks, during fMRI scanning. Face oddity tasks were associated with greater BOLD signal in the PrC and the anterior hippocampus when contrasted with scene oddity tasks, and scene oddity tasks were associated with greater BOLD signal in the posterior hippocampus and parahippocampal cortex when contrasted with face oddity tasks (Lee et al., 2008). Moreover, the individual differences in the extent of hippocampal and PrC BOLD modulation has been associated with scene and face oddity task performance, respectively (Hodgetts et al., 2015).

Further to the roles of the hippocampus and PrC, communication between these areas and extra-MTL areas has also been shown to be important in oddity task completion. Two studies have tested correlations between performance of scene and face oddity tasks with diffusion MRI measures of white-matter tracts in healthy humans to evidence the importance of network communication in complex scene perception (Hodgetts et al., 2015; Postans et al., 2014). They assessed tract properties using Diffusion Tensor Imaging (DTI) and considered high Fractional Anisotropy (FA) and low Mean Diffusivity (MD) of white matter to indicate efficient transfer of information. In one of these studies, fornix FA was found to correlate with scene discrimination performance in two tasks, one which displayed the scene sequentially with a delay (requiring memory) and the other, which displayed the images simultaneously, showing the importance of the fornix-supported communication across memory and perception (Postans et al., 2014). In the second study, low MD in the fornix, and low MD and high FA of the ILF, related to scene oddity and face oddity task performance, respectively (Hodgetts et al., 2015). Since the fornix and ILF are

thought to connect multiple areas in the PMN and AIN, respectively, the results of these studies provide evidence that effective communication within networks aids cognition.

It could be argued that the MTL shows involvement in tasks with differing viewpoints not because of the need to create representations of complex conjunctions for perception, but because they are generally more difficult. However, results from a study by Barense et al. (2010) which specifically tested the effects of viewpoint on MTL involvement in the oddity task, do not support a 'difficulty account'. They used face, scene and object oddity tasks, with and without differing viewpoints. Additionally, they included two types of the size control condition, one difficult and one easy (depending on the range of size changes). To compare the viewpoint effects of faces and scenes, trials were contrasted in the following pattern: (differing views faces – same view faces) – (differing views scenes – same view scenes). Greater viewpoint effects for faces over scenes was seen in the PrC and greater viewpoint effects for scenes over faces was seen in the hippocampus. Aspects of their study reduce the possibility that the results are a confound of task difficulty: only correct trials were included for analysis; there was actually less activity for difficult than for easy size trials in all the MTL regions tested; and activity in the posterior hippocampus was related to the scene processing task and not the size task even though these two task types were matched in terms of behavioural performance. Moreover, a 'difficulty account' cannot explain how the different modality conditions differently modulated activity in MTL regions.

Furthermore, it could be argued that the apparent involvement of MTL regions in the completion of the oddity task is caused by a memory confound. In other words, holding scene or object images in memory may aid task performance. However, the tasks used by Barense et al. (2010) and Lee et al. (2008) comprised trial-unique stimuli, meaning that memory of a scene or object viewed previously, could not aid performance in their tasks. They also asked the participants to indicate the response as quickly as possible, to reduce the risk that measured MTL signals reflected encoding processes, which may dominate after a perceptual decision has been reached. Despite this, it is still difficult to distinguish between perception and memory from the results, as very short-term memory, the holding of visual information during saccades between simultaneously displayed images, may aid task performance and also incite longer term encoding processes in MTL regions.

Lee et al. (2013) specifically attempted to tease apart spatial perception and spatial memory processes in the hippocampus during scene oddity task performance, by analysing

fMRI data using univariate and multivariate analysis. They hypothesized that if the hippocampus's involvement in the scene oddity task was purely of a mnemonic kind, there should be significantly increased hippocampus BOLD signal for correctly answered trials when these are subsequently remembered, and not when they are forgotten. In addition, they hypothesized that if perception and memory were separate, classification between correct and incorrect oddity trials should be possible regardless of the pattern of subsequent memory. The results of the univariate analysis showed greater hippocampal BOLD for correct over incorrect oddity trials and, critically, this was not dependent on whether the trials were subsequently remembered. The results from the multivariate analysis showed that: both classification between subsequently remembered and subsequently forgotten, and between correct and incorrect oddity trials, was possible in the hippocampus; and that the classification result of the latter was not significantly different to the classification results when only subsequently remembered trials were included. Overall, these results indicate that hippocampal processes contribute to the perceptual processing stage, as well as mnemonic stages, in the scene oddity tasks.

However, labelling of 'perceptual' versus 'mnemonic' processes brings about a conceptual issue. In some cases, the distinction between perception and memory becomes unclear. For example, if a system processes information over time, there must be a memory of sorts. For short timescales, this type of memory is referred to as working memory and, in the dichotic view of memory and perception, it is thought to be separate from long-term memory because there are descriptions of spared short-term memory in cases of MTL damage (Baddeley & Warrington, 1970). There are, however, differing opinions on whether short-term and long-term memory are fundamentally different (Norris, 2017; Ranganath & Blumenfeld, 2005). A criticism of the oddity task is that 'very short term' memory or 'saccadic' memory is needed to hold a representation of the one image when focusing on another. Instead of altering the argument to ask whether MTL areas are involved with short-scale memory as well as long-scale memory, the PM-view stresses the need to understand areas of the brain by their computational abilities (for example, spatiotemporal processing), instead of modularizing brain areas by assigned outwardly recognizable functions (for example, LTM).

1.4 Current understanding of PMN and AIN functioning.

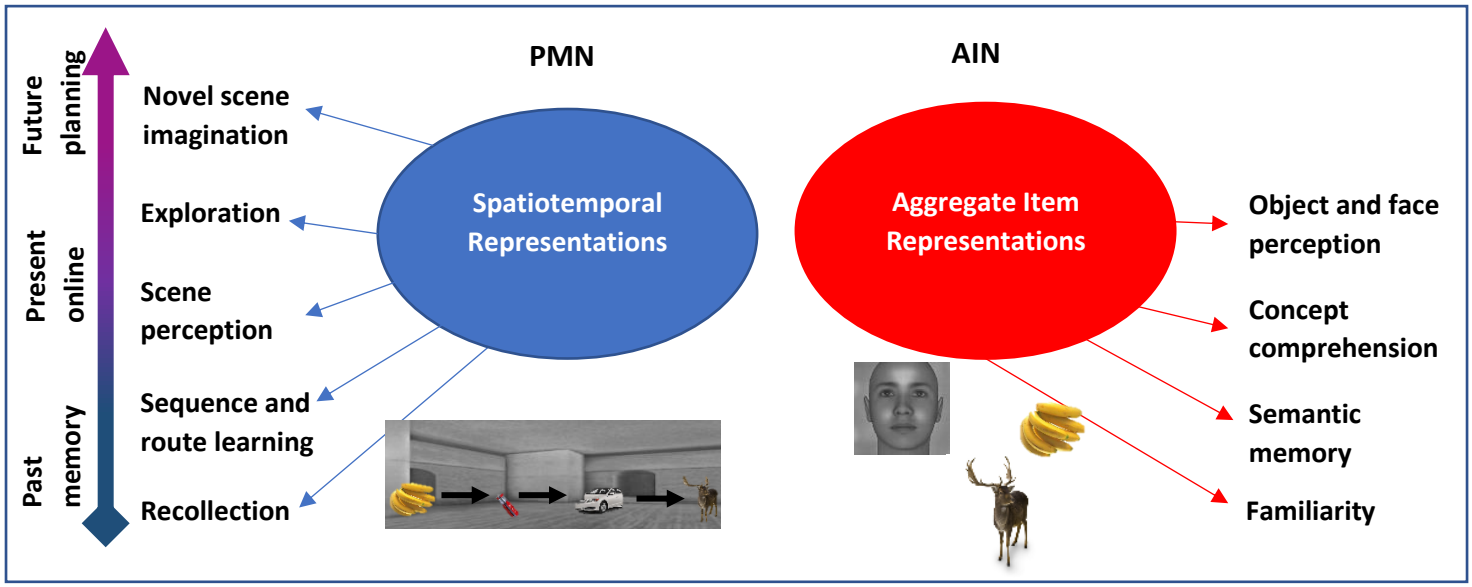

Figure 2. The two proposed types of representations that the PMN (left) and AIN (right) create that aid multiple cognitive processes.

Examples of PMN and AIN functions are shown. Images under the PMN circle are linked by arrows to show that items can be linked in space and time. Images under the AIN circle are placed randomly to show that items and concepts can be understood without context.

(The scene and face images were made using Deus Ex (Ion Storm, 2000) and Facegen (Singular Inversions, 1998) (see *Chapter 3*). The objects are taken from a collection used in the experiment in *Chapter 7*.)

AIN: Anteroinferior Network. PMN: Posteromedial Network.

Figure 2 illustrates the roles of the PMN and AIN as described in this introduction and suggested by the EAM and PMAT models. Concurring with the PM-view, the networks have been demonstrated to have dissociable roles in processing different stimuli that span perception and memory. However, there are aspects of research into these networks which are in their infancy. For example, while simultaneous investigation into the structural and functional aspects of the PMN and AIN supporting complex perception in healthy individuals performed by Hodgetts et al. (2015) highlighted the importance of hippocampal BOLD and fornix microstructure in complex scene perception, and PrC BOLD and ILF microstructure in complex face perception, many unanswered questions remain. Regarding the functional results, scene perception was associated with hippocampal BOLD decrease, which is difficult to interpret due to the complex relationship between neuronal activity, cerebral blood flow and oxygen metabolism, and so the result provides little indication of the hippocampal processes during perceptual decisions. For example, BOLD decrease has been interpreted as inhibition (Devor et al., 2007) and could reflect disengagement of the hippocampus. However, there are haemodynamic circumstances where a change in

neuronal firing patterns, echoing engagement of hippocampal processes, could produce reduced BOLD signals (Hillman, 2014). Similarly, the BOLD signal is slow compared with the underlying neuronal activity (Glover, 2011), so the temporal aspects of hippocampal engagement with the task is unclear. Both shortcomings can be addressed using an electrophysiological technique. Regarding the structural results, Hodgetts et al. (2015) used FA and MD, which are not specific to individual properties of white matter. For example, both axon membrane characteristics and myelin content can influence FA (Beaulieu, 2002). Thus, the importance of underlying biological properties of tracts supporting the PMN and AIN, in complex perception, are unclear. Furthermore, no previous study has assessed the influence of functional connectivity between network areas and complex perception task performance. Therefore, further experimentation into these networks' roles in complex perception is necessary.

Another shortcoming is our understanding of whether structural and functional aspects of these networks equally support the range of roles associated with them. For example, individual differences in fornix microstructure have been associated with recollection (Rudebeck et al., 2009), and scene memory and scene perception (Hodgetts et al., 2015; Postans et al., 2014) performance in healthy adults. However, it is unknown whether its properties similarly relate to temporal sequencing memory.

Additionally, no previous studies have compared the importance of fornix and PHC-supported communication in complex scene perception and temporal sequence memory, both of which are PMN behaviours. Both tracts are thought to support communication between PMN areas but the fornix is the major communicating tract of the hippocampus (Bubb et al., 2017). It would not be possible to conclude that hippocampus-PMN communication is specifically important for spatiotemporal processing if studies have shown correlations between individual differences in fornix microstructure and a PMN behaviour, but have not shown a weaker or non-existent relationship between PHC microstructure and that PMN behaviour.

1.5 The aims of the PhD project.

This PhD project aimed to expand our understanding of how the structure and function of the PMN network supports PMN behaviours, and to contrast this with aspects of structure and function of the AIN network supporting AIN behaviours. This was done by considering the testable implications of the PM-view: the PMN and AIN networks should aid behaviours

in different modalities; MTL areas should be involved in processes across memory and perception; and that the behavioural performance of those modalities should be related to the structural and functional properties of the respective networks (Graham et al., 2010; Murray et al., 2017) (stated again in Box 1 for clarity).

The implications were tested in two contexts, complex perceptual processing and temporal sequence memory. To investigate the networks' roles in complex perception, a scene and face oddity task was performed in conjunction with Magnetoencephalography (MEG) recording, and measurement of microstructural tract properties was carried out with microstructural MRI. The fornix, ILF and PHC were compared. As the functions of PMN was the main focus of this thesis, and the AIN was examined as a contrast, the other tract connecting the AIN, the uncinate fasciculus, was not examined. Correlations between individual differences in structure, function and behaviour were tested. Both online MEG signals and MEG-measured brain connectivity at rest, were examined. To assess the networks' roles in temporal sequence memory, data collected during a previous experiment were used. Correlations were assessed between temporal sequence memory performance and microstructure analysis of the fornix, ILF and PHC similar to that carried out in the oddity task experiment.

Testable Implications of the PM-view

- The PMN and AIN should aid behaviours in different modalities.
- Network areas, including MTL areas, should be involved in processes across memory and perception.
- Behavioural performance in tasks involving network-sensitive modalities should be related to the structural and functional properties of the respective networks.

Box 1: Implications of the PM-view that can be tested to further our understanding of the roles of networks connected to the MTL.

Chapter 2: Methods to measure network properties and functions in humans.

2.1 Using methods which cater to the aims of the research.

The aim of this project was to expand our understanding of how the structure and function of the PMN supports behaviour, and to contrast this with aspects of structure and function of the AIN network, by looking for dissociable associations between individual differences in structure, function and behaviour for the two networks. Structure and function were measured with MRI and MEG, respectively. These techniques are non-invasive so properties of white matter and group neuronal firings can be measured with relative ease, in healthy participants.

MEG allows measurement of synchronised activity of groups of neurones (Singh, 2012) and both MEG and MRI can characterize brain connectivity (Hillebrand et al., 2012; Jones, Knosche, et al., 2013; Marquetand et al., 2019; Messaritaki et al., 2020). Connectivity can be characterized on varying scales, such as between selected brain areas (e.g. Sulpizio et al., 2016) or through the assessment of individual tracts (e.g. Postans et al., 2014), or on a larger scale through whole-brain network analysis (e.g. Messaritaki et al., 2020). While structural connectivity strength can be inferred through microstructure measures (Jones, Knosche, et al., 2013), functional connectivity can be defined as a statistical dependency between measures of brain regions' activity over time, such as correlation or coherence (Fox & Raichle, 2007; van Diessen et al., 2015).

Individual differences can be measured with state or trait properties (Schmitt & Blum, 2020). State characteristics vary across time and relate to the current behaviour. They can include modulations of brain activity between tasks or in task versus rest, giving insight into how individuals' brain networks adapt and engage in different behaviours. Trait characteristics are less variable over time, generalizing over similar situations, and they can be measured irrespective of current behaviour. They can include structural brain properties or functional activity during rest periods, and can indicate how near-static network properties reflect in individual cognitive differences (Schmitt & Blum, 2020). State characteristics are measured in this thesis through completion of the oddity task during MEG recording. Structural trait characteristics are measured using MRI and functional trait associations are characterized using RS MEG.

This chapter outlines the imaging techniques used within this thesis and describes our current understanding of the biological bases of the resulting metrics. The sections describe the techniques and the resulting measures that are thought to be useful for understanding network function.

2.2 The use of inter-individual differences.

Although patient data is useful in providing causational roles of brain areas and tracts in behaviour, there are shortfalls of lesion-based work. For example, not all damage is equally visible with structural MRI (Lee & Newberg, 2005). Also, damage (i.e. abnormal activity) to heavily connected areas which form major nodes in networks (e.g., the hippocampus) can cause structural and functional alterations to connections elsewhere in the network, a phenomenon called 'connectional diaschisis' (Carrera & Tononi, 2014). Therefore, it can be unclear whether an association between a behavioural impairment and injury necessarily means that the affected area supported the behaviour. Moreover, there are benefits to understanding the healthy brain by individual differences research as it enlightens our understanding of normal brain variation.

Individual differences research has already been utilized by a myriad of studies to reveal how properties of communication between areas of the PMN relate to performance across behaviours that require spatiotemporal processing. Examples include: RS fMRI studies that revealed that increased small-worldness (reduced number of steps between nodes) and modularity (existence of groups of nodes which more highly connected which each other than others) of the navigation network (Kong et al., 2017), and increased functional connectivity between the posterior hippocampus and RSC (Sulpizio et al., 2016) are associated with better navigation ability; an RS fMRI study that showed that trait differences in episodic autobiographical remembering have been related to resting neural connectivity patterns between areas including the MTL and the parietal cortex (Sheldon et al., 2016); and a structural-behavioural study that showed that sequential scene discrimination performance correlated with fornix microstructure properties in young healthy adults (Postans et al., 2014).

Experimentation using individual differences has provided support for dissociable PMN and AIN roles. For example, relationships between fornix and ILF tract properties with episodic and semantic aspects of autobiographical memory have been identified in healthy individuals. Episodic detail correlated with fornix microstructure properties and semantic

detail correlated with ILF microstructure properties (Hodgetts, Postans, et al., 2017) (see also Hodgetts et al., 2015).

2.3 Measuring brain rhythms using MEG.

Neurones of the brain operate through electrochemical interactions and groups of neurones spiking synchronously can create oscillating electro-magnetic fields, measurable outside of the head. Multiple healthy brain oscillatory frequency bands have been described, including delta (1-4 Hz) (Park et al., 2014), theta (4-8 Hz) (Herweg et al., 2020), alpha (8-13 Hz) (Becker et al., 2018), beta (12-30 Hz) (MacDonald et al., 2019) and gamma (>40 Hz) (Hanslmayr et al., 2012; Sato et al., 2014; Seymour et al., 2017)[2].

MEG is a functional imaging technique that can measure the weak magnetic fields generated by, and at 90^{o} degrees to, the brain's electrical activity. Most of the signal is thought to come from post-synaptic potentials, including sodium spikes and action potentials (Baillet, 2017). Collective firing of the pyramidal cells of shallow cerebral cortex is thought to produce the strongest signal because of their distance from the sensors and elongated morphology (Baillet, 2017). In humans, neuronal group electrical activity can also be measured with EEG, either at scalp or intracranially. MEG and EEG methods provide a temporal resolution with a timescale of milliseconds. However, MEG provides benefits over EEG techniques. The need for surgical patients makes invasive recording difficult to access and limits the scope of investigation. Non-invasive EEG suffers from poorer source reconstruction because the electrical signal is distorted by the covering tissue. Regarding MEG recording, the cerebrospinal fluid (CSF) and skull have high magnetic permeability so there is little distortion of the magnetic fields (Baillet, 2017).

The magnetic field measured outside the head is around 10 femtoteslas which is considerably smaller than the Earth's magnetic field (Singh, 2014). To measure these weak signals, the MEG machine comprises: a magnetically shielded room; pick-up coils coupled with sensitive magnetometers called SQUIDS (Super Conducting Quantum Interference Devices) held at around −270°C (using liquid helium), stored in the 'Dewar' (a large container with two walls separated by a vacuum); and gradiometers, to calculate background magnetic noise. Along with these are: a helmet and chair connected to the dewar; reference electrodes placed upon the three fiducial points (the nasion and left and

[2] The exact frequency ranges included within the bands can differ between studies and the references included here are example of studies which have used the same frequency band definitions.

right pre-auricular points) to continuously measure head position; and a chin rest to help the participant keep still. It is essential to limit participant movement, as head movement can disrupt the validity of the MEG signals and subsequent source localization (Gross et al., 2013).

A challenge in understanding the signals measured from outside the brain is determining the sources of the activity within the brain. This is referred to as the 'inverse problem' as the modal parameters (the locations) must be estimated from the recorded SQUID signals. However, there are no unique solutions. MEG research aims to create the best solution using prior knowledge of the brain to constrain the calculation. This way, analysis usually involves solving the forward problem before the inverse problem. The forward solution includes a geometrically accurate modelled head using realistic conductor models based on structural MRI and estimations of the contributions each brain source would make to the externally measured signals. These results are then used to inform calculations in the inverse problem, attempting to map the topographical patterns of the real data to likely tissue current sources (Gross et al., 2013).

Source reconstruction techniques vary in their applied constraints. Some assume one or few dipole sources are active at one time (Mosher et al., 1992), while others do not make assumptions about the number of active sources. The latter is called distributed-source imaging (Michel & He, 2019) and includes adaptive and non-adaptive methods (Hämäläinen & Ilmoniemi, 1994). Non-adaptive methods include minimum norm estimates which assumes that the entire cortex is active and provides a solution with the minimum energy (Hämäläinen & Ilmoniemi, 1994). Adaptive methods include beamforming (Michel & He, 2019). Beamformers are signal processing techniques for directional signal reception from phased arrays of sensors, which were developed for radar application but commonly used in MEG analysis (Hillebrand & Barnes, 2005; Van Veen & Buckley, 1988). The main assumption of beamformer techniques is that no two neuronal activity sources are perfectly linearly correlated and only sources that are not correlated are considered locations of interest. Beamformers attempt to focus on signals from locations of interest and attenuate other signals by selectively weighting the contributions from the sensors to the overall beamformer output (Hillebrand & Barnes, 2005; Van Veen & Buckley, 1988). A linear constrained minimum variance (LCMV) beamformer is commonly used (Van Veen et al., 1997). Here, the linear weighting of the sensor array is calculated using theoretical models of the magnetic fields produced by given dipoles as priors and, along with the covariance matrix, the second order statistics of the data. The results make it possible to

estimate wave properties of "virtual channels" at the source locations (Hillebrand & Barnes, 2005).

2.3.1 Measuring oscillatory activity from deep sources.

The possibility of detecting any activity from the MTL or hippocampus has been a source of debate (Riggs et al., 2009; Stephen et al., 2005) for multiple reasons. Foremost, the strength of magnetic signals diminishes with distance 'r' from the source, by $1/r^3$ so measuring MEG signals from deeper sources is more difficult that shallow sources. Additionally, a selection of source localization techniques, such a minimum norm estimation, are biased towards shallower sources (Attal & Schwartz, 2013). Also, the hippocampus' cylindrical shape presents a unique challenge as sections fold over each other, so homogenous activation could lead to signal cancellation (Ahlfors et al., 2010).

However, simulation (Quraan et al., 2011) and empirical (Barry et al., 2019; Cornwell et al., 2012) research, and recent reviews (Pu, Cheyne, et al., 2018; Ruzich et al., 2019) provide substantial evidence that detection of hippocampal activity in MEG sensors is possible. Modelling of magnetic fields have shown that although hippocampal fields are smaller than those of cortical areas, they are still detectable with MEG, and it is suggested that the higher current densities in the hippocampus provide compensation for the distance (Attal & Schwartz, 2013). Furthermore, simulation work has shown that simultaneous activation of hippocampal subfields does not produce complete signal cancellation (Stephen et al., 2005).

The research in this field indicates that successful recording of MEG activity is more feasible with certain experimental designs, analyses and hardware. Quraan et al. (2011) localized hippocampal activation when primary visual sources were also active, which is commonly the case when visual stimuli are used. They found that signal leakage from activity in visual areas causes a challenge for beamformer analysis because the strong visual signal is present simultaneously with the weak hippocampal signal. To increase detection of hippocampal activity, they suggested that stimuli from task and control conditions should have similar visual statistics, and beamformer analyses should involve source image subtraction. A review by Ruzich et al. (2019) suggested a number of techniques to increase sensitivity to hippocampal signals. They stated that: source localization is more accurate with participant structural MRIs, precise head digitization techniques and continuous head movement recording; and analysis should include distributed source or beamforming techniques and not equivalent current dipoles. In line with Quraan et al. (2011), they

recommend contrasting condition task data with two types of control tasks where areas other than the hippocampus are activated. Where MEG is used to measure MTL activity in this thesis, the methods were designed in light of these suggestions.

In addition, separation of signals between MTL areas such as the PrC and hippocampus would be useful for examining the PM-view, but it may not be possible because of their proximity to each other. Stephen et al. (2005) used simulated interictal epileptic activity to investigate whether MEG techniques could dissociate between signals originating from hippocampal subfields (including: CA1, CA3, dentate, entorhinal cortex and presubiculum), parahippocampal cortex and neocortical areas. To make the data more realistic, generated signals were added to real RS-data and the signal dissociation was tested in the context of simultaneous and sequential activation. Cortical activity and activity from the hippocampal subfields or parahippocampus, could be dissociated. However, hippocampal and parahippocampal activity could only be dissociated when the signals were sequential and not if they temporally overlapped. Therefore, in the current experiment, since MTL signals may be distinguishable from other cortical signals but the separation of MTL signals is unlikely, an oscillatory activity in an ROI encompassing both the entire HPC was examined.

While multiple MEG studies have focused on hippocampal processing (Pu, Cheyne, et al., 2018; Ruzich et al., 2019), comparatively few have identified PrC activity (Moses et al., 2009), and previous work has assumed MTL oscillatory modulations to originate from the hippocampus (Guitart-Masip et al., 2013; Ruzich et al., 2019). Moreover, a study attempting to distinguish MTL MEG sources using Independent Components Analysis (ICA) and invasive recordings showed that, when searching for correlations between ICA components from continuous MEG recordings and stereoelectroencephalography recordings from MTL areas, sources from the hippocampus or parahippocampal cortex were more robustly related (correlated in more patients) than signals from the PrC (Pizzo et al., 2019). Importantly, hippocampal oscillations may artefactually appear to affect local surrounding tissue through the phenomenon of tissue volume conduction (Sirota et al., 2008; Vinck et al., 2015). Therefore, in the current project, it was anticipated that MEG measured signals from the MTL would more likely arise from the parahippocampal cortex or hippocampus than PrC. However, there was a possibility that hippocampal and PrC processes during the oddity task manifest as different oscillatory frequencies.

2.3.2 Oscillatory frequencies of interest.

The frequency bands may have specific roles or reflect different processes. They grant differently sized temporal processing windows which may affect the characteristics of the underlying processes. Similarly, they can originate from differently sized cell groups with lower frequency oscillations spanning larger areas than higher frequency oscillations (Canolty & Knight, 2010; von Stein & Sarnthein, 2000).

Modulations in oscillatory patterns are understood to reflect modulations in brain processes (Buzsáki & Draguhn, 2004). Modulations in power of particular frequency bands, in particular brain areas, have been associated with particular functions. For example, theta power modulations in the hippocampus have been associated with memory processes (Cornwell et al., 2008), and beta power modulations in the motor cortex have been associated with movements (Khanna & Carmena, 2015). Relatedly, oscillatory synchrony across brain areas, in the forms of phase-coherence and amplitude-amplitude coupling, is thought to support long-distance communication (Palva et al., 2005; Samogin et al., 2020). For example, increased phase-coherence between the MTL and the frontal cortex has been demonstrated during spatial retrieval (Kaplan et al., 2014). Cross-frequency coupling patterns, such as phase-amplitude coupling (PAC), which is coupling between the amplitude of high frequencies and the phase of low frequencies, also occur (Seymour et al., 2017). Indeed, spatial retrieval was also demonstrated to coincide with increased PAC between frontal cortex theta and medial parietal cortex gamma (Kaplan et al., 2014).

Gamma, theta and alpha were of particular interest in this research because of their involvement in multiple cognitive functions, including perception and memory, and their occurrence in multiple brain regions. Examples include: cortical gamma oscillations are associated with conscious perception (Meador et al., 2002) and MTL gamma has been associated with spatial encoding (Pu, Cornwell, et al., 2018); MTL theta has been associated with spatial memory (Pu et al., 2017) and frontal theta has been associated with working memory processes (Hsieh & Ranganath, 2014); and alpha may suppress off-task processes (Jensen & Mazaheri, 2010) and be associated with perceptual performance (Brüers & VanRullen, 2018). Additionally, alpha coherence across brain areas is a suggested mechanism for long range communication (Chapeton et al., 2019). The following sections briefly describes possible roles of the oscillations and how they might represent underlying neuronal processes.

2.3.2.1 Gamma.

Gamma oscillations have been associated with several cognitive functions including memory, attention and perception (Cabral-Calderin et al., 2015; Carr et al., 2012; Magazzini & Singh, 2018). They can provide real-time characterizations of local circuit operations because they emerge from interactions between excitatory and inhibitory neurones in local cell circuits (Cardin, 2016). Gamma oscillations can arise from multiple network mechanisms, and experimental models have revealed at least two mechanisms in the hippocampus which may work together or independently: strongly activated interneuron-interneuron networks and coactivated reciprocally connected groups of pyramidal cells and interneurons. In the cerebral cortex, the latter may be the dominant mechanism (Cardin, 2016; Whittington et al., 2011).

There are multiple models which attempt to describe the functional role of gamma oscillations (Ray & Maunsell, 2015). The Communication Through Coherence model suggests that it offers communication between select neurones whose oscillations are temporally coherent and thus share inhibitory and excitatory windows. Interactions are established because the neurones' input and output 'communication windows' are open at the same time (Fries, 2005). The Phase Coding model proposes that gamma oscillations are useful for coding sensory information through the timings of spikes (localised depolarisations in individual neurones or small groups) relative to the phase of the ongoing oscillation. Stronger excitation could induce spikes during stronger inhibitory times of the cycles, whereas weaker excitations could only induce spikes when inhibition is weaker, so the pattern of spikes codes stimulus intensity (Fries et al., 2007; Ray & Maunsell, 2015). Regardless of the exact role, gamma provides a useful measure of neuronal activity and has been associated with information processing (Ray & Maunsell, 2015).

Gamma oscillation may be important in spatiotemporal processing. In humans, hippocampal gamma may be associated with spatial learning as gamma power has been found to decrease during repetitions of route navigation (Park et al., 2014) and gamma power post route-learning has been found to positively correlate with subsequent navigation performance (Pu, Cornwell, et al., 2018).

Gamma oscillations may also support face processing. Research into face processing and gamma activity has indicated that face sensitive areas exhibit gamma power modulation between upright faces and inverted faces, at around 300 ms after stimulus presentation (Uono et al., 2017), and that gamma power is higher during the viewing of normally-

configured faces, than scrambled faces (Gao et al., 2013). Also, induced gamma in response to faces is reduced in individuals with congenital prosopagnosia (Dobel et al., 2011). Together, the results indicate that gamma is involved in coherent face perception. They also suggest an underlying mechanism for the deficit in face perception in prosopagnosia.

2.3.2.2 Theta.

The hippocampus is well known for activity in the theta range due to the large amount of literature associating hippocampal theta with place-cell firing in locomotion in rodents (Sosa et al., 2018). Hippocampal theta is also associated with episodic and navigational memory in humans and it is thought that the underlying processes for navigating physical and mental spaces may be the same (Buzsaki & Moser, 2013). The hippocampus is thought to be a major current generator of theta (Buzsaki, 2002) but the emergence of the rhythm stems from the septum/diagonal band of Broca (Leao et al., 2015) and the supramammillary area (Pan & McNaughton, 2004) which are connected to the hippocampus through the fornix (Swanson & Cowan, 1979). Lesions to these areas cause reductions in theta (Rawlins et al., 1979) and memory impairments (Aggleton et al., 1995).

Theta oscillations are thought to link neuronal cell processes, thus creating integrated representations of complex concepts such as spaces or episodic memories (Colgin, 2016). Place and time cells have been shown to fire in relation to the phase of the oscillations of the surrounding group cell activity, in a phenomenon called ‘phase precession’ (Colgin, 2016; Pastalkova et al., 2008). Place cell firing occurs at progressively earlier phases of the theta cycle as the animal moves through the place field such that firing aligns with the beginning of the cycle as the animal leaves the field (O'Keefe & Recce, 1993). Time compressed sequences, called ‘theta sequences’ emerge in each cycle of the theta rhythm and reflect the order of place cell firing and, therefore, the order in which place fields are entered during exploration (Foster & Wilson, 2007). Blocking of theta oscillations in rats has been shown to disrupt theta sequences and spatial memory (Wang et al., 2015).

Although phase precession has not been described in humans, cells equivalent to place cells have been identified using invasive recording (Ekstrom et al., 2003) and properties of human hippocampal theta have been associated with spatial processing, even with non-invasive techniques. For example, a MEG study showed that hippocampal/parahippocampal theta was stronger during an earlier, than later, training phase, of a virtual Morris water maze task, and that individual theta power in the earlier phase correlated with spatial navigation performance (Pu et al., 2017). Conversely, other

studies have found hippocampal theta power decreases during encoding (Crespo-Garcia et al., 2016), that were associated with object and place retrieval accuracy, and during novel scene imagery (Barry et al., 2019). Together, the results indicate the importance of MTL theta in spatial processing in humans.

2.3.2.3 Delta

Hippocampal theta rhythms in humans have been reported to be lower (in the delta range 1-4Hz) than those reported in rodents (Jacobs, 2014). Therefore, although theta is of foremost interest for this project, MTL activity in the delta range was also explored.

Results of invasive studies of rat hippocampi have indicated that hippocampal delta increases during 'offline' periods, where the current behaviour lacks locomotion (Li et al., 2008; Schultheiss et al., 2019) (locomotion is associated with increased hippocampal engagement in the form of increased theta and gamma power (Buzsaki, 2002; Colgin, 2016)). Therefore, human slower hippocampal theta rhythms may occur in delta ranges because human neuroimaging studies often involve immobility (Bohbot et al., 2017).

However, delta rhythms may indicate different processes to theta. Human EEG research suggests that delta oscillations support internal thought by inhibiting other processes, such as processing external stimuli, which may disrupt internal concentration (Harmony, 2013). Similarly, rat hippocampal delta has been demonstrated to become more prominent over repetitions of the same treadmill run, despite no changes in the amount of locomotion, which the researchers attributed to fatigue or task habituation (Furtunato et al., 2020). Therefore, increased hippocampal delta may reflect reduced external sensory input, whereas reduced hippocampal delta may reflect increased online hippocampal processing.

2.3.2.4 Alpha.

It is suggested that alpha suppression reflects disinhibition or information processing because, for a particular task, function-relevant brain regions show decreases in alpha power whereas other regions can show increased alpha power (Jensen & Mazaheri, 2010). Alpha activity is thus associated with 'gating by inhibition' (Jensen & Mazaheri, 2010). In this, top-down modulation of alpha oscillations in sensory areas may enhance a processing stream by exciting task-relevant areas and inhibiting the irrelevant input. For example, in a cross-modal attention task where participants were cued for upcoming visual or auditory discrimination tasks, alpha activity was shown to increase in auditory processing areas, and

decrease in visual processing areas, in response to a visual cue, and vice versa (Mazaheri et al., 2014). Jiang et al. (2015) showed that alpha inhibition can aid other processes. Their MEG study required participants to learn either words or pictures, depending on a prior cue, during trials in which the two were presented simultaneously. They found that alpha increased in regions associated with the modality that was not cued and that memory performance related to alpha decreases in regions relevant to the cued modality (Jiang et al., 2015). The results support the proposal that alpha channels information flow during encoding.

Recently, alpha oscillations have also been shown to have other roles in cognition. A human EEG study attempted to separate working memory and attention in visual tasks (Erickson et al., 2019). Alpha suppression in frontal and posterior electrodes was higher in a task that involved attending to, and memorizing, an array of colours than the task that only involved attending to the array. This suggests that alpha suppression can act beyond generalized gating by inhibition, by supporting memory-specific processes. In information theory terms, alpha suppression may allow increased coding capacity, as information richness may be inversely related to synchrony (Hanslmayr et al., 2012).

It was thus anticipated that alpha power suppression would occur in PMN areas during spatiotemporal processing and in AIN areas during aggregate item processing.

2.3.3 Cognitive functioning can involve interactions between oscillations from different brain areas and in different frequency bands.

Communication between brain areas through oscillatory coupling may support complex behaviours and lower frequencies may be better suited to engage larger networks than higher frequencies (Chapeton et al., 2019; Doesburg et al., 2009; von Stein & Sarnthein, 2000). Kaplan et al. (2017) found that theta phase-coupling between the mPFC and MTL and RSC areas was higher when imagining travelling a path with learned objects than when imagining the objects statically. (The mPFC is associated with working memory maintenance, the RSC with spatial memory.) This suggests that collaboration between these areas allows a more complex cognitive state (Kaplan et al., 2017). Similarly, mental construction of novel scenes has been shown to increase theta coherence between the mPFC and the hippocampus, especially when those scenes are greatly detailed (Barry et al., 2019).

Theta/gamma interplay is common during cognitive functions (Lisman & Jensen, 2013). Gamma activity may be more prominent in the MTL during encoding than theta, which appears to increase in power with experience. Invasive recording in humans, coupled with a virtual reality navigation task which involved learning associations between objects and places, showed that hippocampal theta and delta power was higher in familiar, over novel, environments (Park et al., 2014). High gamma (defined at 51-100 Hz) however, decreased during blocks with high behavioural performance. The authors concluded that low frequency oscillations are associated with encoding novel spaces whereas high gamma is more related to successful object-to-location encoding (Park et al., 2014). Similarly, during a virtual Morris water maze task, MEG-recorded hippocampal/parahippocampal high-gamma power was higher in the inter-trial period after navigation of a novel, than after a familiar, space. This high-gamma power correlated with theta power during navigation and the speed of learning in the subsequent task block (Pu, Cornwell, et al., 2018). This provides evidence that understanding and learning spaces may require theta and gamma oscillations that can covary over time.

Theta and gamma interactions are also reported in perceptual processing (Sato et al., 2014), retrieval (Kaplan et al., 2014), and working memory (Canolty et al., 2006). The 'theta-gamma neural code' hypothesis of Lisamen and Jenson et al. (2013), states that oscillatory coupling allows ordered-storage of multiple items. Gamma oscillations are proposed to allow coding, and separation of, multiple items by synchronising and separating spikes. Theta oscillations are proposed to aid communication of the multiple items between areas by providing a phase reference, shared by the communicating brain regions (Lisman & Jensen, 2013). The oscillations can interact through cross-frequency coupling, such as PAC, which can occur in single areas, or across brain regions (Canolty & Knight, 2010).

2.3.4 Measuring functional connectivity with RS MEG analysis.

RS MEG data analysis is similar to that of task-based data but relies on parcellation of the brain before connectivity analysis. Once the data is in template source space, publicly available atlases such as the Automatic Anatomical Labelling (AAL) atlas can be used for parcellation. Correlation analyses between signals from these parcellations are performed across the whole brain, and the results can be compared between groups or tested for correlations with measures of individual differences.

RS-connectivity patterns can provide information about the quality of a network and can help differentiate different networks' functions. This can be seen in patients with different cognitive deficits. RS analysis across frequency bands has shown that the connectivity of usually-well-connected areas, such as the hippocampus in the PMN, is disrupted in AD (Yu et al., 2017), whereas phase-lag index analysis of EEG signals has shown the importance of frontal networks in behavioural-variant frontotemporal dementia, compared with AD (Yu et al., 2016). Unequal disruption of brain networks may contribute to unequal behavioural impairments in these patients. AD typically involves memory deficits while behavioural-variant frontotemporal dementia patients often display deficits in complex behaviours and can have personality changes (e.g. Bang et al. (2015) and Mielke (2012)).

2.4 Measuring brain structure using MRI.

MRI scanners have three main components: a static magnetic field that aligns the spin axis of protons; radio-frequency coils that transmit energy and increase the proportion of spins in a high energy state (not aligned with the magnetic field); and a receiver coil that measures the energy emitted as the protons return to the low energy state. During excitation, net magnetization moves from the longitudinal to the transverse plane and the spin phases align, giving a higher transverse signal. T2 relaxation is the decay of the transverse component due to a decrease in phase coherence. T1 relaxation is the energy released as the longitudinal net magnetization is recovered. These images are commonly used to delineate brain structure and as a template for other imagining modalities, such as MEG source-space analysis (Gross et al., 2013).

Gradient coils, able to produce magnetic gradients with different orientations, are critical for Diffusion Weighted Imaging (DWI). A temporary magnetic gradient causes a phase shift and a second magnetic gradient, at the same strength for the same duration but in the opposite direction, causes another phase shift that should re-align the phases. However, the resulting emitted signal is reduced because the protons will have moved during this process. Diffusion is the random motion of molecules and if the molecules move randomly, equally in all directions, the resulting signal will be lower than if movement was restricted. The brain's structure results in non-uniform restricted movement. For example, if a voxel contains tracts aligned in a single orientation, the DWI signals for that voxel will differ greatly across different diffusion orientations and be smallest in the orientation with the most movement (the same orientation as the tract). However, in a ventricle, the DWI signal will not differ greatly across orientations. The strength of diffusion effects is determined by

the strength, spacing and duration of the applied magnetic gradients, which are combined into one factor, the b-value (units: s/mm^2).

In this project, DWI was used to indirectly assess the properties of tracts thought to be involved in the PMN and AIN. A DWI experiment requires decisions about: the data acquisition sequence; the model for tractography; and the model for the calculation of MR-derived tract properties.

Diffusion tensor imaging (DTI) is a commonly-used branch of DWI (Jones, Knosche, et al., 2013), that studies the random motion of water molecules in a medium with diffusion-hindering tissue, such as white matter. This hindrance turns diffusion from isotropic to anisotropic (turning dispersion from a point from a sphere to an ellipsoid, Figure 3A). DTI assumes that the probabilities of displacement from a point show Gaussian distribution. Magnetic gradients are applied at right-angles to each other in 3D space. The result is a 3x3 matrix, the tensor. Each voxel contains information about the average diffusion distance, the degree of directionality of the diffusion and its direction. In the ellipsoid constructed (Figure 3A) from the tensor, these data are presented as its size, shape and orientation. The metrics for these are the major-, medium- and minor-eigenvalues, the FA, and the major-eigenvector respectively. Tractography constructs streamlines through voxels based on the major orientation with the expectation that these run parallel to the real white-matter fibres (Alexander et al., 2011; Jones, Knosche, et al., 2013).

When tensors are used to calculate tract streamlines, DTI is vulnerable to errors due to fibre crossing within voxels, which causes areas of incorrect prediction of orientation (Farquharson et al., 2013). ‘Crossing fibres’ includes any situation where multiple fibre orientations appear within one voxel, including fibres brushing past each other or one fibre ‘fanning out’ (Jones, Knosche, et al., 2013). Most tractography algorithms produce streamlines based on local estimates of fibre orientation (Jones, Knosche, et al., 2013), so even very small errors in local orientation estimation can cause a streamline to fall onto a different fibre or stop completely.

For this reason, multi-orientation models can be more accurate. They can involve estimating a reduced representation of the ‘spin propagator’ based on the q-space (Mori & Tournier, 2013). A point in q-space is defined by the gradient strength (b-value) and gradient direction. The spin propagator characterizes the proportion of spins with particular starting positions that have moved particular distances. To obtain the spin propagator from q-space, a 3D Fourier transform is used. Different acquisition models

differ in how they acquire data from different points in q-space. Diffusion spectrum imaging offers the most thorough coverage of q-space – many images are obtained with differing orientations and gradient strengths – and the most complete characterization of diffusion (Tuch, 2004; Wedeen et al., 2005).

For fibre tracking, the spin propagator is used to calculate the diffusion orientation density function (dODF). The dODF displays the directions of diffusion peaks and therefore uses only a subset of diffusion spectrum imaging data. Acquisition times are long considering the amount of information needed for tractography (Tuch, 2004).

High Angular Resolution Diffusion Imaging (HARDI) acquisition offers a compromise. It explores a spherical shell of q-space where the orientation of each image differs, but the gradient strength (b-value) stays constant (Tuch, 2004; Tuch et al., 2002). It is possible to estimate fibre ODF directly (fODF), with HARDI acquisition with spherical deconvolution, which does not require modelling of the diffusion process itself but assumes that the characteristics of the diffusion signal are the same for all fibre bundles (Tournier et al., 2004). An example is the damped Richardson-Lucy (dRL) algorithm, which was designed to reduce isotropic partial volume effects from CSF and grey matter (Dell'acqua et al., 2010).

Scan protocols can include multiple shells (with different b-values). Higher b-values give greater contrast to noise ratios in the angular domain, which helps to resolve crossing fibres (Mori & Tournier, 2013). However, their lower Signal to Noise Ratio (SNR) can make motion and eddy-current correction challenging (Mori & Tournier, 2013). Therefore, low b-value images are also collected. Moreover, higher order models can require multiple shells to gain enough diffusion information for the model fit (Mori & Tournier, 2013).

To estimate tract properties, four measurements are often taken from the diffusion tensor. FA is calculated using metrics related to the difference between the major, medium and minor eigenvalues. It gives an indication of the major direction of diffusion and the extent of restriction of free movement within white matter (range 0 - 1). High FA is often taken to indicate high structural quality (Soares et al., 2013). MD gives an indication of diffusion rate across the three orthogonal directions (units: 10^{-3} mm^2/s), and low MD is often taken to indicate high structural quality (Soares et al., 2013). Axial Diffusivity (AxD) gives the mean diffusion coefficient along the main axis of diffusion (thought to be parallel to the tract) and is thought to relate to axon structure (units: 10^{-3} mm^2/s). Radial diffusivity (RD) is the mean of the two smaller eigenvalues of the tensor model, and is thought to reflect the magnitude of diffusion perpendicular to the fibre tracts (units: 10^{-3} mm^2/s). AxD may reflect axon

structure while RD may reflect myelin proportion (Song et al., 2003). However, the meaningfulness of DTI measures is vulnerable to the effect of crossing fibres on the calculation of the tensor (De Santis et al., 2014). Moreover, they are non-specific to individual properties of the white matter. For example, both axon membranes and myelin content can influence FA (Beaulieu, 2002).

Measures from higher-order models may prove to be more biologically meaningful. DTI assumes that water molecule movement follows a Gaussian distribution, which is unlikely in tissue because of the presence of cell membranes and cellular bodies. Some models do not make this assumption, but view tissue as comprising multiple compartments with differing diffusion properties (Mori & Tournier, 2013).

The Composite Hindered and Restricted Model of Diffusion (CHARMED) protocol requires a multi-shell HARDI acquisition with a wide range of b-values. The model views white matter as a medium containing extra-axonal space with hindered diffusion of water and intra-axonal space with restricted diffusion of water (Assaf & Basser, 2005) (Figure 3B). The latter measure, the Restricted Fraction (FR) (range: 0-1) can be thought of as a probe for axonal density, making it more specific than FA. Furthermore FA values depend on the orientations of fibres within a voxel (Budde & Annese, 2013) whereas FR appears to be independent of this (De Santis et al., 2014).

Neurite Orientation Dispersion and Density imaging (NODDI) shares similarities with CHARMED but was designed to be more clinically feasible, as it can be acquired using a two-shell HARDI acquisition. The resulting measures include intracellular volume fraction (ICVF) (range: 0-1) and Orientation Dispersion (OD) (range: 0-1). OD and FA are negatively related in white matter, while ICVF has a smaller, positive relationship with FA (Zhang et al., 2012).

DTI results can be contaminated by CSF, a problem which may not affect FR or ICVF to the same degree because CSF data would be incorporated into other model compartments (De Santis et al., 2014; Zhang et al., 2012).

Quantitative Magnetization Transfer (qMT) imaging uses the Magnetization Transfer (MT) technique and gives an indication of molecular density, making it more sensitive to measures of myelination. MT overcomes the fact that obtaining MRI information from the protons bound in myelin is unachievable (because the T2 is too short), by utilizing their broad range of resonance frequencies. The free water around these axons has a very

narrow spectrum of resonant frequencies but longer, and therefore measurable, T2 relaxation times. By emitting radiofrequency pulses with frequencies different from free water resonance frequency, free water is unaffected, but bound protons will resonate (Figure 3C). However, by MT, the magnetization of the liquid pool will reduce. The ratio of the free water signal with and without the pulse is the MT ratio. Increases in this ratio correlate with increased concentrations of bound protons, and can imply more myelin in the tissue (Alexander et al., 2011). For qMT, this two-pool model is fitted to data resulting from multiple MT pulses with multiple frequencies and amplitudes (Alexander et al., 2011). The resulting Molecular Proton Fraction (MPF) can be taken as a measure of myelin fraction (Giulietti et al., 2012; Metzler-Baddeley et al., 2019).

2.4.1 The microstructure methods chosen in this thesis.

The temporal-sequence memory experiment described in *Chapter 7* uses a two-shell HARDI acquisition, spherical deconvolution for the streamline calculation, and DTI and NODDI for tract property calculations. Dual-shell data is beneficial because the high b-value (here 2400) gives more angular contrast and the low b-value (here 1200) gives higher SNR (Andersson and Sotiropoulos, 2015; Sotiropoulos et al., 2013), so the former can be used to calculate tractography and the latter can be used to calculate DTI measures. Although DTI measures can be vulnerable to crossing fibres and are difficult to interpret biologically, they can still provide a useful measure for the involvement of a tract in a task when used in an individual differences style experiment. To provide some more direct markers of underlying structure, NODDI measures, ICVF and OD, were also calculated.

The oddity experiment described in *Chapter 5* used data acquired through a CHARMED protocol that comprised diffusion-weighted images acquired over a wide range of b-values with some significantly larger than traditional HARDI acquisitions (e.g., 4000). From this, data acquired using b-values around 1200 and 2400 could still be used to calculate DTI

measures, tractography and NODDI. qMT was also used. Microstructure methods used in this thesis are illistrated in Figure 3.

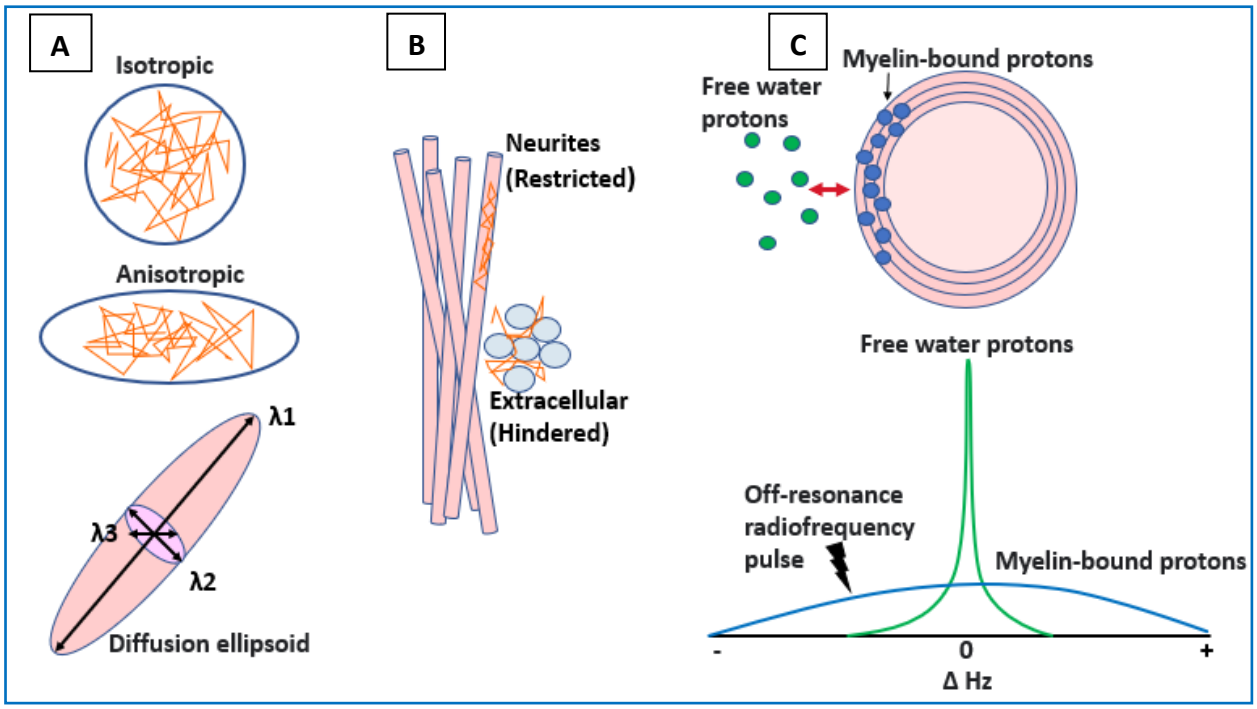

Figure 3. Diagrams of microstructure methods used in this project.

A) Isotropic diffusion is illustrated as diffusion within a perfect sphere (top), where it occurs equally in all directions. Anisotropic diffusion is illustrated as diffusion in an ellipsoid (middle) where it is not equal in all directions. The diffusion ellipsoid is illustrated (bottom) with three eigenvectors (illustrated as arrows) and three eigenvalues (λ1, λ2, and λ3). This can be represented in a 3 by 3 matrix, called the diffusion tensor. Diffusion paths are exemplified in orange.

B) CHARMED and NODDI models assume that there are two compartments, hindered and restricted, the former occurring in extracellular space and the latter occurring in intracellular space. A diffusion path is exemplified in orange.

C) qMT allows the estimation of the proportion of macromolecular protons bound in myelin (top, blue) despite their immeasurably short T2 signals, by utilizing their broad range of resonance frequencies (bottom, blue). Free water has a narrow range of resonance frequencies (bottom, green) but measurably long T2 relaxation times. By emitting a radiofrequency pulse away from the free water resonance frequency, but within the range of the myelin-bound protons, the free water T2 signal can be altered because the spin states of the myelin-bound protons influence those of the protons in the liquid pool by magnetization transfer exchange (top, illustrated as a red arrow).

2.5 Statistical methods to relate functional, structural and behavioural data.

Linear correlation analysis between behavioural data and imaging data (e.g., Hodgetts et al., 2015; Postans et al., 2014; Pu et al., 2017) provide a useful and simple clarification of the relationship between, for example, behaviour and individuals' single tract properties, or between behaviour and brain areas' functional relationship scores.

Whole-brain searches for linear correlations between behaviour and function are also useful. For example, Fieldtrip (Oostenveld et al., 2011), a program for electrophysiological data analysis, allows for a search for correlations between values of interest, such as a behavioural measure, and whole-brain frequency power values.

For instances where coefficients of correlation tests were predicted to be different (for example, in *Chapter 5*, the coefficient of the correlation between fornix microstructure and scene oddity performance was predicted to be stronger than that of the correlation between ILF microstructure and scene oddity performance), the coefficients were compared using the Pearson and Filson's test (Pearson, 1897).

Partial correlations were also used in this thesis, allowing the measurement of correlation between two variables while controlling for a third. For example, in *Chapter 7* the correlation between a fornix microstructure property and an object-in-sequence retrieval score was tested while controlling for an object-in-sequence 'learning score', to test if a relationship existed between fornix microstructure and object-in-sequence retrieval that was independent of learning. Similarly, multiple linear regression analyses were useful on occasions where it was of interest to understand whether a variable independently predicted another variable or whether other measures also contributed. For example, to ask whether microstructure properties from all three tracts contribute to a behaviour score and whether fornix microstructure is an independent contributor.

Some of the hypotheses in this project were that specific phenomena should *not* occur. For example, when designing the stimuli for the oddity study through piloting (described in *Chapter 3*), Bayesian Repeated Measures Analysis of Variance (RM ANOVA) was used to assess whether accuracy scores for the conditions (scene, face or size) did not differ. Therefore, along with inferential statistics, Bayes Factors (BFs) were also calculated using BayesFactor package in R (Morey & Rouder, 2018) or using JASP (JASP Team, 2020), and were reported as BF_{10} (evidence of the alternative model over the null model). BF_{10} values between 1 and 3 can be taken as weak evidence in favour of the alternative model, values exceeding 3 taken to reflect stronger evidence, and values between 1 and 0.33, and below 0.33, taken as weak and stronger evidence in favour of the null, respectively (Raftery, 1995). In the cases where a third variable needed to be controlled for, Bayesian correlations between the residuals of variables were tested (as with traditional partial correlations).

PCA is useful when there is high multicollinearity among variables. Here, it was used to reduce microstructure data, as different measures can give overlapping information. PCA identifies components in the data by looking for linear correlations between the variables. The first component explains the largest amount of variance in the data and subsequent orthogonal components explain sequentially smaller amounts of resulting variance (Abdi & Williams, 2010). As an example of the advantages of this technique, Chamberland et al. (2019) used PCA to reduce 10 MRI-derived tract properties, and found that the first component of the inferior fronto-occipital fasciculus correlated with age.

Chapter 3. Adapting the oddity task for use with MEG.

3.1 Introduction

3.1.1 Background.

The oddity task predominantly tests complex perceptual processing as it involves online discriminations of items displayed simultaneously, but with differing view-angles. The task can include scenes, faces/objects and shape-sizes (control). It has been used to reveal impairments in MTL-lesioned patients (Barense et al., 2007; Lee, Buckley, et al., 2005). It produces MTL BOLD modulation in healthy participants (Barense et al., 2010; Hodgetts et al., 2015; Hodgetts, Voets, et al., 2017; Lee et al., 2008). Importantly, these patterns were only seen when the images were displayed at differing angles, suggesting that the MTL areas aid in the creation of online view-invariant internal models (the shape-size control task, in which participants identify a shape of a different size, does not require the creation of a view-invariant internal model and does not produce these patterns). Examples of the stimuli used in these previous oddity studies are shown in Figure 4. This project used the oddity task in conjunction with MEG to examine the roles of the PMN and AIN in complex perception. This had not previously been done. MEG records brain activity with precise timings but its ability to localise deep brain sources is challenging, and eye-movements can influence MEG signals (Gross et al., 2013; Quraan et al., 2011). This chapter discusses the design and piloting of an oddity task adapted for use with MEG.

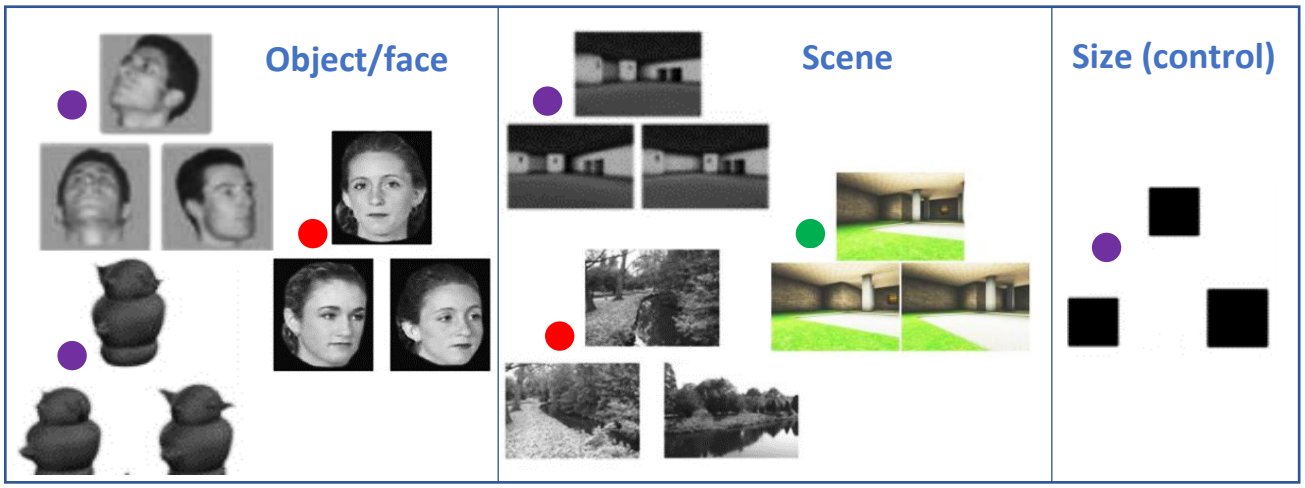

Figure 4. Examples of oddity task stimuli used in previous studies.

Images copied from: ● Barense et al. (2010); ●Hodgetts et al. (2015); and ●Lee et al. (2013), without permission.

3.1.2 Aims and considerations.

Like previous oddity studies, trials in the current oddity task comprised three images, presented simultaneously. These were virtual scenes or faces, from three different angles. To make this study comparable to Hodgetts et al. (2015), scenes, face and shape stimuli were used. The odd scene had different spatial relationships between the objects within the image, different orientations or locations. Similarly, the odd face had altered features, for example the eyes and mouth might have altered shapes or distance between them. The control task was designed not to require online internal model generation and involved identifying the different-sized circle. Although previous work had used squares (e.g. Hodgetts et al., 2015), rather than circles, there was a risk that the prominent edge orientation information in these images may make MEG-measured visual signals comparatively stronger in this condition than in the scene or face conditions (the importance of matching image statistics is discussed further below in section 3.1.2.2).

While this project used MEG, previous research combining oddity task completion with neuroimaging in humans had used fMRI (Barense et al., 2010; Hodgetts et al., 2015; Hodgetts, Voets, et al., 2017; Lee et al., 2013; Lee et al., 2008). There are several methodological considerations involved in adapting the stimuli and paradigms of fMRI studies for MEG research. Different designs were tested over six behavioural pilot studies, which are collectively described in this chapter. The specific considerations and aims are described below (sections 3.1.2.1 - 3.1.2.4).

3.1.2.1 Increasing temporal precision.

Due to the time-lag of the BOLD response, the temporal qualities of MTL and outer network involvement in online processing is unclear. The current experiment was designed to utilize the precise timing of MEG. Whereas previous experiments gave participants a fixed time period to view the stimuli (e.g. 5.5 s in Lee et al., 2013), here the trial ended as soon as the participant made their choice. It is likely that online perceptual processes and mnemonic processes temporally overlap (and they are thought to be intimately related in the PM-view), but it was postulated that the time-period after a decision, where the participant passively views the stimulus for the remainder of the trial, would be dominated by mnemonic processes. Therefore, the current method may reduce mnemonic-dominant brain signals in the trial periods. The previous fMRI studies did not take this approach, presumably because of restraints regarding the temporal characteristics of the haemodynamic response function (Amaro & Barker, 2006).

The design meant that trials could be of variable lengths. Therefore, it was important that trials were viewed long enough so that sufficient recording of the low oscillation frequencies of interest (e.g. those within the delta/theta bands) was possible. An aim was for trials to last longer than 1.5s. This would allow at least one whole cycle of the lowest delta frequency (1 Hz) and at least 6 cycles of theta (4-8 Hz) frequencies. Participants were given 6 s (pilots 1-2) or 8 s (pilot 3-6) in total for each trial but were asked to indicate their answer as soon as they had come to a decision. They were advised that accuracy was more important than speed, and that the response could be made any time during the trial. This differed from a previous administration of the oddity task in fMRI, where the researchers asked participants to respond "as quickly but as accurately as possible" (Lee et al., 2008). It was important that the stimuli were difficult enough so that completion of most trials would take longer than 1.5 s and, ideally, up to 8 s. Although part of the aim of this project was to replicate the findings of Hodgetts et al. (2015), the scene stimuli used in Lee at al. (2013) were chosen as they were more difficult. This latter study gave participants 5.5 s to complete each trial and had around a 50% accuracy rate (chance level at 33%). The current pilot studies initially aimed for accuracy of around 50% (Pilots 1-3) but this was then increased to 60% (Pilots 4-6) to allow for a 'safety net' in case the MEG environment caused a reduction in accuracy scores. It was hoped that this higher accuracy level would be achieved through the longer trial times.

The face and size stimuli were generated with the aim of matching the scene stimuli in mean and distribution of accuracy. There was a jittered 1-1.5 s interval in between task trials (except those preceded by a 'fixation trial', see below) in which a fixation cross was displayed. A jittered time-length is important to reduce the effects of participants' expectations of upcoming trials and the accumulation of recurring cyclic interference from line noise, for example, when calculating the average over trials (Gross et al., 2013).

3.1.2.2 Increasing the likelihood of deep source localization by matching image statistics between conditions.

As discussed in *Chapter 2*, localization of deep sources is a challenge in MEG research, but it is feasible (Pu, Cheyne, et al., 2018). Quraan et al. (2011) localized hippocampal activation when primary visual sources were also active, which is commonly the case when visual stimuli are used and is likely the case in the current study. They found that signal leakage from activity in visual areas causes a challenge for beamformer analysis because the strong visual signal is present simultaneously with the weak hippocampal signal. Source image

subtraction is a viable solution. The comparison of two sets of MEG data with similar visual cortex activity but differing deep brain activity, should expose the deep brain activity. Image properties can modulate visual area activity. Therefore, in the current project, the stimulus images were created and modified with the aim of making the low-level statistics of the images of each category as similar as possible, without changing the nature of the tasks. The following describes the image properties of interest and how they can influence visual cortex activity.

Image statistics can be classified as first-order, second-order or higher-order, which corresponds to the number of pixel values included in a calculation. First-order statistics includes data from individual pixels, and they can be represented through histograms that possess several descriptive qualities such as mean and dispersion. A common first order image property is luminance, which has been shown to affect low level visual processing areas. For example, mean luminance has been shown to influence the time course of event-related potentials in response to faces (Bieniek et al., 2013).

Second-order statistics describe the comparison of two spatially separate pixel values (van der Schaaf, 1998) and have been shown to modulate activity in low level visual processing areas. For example, V1 responses increase with increasing image contrast (Albrecht & Hamilton, 1982; Gardner et al., 2005). Perry et al. (2015) used MEG recording in conjunction with patterns of varying luminance contrast and showed that varying luminance contrast over time modulated the contrast tuning of the amplitude and frequency of the visual gamma response. The autocorrelation function and the power spectrum are commonly used measures of luminance contrast in second-order statistics. The former measures the correlation between intensity values of two spatially separate pixels and the power spectrum is the Fourier transform of this (van der Schaaf, 1998). Fourier analysis allows for any 2D image to be reduced into the sum of a set of sinusoidal gratings described by spatial frequency (the width of the grating bars), orientation (angle of the grating bars), amplitude (difference in luminance in the grating) and phase (the position of the sinusoidal grating relative to a reference point) (Willenbockel et al., 2010). Performing Fourier analysis on an image produces two spectra, an amplitude spectrum and a phase spectrum, which illustrate the amplitudes and phases of each grating at particular spatial frequencies and orientations, respectively (van der Schaaf, 1998). Natural images have an amplitude power spectrum that follows a pattern of $1/f^2$, where spectral amplitude decreases with increasing spatial frequencies. Images with finer detail will have higher powers of high spatial frequencies and the slope will be shallower. The opposite applies to

images with more coarseness and higher powers of low spatial frequencies. The size of the spectral signature is correlated with the slope of the frequency spectrum (Torralba & Oliva, 2003). Lescroart et al. (2015) investigated how Fourier power spectrums, object category and subjective distance of images, affected BOLD response patterns in scene processing areas and found that their Fourier power model was the best predictor of these patterns in V1. Therefore, it can be assumed that equivalent V1 oscillatory signals are modulated by Fourier power spectra of images, and these signals may pervade the recordings of MTL signals.

In an effort to match the low-level statistics (luminance and Fourier spectra) between categories, the face, scene and size stimuli underwent statistics matching using the SHINE toolbox for MATLAB (MATLAB, 2015), which reduced differences between condition images' Fourier amplitude and luminance patterns (Willenbockel et al., 2010).

In previous studies the control condition required participants to judge the size of black squares on white backgrounds. This straight-edge high-contrast shape does not visually match the scene and face stimuli, which are more complex, and such properties can strongly affect visual cortex oscillatory activity (Hadjipapas et al., 2015). The control task needed to be adapted without changing its lack of requirement for view-invariant internal representations. The task was changed to size judgment of semi-translucent circles overlaid on phase scrambled face and scene stimuli.

3.1.2.3 Increasing the likelihood of deep source localization by adapting layout and timing.

The layout and timing of the presentation of the stimuli differed from previous oddity task studies with the aim of limiting head movement while also increasing trial number. Quraan et al. (2011) simulated hippocampal localization in datasets with 10 to 150 trials. They found that localization error did not increase when reducing from 150 to 100 trials, but it increased when reducing from 100 to 50 trials and increased again between 50 and 10 trials. Previous studies had used relatively few trials (e.g. Hodgetts et al. (2015) used 18 per condition). To limit scan time, and to assist with counterbalancing, the current study used 96 trials per condition.

To allow for breaks and reduce head-movement distance within recording sessions, trials were split into 4 blocks, lasting around 10-minutes each. The head position was re-mapped before each recording block.

Eye-movement can create physiological artefacts in the MEG recording (Gross et al., 2013) so it was important that the extent of saccades between images within the trials was kept to a minimum. The ocular angle of the first pilot was estimated to be the smallest possible while still visible to the participant. The intention was to reduce this angle in subsequent pilots if possible. However, accuracy scores did not reach the target mean of 60% so ocular angle was not reduced. The distance between participant and screen and the screen size differed between the behavioural laboratory setting and the MEG lab setting so the image size was altered to keep ocular angle the same in the two settings.

3.1.2.4 The importance of a subsequent unforeseen memory test.

In addition to the oddity task, it is important to include a post scanning memory test of the oddity trials. A criticism of previous work is that MTL BOLD changes during the trial could be a result of incidental encoding processes. Although this can be countered by the evidence that the association between hippocampal signal strength and oddity task performance is independent of subsequent memory for the oddity stimuli (Lee et al., 2013), it is important to test for incidental encoding as well as complex perception performance. This allows the researchers to ensure that associations between structure or function neuroimaging measures and performance in this complex perceptual task, are not simply reflections of an association between these neuroimaging measures and incidental encoding, and that incidental encoding aids performance in the complex perceptual task. Pilots 1 and 5 included an unexpected memory test, following the oddity task, to test the paradigms' feasibility and to examine whether incidental encoding of scene and face stimuli facilitates oddity task completion.

3.2 Methods

3.2.1 Participants.

Participants for all pilots, and all subsequent experiments presented in this thesis, were recruited through Cardiff University School of Psychology's participant panel after the projects were approved by Cardiff University School of Psychology ethics department. Participants were asked to volunteer only if they were taking no psychoactive medication and had normal, or corrected-to-normal, vision. All volunteers gave informed consent prior to participation.

Since the aim was to create an adaptation of the oddity task, a task that has been used in several studies previously, the purpose of the pilots was to check that the trials were answerable, and that the condition accuracies were equal. Therefore, small sample sizes were sufficient. The participant demographics for each oddity pilot are shown in Table 1. For each pilot, there was a target of 10-15 participants and the resulting sample size varied according to the number sessions that could be run within the time allocated to the pilots (for example, more volunteers are available at certain times of the year). Note that participants could not contribute to more than one pilot. Due to a recording error, the ages of the participants in pilots 1 and 2 were not recorded. However, the age range is likely to be similar to other pilots because they were recruited from the same participant pool.

Pilot Number	Number of Participants	Number of Males	Mean Age	Number Left-handed
1	15	3	n/a	2
2	9	3	n/a	1
3	15	2	20 SD: 1.3	2
4	10	0	22 SD: 1.9	0
5	9	3	23 SD: 2.6	1
6	9	1	20 SD: 1.5	0

Table 1. Participant demographics for oddity task pilots 1-6.

Age was not collected for pilots 1 and 2. 10 participants' data were collected for pilot 4 in total but one individual did not appear to engage with the task so this dataset was not used and another participant was recruited. 15 participants were originally recruited for pilot 1 but two datasets were not fully collected due to recording errors.
n/a = 'not available'

3.2.2 The oddity task.

3.2.2.1 Layout and timing of presentation of the stimuli.

The oddity task required participants to examine triplet images of scenes, faces or circles and to identify the odd-one-out. For the scene and face stimuli, the images were shown at three different angles and different locations. One image had either differing object relationships (scene condition) or differing facial features (face condition). For the control

task (size condition), 3 circles were shown with different locations and one circle differed in size.

There was a total of 96 size trials and 144 face and scene trials. For each participant, the oddity task included all 96 size trials, 96 of the face trials, and 96 of the scene trials. To reduce fatigue and head movement over trials, the resulting 288 trials of the oddity task were split into four counterbalanced blocks of 72 trials. Participants responded using a keyboard with their right hand. In the oddity task, three keys represented the three images.

To reduce predictability, there was an element of random ordering of stimuli within blocks. However, complete randomness of trial order may increase the time taken for networks to fully engage. The trials were grouped into mini-blocks of three trials of the same condition, with the aim of inducing maximal engagement of the scene and face networks. These mini-blocks were then presented within blocks in a pseudo-random order, such that each mini-block was different from the previous one. An illustration of the mini-block design is shown in Figure 5.

In the oddity task, the first trial of each mini-block was preceded by a 5 s fixation period of a black screen with a white cross at the centre. The second and third trial of each mini-block were preceded by an inter-trial fixation period for a time that randomly varied between 1 s and 1.5 s. Participants were shown trials for up to 6 s (pilots 1 and 2) or 8 s (pilots 3-6) but each trial ended as soon as a response was made.

To make the behavioural laboratory setting similar to the MEG laboratory setting, participants were asked to sit with their head 1m from the screen and to keep as still as possible during the experiment blocks.

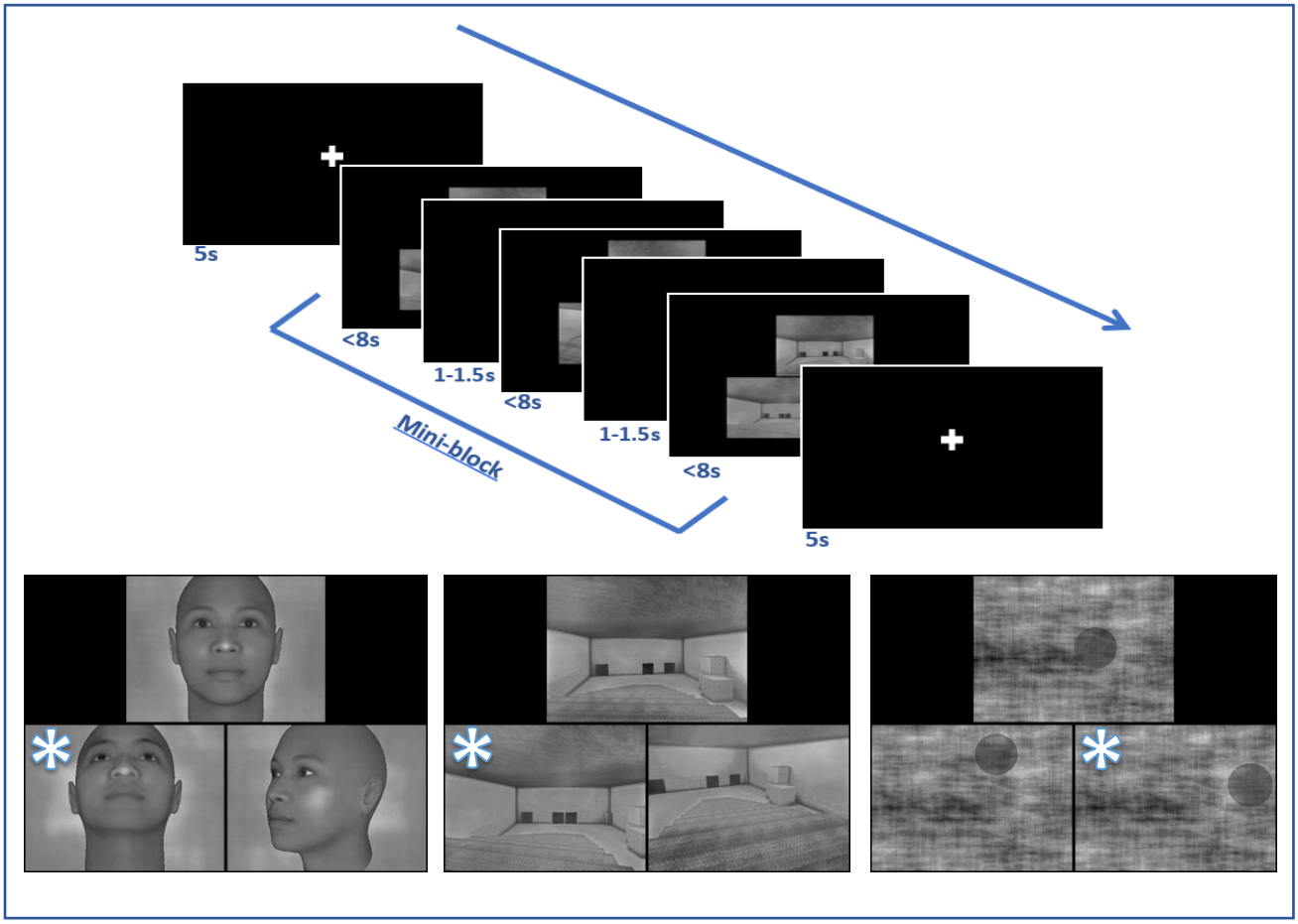

Figure 5. Layout of the oddity task.

The upper image illustrates a mini-block comprising 3 scene, face or size stimuli, separated by short (1 - 1.5s) inter-trial fixation periods, preceded and followed by 5 s fixation periods. The trials could be displayed up to 6 or 8s in total (depending on pilot number) but ended as soon as the participant made a response. The 3 lower images are examples of the final (pilot 6) oddity stimuli. The asterisk indicates the odd-one-out.

3.2.2.2 Stimulus design

Scene stimuli were made using a commercially available computer game, Deus Ex (Ion Storm, 2000) and the majority had been previously made by Lee et al. (2013). Screenshots were taken from the virtual character's perspective from different angles within the scene, by placing the character in different positions in the room.

Face stimuli were made using Facegen (Singular Inversions, 1998). After applying the default settings for face type (race, age, symmetry) and setting the sex rating equidistant between male and female, the 'generate random face' function was used. It was important that facial characteristics pertaining to race and gender did not vary greatly because they can influence individual differences in recognition of faces (Mukudi & Hills, 2019). In light of this some faces needed additional editing to remove shading emulating facial hair, as this

made faces look male. The odd-one-out was constructed by using the 'genetics' tab and applying a variation of 0.4.

All faces within a trial were presented from three different viewpoints from four possibilities, 'right' (45^{o} right), 'left-up' (45^{o} left and 20^{o} up), 'up' (20^{o} up) and ‘straight-on’ (0^{o}). Viewing angle and location oddity were counterbalanced across trials.

To reduce differences in image statistics between the task and control conditions, the size images were constructed using 24 phase-scrambled scene images and 24 phase-scrambled face images, equally taken from each stimulus group (described below in 3.2.3). Phase-scrambling was performed using a technique (Perry, 2016) which allows the user to determine the level of phase scrambling by using the ‘weighted mean phase’ method (Dakin et al., 2002). This adds noise to spatial phases of images according to ‘w’, a weighting factor, in the range of 0 - 1. The weighting factor determines the proportion of unaltered spatial phase kept in the scrambled image. A ‘w’ of 0.16 was used because this has been shown to produce a subthreshold detection rate (Perry, 2016). To reflect the similarity in spatial phase between three similar scenes and faces portrayed at different angles, each scrambled image was used 3 times in each size triplet.

Using the python package ‘PIL’ (Umesh, 2012), translucent homogenous black circles were placed over the scrambled images. Circles were rendered inside square areas randomly sized between 60x60 pixels to 90x90 pixels. These square areas were randomly placed within a larger area covering 305x205 pixels. Three circle images were made for each triplet (each with the same scrambled background), two with the same size dimensions and one with a different sized square. The changes in size in pixels of the pilots are as follows: pilot 1 = 5, 7, 9, 11; pilot 2 = 6; pilot 3 = 5, 6; and pilots 4 to 6 = 4. For example, in pilot 6, if two square areas were size 60x60, the third would be 64x64.

Images for all three conditions, face, scene and size, were converted to greyscale, cropped to a size of 400x300 pixels and ordered into a triplet pattern on a black background.

3.2.2.3 Matching image statistics with the SHINE toolbox.

Triplet[3] greyscale images were altered using SHINE (Willenbockel et al., 2010). Luminance was normalized across images using the 'lumMatch' function and the luminance histograms were matched using the 'histMatch' function. The SHINE toolbox provides two ways of equating Fourier amplitudes across stimuli, 'spec Match' and 'sfMatch'. The latter is more lenient as it preserves the amplitude distribution across orientations but ensures that the rotational average amplitudes for given spatial frequencies are equated across images. sfMatch was used here because the tasks in this experiment require the participant to judge differences between similar images and, therefore, image quality is important.

SHINE incorporates a method by Avanaki (2009) which can improve the quality of the histogram-matched images through optimising the Structural Similarity Index Measure (SSIM) (Wang et al., 2004) over a series of steps. SSIM is a measure of the similarity between the original and output images and is used as a proxy for quality: measured 0-1, where 1 would imply identical images. For each iteration, an image with a target histogram is produced, the SSIM index and gradient are then calculated and the gradient is used to improve the SSIM of the output image. For the stimuli of the final pilot, the SSIM index was 0.88.

Histogram and Fourier amplitude specifications can affect each other so SHINE facilitates an iterative approach where the targets are recalculated in each repetition. 15 iterations were used.

To visualize the effects of SHINE, images of the Fourier spectrum and frequency spectrum were made using the inbuilt MATLAB Fourier Transform function (MATLAB, 2015) and the luminance histograms were made using the 'imstats' function in SHINE. Figure 6 shows the averaged image properties from each condition before and after undergoing SHINE alterations.

[3] Note that in pilots 1-4, SHINE editing occurred before triplet images were stitched together, causing unequal noise to be added to each image, which was thought to be making the task more difficult. In pilots 5 and 6, SHINE editing occurred after the triplet images were stitched together.

Before SHINE	Averaged Fourier Spectrum	Averaged Frequency Spectrum	Averaged Luminance Histogram	Example Image
Scene Stimuli	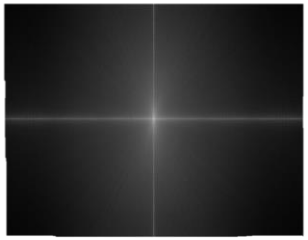	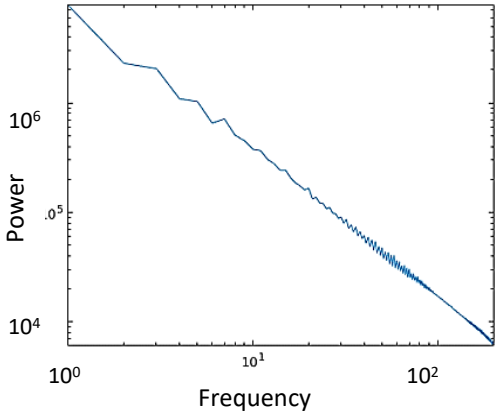	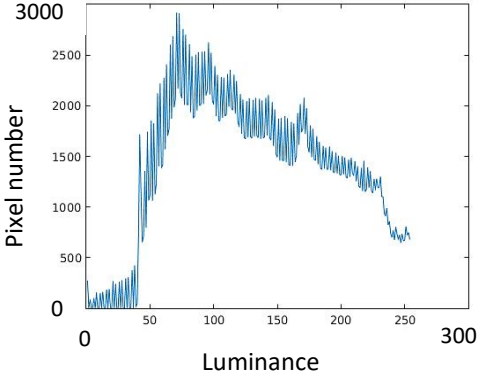	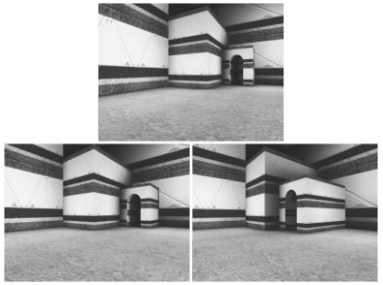
Face Stimuli	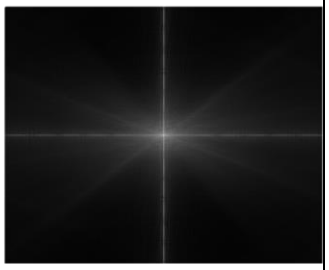	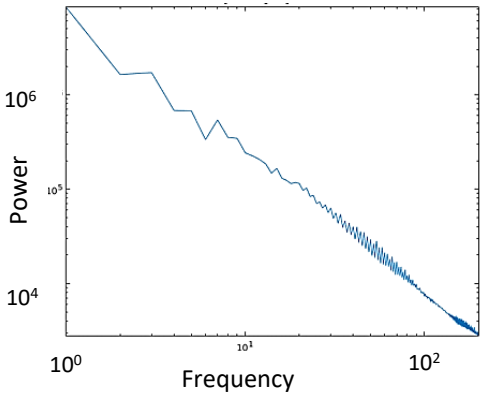	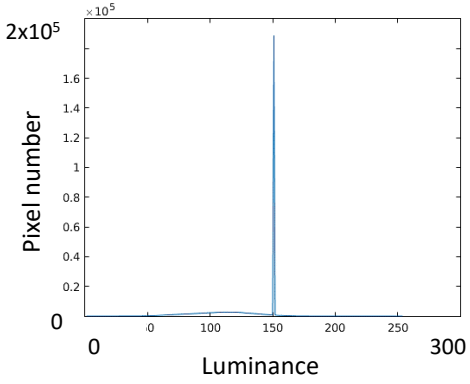	

Size Stimuli	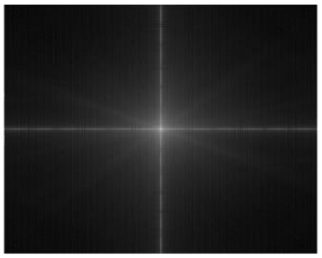	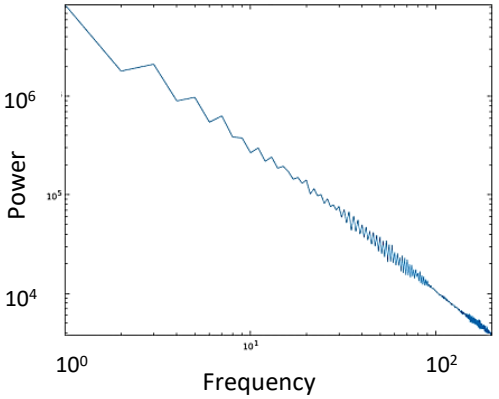	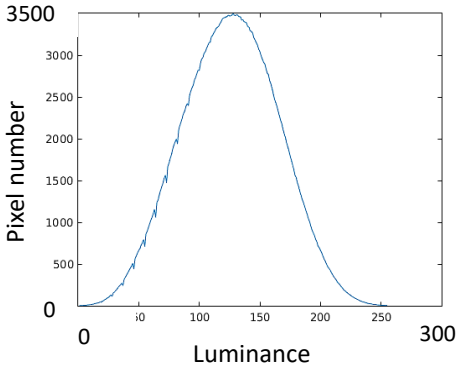	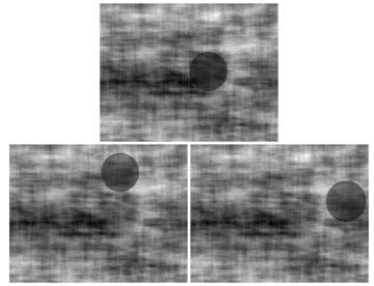

After SHINE	Averaged Fourier Spectrum	Averaged Frequency Spectrum	Averaged Luminance Histogram	Example Image
Scene Stimuli	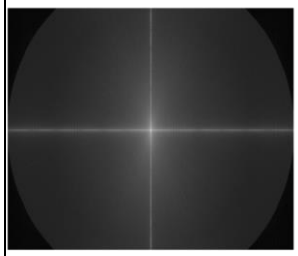	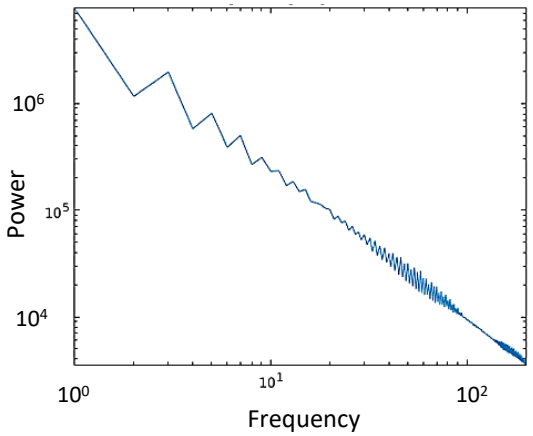	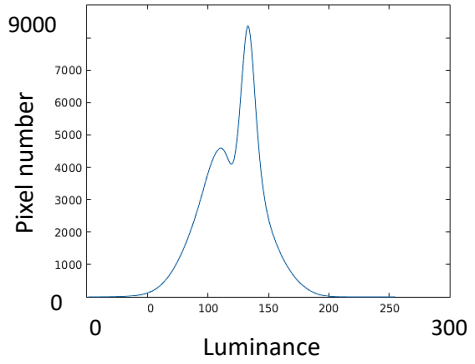	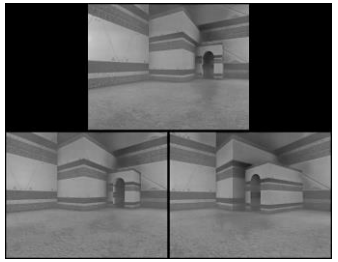
Face Stimuli	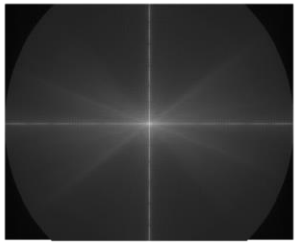	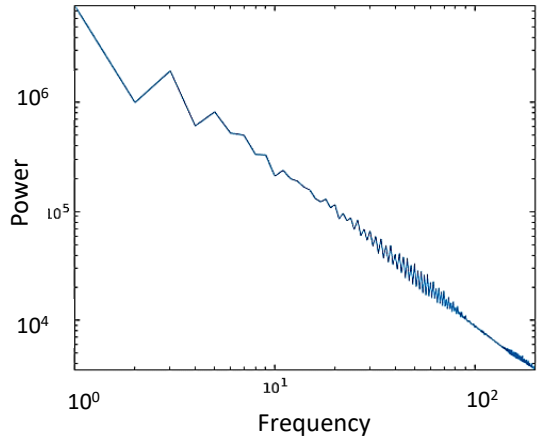	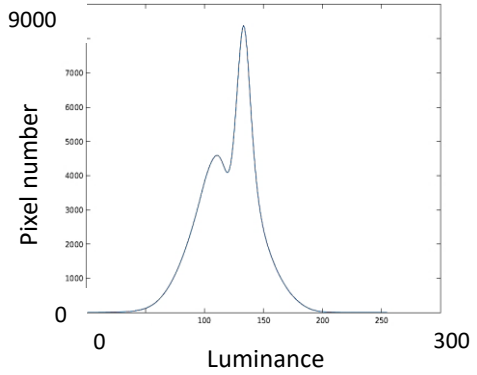	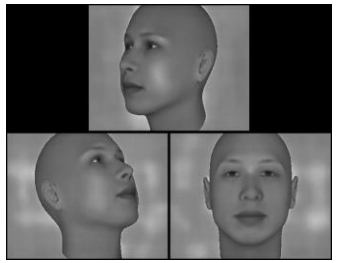

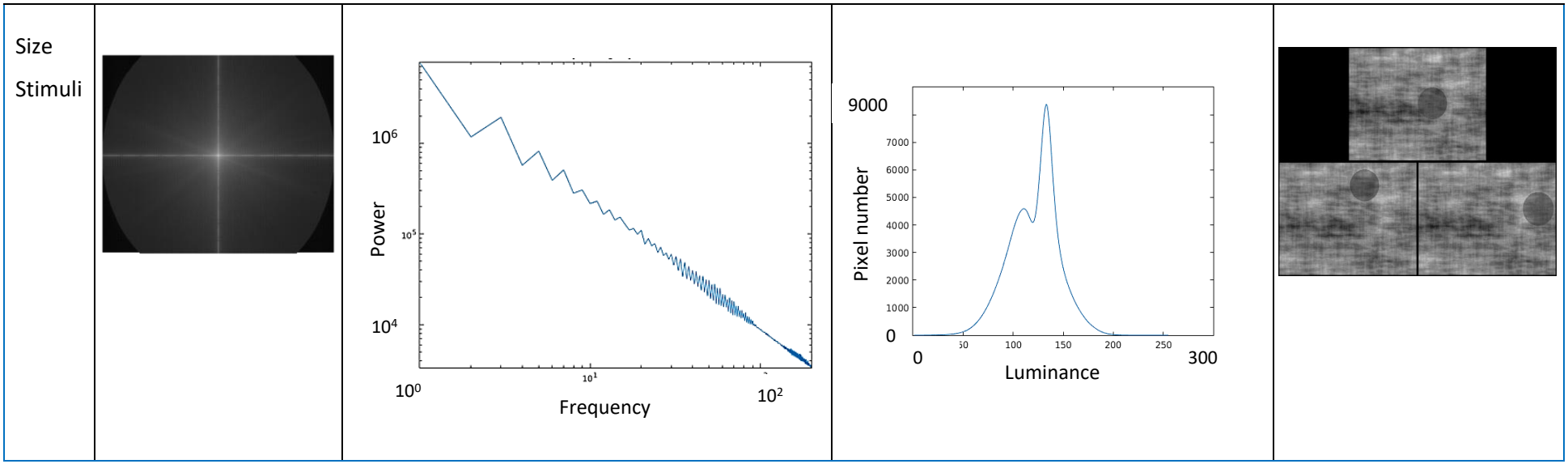

Figure 6. The averaged image properties from each condition before and after undergoing SHINE alterations.

Average image statistics for each condition are shown, before and after SHINE. The stimuli after SHINE application in pilot 6 were used for the subsequent experiments in this thesis. From left to right the boxes display: the Fourier spectra in polar plots; the power per frequency (averaged across orientations) in log plots; luminance histograms and example images.

3.2.3 The memory task.

3.2.3.1 Layout and timing of presentation of the stimuli.

The memory task included the remaining 48 scene and 48 face trials not used in the oddity task, plus 48 of the previously used scene trials and 48 of the previously used face trials (192 trials in total). To be consistent with the methods of Lee et al. (2013), the trials were presented in the same layout as those of the oddity task (triplet images). To ensure a balanced split between scenes and faces used for the oddity and memory tasks, the stimuli were split into 3 groups of 48: A, B, C. The participants were also split into three groups with each group receiving different combinations of stimulus groups for the oddity and memory tasks. For example, if scene stimuli groups A and B were used in the oddity task, then the memory task would use scene stimulus group C as 'novel' trials and 48 randomly chosen trials from scene stimuli groups A and B as 'old' trials.

Participants responded using a keyboard with their right hand. Four keys represented four answers: 'definitely old', 'I think it's old', 'I think it's new' and 'definitely new'. The reason for this integrated response in the memory task (combining old/new discrimination with confident/unconfident) was to allow for further detail on the memorability of the stimuli, without lengthening the duration of the experiment with an additional question.

As in the oddity task, memory trials were grouped into mini-blocks of three trials of the same condition which were then displayed in a pseudorandomized order. Decision making in the memory task was predicted to be faster than that of the oddity task, so trials lasted only for up to 3.5 s and mini-blocks were separated by 2 s fixation periods. Previous studies using delayed recognition tests of scenes and faces have reported RTs shorter than 3.5 s (Blondin & Lepage, 2008; Burns et al., 2014), so this was expected to give enough time for a recognition decision. Similar to the oddity task, the inter-trial fixation period also randomly varied between 1 s and 1.5 s. An illustration of the memory task is shown in Figure 7.

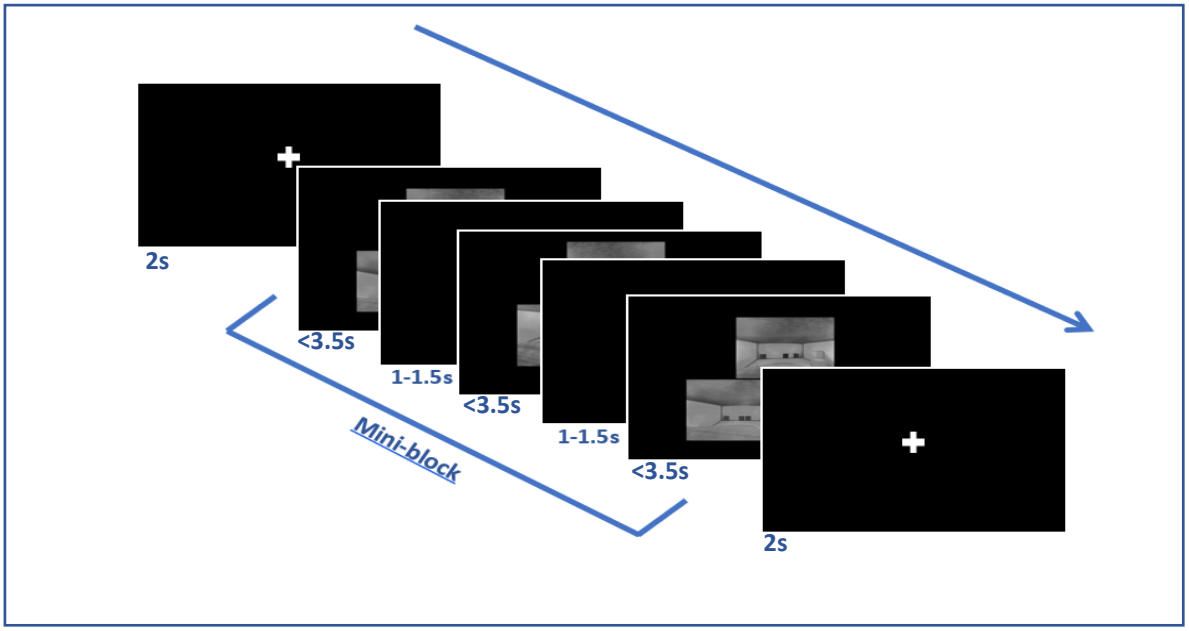

Figure 7. The layout of the unexpected memory task.

Illustration of a mini-block comprising 3 scene or face stimuli, separated by short (1 - 1.5s) inter-trial fixation periods, preceded and followed by 2 s fixation periods. The trials could be displayed up to 3.5 s in total but ended as soon as the participant made a response. Participants were asked to indicate whether they had previously seen the triplet image within the oddity task blocks, or whether it was new, and to indicate their confidence. Using four keys, participants could respond: 'definitely old'; 'I think it's old'; 'I think it's new'; and 'definitely new'.

3.2.4 Statistical analyses.

Statistical analyses were carried out using RStudio (R Core Team, 2018; RStudio Team, 2015) and JASP (JASP Team, 2019). Bayesian RM ANOVA was used to assess the evidence that the stimuli groups were equally difficult in the oddity task. When comparing the oddity task accuracies to chance level (using frequentist statistics), an alpha level of 0.016 (0.05/3) was applied to correct for the three conditions. For the memory task, an alpha level of 0.025 (0.05/2) was applied when comparing memory scores to chance level. A traditional alpha level of 0.05 was used for all other tests, to maximise sensitivity.

3.3 Results

3.3.1 Oddity task results.

The aims were: to have accuracy scores significantly above chance level (33%), which was achieved in Pilot 1; to have equal means and spreads of accuracy scores in the scene, face and size conditions, which were achieved by Pilot 4; and to have mean accuracies of around

60%, which was achieved by Pilot 6. The accuracies and Reaction Times (RTs) across the pilot studies are shown in Figures 8 and 9.

3.3.1.1 Accuracy in Pilots 1-6.

Equal accuracy scores across the conditions were achieved by pilot 6. Table 2 gives a summary of the accuracy results, as means and standard deviations (SD), for each pilot.

<table>
<tr><th>Pilot</th><th>Stimulus details</th><th>Results</th><th>Comments</th></tr>
<tr><td>1</td><td>Edited scene stimuli from Lee et al. (2013).</td><td>Aiming for accuracy means at 50%.
It was possible to complete the task above chance level, but accuracy means across conditions were not equal.

<table><tr><th>ACCURACY (%)</th><th>SCENE</th><th>FACE</th><th>SIZE</th></tr><tr><td>MEAN</td><td>45.03</td><td>48.48</td><td>61.54</td></tr><tr><td>SD</td><td>7.40</td><td>5.59</td><td>17.89</td></tr></table>
Chance level 33% exceeded (p<0.01).
Bayesian RM ANOVA results provided evidence that accuracy means were different (BF_{10} = 200.354).</td><td>The stimuli needed altering to get equal accuracy means and spreads across conditions.
Accuracy scores of individual circle size changes inspected. 5 was too low (40%) and 7 was too high (59%), so size change 6 was used in the next pilot.</td></tr>
<tr><td>2</td><td>Scene and face stimuli unchanged, circle size change of 6 used.</td><td><table><tr><th>ACCURACY (%)</th><th>SCENE</th><th>FACE</th><th>SIZE</th></tr><tr><td>MEAN</td><td>48.38</td><td>50.35</td><td>62.15</td></tr><tr><td>SD</td><td>5.314</td><td>6.400</td><td>15.256</td></tr></table>
Chance level 33% exceeded (p<0.01).
Bayesian RM ANOVA results provided evidence that accuracy means were different (BF_{10} = 11.760).</td><td>Aimed to increase performance means and spreads with increased trial times.</td></tr>
<tr><td>3</td><td>Scene and face stimuli unchanged, circle size change of 5 and 6 used.</td><td><table><tr><th>ACCURACY (%)</th><th>SCENE</th><th>FACE</th><th>SIZE</th></tr><tr><td>MEAN</td><td>51.04</td><td>48.89</td><td>60.21</td></tr></table></td><td>Circle size change needed to be reduced to increase difficulty.</td></tr>
</table>

<table>
<tr><td></td><td>Trial times extended from 6s to 8s.</td><td><table><tr><td>SD</td><td>6.09</td><td>7.00</td><td>11.65</td></tr></table>
Chance level 33% exceeded (p<0.01).
Bayesian RM ANOVA results provided evidence that accuracy means were different (BF_{10} = 36.502).</td><td></td></tr>
<tr><td>4</td><td>Scene and face stimuli unchanged, circle size change of 4 used.</td><td>Aiming for accuracy means at 60%.<table><tr><th>ACCURACY (%)</th><th>SCENE</th><th>FACE</th><th>SIZE</th></tr><tr><td>MEAN</td><td>48.85</td><td>51.04</td><td>48.85</td></tr><tr><td>SD</td><td>7.97</td><td>4.66</td><td>11.48</td></tr></table>Chance level 33% exceeded (p<0.01).
Bayesian RM ANOVA results provided evidence that accuracy means were not different (BF_{10} = 0.272).</td><td>Aimed to increase accuracy scores to 60% and increase spread for scenes and faces.
Additionally, performance of individual scene trials was inspected to see if some scene trials were consistently answered incorrectly. Those answered correctly by less than 40% of participants were removed and replaced with new scene stimuli.</td></tr>
<tr><td>5</td><td>SHINE processing moved to after triplet image stitching. New scene stimuli replaced difficult scene trials.</td><td>Face and size accuracy increased but not scene accuracy<table><tr><th>ACCURACY (%)</th><th>SCENE</th><th>FACE</th><th>SIZE</th></tr><tr><td>MEAN</td><td>51.74</td><td>60.30</td><td>60.30</td></tr><tr><td>SD</td><td>8.64</td><td>12.69</td><td>13.90</td></tr></table>Chance level 33% exceeded (p<0.01).
Bayesian RM ANOVA results provided weak evidence that accuracy means were different (BF_{10} = 1.334).</td><td>Performance of individual scene trials over pilots 4 and 5 were inspected to assess accuracy levels of new scene stimuli.
Additional new scene stimuli were added to pilot 6.</td></tr>
<tr><td>6</td><td>New scene stimuli replaced difficult scene trials.</td><td>Scene accuracy score raised and spread increased.<table><tr><th>ACCURACY (%)</th><th>SCENE</th><th>FACE</th><th>SIZE</th></tr><tr><td>MEAN</td><td>58.56</td><td>55.44</td><td>63.77</td></tr></table></td><td>Accuracy and spread between groups matched more closely.</td></tr>
</table>

		SD	15.25	8.80	14.53	
		Chance level 33% exceeded ($p<0.01$). Bayesian RM ANOVA results provided weak evidence that accuracy means were equal ($BF_{10} = 0.527$).				

Table 2. Summary of accuracy results of oddity pilots 1-6.

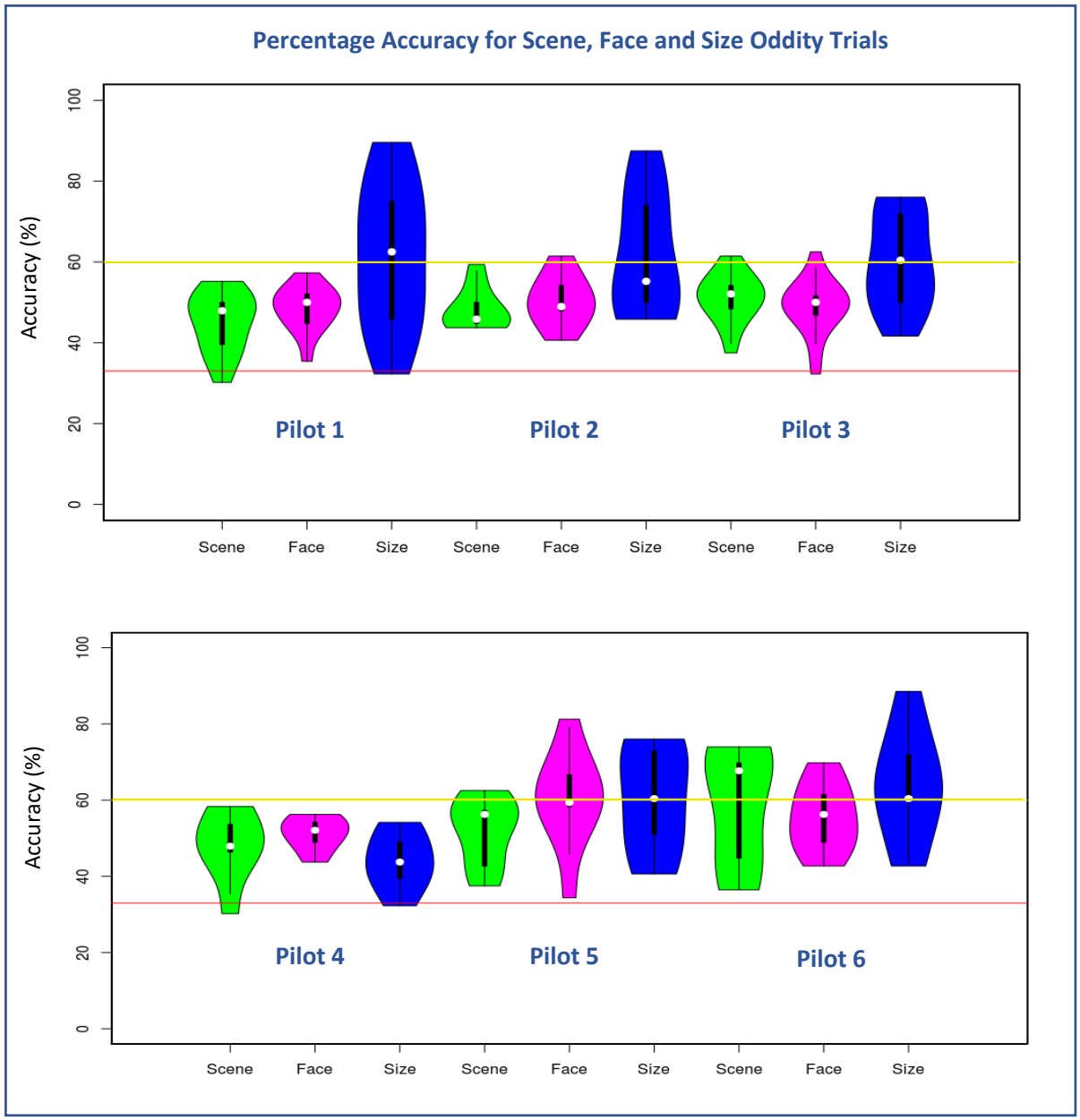

Figure 8. Violin plots showing condition accuracies for pilots 1-6.

The scene data are green, the face data are pink, and the size data are blue. The horizontal red line indicates the chance level at 33%. As a visual aid, horizontal yellow line indicates 60%. The white dots indicate the median, the thick vertical black lines indicate the interquartile ranges and the thin vertical black lines indicate the 1.5 x interquartile ranges.

By pilot 6, distribution and means of the accuracy scores are well matched between conditions.

3.3.1.2 RTs in Pilots 1-6.

The RTs across the conditions could not be matched and there were consistent relationships between the groups: scene RT > face RT > size RT. RTs in pilot 6 for scene, face and size trials (mean (SD)) were 4713 (1079), 3691 (1230), 2664 (946) ms respectively. However, the majority of trials exceeded the aim of 1.5 second minimum length and the spread across conditions was reasonably matched in pilot 6.

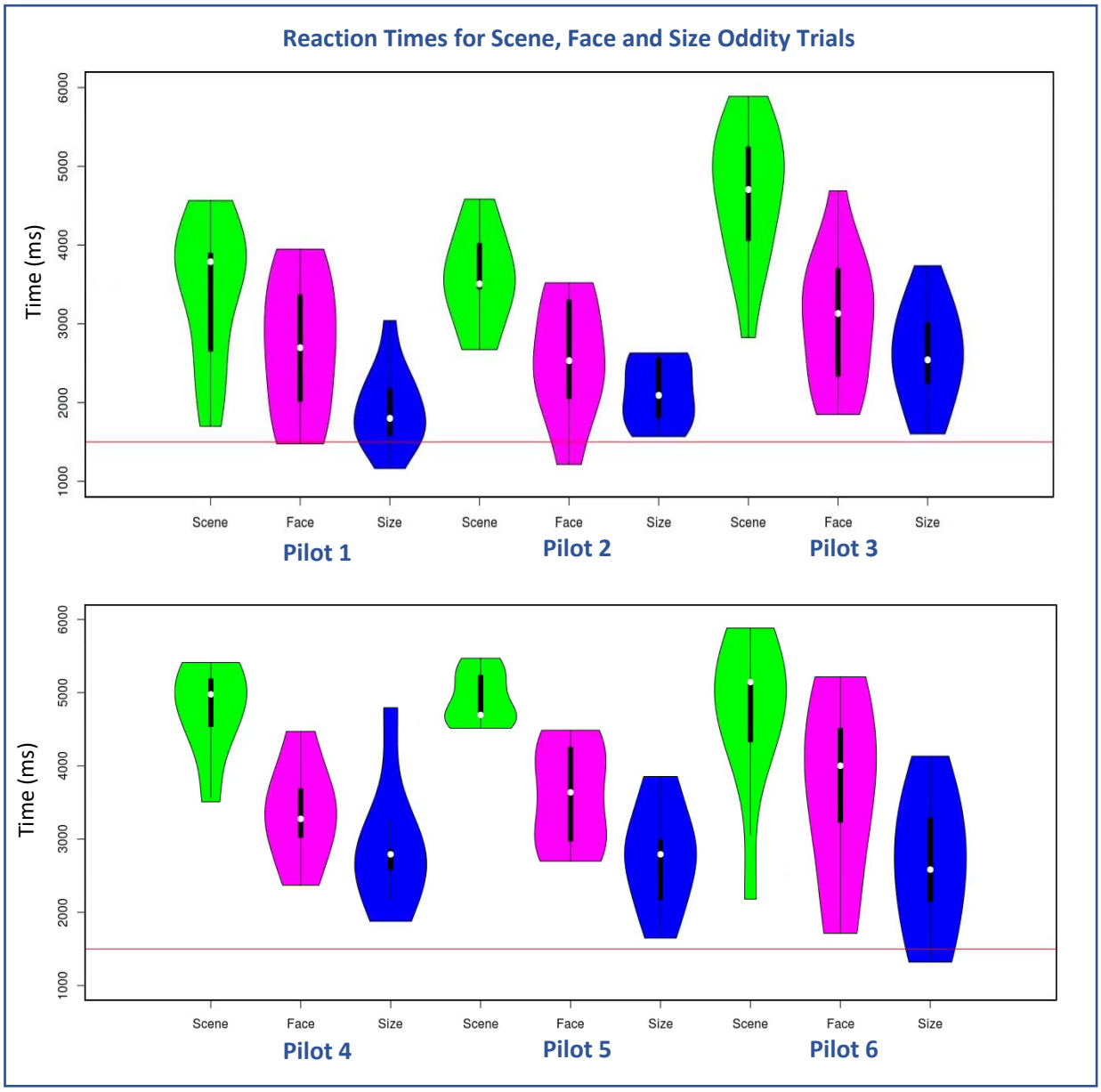

Figure 9. Violin plots showing condition RTs for pilots 1-6.

The scene data are green, the face data are pink, and the size data are blue. The horizontal red line indicates the target minimum trial length of 1.5s. The white dots indicate the median, the thick vertical black lines indicate the interquartile ranges and the thin vertical black lines indicate the 1.5 x interquartile ranges.

3.3.2 Memory task results.

3.3.2.1 Pilot 1 memory task results.

Overall, memory performance was poor. The mean of scene hit rates was 0.50 (SD = 0.143), with a mean false alarm rate of 0.36 (SD = 0.083). The mean of face hit rates was 0.54 (SD = 0.119), with a false alarm rate of 0.44 (SD = 0.129). To compare memory performance across conditions, d-prime (d') scores (z(P(hits) – z(P(false alarms)) were calculated for scenes and faces. The mean d' scores for scenes and faces were 0.57 and 0.29, respectively, and were both above the chance level of 0 ($t_{(12)}$ = 3.873, p = 0.002; $t_{(12)}$ = 3.653, p = 0.003). A paired t-test, testing the difference in d' scores between conditions, was significant ($t_{(12)}$ = 2.39, p = 0.034).

The mean proportion of hits answered with high confidence ('It's definitely old') (as opposed to low confidence ('I think it's old')) for the scenes was 0.56 (SD = 0.333) and for the faces was 0.39 (SD = 0.304) (fractions of total number of correct remembered responses). There was no significant difference between these values ($t_{(12)}$ = 1.35, p = 0.19).

For both scene and face trials, there was no significant difference between the number of oddity-correct and subsequently remembered stimuli and oddity-incorrect and subsequently remembered stimuli ($t_{(12)}$ = 1.56, p = 0.15; $t_{(12)}$ = -0.51, p = 0.62, respectively for scenes and faces).

3.3.2.2 Pilot 5 memory task results.

The mean of scene hit rates was 0.61 (SD = 0.140), with a mean false alarm rate of 0.41 (SD = 0.131). The mean of face hit rates was 0.58 (SD = 0.165), with a false alarm rate of 0.45 (SD = 0.144). The mean d' scores for scenes and faces were 0.62 and 0.34, respectively, and were both above the chance level of 0 ($t_{(8)}$ = 3.513, p = 0.004; $t_{(8)}$ = 2.178, p = 0.050). A paired t-test, testing the difference in d' scores between conditions, just surpassed traditional alpha threshold ($t_{(8)}$ = 2.21, p = 0.054).

The mean proportion of hits answered with high confidence ('It's definitely old') (as opposed to low confidence ('I think it's old')) for the scenes was 0.65 (SD = 0.158) and for the faces was 0.32 (SD = 0.220) (fractions of total number of correct remembered responses). There was a significant difference between these values ($t_{(8)}$ = 4.23, p = 0.003).

For both scene and face trials, there was no significant difference between the number of correctly answered and subsequently remembered stimuli and incorrectly answered and subsequently remembered stimuli ($t_{(8)} = -0.89$, $p = 0.34$; $t_{(8)} = -0.18$, $p = 0.86$, respectively).

3.4 Discussion

The pilot behavioural studies allowed the stimuli, their layout and presentation sequences to be adapted for an oddity study in the MEG environment. One consideration is that trials had to be long enough for multiple delta/theta cycles to occur during decision time and therefore the trials had to be made difficult enough so that RTs would be longer than 1.5 s. The scene stimuli of Lee et al. (2015) were chosen because of their difficulty, and face and size stimuli were developed to match the scene accuracy levels. A second challenge was to minimise the differences in image properties across the stimuli conditions, which involved redesigning the control size task and matching the images with the SHINE toolbox. In sum, aims of the piloting included: producing matched accuracy scores across image-statistics-matched conditions, accuracy scores averaging at around 60%, and to design an unforeseen memory test appropriate to examine incidental encoding of stimuli. The first two were achieved by Pilot 6 and the last was achieved by Pilot 1 but re-tested in Pilot 5 due to the stimuli and paradigm changes.

Although oddity accuracy matched between groups, RT did not. Altering the stimuli with the aim of matching RTs would likely alter accuracy scores and it may be that the brain processes involved in making perceptual decisions on scene, face and circle images take different lengths of time. Supporting this, an early MEG study compared the time course of predominant evoked MEG signals in response to viewing scenes and faces (Sato et al., 1999) and found that scene-related signals were localised to the right parietooccipital junction and parahippocampal gyrus and had a latency of around 300ms, whereas face-related signals were localised to the FG and had a latency of around 160ms. More recent studies examining scene-viewing related electrophysiological signals have also reported timescales longer than those reported in more recent studies examining face-viewing (Gao et al., 2013; Halgren et al., 2000; Mormann et al., 2017; Vlcek et al., 2020). Moreover, the hypothesis tested in this thesis is that scenes and faces require different processing and that two brain networks possess the respective processing qualities required. It is conceivable that these networks may function at different speeds.

The d’ results of the memory task indicated that the stimuli were memorable above chance level and that the scene stimuli were more memorable than face stimuli. However, the d’ scores also indicated that memory for both was poor. This may be due to the number of trials shown in the oddity and the length of the sessions. There were 96 scenes and faces shown in the oddity task which could last up to 50 minutes. Furthermore, participants were

not told about a subsequent memory task because active encoding of the stimuli was not an aim of the task. Interestingly, the memory results of Lee et al. (2013), who also used large numbers of stimuli and an unforeseen subsequent memory test, also showed poor recollection of scene oddity trials (d' = 0.562). These results may indicate a success in oddity paradigm design, as the aim is to incite online perceptual processes and not incidental encoding processes. Importantly, there was no difference between the number of remembered correct scenes or faces (answered correctly during the oddity task) and the number of remembered incorrect scenes or faces (answered incorrectly during the oddity task), in either Pilots 1 or 5, suggesting that recognition memory performance was not modulated by successful completion of this complex perceptual task.

The higher memorability of scene stimuli than face stimuli may mean that scene and face stimuli have differing effects on memory processes. The difference in memorability was also echoed in the proportion of confidently remembered scenes and faces. In pilot 5, the proportion of scene hits answered with high confidence was higher than that of faces. The objects within scenes vary more than features on faces. This pattern may be due to the higher similarity between images in the face condition. However, this finding may not undermine the use of the oddity task to measure complex perception. Since scene oddity accuracy was lower than that of faces in pilots 1 and 5, it is unlikely that previous studies' findings that scene oddity and face oddity completion incite neuronal activity in different brain areas (Hodgetts et al., 2015; Lee et al., 2008) are reflections of the differing propensities of the stimuli to incite beneficial incidental encoding processes. On the other hand, it could be that the more a trial incites memory processes, the poorer the perceptual performance. Considering this, the relationship between hippocampal BOLD and scene oddity performance found by Hodgetts et al. (2015) may be mediated by the amount of memory processes during the task, and the hippocampal activity may reflect memory encoding rather than reflect the involvement of the hippocampus in scene perception. Therefore, it is important that in any research where a correlation between a neuroimaging measure and scene/face oddity performance is demonstrated, the relationship between the same neuroimaging measure and subsequent scene/face memory performance must also be tested (see *Chapter 5* section 5.3.5).

The level at which to match image statistics between the conditions was a compromise. It was important that the conditions were as visually similar as possible because a challenge with recording deep brain signals in MEG is the spread of stronger visual signals from visual areas, which can pervade into the deep brain signal recordings (Quraan et al., 2011).

However, complete matching would result in identical images and all levels below this cause graded improvements on the image quality. It was important to match the condition images as closely as possible without degrading image quality to the extent that the task was too difficult to complete. Therefore, applying SHINE, the rotational average amplitudes for the spatial frequencies were matched across images while the amplitude distributions across the orientations were unchanged as this helps to preserve image quality (Willenbockel et al., 2010).

As the aim was to use this study design in conjunction with MEG, it is important to note similarities and differences between the behavioural laboratory and MEG laboratory settings. To make these similar, participants were asked to sit with their head at a fixed distance from the monitor and keep as still as possible during the experimental blocks. However, MEG sessions differ from behavioural-only sessions in several ways: the timing, due to set-up time before MEG recording; the environment, for example participants must wear reference electrodes and sit in a shielded room; and comfort and freedom of movement, as participants' movement is physically restricted when in the MEG system. For these reasons, it was noted that the accuracy scores could decrease in the MEG setting. It was hoped that the final average oddity accuracy score of 60% would provide a large enough safety net so that accuracy levels could drop without reaching chance level.

In conclusion, the oddity task was adapted to be suitable for a MEG study and to allow further investigation into the timing and nature of processes underlying complex online scene and face processing. The target results were decided before the pilot studies began and included target accuracy scores that matched between conditions. The stimuli and their timing and layout in Pilot 6 were used in the subsequent MEG and microstructure study.

Chapter 4: Examining oscillatory power modulation within PMN areas during complex scene perception, using MEG.

4.1 Introduction

4.1.1 Background.

Implications of the PM-view include: the PMN and AIN networks should aid behaviours in different modalities; network areas, including MTL areas, should be involved in processes across memory and perception; and that the behavioural performance of those modalities should be related to the structural and functional properties of the respective networks (Graham et al., 2010; Murray et al., 2017). This chapter continues the investigation of the first two implications by measuring brain oscillatory behaviour during completion of the oddity task, using MEG.

Oddity tasks can be used to incite complex perceptual processes. The task requires the participants to pick the odd-one-out from multiple images of scenes or faces, each presented at a different view angle. It is understood that successful completion of the task requires the construction of a view-invariant internal model of a scene or face (Barense et al., 2010). Previous fMRI work has shown BOLD increases in the hippocampus and PrC during the completion of scene and face visual oddity tasks, respectively (Barense et al., 2010; Hodgetts, Voets, et al., 2017), and increased hippocampal BOLD during correct versus incorrect scene oddity trials (Lee et al., 2013). These studies indicate the importance of these MTL areas in complex visual processing in two modalities. Moreover, Hodgetts et al. (2015) found an increase in PrC BOLD during the face task that selectively correlated with face task performance, and not with performances in the scene task or a size judgment control task. In contrast, hippocampal BOLD decrease during the scene task selectively correlated with scene task performance and not with face or size task performance. Together, since the PrC and hippocampus are thought to be members of the AIN and the PMN, respectively, the results support the proposal that the AIN and PMN cater for different modalities, but they leave some unanswered questions. The discrepancy in relationship between the scene task and hippocampal BOLD increase or decrease is difficult to interpret due to the complex relationship between neuronal activity and the BOLD response (Ekstrom, 2010; Ekstrom et al., 2009). Moreover, the BOLD signal is slow compared with the underlying neuronal activity, and so the result provides little detail of

the temporal dynamics of hippocampal processes during perceptual decisions. Indeed, the results of Hodgetts et al. (2015) were created from averaging BOLD in 6 s trials. In addition, Hodgetts et al. (2015) like previous work (Barense et al., 2010; Lee et al., 2013), focused on activity in single areas of the networks. Further investigation of the PM-view requires assessment of functional modulation across networks.

The current study aimed to expand on previous work using fMRI and the oddity task by measuring oscillatory power modulation, PAC and phase-coherence across multiple network areas in the first 2 s of oddity task completion, using MEG. There was a particular focus on the oscillatory power modulations of PMN areas, during the scene oddity condition, and this was contrasted with oscillatory power modulations of AIN areas during the face oddity condition. Assessment of area-to-area communication was also used to study how the HPC and other PMN structures interact during complex scene perception.

A whole-brain assessment of time-averaged oscillatory power was carried out, to assess the differential involvement of brain regions in complex scene and face processing. Virtual Sensors (VSs) of six PMN regions were then extracted: right and left HPC (comprising the hippocampus and parahippocampal areas); right and left IPL (including the supramarginal gyrus and the angular gyrus); PCC; and mPFC. Time-frequency analysis was carried out on each. PAC within right and left HPC and mPFC VS data, and theta/alpha phase-coherence modulations between all VSs, were then measured.

4.1.1.1 Electrophysiological correlates of activity in the PMN and AIN.

MTL oscillatory activity had not previously been explored during complex visual perceptual processes but previous human memory research examining the MTL, or perceptual work examining other ROIs, points towards the importance of oscillations in the gamma (40-80Hz) and theta (4-8Hz) ranges (Colgin & Moser, 2010; Fell et al., 2011; Monk et al., 2020; Pu et al., 2017; Pu, Cornwell, et al., 2018; Sweeney-Reed et al., 2016).

The hippocampus is well known for activity in the theta range due to the wealth of literature associating hippocampal theta with place-cell firing in locomotion in rodents (Sosa et al., 2018), and episodic and navigational processes in humans (Lin et al., 2017; Pu et al., 2017). The hippocampus is understood to be a major current generator (contributor to magnitude of power) of the hippocampal and limbic theta rhythm (Kocsis et al., 1999). Theta rhythms could allow grouping and separation of information and processes in an extended hippocampal network (Buzsaki, 2002) and this ability to sequence and separate

may underly both memory and navigation processes (Eichenbaum, 2017b). It is thought that the underlying processes for navigating physical and mental spaces may be the same (Buzsaki & Moser, 2013) and, therefore, theta rhythms may also be important during complex scene perception, which requires the construction of view-invariant internal representations. Indeed, the reduction in hippocampal BOLD during scene task completion, compared with a size judgment control task, reported in Hodgetts et al. (2015) may correspond to underlying increase in hippocampal theta. BOLD decreases have been reported to relate to increases in low frequency power (Fellner et al., 2016; Scheeringa et al., 2011) and, in particular, to MTL theta power increases during mnemonic encoding (Fellner et al., 2016).

However, previous research that used a similar oddity task found hippocampal voxels that displayed increased BOLD during viewing of scene oddity trials involving images of scenes displayed at differing angles (requiring internal representation construction) in contrast to scene oddity trials involving images of scenes displayed at consistent angles (Barense et al., 2010). Additionally, two studies using a mental scene construction task reported a decrease in anterior hippocampal theta (Monk et al., 2020) and an increase in anterior hippocampal BOLD (Dalton et al., 2018), when compared with construction of a non-scene mental array. Power decreases in lower frequency bands can coincide with power increases in higher frequency ranges, such as gamma (Mukamel et al., 2005; Scheeringa et al., 2011). This pattern has been related to increased BOLD (Conner et al., 2011; Kilner et al., 2005), and therefore implies increased engagement of a brain area. It is likely that different hippocampal processes are reflected in theta and gamma oscillations. For example, a study inspecting virtual navigation in humans found that delta and theta power were lower in novel environments compared with familiar ones, whereas low gamma (defined as 31-50 Hz) power showed an opposite pattern (Park et al., 2014). The discrepancy in BOLD change direction between these findings and those of Hodgetts et al. (2015) may be due to the blurred BOLD representation of multiple processes with different temporal or oscillatory characteristics taking place during the trial. Therefore, in the current study, it was hypothesized that hippocampal theta and gamma would be modulated during completion of the scene oddity task, when compared with face or size judgment oddity conditions. However, due to the discrepant BOLD results, and the lack of previous research into oscillatory correlates of hippocampal perceptual processes, the direction of modulation was unspecified. Moreover, time-frequency analysis was carried out on multiple VSs to study the duration of the oscillatory patterns that were observed.

In conjunction with changes in hippocampal oscillatory activity, it was hypothesized that other areas of the PMN network would specifically engage in the scene oddity task. Theta in the mPFC has been reported to increase during spatial working memory delay (Kaplan et al., 2017) and spatial memory retrieval (Kaplan et al., 2014). Scalp-recorded frontal midline theta is associated with several PMN functions, such as episodic memory encoding and retrieval, and is thought to be largely contributed to by the mPFC, and influenced by other areas of the DMN and the hippocampus (Hsieh & Ranganath, 2014). In addition, the inferior parietal cortex is understood to be important for spatiotemporal integration in visual-spatial working memory (Pisella, 2017), and parietal gamma oscillations have been associated with manipulation of visual and spatial representations in working memory (Morgan et al., 2011). The PCC may also play a role in the PMN processing as inhibitory stimulation of this area during encoding disrupts subsequent recall (Natu et al., 2019), and successful item encoding is associated with decreased low frequency power and increased gamma power (Lega et al., 2017). Considering these findings, theta and gamma oscillations may be a marker of spatiotemporal processing, not only in the hippocampus, but across the PMN.

Increased power in the gamma range in response to object or face processing has been reported in areas across the ventral visual hierarchy including early visual areas (Gao et al., 2013; Magazzini & Singh, 2018; Perry & Singh, 2014), ventral occipitotemporal cortex (Engell & McCarthy, 2010) and fusiform cortex (Gao et al., 2013). Moreover, PrC cells responsive to object repetition show 'phase-pruning' (more concentration of spiking phases around the rhythm peak) in the gamma band, after repeated experience of an object (Ahn et al., 2019), and it is thought that PrC gamma may be a result of a transfer of gamma oscillations from other visual areas carrying object information (Ahn et al., 2019; Collins et al., 2001). It is suggested that unified percepts are brought about by oscillatory synchronisation in the gamma range in distributed networks (Bertrand & Tallon-Baudry, 2000), and that gamma activity facilitates the integration of new visual input into internal perceptual models (Gao et al., 2013). Indeed, previous MEG research has indicated a feed-forward role of gamma activity, passing sensory information up the ventral visual hierarchy (Magazzini & Singh, 2018; Michalareas et al., 2016). Therefore, in this work, ventral visual stream gamma power was predicted to be elevated during the face oddity task, in contrast to scene or size judgment oddity conditions.

In accordance with the increased PrC BOLD during face oddity task completion reported in Hodgetts et al. (2015), it might be expected that power in low frequency oscillations of the

PrC would decrease, while power in high frequency oscillations would increase, during the face oddity task, in contrast to scene or size judgment oddity conditions. However, distinguishing between different sources among MTL structures (such as between the hippocampus and the PrC) is challenging with MEG. This is because of the low SNR of signals originating from deep tissue and, because of their proximity, the influence of head movements (Ruzich et al., 2019). Since successful separation of hippocampal and PrC sources with MEG was unlikely, and hippocampal signals may be more reliably detected (see *Chapter 2*), it was assumed that modulation of MTL oscillations would predominantly reflect hippocampal or parahippocampal processing, rather than PrC processing. Therefore, it was predicted that MTL oscillatory modulation be unique to the scene condition.

For the whole-brain analysis, the theta band chosen was 4-8 Hz, as human hippocampal signals have previously been measured in this range with MEG (Barry et al., 2019). The gamma band chosen was 40-80Hz, but this was analysed in two bands: low (40-60Hz) and high (60-80Hz) gamma. This was to aid specificity about signal ranges important to the current task, given the wide range of frequencies included in the term 'gamma'. Moreover, in the context of novel spatial encoding, higher and lower gamma signals have been shown to have different functions in the hippocampus, with the latter relating to encoding success (Park et al., 2014).

These frequency band definitions vary across studies. In previous studies, and in the present study, the definitions are somewhat arbitrary. However, broadband time-frequency analysis of PMN ROIs (e.g., using 1-90 Hz) help in understanding the spread of frequency modulation. For example, theta band modulations could be accompanied by modulations in delta (1-4 Hz) and alpha (8-13 Hz). If only theta is inspected, it is unclear whether modulation in this band is specific to this band, or represents a general modulation of lower frequencies. Similarly, homologues of rodent theta in humans are often reported to be lower, residing in the delta band (Watrous et al., 2013). There were no specific hypotheses regarding hippocampal oscillatory modulation in the range between alpha and gamma (beta, 15-30 Hz), but this is included so that: broadband modulations can be appropriately captured; and to include high-beta (although not commonly reported, high beta modulation of the hippocampus has been described (França et al., 2014)). In addition, the time-frequency analysis allowed inspection of the temporal dynamics of oscillatory power modulations within the first 2 s, with the aim of illustrating a complete picture of oscillation modulation during the oddity task.

4.1.1.2 Communication within and between brain areas by PAC and phase-coherence in the PMN.

Interactions between oscillations of different frequencies are understood to reflect the coordination of information processing within local groups of neurones. PAC describes a phenomenon whereby the phase of the lower frequency range provides a temporal reference for amplitude modulation in higher frequencies (Bonnefond et al., 2017). Although PAC is thought to occur across the brain (Bonnefond et al., 2017), to assess its role in the PMN, the current study focused on PAC in MTL and mPFC regions, which have been associated with mnemonic functions. For example, PAC between theta and beta/gamma within the human hippocampus has been associated with memory load in a task requiring maintaining multiple items in working memory (Axmacher et al., 2010), and PAC between theta and low gamma within the rat mPFC was more pronounced during correct trials of a Y-maze working memory task than with incorrect trials (Li et al., 2012). A study exploring the association between hippocampal PAC and encoding discovered two sets of neurones, one displaying increased PAC, and the other displaying decreased PAC, during successful encoding (Lega et al., 2016). In the former subset the higher frequency range was predominantly modulated by low theta/delta (2.5-5 Hz), rather than the traditional theta band, and this low frequency also showed an increase in power during successful encoding. In addition, neurones displaying increased PAC (with traditional theta, 4-9 Hz) with successful encoding were found in the frontal cortex (Lega et al., 2016). Considering these results, modulation of PAC within the mPFC and hippocampus may be a hallmark of successful PMN functioning.

Phase-coherence between brain regions may also signify network communication. For example, theta phase-coherence between the hippocampus and mPFC has been shown to increase during retrieval in free recall compared to baseline (Anderson et al., 2010) and to be associated with successful memory integration (Backus et al., 2016) and encoding of spatial position (Zielinski et al., 2019). Kaplan et al. (2014) used MEG to investigate spatial memory retrieval and revealed modulations of phase-coherence and PAC between the hippocampus, the mPFC and the parietal cortex. Increases in mPFC theta power, mPFC-hippocampus theta coherence, and PAC between mPFC theta and parietal cortex gamma, occurred during cued retrieval of spatial representations compared with fixation baseline. More recently, phase-coherence between these regions was investigated in the context of a dynamic mental sequence recall task, in which participants were asked to mentally 'walk' through a learned scene, passing the learned objects sequentially (Kaplan et al., 2017). This

task incited increased theta phase-coupling between the mPFC and posterior MTL/RSC compared to baseline. Together, these results suggest that inter-area phase-coherence is important for PMN processing and may support the maintenance of internal mental representations of scenes, associations, and sequences.

Beneficial phase-coherence may extend outside of the theta range. Work combining fMRI and EEG found that functional binding between the hippocampus and the PFC during recollection related to hippocampal low frequency oscillations, spanning the theta and alpha bands (Herweg et al., 2016). Therefore, the current experiment explored phase-coherence over 4-12 Hz between the HPC and mPFC ROIs (and then exploratorily between in the remaining PMN ROIs).

4.1.1.3 The overlap between the PMN and the DMN.

Understanding the role of the mPFC and PCC in complex scene processing is of particular interest because they are also members of the DMN, a collection of areas which display reduced activity during active engagement with a task (Raichle, 2015). Whereas multiple studies have evidenced the importance of complementary mPFC and hippocampal processing in spatial processing and memory (Backus et al., 2016; Dahmani & Bohbot, 2015; Kaplan et al., 2017; Kaplan et al., 2014), in line with the mPFC being within the PMN network, others have shown an association between increased task difficulty and reduced DMN activation, in the form of broadband gamma suppression (Ossandón et al., 2011) and reduced BOLD (de Dreu et al., 2019) in the mPFC. In addition, the PCC is commonly associated with the DMN and shows task-related activation decreases (Shulman et al., 1997) but has also been reported to show increased communication with the hippocampus during encoding (Lega et al., 2017).

It may be that mPFC and PCC engagements are not always consistent with hippocampal engagement across PMN functions. There is evidence that DMN areas show reduced activity during encoding but increased activity during retrieval, a process known as the encoding-retrieval flip (Huijbers et al., 2012), whereas the hippocampus does not display this pattern (Huijbers et al., 2011). This may be because encoding phases tend to involve processing of external information (e.g. a visually presented sequence) whereas retrieval involves internal processes (e.g. mentally re-imagining a sequence). Therefore, while it was hypothesized that oscillatory power modulation in the mPFC and PCC, and increased coherence between the HPC and mPFC ROIs, would be associated with the scene task because of their roles in the PMN, if these areas showed activity in line with their

involvement in the DMN, there may be no detectable differences between the scene and face tasks. This may help to clarify the roles of these areas in complex visual perceptual processes.

4.1.2 Aims and hypotheses.

This project aimed to investigate the role of the PMN in complex scene processing, and contrast this with complex face processing, using the oddity task and MEG recordings. This work builds upon previous fMRI work (Barense et al., 2010; Hodgetts et al., 2015; Hodgetts, Postans, et al., 2017) by investigating oscillatory modulations associated with complex scene perception, not only in the MTL, but in several areas of the PMN. Furthermore, whereas previous fMRI work had averaged BOLD modulations over long trials (e.g. 6 s in Hodgetts et al., 2015), in the current study the trial ended as soon as participants indicated their perceptual decision and trial analysis was restricted to the first 2 s (permissible with the temporal precision provided by MEG). This was done with the aim of reducing measurements of oscillatory modulations reflecting off-task thoughts and to increase the proportion of oscillatory modulations reflecting perceptual processes.

First, whole-brain theta and gamma power during the first 2 s of the scene and face tasks were contrasted with the first 2 s of the size task, and each other. It was hypothesized that there would be theta and gamma modulations in the PMN areas, including the MTL, that would be specific to the scene task, and that there would be increased gamma power in areas of the ventral visual stream specific to the face task.

Second, broadband time-frequency analysis was carried out on virtual sensor data on six PMN ROIs (left HPC, right HPC, mPFC, PCC, left IPL and right IPL). It was hypothesized that these would also reflect modulations in theta and gamma power, specific to the scene task. However, this additional analysis was included mainly to aid understanding of the frequency band specificity, laterality and temporal dynamics of effects found in the whole-brain analysis.

Lastly, PAC within the mPFC and HPC ROIs, and phase-coherence between all PMN ROIs, were investigated. It was hypothesized that increased mPFC and HPC PAC, and HPC - mPFC phase-coherence, would be specific to the scene task. Additional exploratory analyses investigated whether scene specific phase-coherence modulations occurred between the remaining PMN ROIs.

4.2 Methods

This chapter, *Chapter 5* and *Chapter 6* describe different aspects of the same experiment.

4.2.1 Participants.

The sample size of this study was based on the microstructure-behaviour correlation results of Hodgetts et al. (2015), which reported a Pearson's correlation of 0.46 between fornix MD[4] and scene oddity accuracy (microstructure-behaviour correlation tests are relevant to *Chapter 5*). Therefore, using G*Power (Faul et al., 2009; Faul et al., 2007) it was calculated that 38 participants were needed to achieve an 80% chance of detecting a Bonferroni-adjusted (0.017, adjusted for 3 conditions) one-sided correlation. To ensure enough data were collected if some collection sessions were unsuccessful or produced outliers, the number of participants recruited was 43, this being approximately 10% above the calculated requirement. Relevant to the current chapter, this sample size exceeded that reported in multiple previous MEG studies that produced significant results when examining MTL oscillatory patterns in healthy participants with MEG (Ruzich et al., 2019).

Forty-three volunteers (mean age: 22.4 years, SD 4.0, range: 18-38 years; 31 female), with no reported neurological pathology, were recruited. After giving informed consent, they participated in a MEG session, in which they undertook the behavioural task, and a follow-up dMRI session. Due to data collection disruptions, data from three participants were incomplete, leaving forty datasets (mean age: 22.5 years, SD 4.0, range: 18-38 years; 30 female).

4.2.2 The oddity task.

Participants were asked to perform scene, face and size oddity tasks. The creation of the stimuli and further details of the paradigm are described in *Chapter 3*. Three further examples of the stimuli are shown in Figure 10.

There were 96 trials of each condition (288 trials in total), displayed in a pseudo-randomised order. The 288 trials were split into 4 counterbalanced blocks (72 trials in each block, 24 of each condition).

[4] Note that the correlation between ILF MD and face oddity accuracy was also of interest, but the reported Pearson's r was a higher value.

Participants indicated their answer using a button box placed in their right hand. Each trial could last up to 8 seconds, but participants could answer at any point during trial display and their response would end the trial. Trials of the same type were grouped into 'mini-blocks'. Trials within mini-blocks were preceded by a baseline screen of a white fixation cross on a black background with a duration that varied between 1 and 1.5s. There were also longer fixation screens, of 5 s, between mini-blocks.

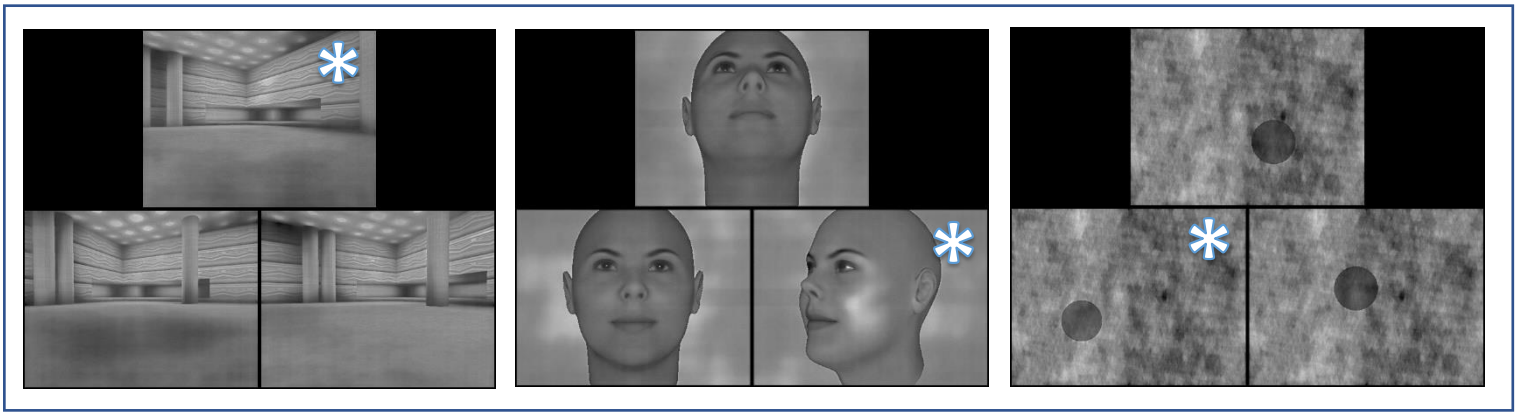

Figure 10. Examples of the scene, face and size trials.

The triplets of images were presented simultaneously. For this example, an asterisk is placed over the odd-one-out.

4.2.3 MRI scanning protocol.

Structural MRI data were collected using a Siemens Prisma GE 3T MRI system with a 32-channel head coil. T1-weighted anatomical images were obtained using an MPRAGE sequence with the following parameters: slices = 176, time to repetition (TR) = 2300 ms, field of view (FOV) = 256 mm x 256 mm, matrix size = 256 mm x 256 mm, flip angle = 9°, echo time (TE) = 3.06 ms, slice thickness = 1 mm.

4.2.4 MEG recording and analyses.

4.2.4.1 MEG acquisition.

The MEG recordings were performed using a 275-channel (1 channel was faulty) axial gradiometer CTF system, located inside a magnetically shielded room. The data were acquired continuously, with a sampling rate of 1200 Hz. Electromagnetic coils were placed on three fiducial locations, the nasion, and left and right pre-auricular regions. During the MEG recording, these sensors were energised with a high-frequency signal, in order to locate their positions relative to the MEG sensors. The locations of the fiducial points for

each participant, and head shape, were recorded digitally using an Xsensor camera system (ANT Neuro, Enschede, The Netherlands). These data were subsequently used to co-register the MEG data to each participant's individual T1-weighted MRI scan. There were individual MEG scans for each of the four oddity task blocks, each beginning with head localization.

4.2.4.2 MEG data pre-processing.

All MEG analyses were carried out using the Fieldtrip toolbox (Oostenveld et al., 2011) for MATLAB (MATLAB, 2015). The recordings were inspected manually for muscle and system artefacts before being downsampled (600Hz) and decomposed into 100 components using ICA (using Fieldtrip's fast ICA) (Hyvärinen, 1999; Oostenveld et al., 2011). Components relating to eye-movement, heart rate, and movement, were removed from the original data. These data were then cut into trials. These were visually inspected, and any left-over artefacts were manually excluded. Two participants each had one block removed due to large head movements, resulting in fewer trials surviving artefact removal (for each participant, the remaining numbers of trials for each condition, after data cleaning and cutting for two differently sized epochs, can be found in *Appendix 1*).

4.2.4.3 MEG to MRI co-registration.

Volume conduction models for each participant were computed using segmented individual T1-weighted images (brain, skull and scalp) and a semi-realistic model (Nolte, 2003). The source model was computed using an inverse-warping procedure to create subject-specific grids that are equivalent across subjects in normalized space. For this, a template MNI brain was divided into a 5-mm resolution grid (provided by Fieldtrip)(Oostenveld et al., 2011) and each individual anatomical MRI was warped to the template MRI. The inverse transformation matrix was then used to warp the template grid into an individual grid for each participant. The source models and head models were used to compute the leadfield matrix.

4.2.4.4 Whole-brain frequency and source analysis.

This study is primarily concerned with earlier perceptual processes, rather than later encoding processes (though these likely overlap), so analyses were focused on the first 2s of the trials. For whole-brain analysis, trials were cut to include -1 s pre-stimulus and 2 s post-stimulus onset. Oscillatory power in the frequency bands theta (4-8 Hz), low gamma

(40-60 Hz) and high gamma (60-80 Hz) were calculated using Fieldtrip's ft_freqanalysis and the 'mtmfft' (multi-taper method fast Fourier transform) method (Oostenveld et al., 2011), which entails windowing the data and performing a Fast-Fourier-Transform. Source localization was carried out using the Linearly Constrained Minimum Variance (LCMV) beamforming method (Van Veen et al., 1997). To reduce the magnitude of participant movement in each beamformer calculation, data were not concatenated across the experimental blocks. For each frequency band, common filters were calculated using all task conditions (face, scene, size). The source images were interpolated to a template source model included with Fieldtrip and anatomically parcellated using the AAL atlas (Tzourio-Mazoyer et al., 2002), also included with Fieldtrip.

All calculations were carried out per trial (rather than on averaged trial data), and the resulting trial source images were collated within conditions across blocks, for each participant.

4.2.4.5 Extraction of VS time series, and time-frequency, PAC and coherence analysis.

Adaptations of freely available code by Seymour et al. (2017) (available here: https://github.com/neurofractal/PACmeg/tree/master/frontiers_paper) were used to create VS time series and to perform subsequent PAC analysis.

ROI masks of the left and right HPC were made using the AAL ROIs: right hippocampus and parahippocampal regions, and left hippocampus and parahippocampal regions, respectively. An ROI mask of the mPFC was made using AAL ROIs: bilateral frontal medial orbital, bilateral middle frontal, and bilateral superior medial frontal regions. ROI masks of the right and left IPL were made using AAL ROIs: left and right IPL (inferior parietal gyrus, angular gyrus and supramarginal gyrus AAL ROIs), respectively. Lastly, a PCC ROI mask was made using the right and left PCC AAL ROIs. Whole-brain frequency analysis and source analysis was recomputed as above but over the frequency range 1-100Hz. To construct VS time-series data, a single spatial filter for each ROI was obtained by multiplying the spatial vertices extracted from an ROI mask by the sensor-level covariance matrix, and then performing PCA and taking the first principal component. The sensor-level data was then multiplied by the spatial filters for each ROI (Seymour et al., 2017).

Time-frequency analysis of the VSs was calculated over a time-window of 0-1.2 s with fixed sliding time window of 0.2 s (but the last 0.2 s were disregarded to remove edge artefacts) in two frequency windows. The 'mtmconvol' (multi-taper method fast Convolution)

method was used. A lower window of 1-15 Hz was analysed in 1 Hz intervals with 5 Hz frequency smoothing, and a higher window of 15-90 Hz was analysed in 5 Hz intervals with 10 Hz frequency smoothing. This was because increased smoothing for higher frequencies (>30H z) increases sensitivity as the gamma bandwidth is larger than the lower frequency bands and subject variability in peak frequency is more pronounced in higher frequency bands (Gross et al., 2013).

For PAC analysis, edge artefacts are particularly problematic (Kramer et al., 2008), but a long time window is necessary for reliable calculations (Seymour et al., 2017). Therefore, trials were cut to include -1 s pre-stimulus and 2.2 s post-stimulus onset. PAC was then calculated using times 0-2 s, to reduce spurious PAC from edge artefacts. The low and high frequency windows spanned 1-10 Hz and 24-90 Hz, respectively. The phase of the lower window, and the amplitude of the higher window, were extracted using a fourth order, two-pass Butterworth filter before applying the Hilbert transform. As in Seymour et al. (2017), a variable bandwidth, of 0.4 x centre frequency, was used for filtering to improve the ability to detect PAC. Coupling between the phases and amplitudes was calculated using the phase-locking value modulation index (Cohen, 2008). In this, the Hilbert transform is used to construct envelopes of the signals in the higher frequency band and then the relationships between the phases of these envelopes, and the phases of the signals in the lower frequency band, are expressed with phase-locking values.

Phase-coherence analysis was carried out between each VS over a time-window of 0-1.8 s, using Fieldtrip's 'ft_connectivity' analysis (Oostenveld et al., 2011), after frequency analysis was carried out at 8 Hz with 4 Hz smoothing. The imaginary aspect was analysed, removing 0 phase-lag, thereby suppressing spurious coherence resulting from electromagnetic field spread (Nolte et al., 2004).

4.2.5 Variable trial lengths.

Trials ended as soon as participants had responded with the button box, which meant that the trial lengths varied. It also resulted in different average trial length between the conditions (see Results section 4.3.1 for RTs). This study is primarily concerned with earlier perceptual processes, rather than later encoding processes (though these likely overlap) but trials needed to be long enough so that lower frequencies could be reliably measured. Therefore, the first 2 s were explored. However, some trials were shorter than 2 s, so they were not included in the whole-brain power analysis and VS time-frequency analysis. This length inclusion criterion, in combination with data cleaning during pre-processing,

resulted in different trial numbers within conditions. Although a common solution to this problem is to randomly remove trials to equalise trial numbers across conditions (Gross et al., 2013), this is wasteful, and large trial numbers are required to localise signals to deep brain structures (Quraan et al., 2011). Moreover, unequal trial numbers are less of an issue when measuring mean amplitudes, as done in whole-brain source analysis here, than when measuring peak amplitudes (Thomas et al., 2004).

Nonetheless, trial numbers affect SNR and comparing one condition with higher SNR to another with lower SNR would bias the results. There were consistently fewer size condition trials than scene or face condition trials. For example, trials cut at 2s post stimulus onset, resulted in 82 scene trials, 82 face trials and 65 size trials, on average. *Appendices 1a and 1b* show the trial numbers for each participant. To combat this bias in the whole-brain source analysis and VS time-frequency analysis, variance information was included in the statistical tests (see below, section 4.2.6).

4.2.6 Statistical analysis.

Statistical comparisons of whole-brain source images of the three conditions, face, scene and size, were carried out in two stages, to account for unequal trial numbers between conditions. First the conditions were compared at the individual level with Fieldtrip's 'ft_sourcestatistics' (Oostenveld et al., 2011) using MATLAB's t-test with unequal variance (MATLAB, 2015). This resulted in t-maps for each condition comparison (scene vs size, face vs size, scene vs face) for each individual. Additional t-maps were created by sign-flipping each t-map and the conditions were then compared with their sign-flipped counterparts, at the group level, using a dependent-samples t-test with Monte Carlo sampling and 5000 permutations. Locations of significant clusters were interpreted using an AAL atlas overlay. Statistical comparisons of VS time-frequency data were carried out using Fieldtrip's ft_freqstatistics (and involved the same two-stage statistical analysis described above, to account for unequal trial numbers across conditions), with equivalent parameters.

The alpha thresholds in these analyses were Bonferroni-corrected in accordance with the number of tests included in a section (with one hypothesis per section). The alpha threshold applied in the whole-brain power comparisons was 0.017 (0.05 / 3 conditions). The alpha threshold applied in the VS time-frequency power comparisons was 0.008 (0.05 / 6 tests per section, 3 conditions with frequency range split into 2 parts). For both, the cluster alpha threshold was 0.001. Fieldtrip's 'correct tail = alpha' option was applied to further correct for two-sided tests.

Unequal variance, caused by unequal trial numbers, could not be overcome for PAC and coherence analyses as the Fieldtrip functions do not permit single-trial analysis. Moreover, the trials were cut longer (2.2 s) for PAC, resulting in fewer trials per condition (see *Appendix 1B*). Therefore, rather than delete trials and reduce SNR, these analyses were carried out with unequal trial numbers and were classed as exploratory in nature, with the understanding that the method may create false positives and false negatives. Alpha threshold was not as strict, and no Bonferroni-corrections were applied. Statistical comparisons of PMN ROI PAC results were carried out using the methods of Seymour et al. (2017), utilizing Fieldtrip's ft_freqstatistics (Oostenveld et al., 2011) and a dependent-samples t-test with Monte Carlo sampling and 5000 permutations. The alpha, and cluster alpha, thresholds were both 0.05. For statistical comparisons in the coherence analysis, phase-coherence statistics from each condition were contrasted through subtraction, for each individual. Then, a group-level one-tailed t-test was carried out on each comparison, comparing to 0 (no difference) and the alpha threshold was kept at the traditional alpha threshold of 0.05.

4.3 Results

4.3.1 Oddity behavioural data.

Descriptive statistics of the oddity behavioural task results are shown in Table 3. No outliers (values larger than three SDs from the mean) were identified. There was no evidence that mean accuracies differed across conditions. An RM ANOVA to test for differences between accuracy scores for the three conditions gave a non-significant result ($F_{(1.59,62.13)} = 0.010$, $p = 0.868$)[5], and the equivalent Bayesian ANOVA test indicated evidence in favour of the null ($BF_{10} = 0.09$), suggesting that task difficulties were well matched. However, RTs did significantly differ between conditions ($F_{(2,78)} = 250.2$, $p<0.001$; $BF_{10} = 3x10^{32}$). Post hoc analysis with Bonferroni correction identified that scene RT was significantly larger than face RT ($p >0.001$) which in turn was significantly larger than size RT ($p >0.001$). This may have implications for subsequent analysis and interpretation of the results (see *Discussion* section 4.4).

	Scene Accuracy (%)	Face Accuracy (%)	Size Accuracy (%)	Scene RT (s)	Face RT (s)	Size RT (s)
Mean	60.52	60.68	61.30	5.14	4.16	3.14
SD	7.18	8.841	13.00	0.51	0.78	0.70
Minimum	38.54	39.58	29.17	3.95	2.56	2.14
Maximum	70.83	80.21	89.58	6.00	5.48	4.96

Table 3. Descriptive statistics of oddity task performance results.

RT: Reaction Time. SD: Standard Deviation.

[5] Mauchly's test of sphericity was significant at p = 0.004, so the Greenhouse-Geisser correction was used.

4.3.2 Dissociability of complex scene and face processing networks through oscillatory power changes.

Whole-brain theta and gamma power differences in scene, face and size conditions were assessed first. Cluster-based permutation tests revealed differences in oscillatory power within the selected 2 s time window, between the task conditions.

4.3.2.1 Differences in theta (4-8 Hz) power between scene and face conditions.

It had been hypothesized that theta power modulation in the MTL and other PMN areas would occur during the scene condition, and not the face condition, when compared with the size condition. The cluster-based permutation test, comparing the scene condition with the size condition revealed two significant clusters of theta reduction (both cluster p-values = 0.0002; 0.0008). These encompassed areas of left medial and inferior temporal lobe (including the hippocampus), and the medial occipital cortex (Figure 11).

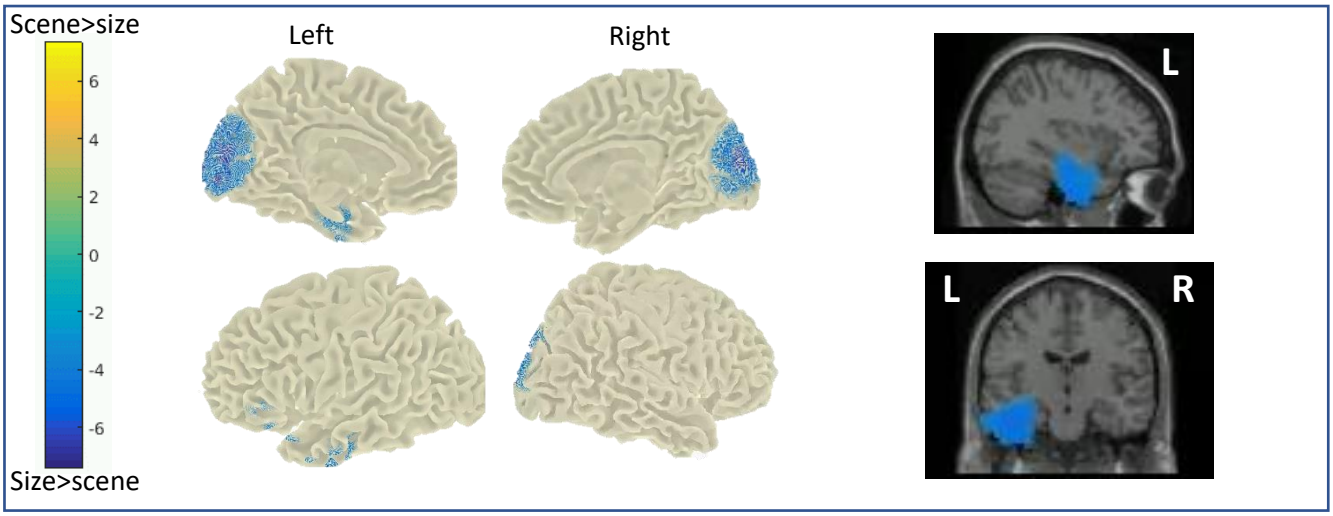

Figure 11. Theta power difference between scene and size trials.

Reduced theta power was localized to the left medial and inferior temporal lobes, and the medial occipital cortex. Colours represent t-values, and the scale is shown on the left-side bar. L = left. R = right.

The cluster-based permutation test comparing the face condition with the size condition revealed two significant clusters. A positive cluster (cluster p-value = 0.0002) encompassed areas of the IOC. A negative cluster (cluster p-value = 0.0016) encompassed areas of the left lateral and inferior frontal cortices (Figure 12).

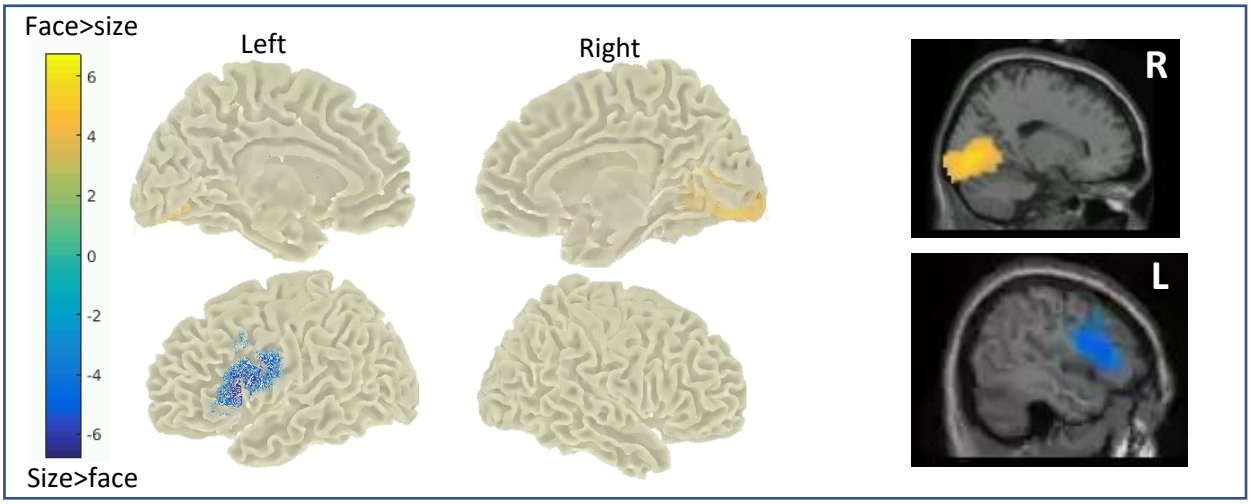

Figure 12. Theta power difference between face and size trials.

Increased theta power was localized to the inferior medial occipital cortex. Decreased theta power was localized to left lateral and inferior frontal cortices.
Colours represent t-values, and the scale is shown on the left-side bar. L = left. R = right.

The cluster-based permutation test comparing the scene condition with the face condition revealed a significant negative cluster (cluster p-value = 0.0002). This encompassed areas of occipital cortex that also showed decreased and increased theta power in the previous scene and face versus size contrasts, respectively. Additionally the cluster included the right MTL areas including the hippocampus (Figure 13).

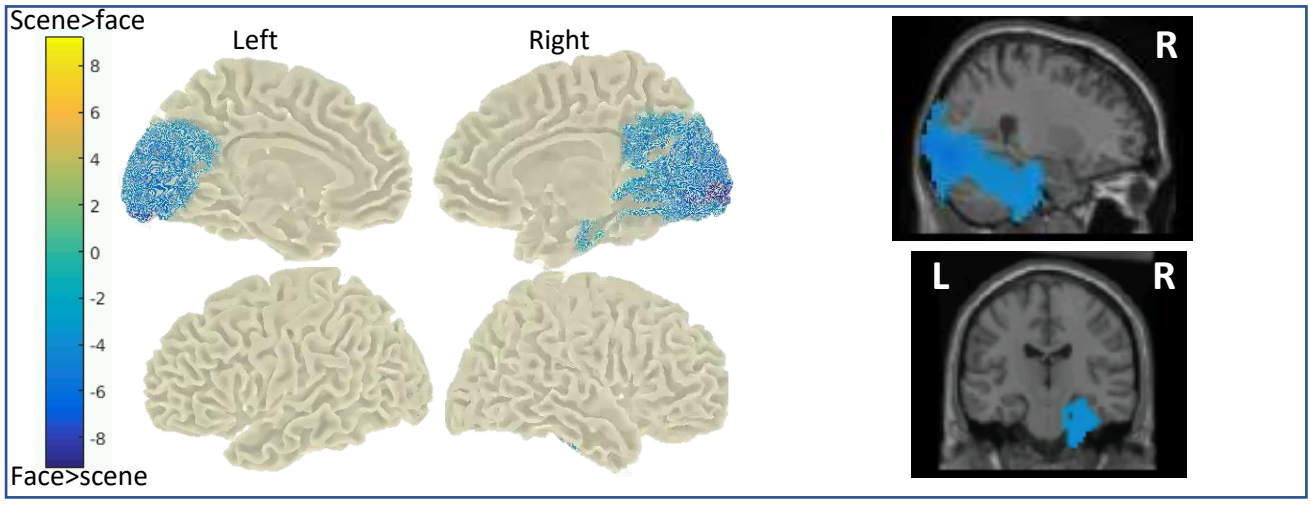

Figure 13. Theta power difference between scene and face trials.

Decreased theta power was localized to occipital, midline and right medial temporal structures, including the hippocampus.
Colours represent t-values, and the scale is shown on the left-side bar. L = left. R = right.

4.3.2.2 Differences in low gamma (40-60 Hz) power between scene and face conditions.

The cluster-based permutation test comparing the scene condition to the size condition revealed a significant negative cluster (cluster p-values = 0.0058), encompassing areas of the medial occipital cortex (Figure 14).

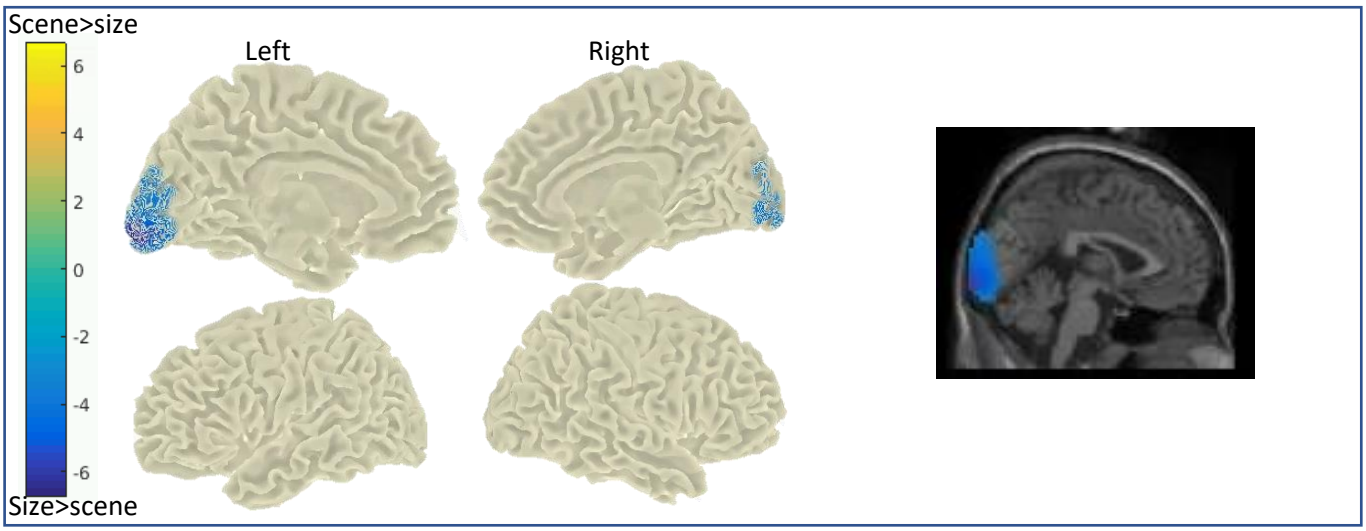

Figure 14. Low gamma power difference between scene and size trials.

Decreased gamma power was localised medial occipital cortex.
Colours represent t-values, and the scale is shown on the left-side bar. L = left. R = right.

The cluster-based permutation test comparing the face condition with the size condition revealed a positive cluster (cluster p-value = 0.0078) encompassing right posterior inferior temporal cortex, including the FG (Figure 15).

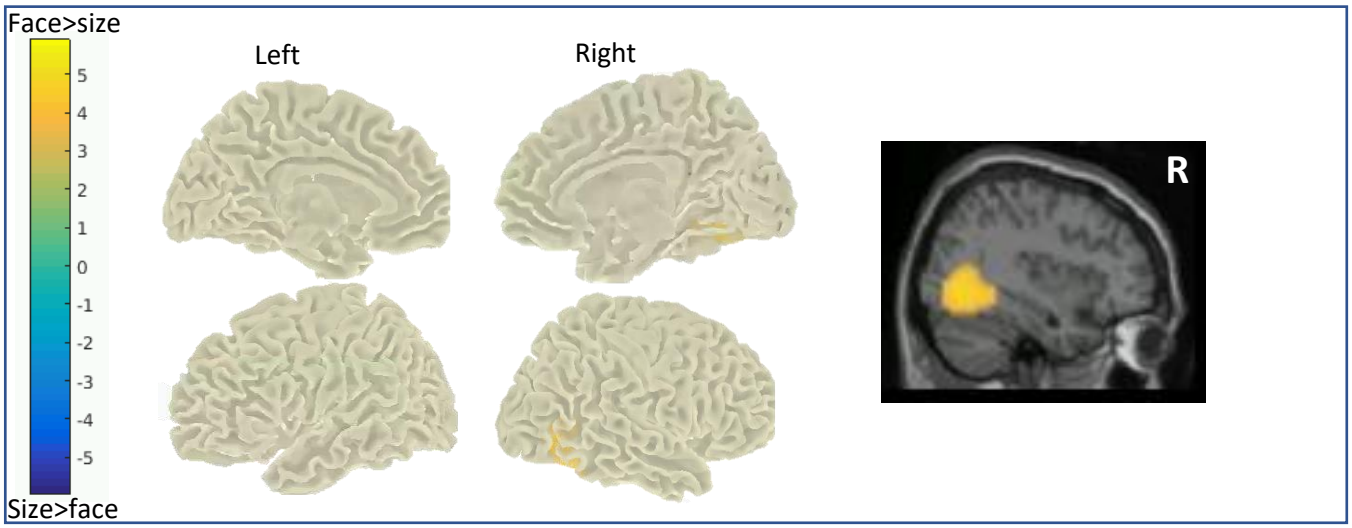

Figure 15. Low gamma power difference between face and size trials.

Increased low gamma power was localised to the right inferior temporal cortex, including the fusiform gyrus.
Colours represent t-values, and the scale is shown on the left-side bar. L = left. R = right.

The cluster-based permutation test comparing the scene condition with the face condition revealed one positive cluster (cluster p-value = 0.0040) and one negative cluster (cluster p-value = 0.0046), The positive cluster encompassed the left inferior parietal cortex and the negative cluster encompassed areas of the right IOC and inferior posterior temporal cortex, including the FG (Figure 16).

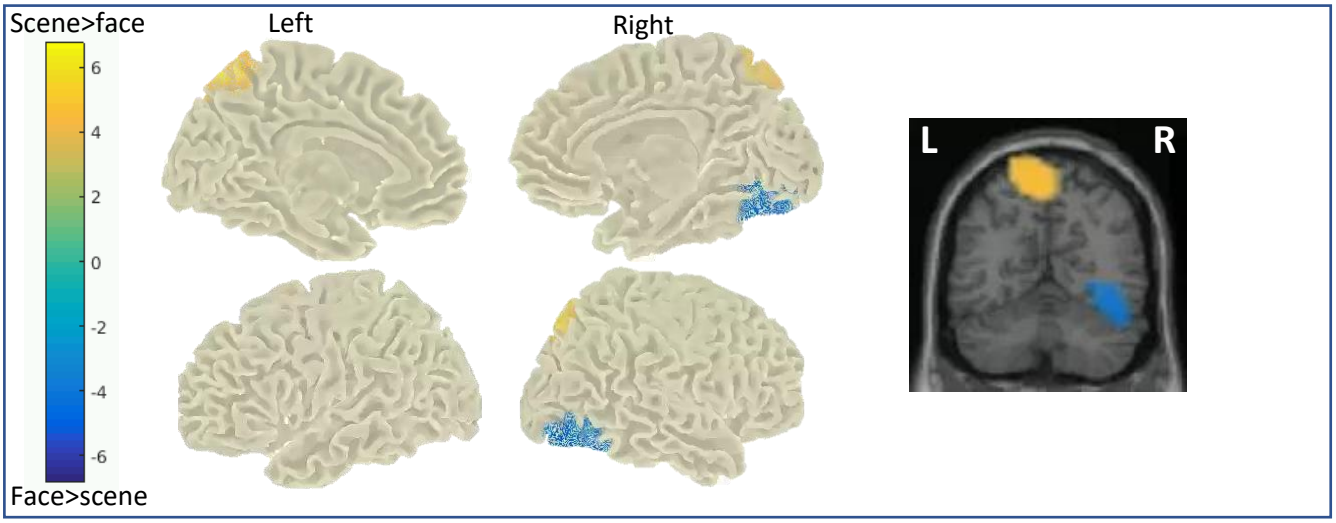

Figure 16. Low gamma power difference between scene and face trials.

Increased low gamma power was localised to the left parietal cortex. Decreased gamma power was localised to the right posterior inferior temporal cortex.
Colours represent t-values, and the scale is shown on the left-side bar. L = left. R = right.

4.3.2.3 Differences in high gamma (60-80 Hz) power between scene and face conditions.

The cluster-based permutation test comparing the scene condition with the size condition revealed one positive cluster (cluster p-value = 0.0004) encompassing areas of the bilateral medial occipital lobes and extending: superiorly and anteriorly to include areas of the IPL; and medially and anteriorly to include the right precuneus (Figure 17).

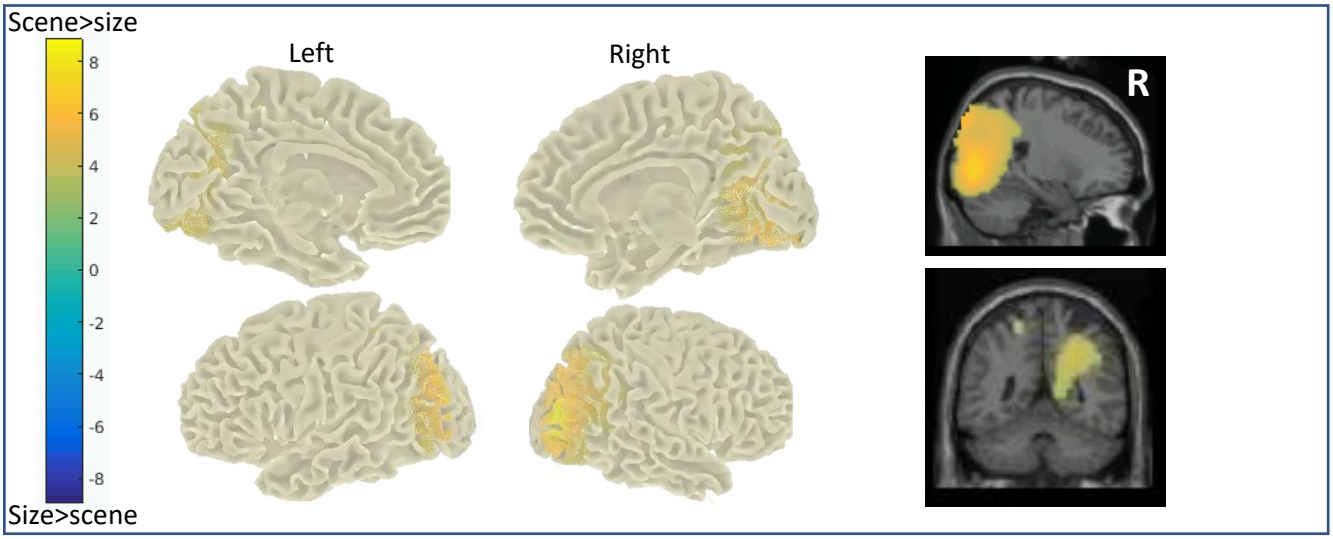

Figure 17. High gamma power difference between scene and size trials.

Increased high gamma power was localized to bilateral medial occipital lobes, inferior parietal lobule and the right precuneus.
Colours represent t-values, and the scale is shown on the left-side bar. L = left. R = right.

The cluster-based permutation test comparing the face condition with the size condition revealed two positive clusters (cluster p-values = 0.0004; 0.004) both encompassing IOC, and one also extending anteriorly to include the right FG (Figure 18).

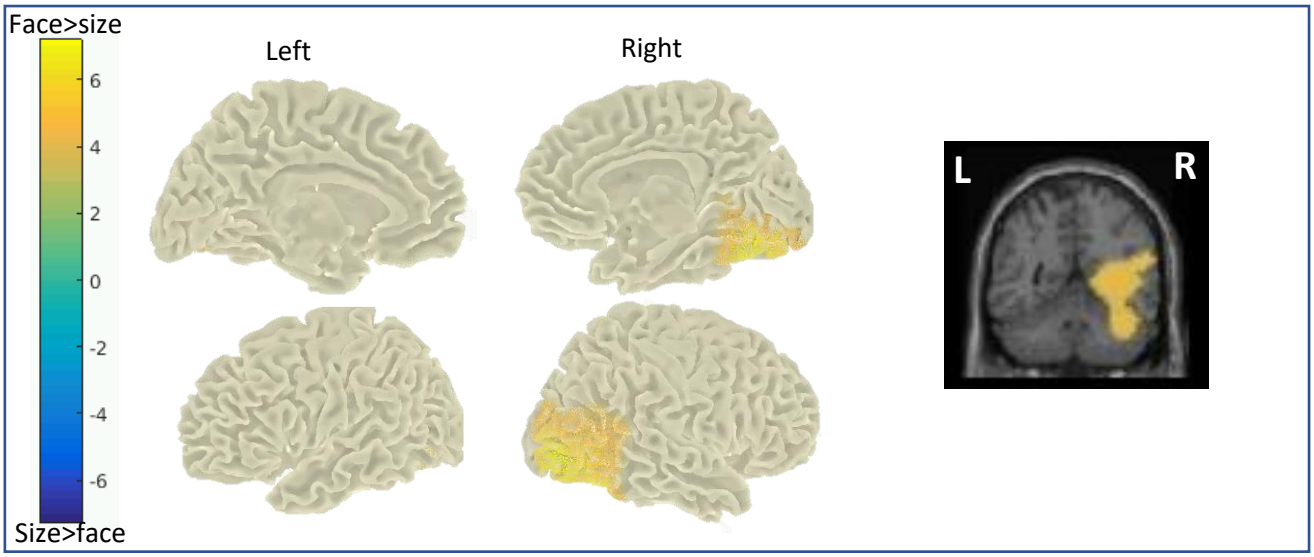

Figure 18. High gamma power difference between face and size trials.

Increased high gamma power was localized to right inferior occipital and right inferior temporal lobes. Colours represent t-values, and the scale is shown on the left-side bar. L = left. R = right.

The cluster-based permutation test comparing the scene condition with the face condition revealed one positive cluster (cluster p-value = 0.0006) encompassing bilateral areas of the superior parietal cortex, inferior parietal lobule and precuneus (Figure 19).

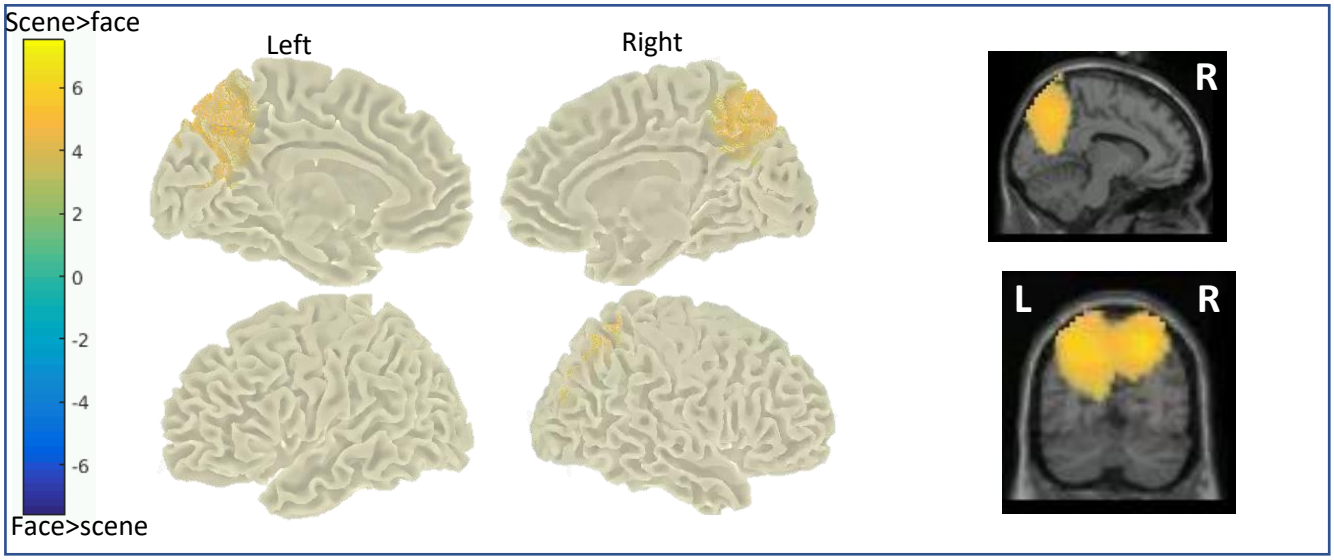

Figure 19. High gamma power difference between scene and face trials.

Increased high gamma power was localized to bilateral superior parietal cortex, inferior parietal lobule and precuneus. Colours represent t-values, and the scale is shown on the left-side bar. L = left. R = right.

4.3.3 Time-frequency analysis of regions of the PMN.

4.3.3.1 Right HPC virtual sensor time-frequency analysis.

Time-frequency analysis of the right HPC VS, in the lower frequencies (1-15 Hz), revealed a significant decrease in power in the scene condition compared with the size condition, starting at approximately 1.6 s post stimulus-onset (cluster p-value = 0.0008). Equivalent tests in the higher frequencies (15-90 Hz) revealed a significant increase in power in the scene condition compared with the size condition, starting at approximately 0.5 s post stimulus-onset (cluster p-value = 0.0072). No significant clusters were revealed in the low or high right HPC VS time-frequency data in the comparison of the face and size conditions, or between the scene and face conditions (Figure 20B).

4.3.3.2 Left HPC virtual sensor time-frequency analysis.

Time-frequency analysis of the left HPC VS, in the lower frequencies, revealed significant decreases in power in the scene condition compared with the size condition, starting at approximately 1.3 s post stimulus-onset, and appearing as two clusters on the spectrogram (cluster p-values = 0.0002; 0.0004). There were significant increases and decreases in power in the face condition compared with the size condition, starting within 0.2 s of stimulus onset (cluster p-value = 0.0026), and at approximately 1.4 s post stimulus-onset (cluster p-value = 0.0028), respectively. No significant clusters were revealed in the low left HPC VS time-frequency data in the comparison of the scene and face conditions. Time-frequency analysis of the left HPC in the higher frequencies revealed no significant differences between any of the conditions (Figure 20C).

4.3.3.3 Right IPL virtual sensor time-frequency analysis.

Time-frequency analysis of the right IPL VS in the lower frequencies revealed a significant increase in high theta/alpha in the scene condition compared with the size condition, starting at approximately 0.3 s post stimulus-onset (cluster p-value = 0.0002). There was also a decrease in delta power starting at approximately 1.6 s post stimulus-onset (cluster p-value = 0.003). There was an increase in theta/alpha in the scene condition compared to the face condition, starting at approximately 0.2 s post stimulus-onset (cluster p-value = 0.0003). There were no significant differences between the face and size conditions.

Equivalent tests in the higher frequencies, revealed a significant increase in high beta power in the scene condition compared with the size condition, appearing as two clusters

starting within 0.2 s of stimulus onset (cluster p-values = 0.0016; 0.0020). An equivalent increase in high beta power was also seen in the scene condition compared to the face condition, starting at approximately 0.5 s post stimulus-onset (cluster p-value = 0.0002). There were no significant differences between the face and size conditions (Figure 20E).

4.3.3.4 Left IPL virtual sensor time-frequency analysis.

Time-frequency analysis of the left IPL VS, in the lower frequencies revealed a significant increase in high alpha power in the scene condition compared with the size condition, starting at less than 0.2 s post stimulus-onset (cluster p-value = 0.0002). There was also a significant decrease in theta/delta starting at approximately 1.6 s post stimulus-onset (cluster p-value = 0.0038). There was a significant increase in high alpha power in the face condition compared with the size condition, starting at approximately 0.7 s post stimulus-onset (cluster p-value = 0.0002). There was a significant increase in theta/alpha power in the scene condition compared with the face condition, starting at approximately 0.2 s post stimulus-onset (cluster alpha = 0.0022).

Equivalent tests in the higher frequencies revealed broad increases in low gamma/beta power in the scene condition compared to the size condition, appearing as two clusters starting at less than 0.2 s post stimulus-onset (cluster p-values = 0.0002; 0.0036). There were similar increases in low gamma/beta power in the face condition compared with the size condition, appearing as two clusters, but these had a later onset, starting at approximately 0.4 s post stimulus-onset (cluster p-values = 0.0014; 0.002). There was a significant increase in low gamma/beta power in the scene conditions compared with the face condition, starting at approximately 0.2 s post stimulus-onset (cluster p-value = 0.0068; Figure 20F).

4.3.3.5 mPFC virtual sensor time-frequency analysis.

Time-frequency analysis of the mPFC VS, in the lower frequencies, revealed no significant differences between any of the conditions.

Equivalent tests in the higher frequencies, revealed a significant decrease in gamma power in the scene condition compared with the size condition, starting at approximately 0.8 s post stimulus-onset (cluster p-value = 0.0024). There was a significant decrease in gamma power in the face conditions compared with the size condition, starting at around 0.2 s post stimulus-onset (cluster p-value = 0.0074). No significant clusters were revealed in the

comparison between high mPFC VS time-frequency data in the face and the scene conditions (Figure 20H).

4.3.3.6 PCC virtual sensor time-frequency analysis.

Time-frequency analysis of the PCC VS in the lower frequencies revealed a significant increase in alpha power in the scene condition compared with the size condition, starting at approximately 0.6 s post stimulus-onset (cluster p-value = 0.0078). There was a significant increase in alpha power in the face conditions compared with the size condition, appearing as three clusters, starting at approximately 0.4 s post stimulus-onset (cluster p-values = 0.0002, 0.0002, 0.0018). There was a significant decrease in alpha/theta power in the scene condition compared with the face condition, starting at approximately 0.4 s post stimulus-onset (cluster p-value = 0.0002).

Equivalent tests in the higher frequencies revealed a significant decrease in beta power in the face condition compared with the size condition, at approximately 0.4 s post stimulus-onset (cluster p-value = 0.0068). There were no significant differences between the scene and size conditions, or between the scene and face conditions (Figure 20J).

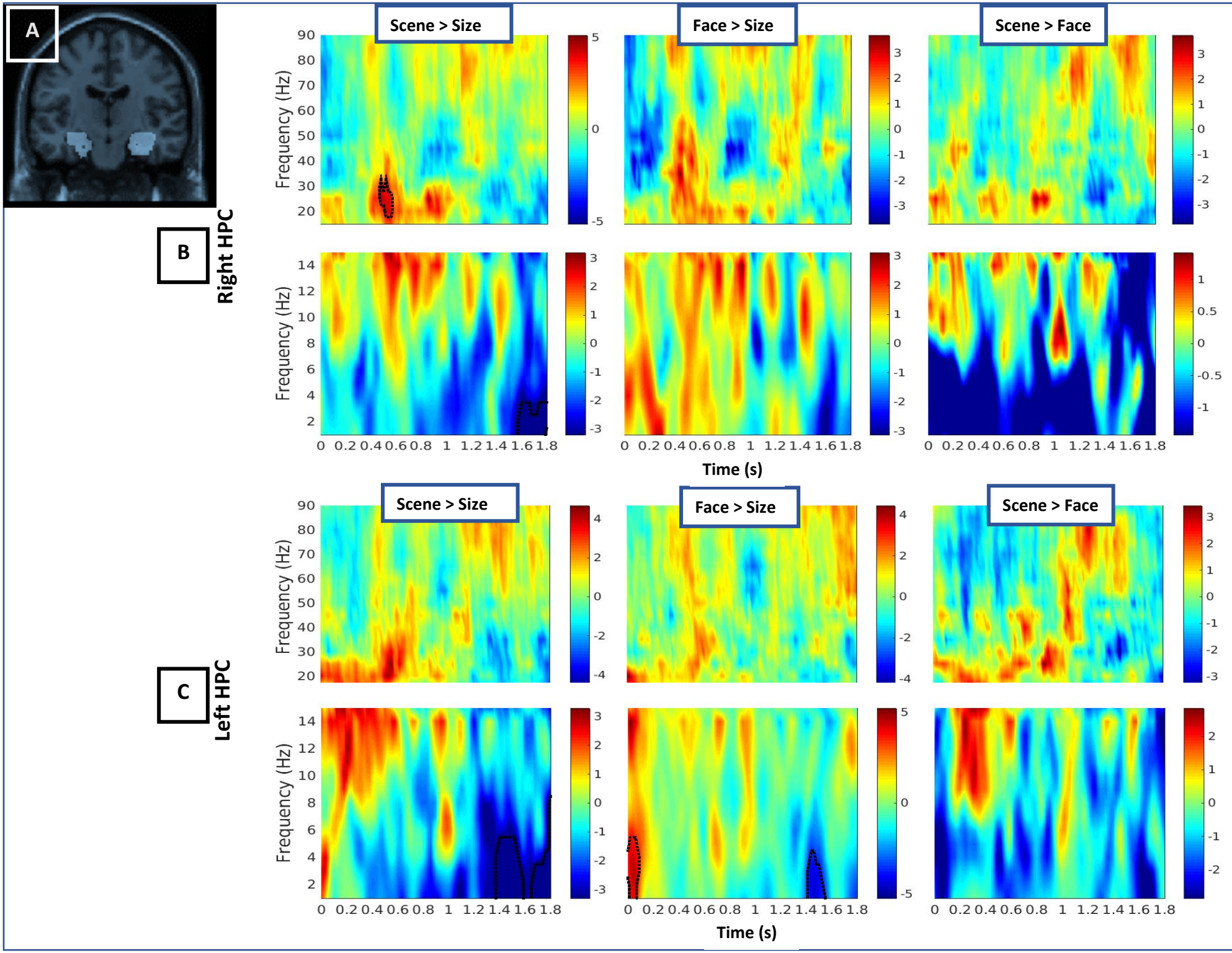
A
B
Right HPC
C
Left HPC
Scene > Size
Face > Size
Scene > Face
Frequency (Hz)
Time (s)

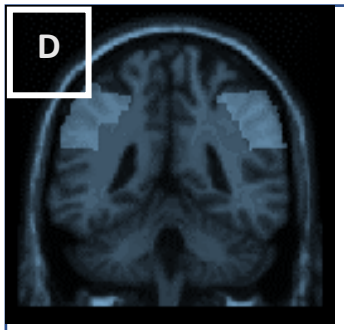

E

Right IPL

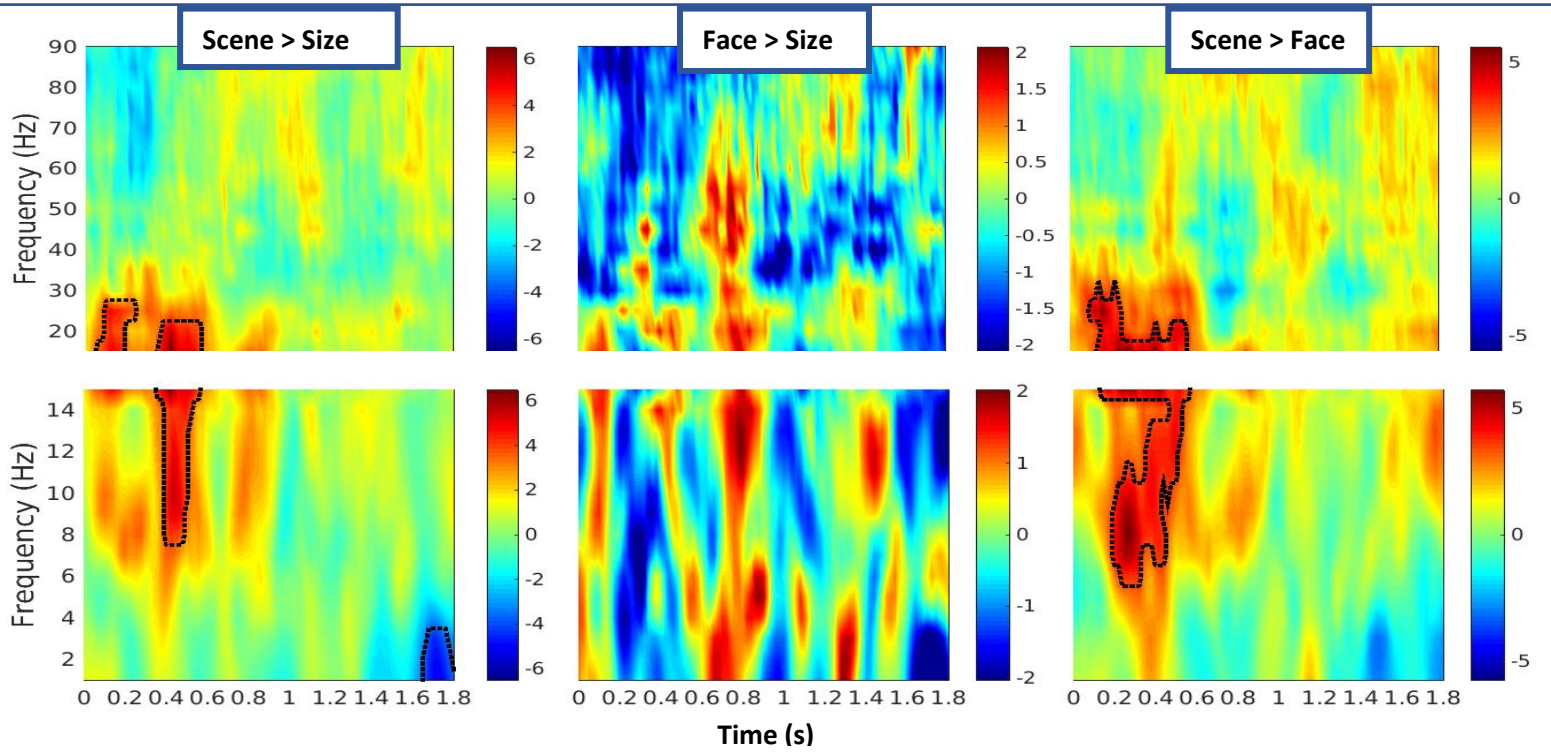

F

Left IPL

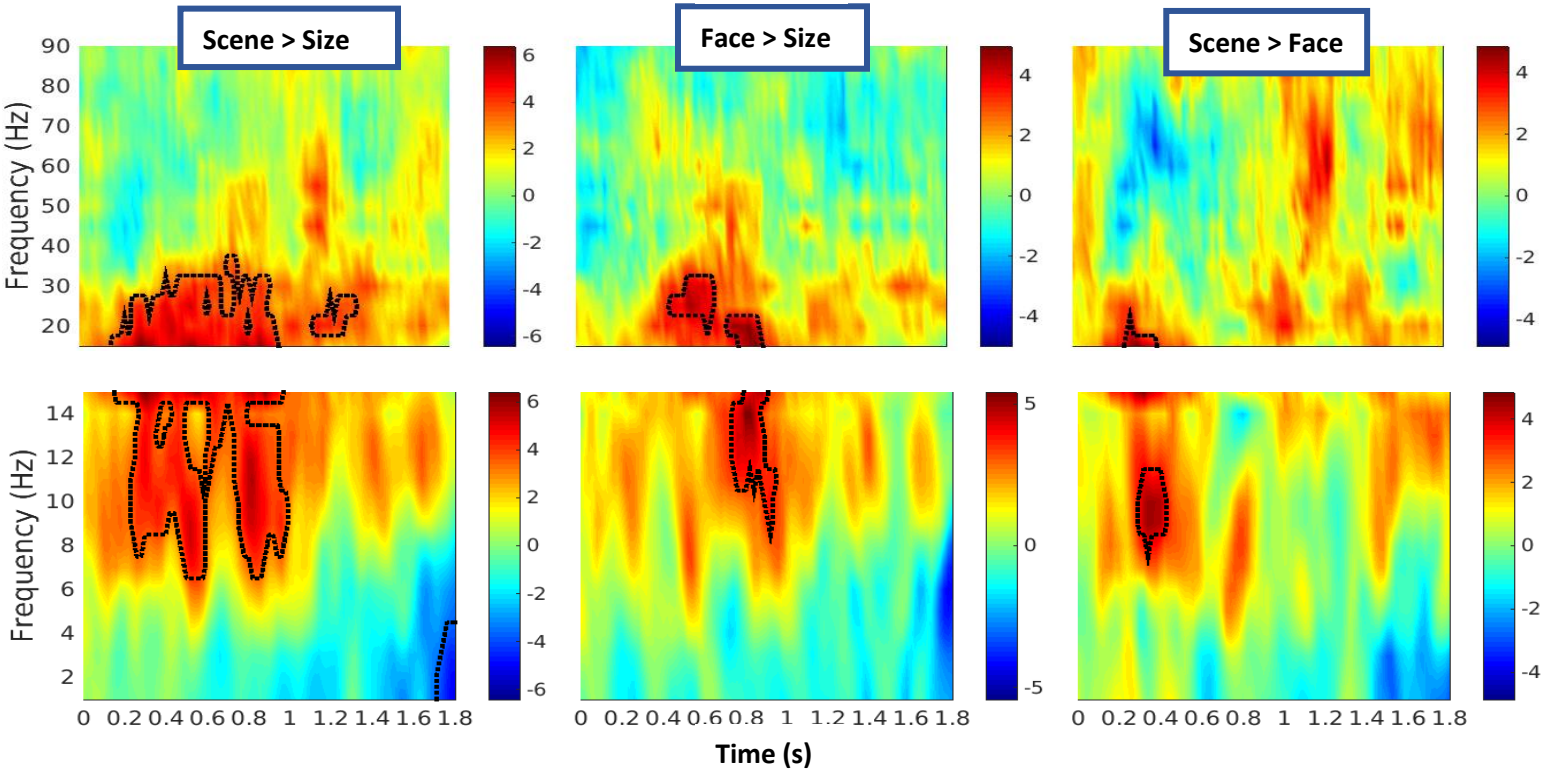

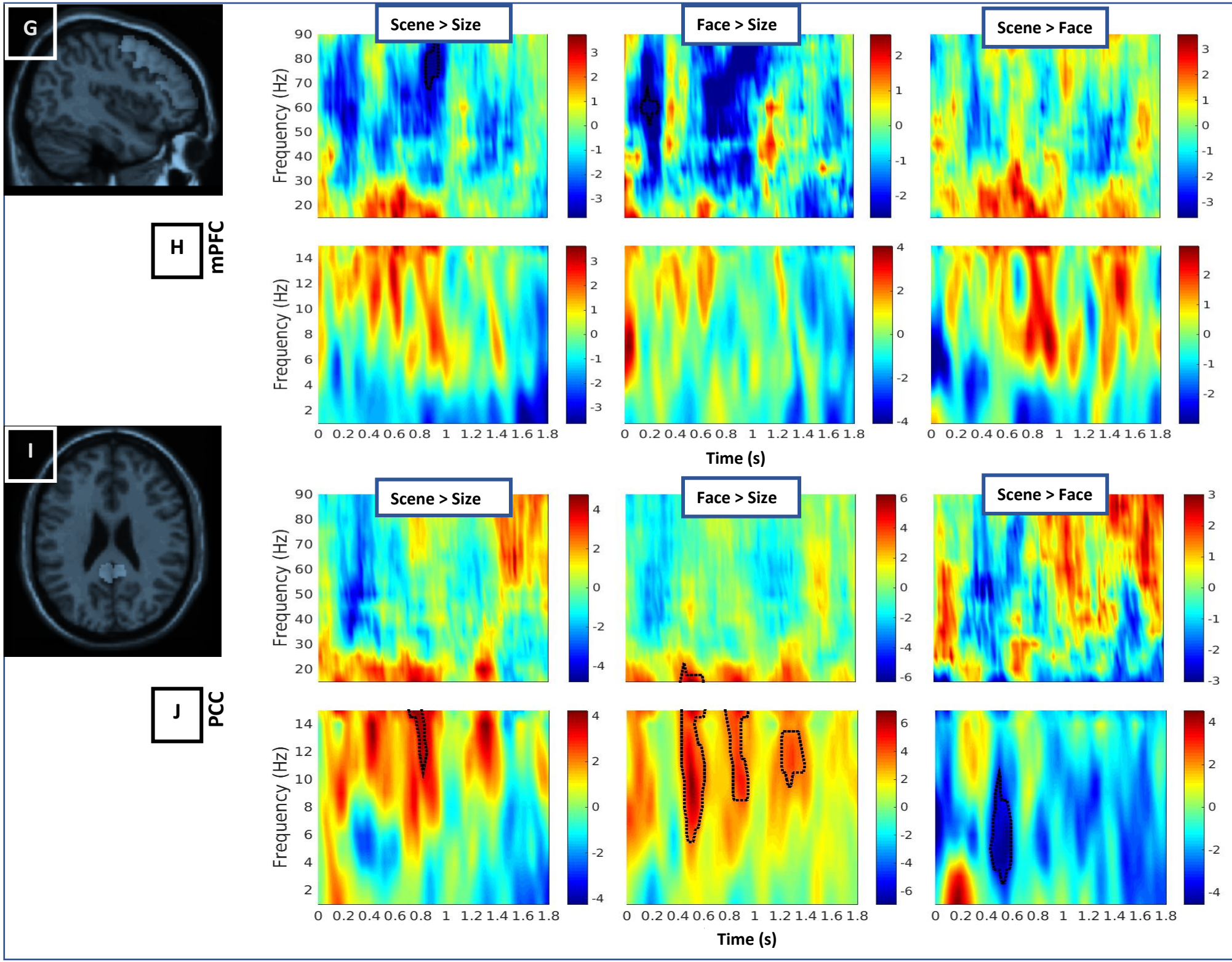
G
H
mPFC
I
J
PCC
Scene > Size
Face > Size
Scene > Face
Frequency (Hz)
Time (s)

Figure 20. Comparison of VS time-frequency data between conditions.

ROI masks of the HPC (A), IPL (D), mPFC (G), PCC (I), illustrated over template brains are shown to the left of the time-frequency results of each corresponding VS. Time-frequency spectrograms of the right HPC (B), left HPC (C), right IPL (E), left IPL (F), mPFC (H) and PCC (J) virtual sensors are shown for three contrasts: scene versus size; face versus size and scene versus face. The black dotted lines outline clusters significant at an alpha threshold of 0.008. Colours represent t-values, and the scale is shown on the bar to the right of each spectrogram.

4.3.4 Phase-Amplitude Coupling Within Regions of the PMN.

Contrary to the hypothesis, comparison between PAC values in the scene and size conditions revealed reduced mPFC delta-gamma coupling in the scene condition compared with the size condition (cluster p-value = 0.0280). There were no other significant differences in the other comparisons (Figure 21).

An exploratory search of PAC in the HPC VSs revealed no significant differences in the right or left HPC PAC between any of the conditions (see *Appendix 4C*).

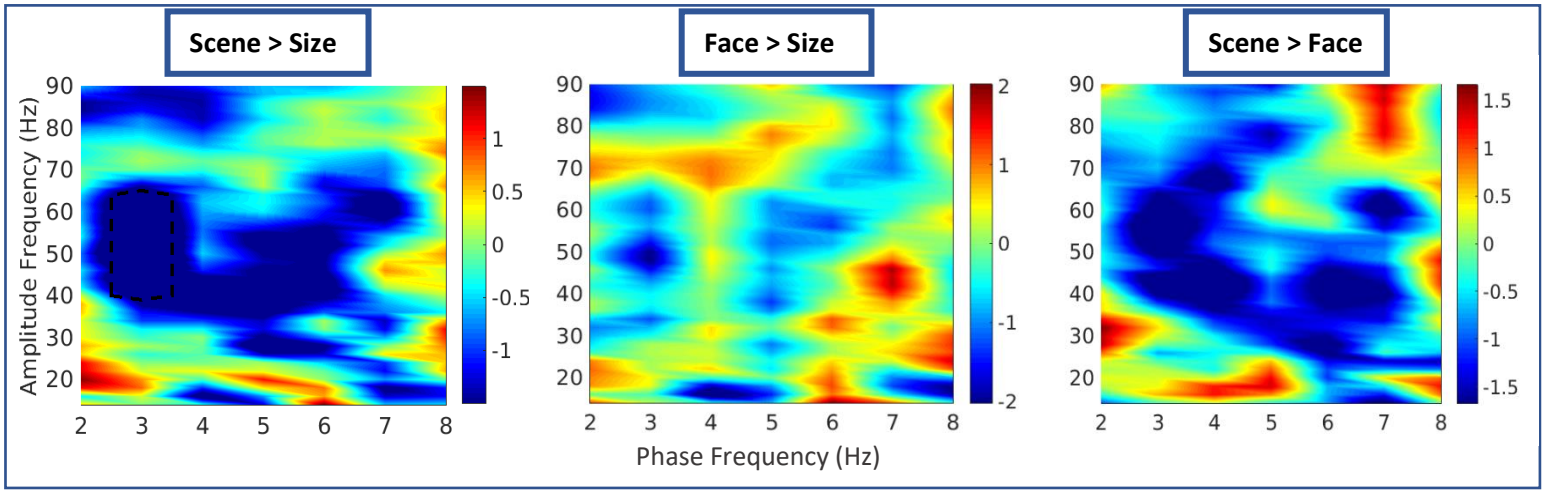

Figure 21. mPFC PAC in scene and face trials.

The scene and size conditions comparison revealed decreased delta-gamma PAC. This was also indicated in the scene and face conditions comparison, but it was not significant.
The colours represent t-values. The colour scale bar is shown to the right of each image. The black dashed line outlines a cluster significant at an alpha threshold of 0.05.

4.3.5 Phase-coherence between regions of the PMN.

Contrary to the hypothesis, analysis of theta-alpha phase-coherence (4-12Hz) revealed no differences in right or left HPC-mPFC coherence, between any of the conditions (p >0.2489). An exploratory search (alpha threshold set at uncorrected 0.05) for coherence between all VSs, compared between the conditions, indicated increased coherence between the right HPC and left IPL in the scene and size conditions comparison (p = 0.0331). In the scene and face conditions comparison, there was increased coherence between the left HPC and the left IPL (p = 0.0494), and decreased coherence between the left IPL and the PCC (p = 0.0110) There were no significant differences in coherence in the face and size conditions comparison (Figure 22).

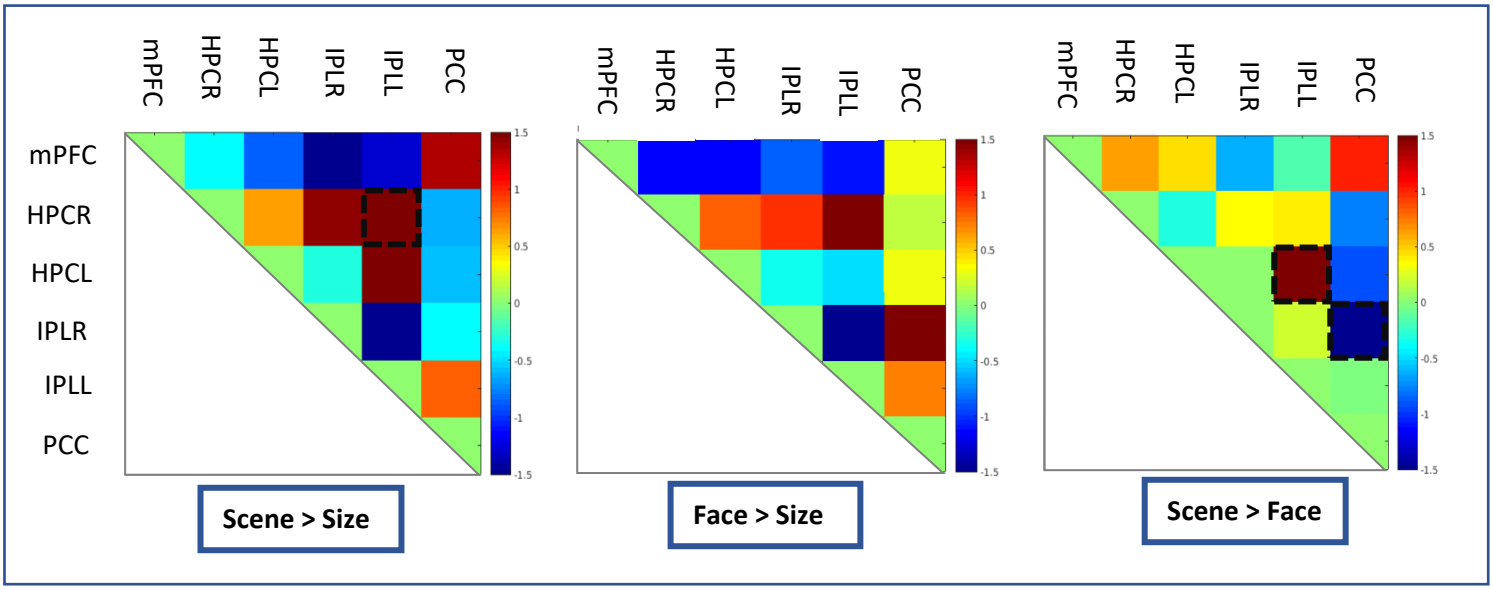

Figure 22. Differences in theta-alpha phase-coherence between conditions.

The scene and size conditions comparison revealed increased coherence between the right HPC and left IPL. The scene and face conditions comparison showed increased coherence between the left HPC and left IPL and reduced coherence between the right IPL and the PCC.
The colours represent t-values. The colour scale bar for each image is shown to the right of each image. The black dashed line outlines significance at an alpha threshold of 0.05.

HPCR: right Hippocampal Complex. HPCL: left Hippocampal Complex. IPLR: right Inferior Parietal Lobule. IPLL: left Inferior Parietal Lobule. mPFC: medial Prefrontal Cortex. PCC: Posterior Cingulate Cortex.

4.4 Discussion

This project aimed to investigate the role of the PMN in complex scene processing, and contrast this with complex face processing, using the oddity task and MEG recording. The results build upon previous fMRI work (Barense et al., 2010; Hodgetts et al., 2015; Hodgetts et al., 2017) by revealing oscillatory modulations associated with complex scene perception, not only in the MTL, but in several areas of the PMN. Whole-brain theta (4-8 Hz) power analyses revealed power modulations in MTL and other posteromedial areas that were specific to complex scene perceptual processing. Whole-brain gamma power analyses revealed power modulations in low gamma (40-60 Hz) in the right IOC and FG areas that were specific to complex face processing, and high gamma (60-80 Hz) in the inferior parietal cortex and precuneus that were specific to complex scene processing. Time-frequency analysis of the VS data revealed further temporal and frequency detail of the engagements of PMN ROIs during the scene condition. Although the decreased low frequency power during the scene condition compared with the face condition was not significant, it indicated that the scene specific decrease in right HPC theta power, found in the whole-brain analysis, was a long-lasting effect throughout the 2 s time-period. The right IPL and PCC regions also showed power modulations during the scene condition, compared with the face and size oddity conditions, but these lasted shorter durations. Exploratory PAC and phase-coherence analysis results differed from the hypotheses, as the mPFC VS data showed reduced PAC during the scene task and phase-coherence between the hippocampus and mPFC VSs did not differ between any conditions. Together, the results suggest that areas within the PMN network engaged during complex scene processing, and not during face or size processing.

4.4.1 Results of whole-brain theta and gamma power analyses provide some support for a dissociation between the networks.

In accordance with the hypotheses, there were brain areas displaying dissociable oscillatory power modulations in PMN areas during the scene condition, and in AIN areas during the face condition.

Whole-brain theta power comparison between the scene and size conditions revealed significant differences in the oscillatory power in areas including the medial occipital cortex and left MTL. The comparison between the face and size conditions did not reveal any power differences in MTL regions, but instead showed increased theta power in an area including the IOC and decreased theta in an area including left lateral and inferior frontal cortex. Since the size control task is thought not to incite the creation of an internal representation, the results reveal brain areas that are involved in creating representations to aid complex perception (Barense et al., 2010). Further comparison

between scene and face conditions, revealed reduced theta power in the right MTL. Together, the results suggest that power reduction in the MTL was specific to complex scene processing which aligns with the results of previous MEG studies, which identified reduced hippocampal theta power during novel scene imagery (Barry et al., 2019; Monk et al., 2020). A commonality between this novel scene imagery task and the scene oddity task, is the requirement to construct view-invariant internal representations of scenes, so the current finding of a reduction in MTL theta may reflect hippocampal processes that support internal scene representations.

Whole-brain gamma power comparison between the scene and size condition revealed decreased low gamma power and increased high gamma power in the medial occipital cortex. This could relate to the engagement of the OPA, a member of the scene network (Nasr et al., 2013). Indeed, the OPA has been implicated in several functions including local scene elements (items within a scene) processing (Kamps et al., 2016), and inhibition of the OPA by transcranial magnetic stimulation has been shown to selectively disrupt scene discrimination but leave face discrimination intact (Dilks et al., 2013). The decrease in power in low gamma and the increase in power in high gamma could reflect a shift in gamma frequency power in this area, but this is challenging to interpret as the primary visual cortex was anticipated to be engaged during the size task. Indeed, visual evoked gamma measured from occipital lobes, has been shown to occur during a simple circle size discrimination task (Ghorashi & Spencer, 2015). Therefore, for example, this apparent shift in frequency power could arise if the size condition induced a weaker, broadband effect, and the scene condition induced a larger increase in a narrower higher frequency range. However, these significant differences in medial occipital gamma power between scene and size conditions were not present in the comparison between scene and face conditions, implying that this power modulation may not reflect scene-specific processes. Further research, combining MEG and fMRI, for more accurate spatial localization, may allow confirmation, and/or further understanding, of the role of OPA gamma power increase in scene oddity task completion.

Increased low and high gamma power in the left parietal cortex was also seen in the scene condition compared with the face condition. It was hypothesized that the IPL would be engaged in complex scene processing because of its role in the PMN. The IPL has been identified as a member of the 'anterior scene network', a collection of scene processing areas which are highly connected with areas of the DMN and the hippocampus (Baldassano et al., 2016). Contradictory to the current results, the anterior scene network, in particular the IPL, is associated with mnemonic rather than perceptual functions, because it seems unresponsive to standard scene localizers in fMRI studies using unfamiliar scenes or sequences of unrelated scenes (Baldassano et al., 2016). However, it is thought to act as a cross-modal hub (Seghier, 2013), integrating visual information with internal memory information, allowing recognition of an image of a scene and relating to the place it depicts

(Baldassano et al., 2016; Montaldi et al., 2006). In the case of the oddity task, it may be that this area integrates incoming visual information, from visual sampling of the triplet images, into the internal scene model concurrently being constructed elsewhere in the PMN, such as in the hippocampus.

For the face condition, there was a significant increase in low and high gamma power in the right inferior occipital and temporal lobes, including the FG, compared with the size task. The low gamma change was also significantly different from the scene condition, indicating that this process is specific to complex face processing. The brain areas included in the cluster contain the OFA and the FFA, two areas of the core face processing network (Haxby et al., 2000). These results align with those of a transcranial magnetic stimulation study, which showed that inhibition of the right OFA impaired face discrimination but left scene discrimination unimpaired (Dilks et al., 2013), and a MEG study which showed low and high gamma power increases in both the right IOC and the right FG in response to images of faces as opposed to houses (Uono et al., 2017). Modulations in gamma power in these areas has been shown to be sensitive to gestalt face processing, displaying increased activity to whole faces over facial features not presented on a face (Gao et al., 2013), and over scrambled face images (Perry & Singh, 2014). Therefore, gamma oscillations in the IOC and FG may aid completion of the face oddity task since it was proposed that it requires aggregate processing of faces to complete.

In general, the whole-brain power analyses support the PM-view by showing MTL involvement in scene perceptual processing, and revealing PMN and AIN brain areas which were differently modulated during scene or face perceptual processing. In line with the hypotheses regarding the PMN, activity in the MTL, parietal and medial occipital areas was modulated during scene perception. In line with the hypotheses regarding the AIN, activity in areas along the ventral visual stream, including the FG, was modulated during the face task.

4.4.2 Time-frequency analysis of PMN virtual sensors elaborated on the temporal and frequency properties of the responses.

4.4.2.1 Results from the Right and Left HPC suggest a mixture of short and long-lasting oscillatory modulations in response to scenes.

The right and left HPC VSs displayed decreased theta/delta power near the end of the time window in the comparison between scene and size conditions. Although this could be interpreted as a bilateral late-appearing frequency-specific effect, the comparison between the right HPC VS data in the scene and face conditions indicated a long-lasting decrease in power covering delta and theta ranges starting at the beginning of the time window. This trend was apparent, but the p-value of the cluster did not survive multiple-comparison correction. Nonetheless, this pattern would explain the

decreased right MTL theta power between scene and face conditions resulting from the whole-brain analysis. The results do not support a specific theta effect in the MTL for scenes, but rather a general power decrease in the lower frequencies. This has been postulated to mirror engagement of a brain area in encoding and retrieval tasks (Hanslmayr et al., 2016), and may reflect a shift in power to higher frequencies, which is associated with increased BOLD (Conner et al., 2011).

In this way, the results of the right HPC VS do not adhere to predictions made from the results of Hodgetts et al. (2015) but might reflect the results of Barense et al. (2010). The latter used a similar oddity task, comparing BOLD signals in the PrC and the hippocampus in response to scene, face and object oddity tasks. Some of these contained images with differing angles (like the stimuli used here; to incite the creation of view-invariant internal models) and some contained images with fixed angles. They found voxels in the right hippocampus which showed increased BOLD when comparing scene viewpoint effects (an increase in BOLD when comparing scene oddity trials comprising images with differing image angles over oddity trials comprising images shown at fixed angles) with face and object viewpoint effects. However, considering the results of Barense et al. (2010), considering that decreases in low frequency power have been shown to accompany increases in power in higher frequencies (Scheeringa et al., 2011), and considering that an increase in BOLD signal can reflect a shift in power from lower to higher frequencies, an increase in HPC gamma power may have been expected in the current results. This was not the case. Interestingly, Barry et al. (2019), who identified a MEG-measured decrease in hippocampal theta in response to novel scene imagery, also reported no equivalent power change in higher frequencies. It may be the case that increased power in higher frequencies did occur but were undetected, because accurate localization of higher frequency signals from deep sources with MEG is more challenging than localization of lower frequency signals, because of decreased SNR due to source-sensor distance and muscle artefacts (Muthukumaraswamy, 2013). Invasive recording of MTL oscillatory signals during scene oddity performance may help address this uncertainty.

There was, however, a transient increase in power in the range 20-30 Hz in the right HPC VS data, during the scene condition compared with the size condition, which may motivate further research. This range has been described as beta2 and modulation of beta2 was associated with novel scene perception in an invasive recording study in rats (Berke et al., 2008). During early stages of novel environment exploration, local field potential recordings revealed pulses of increased beta2 (23-30 Hz) which decreased during subsequent laps of the environment and during a revisit to the same environment the following day. The authors suggested that hippocampal activity within the beta range may reflect, or facilitate, a plastic state aiding the construction of contextual representations. However, further research is needed to understand the role of modulations of right HPC beta2 during the scene oddity task, as this effect was not found in the comparison between right HPC VS

data in the scene and face conditions, indicating that it may not be specific to complex scene processing.

Results from the left HPC VS do not support its unique involvement in scene processing. Similar to the right HPC, there was a decrease in delta power near the end of the time-window in the scene and size condition comparison. However, a similar delta power decrease was also revealed in the face and size comparison, and there were no significant differences revealed in the scene and face conditions comparison. These results match the whole-brain theta power analysis, which also did not reveal any power differences between scene and face conditions in left MTL areas.

Considering the whole-brain and VS time-frequency analysis together, the results may indicate bilateral MTL involvement in complex scene processing, but that only the right HPC is selectively engaged during scene, as opposed to face, processing. Although this is in disagreement with Hodgetts et al. (2017), who found increased bilateral hippocampal BOLD during scene oddity trials over face or object oddity trials, asymmetrical hippocampal involvement in spatial processing has been previously demonstrated (Lee et al., 2016). In a study that compared hippocampal BOLD during two stages of a virtual reality task, one requiring object-place association retrieval and the other requiring spatial navigation, it was shown that the left hippocampus was more engaged in retrieval of object-place pairs while the right hippocampus was more engaged in retrieval of spatial memory (Lee et al., 2016). Together with the current results, this may suggest that the bilateral hippocampi are involved in conjunctive processes but that the right hippocampus is specific to spatial processing. As left and right HPC oscillatory power modulations were not directly compared in the current project, a future study would be necessary to elaborate on lateralized MTL processing in complex scene perception.

4.4.2.2 Results from the mPFC may reflect its role in the DMN.

Previous studies have demonstrated increased mPFC theta power during spatial memory retrieval (Kaplan et al., 2014), theta-gamma PAC during working memory (Li et al., 2012), and hippocampal-mPFC communication during spatial processing in dynamic mental exploration of previously-learnt scenes (Kaplan et al., 2017). Therefore, it was hypothesized that the same phenomena would be more prevalent during the scene condition than during the face or size conditions. However, increased theta power was not revealed in either the whole-brain analysis or the VS data. Rather, the mPFC results may reflect DMN processes, as time-frequency analysis of the VS data revealed decreased gamma power in both the scene and face conditions compared with the size condition. A decrease in dorsal-mPFC gamma, has been reported to occur in response to task difficulty (Ossandón et al., 2011). Although the oddity task was designed to result in equal accuracy scores across conditions (see C*hapter 3*) and the accuracy scores were equal across conditions in this experiment,

the RT differed across conditions such that scene RT > face RT > size RT (a pattern that was also consistent in task piloting, see *Chapter 3*). Longer RTs may imply that a task differs in cognitive demand inasmuch as the necessary processes took longer. Moreover, the size condition does not necessitate the creation of an internal representation, making it an appropriate control task, but this may also reduce cognitive demand.

If the mPFC oscillatory modulations recorded in the present study do indicate functioning akin to the DMN, it implies that HPC and DMN areas display differing engagements during the scene oddity task, despite these areas featuring in both the PMN and the DMN. Relatedly, Huijbers et al. (2011) assessed whether DMN areas worked cohesively with the hippocampus during encoding and retrieval if both were 'internal' (encoding and retrieving internally generated events). For this, some encoding trials asked participants to imagine a sound or image when presented with a word and to remember this association. They found evidence of differing BOLD modulations within the two phases: the PCC, mPFC and ventral parietal cortex displayed reduced BOLD during encoding, and increased BOLD during retrieval, whereas the hippocampus displayed increased BOLD during both encoding and retrieval. It may be that functional coupling between HPC and mPFC areas occurs during spatiotemporal processing in some circumstances but not others.

The reduction in mPFC theta-gamma PAC resulting from the scene and size conditions comparison may be related to the decreased gamma power in the equivalent comparison in the mPFC VS, and further supports the suggestion that the mPFC disengaged during scene trials. On the other hand, while increased PAC is often reported as functionally beneficial (Canolty & Knight, 2010), it has been suggested that it yields an inflexibility in cortical processing, and PAC has also been found to diminish in memory-related brain areas during encoding and retrieval (Vaz et al., 2017). Due to this uncertainty, and because this analysis was exploratory, further research is necessary to understand modulations in mPFC PAC during complex scene processing.

The difference between the current results and previous work relating mPFC processes to spatial processing may also have come about because of the specific requirements of the scene oddity task. The hypotheses of mPFC scene specific modulations were based upon previous work examining memory functions (Kaplan et al., 2017; Kaplan et al., 2014), whereas the oddity task has been shown to incite non-mnemonic processes (Lee et al., 2013). Together, these results imply that scene-selective engagement of the mPFC, PAC within the mPFC, and hippocampal-mPFC communication, may be restricted to PMN processes involved in memory, and that the processing of trial-unique novel stimuli, used in the oddity task, may incite different network dynamics. Future work could attempt to clarify the role of the mPFC in the PMN by using an adapted oddity task with differing levels of mnemonic demand. For example, by comparing PMN activity during online scene oddity task completion (trials comprise simultaneously displayed images and require an immediate

response, as done here), with PMN activity during oddity task completion where images are displayed sequentially with delays in which the internal representation must be held (an example of the latter was used by Postans et al. (2014)).

4.4.2.3 Results from the Right and Left IPL suggest a unique role of the inferior parietal areas in scene processing.

The right IPL VS demonstrated a broadband increase in power spreading across alpha to gamma bands, commencing early in the time window, which was specific to the scene condition. The left IPL VS, however, did not display specificity for the scene task over the face task: increased broadband power modulation was also present in the face condition compared to the size condition. These results were contrary to the whole-brain gamma analyses which showed increased low gamma power in the left inferior parietal cortex and increased high gamma power in bilateral inferior parietal areas in the scene over face conditions comparison. The whole-brain analyses involved averaging activity over time, so the conflicting results may arise through differences in temporal dynamics in left and right inferior parietal processes.

The parietal cortex is known to be important for spatial cognition, as lesions can cause spatial neglect (Karnath & Rorden, 2012), mental rotation deficits (Bestmann et al., 2002) and spatial working memory deficits (Mackey et al., 2016). The results of an experiment showing that areas of the posterior parietal cortex (containing the IPL) respond differently to changes in perspective of familiar and unfamiliar scene images, may provide insight into the role of the parietal cortex in the scene oddity task. Van Assche et al. (2016) showed participants sequential images portraying the same scene at different angles, either in a sequential order or a scrambled order, to test the role of the posterior parietal cortex in integration of information to create coherent spatial representations. Using fMRI, they found that the rostral IPL differed from other parietal areas examined, as it showed increased BOLD for unfamiliar scenes versus familiar scenes, when the angle images were presented in a coherent order. The results suggested that this area played a role in spatiotemporally mapping different viewpoints into a coherent internal scene representation (van Assche et al., 2016). Similarly, it is postulated that the contribution of the posterior parietal cortex to visual perception is to support working memory, allowing the integration of information over saccades (Pisella, 2017). In particular, the right IPL may be important in spatiotemporal mapping, as unilateral damage here can produce bilateral deficits in spatial attention (Malhotra et al., 2009) and spatial working memory (Malhotra et al., 2005).

The increase in broadband power in the IPL VSs warrants further investigation. It may reflect a phase-locked event-related field, rather than an induced response spanning multiple frequency ranges. A follow up analysis extracting only phase-locked signals would be beneficial.

Aligning with the whole-brain and VS time-frequency results, exploratory phase-coherence analysis indicated increased HPC-IPL coherence during the scene task, suggesting that, in addition to their processes being contributory to PMN functioning, communication between these areas may also have been important. However, this conclusion would need to be further supported by confirmatory analyses.

4.4.2.4 PCC patterns are complex, displaying DMN and PMN characteristics.

The PCC VS showed increased alpha power in both the scene and face conditions compared with the size condition. Previous studies have shown positive associations between BOLD and alpha power in the PCC (Javadi et al., 2019) and DMN areas (Mayhew et al., 2013), so the current results may indicate similar engagement of the PCC in complex scene and face processing, perhaps by supporting internal representations in both tasks (Leech & Smallwood, 2019). However, there was a transient decrease in lower frequency power in the scene condition when compared with the face condition, indicating that PCC processes during these tasks were not identical. It may be that, despite it being in the DMN, the PCC contributes processing specific to the PMN, displaying scene-specific decreases in low frequency power resembling those seen in the MTL.

The results of Shine et al. (2015) also illustrate complex PCC activity dynamics with the scene oddity task. They used fMRI to compare PCC BOLD in scene, face and object oddity conditions in APOE-ε4 [6] carriers and non-carriers, and found PCC deactivation, compared with baseline, for all conditions in the non-carriers, and for the face and object conditions in the carriers. Carriers showed increased PCC BOLD in the scene condition compared to the face and object conditions (Shine et al., 2015). Shine et al. interpreted their results as an impairment in APOE-ε4 carriers to modulate PCC activity. However, this modulation did not relate to performance in the task, so these results cannot elaborate further on the function of the PCC during complex scene processing. The following chapter will explore relationships between oscillatory activity and task performance, potentially indicating the importance of scene-specific PCC oscillatory power modulation.

4.4.3 Limitations.

One limitation of this study is the uncertainty that modulations of signals appearing to originate from the hippocampus, do in fact originate from this area. The ability of MEG to localize deep source activity such as that from the hippocampus has been debated (Riggs et al., 2009; Stephen et al., 2005), but it is becoming accepted in the literature and techniques for best revealing these signals are being reported (Mills et al., 2012; Quraan et al., 2011; Ruzich et al., 2019). However, it is known

[6] APOE-ε4 is a major genetic risk factor for Alzheimer's disease (Genin et al., 2011), suggested to be a disease of the PMN (Ranganath and Ritchey, 2012).

that source localization becomes more difficult to solve when co-registration error exceeds 3 mm (Meyer et al., 2017), a plausible amount of movement for a MEG recording block. The trials across the blocks were not concatenated before conducting the analysis for this reason. However, the fewer the trials entered frequency analysis, the less noise is removed by averaging, and this may affect the accuracy of the frequency and source results.

Furthermore, due to the challenge in accurately localizing MEG signals, the HPC ROI was made using AAL hippocampal and parahippocampal regions. This included the hippocampus, parahippocampal cortex and PrC, and it should be noted that signals from this ROI were assumed to be predominantly originating from the hippocampus and parahippocampal cortex. This was because: multiple studies have shown hippocampal/parahippocampal cortex activity to be detectable with MEG (Mills et al., 2012; Pu, Cheyne, et al., 2018), while comparatively few have shown PrC activity with MEG (Moses et al., 2009); hippocampal signals have previously been shown to influence measurement from nearby cortex, such as the PrC, through tissue volume conduction (Sirota et al., 2008; Vinck et al., 2015); and, in a previous study, the number of participants in which components of MEG signals correlated with hippocampal/parahippocampal cortex signals was larger than the number of participants in which they correlated with PrC signals (Pizzo et al., 2019). Previous MEG work has attributed MTL oscillatory modulations to hippocampal signals (Guitart-Masip et al., 2013), but confirming this is challenging. In the current study, it may be that changes in neuronal activity occurring during the scene task may be related to hippocampal processes specifically, or to processes in another region within this ROI. Previous fMRI-based studies of MTL activity during oddity task completion provide partial support for the assumption that these signals are from the hippocampus. Barense et al. (2010) reported that no voxels in the PrC showed increased BOLD for scene viewpoint effects compared with face viewpoint effects, but also found that the parahippocampal place area responded to both fixed angle and differing angle scene conditions. On the other hand, Hodgetts et al. (2015), who found a three-part relationship between hippocampal BOLD, the fornix and scene performance, did not find any voxels in the posterior parahippocampal gyrus that showed a relationship between increased BOLD in response to scene trials (versus face trials) and fornix microstructure. Therefore, the following chapter in this thesis (*Chapter 5)* may allow some confirmation that these scene-related signals were specific to the hippocampus, if they relate to fornix microstructure.

Further limitations of this study are the low trial numbers in the size task, and the unequal trial numbers across conditions. Due to the differences in RT between conditions, for most participants, there were more scene trials than face or size trials. This can create a bias because if one condition has a low SNR and is compared to another with a high SNR, then the comparison may not be between brain activity during two behaviours but rather between brain activity in one behaviour,

and noise. However, it is unlikely that the size condition had too few trials in any participant to adequately match the SNR in the scene condition, because there were areas showing significant power differences in the whole-brain scene and size condition comparisons that also showed significant power differences in the scene and face condition comparisons (such as increased high gamma power in the IPL), and the face and scene conditions were well matched in terms of trial numbers. Moreover, the purpose of this control condition was to remove visual signals that were non-specific to complex visual processing that likely reside in the primary visual cortex, and sources from this area are stronger than those in the MTL, making them more easily detectable (Quraan et al., 2011). Although the minimum number of size trials per participant to reliably measure visual signals during the size task is unknown, it is interesting to note that significant classifier performance of MEG recordings during speech perception, significant detection of cortical MEG-measured evoked potentials, and significant detection of EEG-measured event-related potentials have been shown to be obtainable with 40 or fewer trials (Boudewyn et al., 2018; Chaumon et al., 2021; Dash et al., 2019).

Regardless, to reduce the risk of spurious results arising from unequal trial numbers across conditions, unequal variance was accounted for in the statistical analyses for whole-brain power comparisons and VS time-frequency comparisons. Moreover, unequal trial numbers are less of an issue when measuring mean amplitudes, as done in whole-brain source analysis here, than when measuring peak amplitudes (see "ERP Methodology Blog" [7]). However, SNR can have substantial effects on PAC and phase-coherence analysis (see this Fieldtrip tutorial[8] for an example) and these analyses could not be corrected for unequal variance. Also, shortening the time-window, and therefore including more short trials and evening trial numbers across conditions, would have reduced the capacity for measuring lower frequency bands. Therefore, while the exploration of PMN PAC and phase-coherence illustrated an interesting picture of reduced mPFC engagement, unchanged mPFC-HPC communication, and increased HPC-IPL communication, complementing the whole-brain and VS data analyses, conclusions cannot be drawn without further replication.

An additional obstacle in interpreting the results is the ambiguity in the functional processes being represented by oscillatory power modulation. The role of MTL structures in perceptual processes is controversial, with some arguing that any apparent involvement is a reflection of memory processes (Squire et al., 2006; Urgolites et al., 2018). Although the oddity task used here comprised novel images in every trial and did not require memory over a delay, there is a possibility that incidental mnemonic processes are responsible for the modulations in MTL activity. To address this,

[7] https://erpinfo.org/blog/2018/6/26/different-ntrials
[8] http://www.fieldtriptoolbox.org/example/coherence_snr/

participants also underwent a subsequent surprise memory test, and relationships between the HPC activity modulations and subsequent memory performance are tested in *Chapter 5*.

4.5 Conclusions

The aims of the work described in this chapter were to expand on previous work investigating the roles of the PMN and AIN in complex scene and face processing. The results further support the notion described in previous studies that MTL areas are involved in perceptual processes when constructions of internal representations are required. Modulation of theta power in the MTL, thought to be contributed to by hippocampal/parahippocampal cortex processes, was specific to the scene task. Moreover, two collections of brain areas showed dissociable engagements with scene or face conditions, matching the PMN and AIN networks, respectively. Pertaining to the AIN, activity modulation in areas along the right visual ventral stream was specific to the face condition. Pertaining to the PMN, activity modulation in the right MTL, inferior parietal cortex and posteromedial areas was specific to the scene condition. Time-frequency analysis allowed some further understanding of the temporal dynamics of these network processes, giving indications of which processes were long- or short- lasting, or appearing earlier or later in the time-window. Exploratory PAC and phase-coherence analysis indicated differences in PMN processes involved in the oddity task compared with those described in previous work investigating other PMN-related behaviours, such as memory retrieval. This study highlighted PMN processes that are distinct from DMN and that are specific to complex scene processing.

Chapter 5: Examining relationships between structure, function, and oddity performance in the PMN and AIN.

5.1 Introduction

5.1.1 Background.

Implications of the PM-view include: the PMN and AIN networks should aid behaviours in different modalities; network areas, including MTL areas, should be involved in processes across memory and perception; and that the behavioural performance of those modalities should be related to the structural and functional properties of the respective networks (Graham et al., 2010; Murray et al., 2017). This chapter continues the investigation, focussing on the last implication, by testing correlations between individual differences in oddity task performance, MEG-measured brain oscillatory power modulation during the oddity task, and microstructure of the tracts that connect areas of the PMN and AIN networks. The aim of the experiment was to identify three-part relationships between structure, function and performance.

The investigations of the roles of PMN and AIN networks, including MTL areas, in complex perceptual processing are reported in *Chapter 4*. PMN areas, including the IPL, PCC and HPC, displayed oscillatory power modulations during scene oddity trials, and areas of the AIN, including the FG, displayed oscillatory power modulations during face oddity trials. Of particular note, is the scene-oddity-related decrease in HPC theta power.

As briefly described in *Chapter 4*, the implications of the PM-view have been investigated previously by Hodgetts et al. (2015), who correlated performance of scene and face oddity tasks with diffusion MRI measures of white-matter tracts and BOLD changes in MTL areas. They assessed fornix and ILF properties using DTI and found that fornix MD and ILF MD negatively correlated with scene oddity and face oddity accuracy, respectively. They also found positive trends between fornix FA and ILF FA, and scene oddity and face oddity accuracy, respectively. Similarly, they found PrC and FFA BOLD increases associated with, and positively correlated with, face task accuracy. FFA BOLD also correlated negatively with ILF MD. In addition, they found hippocampal BOLD decreases associated with, and correlated with, scene task accuracy. Although these results provide evidence that the AIN and PMN cater for different modalities, they leave some unanswered questions. Critically, they found a three-part mediation between FFA BOLD, ILF MD and face task accuracy, but

no three-part mediation between hippocampal BOLD, fornix MD and scene task accuracy was found. Regarding the functional results, the hippocampal BOLD decrease is difficult to interpret due to the complex relationship between hippocampal neuronal activity and BOLD (Ekstrom, 2010; Ekstrom et al., 2009), and so the results provide little information about the hippocampal processes during perceptual decisions. Regarding the structural results, Hodgetts et al. (2015) used FA and MD which are non-specific to individual properties of the white matter. For example, both axon membranes and myelin content can influence FA (Beaulieu, 2002). It may be that structure-function-behaviour relationships can be further unveiled by using different imaging techniques.

Therefore, in the current study, functional aspects were measured with MEG, which provided more precise timing and added oscillatory information, and structural properties were derived from several microstructure models. These included CHARMED (Assaf & Basser, 2005), qMT (Cercignani & Alexander, 2006; Henkelman et al., 1993; Henkelman et al., 2001), and NODDI (Zhang et al. 2012), as well as DTI.

From CHARMED, the FR, was extracted. It can be thought of as a probe for axonal density, so it is more specific than FA. From NODDI, two measures were extracted: ICVF, which is a marker of neuronal density, and OD which quantifies the coherence of fibre orientations. Both of these have been shown to relate to FA (Zhang et al., 2012). CHARMED and NODDI can be especially useful when studying the fornix. Fornix DTI results can be contaminated by CSF from the lateral ventricles (De Santis et al., 2014), a problem which may not affect FR or ICVF to the same degree (as explained in *Chapter 2*). Lastly, from qMT, MPF[9] (Cercignani & Alexander, 2006) was extracted. This has been shown to be sensitive to myelin content (Turati et al., 2015).

With the aim of reducing multiple-comparisons problems and to collate microstructure information in a biologically interpretable way, inter-individual differences in tract properties were scored by reducing multiple microstructure measures to component scores using PCA (Chamberland et al., 2019; Geeraert et al., 2020).

In addition to confirming the importance of the fornix and ILF in scene and face processing, this study also inspected the importance of the PHC. The PHC, along with the fornix, is an important pathway within the hippocampal–diencephalic–cingulate loop, connecting parahippocampal areas to other areas of the posteromedial network, including the RSC

[9] Also often referred to as "F" (Cercignani & Alexander, 2006; Turati et al., 2015).

(Bubb et al., 2017). It was of interest to know whether relationships between fornix microstructure and scene oddity performance were specific to the fornix or whether there was a similar relationship between the PHC and scene oddity accuracy, since both the hippocampus and parahippocampal areas have been shown to display BOLD modulation during complex scene processing (Hodgetts et al., 2016). However, the hippocampus is thought to be particularly important when the oddity images are presented at differing angles (Barense et al., 2010) and BOLD modulation of the hippocampus and not parahippocampal cortex, has been found to correlate with scene oddity performance (Hodgetts et al., 2015). Therefore, communication through the fornix pathway may relate to scene oddity performance more strongly than communication through the PHC pathway.

Since theta and gamma power modulations were found in PMN areas during scene oddity task completion (*Chapter 4*) and previous studies have found correlations between MTL theta/gamma power and spatial processing performance (Park et al., 2014; Pu et al., 2017; Y. Pu et al., 2020), MTL theta/gamma power was predicted to correlate with scene oddity performance. MTL localization of hippocampal and parahippocampal signals are challenging to differentiate with MEG. With small head movements, resolved localization of one region's signals may be shifted to the other. Previous MEG research has analysed them together (Pu et al., 2017). For this reason, the HPC ROI used here encompassed both the hippocampus and parahippocampal regions, creating a risk that any correlations between oscillatory power in this ROI and behaviour may be produced by parahippocampal activity. Assessing the relationships between the HPC ROI activity and fornix and PHC microstructure may help clarify the location from which the signals arise. For example, if HPC ROI oscillatory power relates to fornix microstructure only, then this could support the suggestion that the signals arose from the hippocampus.

Regarding the AIN, no studies have focused on the relationship between face perception performance, oscillatory power in areas of the AIN, and the microstructure of the ILF. Increased power in the gamma range (including the both the higher and lower bands defined here) in response to object or face processing has been reported in areas across the ventral visual hierarchy including early visual areas (Gao et al., 2013; Magazzini & Singh, 2018; Perry, 2016), the ventral occipitotemporal cortex (Engell & McCarthy, 2010) and the FG (Gao et al., 2013). Since the ILF connects the ventral visual pathway (Herbet et al., 2018), there may be correlations between FG gamma power, ILF microstructure and face oddity performance.

This study also investigated incidental encoding of oddity stimuli with the use of an unforeseen recognition test following the oddity task. It was important to investigate if oddity-related HPC signals were the consequences of incidental encoding, by testing whether HPC oscillatory signals that correlated with oddity performance, also correlated with subsequent memory of the stimuli. From a mnemonic-only view of the MTL, it could be argued that MTL signals during the oddity task, or poor performance from patients with MTL damage, could be explained by MTL encoding processes which support memory of items within each trial. Previous work by Lee at al. (2013), which measured hippocampal BOLD signals during a scene oddity task and a subsequent surprise recognition test, provided evidence against a mnemonic-only view of the MTL. In line with the PM-view, they found that hippocampal BOLD signals during correct and incorrect oddity trials were not associated with subsequent recognition performance, and that there was no correlation between scene oddity accuracy and d' scores from the scene memory test. However, their experiment did not include equivalent tests for face oddity stimuli or correlations with microstructure data. Therefore, since the memorability of scene and face oddity trials has not been compared in the context of oddity tasks, there is still the possibility that differences found from functional imaging of the MTL during face and scene oddity trials reflected differences in the propensity of the stimuli to incite incidental encoding. The current work aimed to test whether scene and face HPC oscillatory responses during the oddity trials related to recognition memory accuracy (measured as d'). Similarly, previous work has not compared the relationships between fornix and ILF microstructure properties and oddity task performance, and fornix and ILF microstructure properties and incidental stimulus encoding. Therefore, there is a risk that relationships found between fornix microstructure and scene oddity performance, for example, arise because incidental encoding aids task performance and fornix microstructure aids incidental encoding. In this study, correlations between fornix and ILF microstructure properties and scene and face d', respectively, were tested.

5.1.2 Aims and hypotheses.

Regarding structure, function and behaviour correlations, it was hypothesized that the current study's results would follow the same patterns as those of Hodgetts et al. (2015). Relationships between fornix microstructure and ILF microstructure and scene oddity and face oddity performance, respectively, were hypothesized. Moreover, since the PHC connects the PMN, but not predominantly the hippocampus, it was hypothesized that PHC microstructure would not correlate with scene oddity performance as strongly as fornix

microstructure, and that PHC microstructure would not correlate with face oddity performance.

Also, it was hypothesized that modulation of HPC theta (4-8 Hz) and low or high gamma power (40-60 Hz, 60-80 Hz) during the scene task, as compared to baseline, would correlate with scene oddity performance, reflecting hippocampal neuronal activity. Oscillatory power modulations were calculations of the differences between scene, face or size conditions compared to the fixation condition (to create a modulation from baseline measure). These comparisons (with the fixation condition) differed from those carried out in *Chapter 4*, in which contained comparisons between conditions. Comparing with the fixation condition was equivalent to the BOLD-behaviour analyses carried out by Hodgetts et al. (2015). It allowed a characterization of ROI 'engagement' in a task, from rest, rather than differences in engagement between tasks. However, oscillatory power modulations were also calculated as differences between scene or face conditions compared to the size condition, to create a difference from control measure which is equivalent to the comparisons made in *Chapter 4*.

In particular, it was hypothesized that there would be a three-part relationship between MTL oscillatory power, fornix microstructure and scene oddity performance. Although the results of Hodgetts et al. (2015) indicated that fornix microstructure and hippocampal BOLD correlated with scene oddity accuracy, but not with each other, it could be that structure and function measures other than those they used would correlate with each other. It was considered that the inclusion of further functional and structural information would reveal a three-part relationship.

Since the ILF connects lower and higher ventral visual stream areas (Catani et al., 2003; Latini et al., 2017), it was hypothesized that gamma power modulations in the FG during face processing would be associated with ILF tract properties and face oddity accuracy. Although Hodgetts et al. (2015) included the PrC as a focus in their investigation, signals from this brain area are likely unmeasurable with MEG (see *chapter 4*), so, in the current study, the focus was to replicate and expand on the findings that FFA activity modulation (BOLD increase) correlated with face oddity performance.

This project included a mixture of confirmatory and exploratory analyses. Confirmatory analyses related to the outlined hypotheses. Additional questions were addressed through exploratory analyses. Exploratory questions included: whether associations between tract microstructure and oddity task performance were specific to accuracy, or whether they

also related to RT; whether associations between HPC theta/gamma power modulation and scene oddity task were specific to that brain region or whether theta/gamma power modulations of other PMN regions also correlated with scene oddity performance; whether associations between HPC theta/gamma power modulation and scene oddity task were specific to that frequency band or whether power modulations in other frequency bands also correlated with scene oddity performance; and whether associations between fornix microstructure and HPC theta power were specific to that brain region or whether fornix microstructure related to power modulation in other PMN regions.

To test whether any relationships between scene HPC theta and gamma power and scene oddity performance were specific to that ROI, exploratory correlation tests between theta and gamma power in other PMN ROIs (mPFC, PCC, IPL) and oddity performance were carried out. It was anticipated that, if oscillatory power in the HPC, and the microstructure of the fornix (which connects the HPC to other PMN structures), both correlated with scene oddity performance, then another theta and gamma power modulation in another PMN structure, connected via the fornix, may also correlate with performance. Coherent oscillatory activity between regions can be a reflection of network communication and complementary processing (e.g. Barry et al., 2019).

To assess whether any relationships between scene HPC theta and gamma power and scene oddity performance were specific to those frequency bands, associations between scene HPC delta (1-4 Hz), alpha (8-12 Hz), beta (12-30 Hz) and scene oddity performance were also tested. Similarly, correlations with performance were also searched for in broadband (1-90 Hz) time frequency data for the right and left HPC. This also allowed exploration of bilateral differences and timescales of behaviour-oscillatory power associations. It was predicted that HPC theta and gamma would be uniquely important in complex scene processing but there were no predictions about the laterality or temporal dynamics of these relationships. Although there is some overlap in these analyses, it is important to include both the individual frequency bands and the broadband time frequency data. This is because a signal spatial filter over a broadband range of frequencies can be inaccurate, as the spatial structure of background activity is different for different frequencies, so one spatial filter cannot be optimal for all frequencies (Liu & Weiss, 2010).

Lastly, correlations were also tested between oddity performance and whole-brain t-maps of differences between theta and gamma power in the three conditions (scene>size, face>size, scene>face; see *chapter 4*). This differs from the methods of the main results of

Hodgetts et al. (2015), and part of the methods of the confirmatory analysis presented here, which compared online data to fixation data. It was thought that this comparison (of in-task data to other in-task data) may improve localization of correlations between oddity performance and deep-source oscillatory power. MEG measurements of deep sources can be influenced by stronger signals from shallower sources, such as those from the occipital cortex relating to visual processing (Quraan et al., 2011). Therefore, the aim was to 'cancel out' these visual signals by comparing the scene and face oddity tasks, which should incite more similar visual processing signals than those incited by the fixation trials. This analysis addresses a different question to that of the confirmatory analysis: 'do activation differences between oddity conditions relate to performance?', rather than 'do activation differences within oddity conditions, compared with baseline, relate to performance?'.

Since the PM-view implies that MTL responses during the oddity task are not purely reflections of incidental encoding, it was hypothesized that structure-function-behaviour correlations found for the oddity task would not be explained by subsequent memory behaviour. Therefore, correlations between oddity performance and subsequent recognition performance would be weak or non-existent. Moreover, it was predicted that HPC oscillatory changes that associated with oddity performance would not correlate, or only correlate weakly, with subsequent recognition performance. Furthermore, although the fornix and ILF have been shown to be important in spatial (Hodgetts et al., 2020) and face memory (Unger et al., 2016), respectively, it was hypothesized that associations between tract microstructure and subsequent recognition performance would be weaker than associations between tract microstructure and oddity performance, or non-existent.

5.2 Methods

5.2.1 Participants.

The 40 participants were the same as described in *Chapter 4*. However, one participant asked to leave the scanner before completing all the qMT-weighted scans, so this dataset is included in MEG-behaviour correlations but not in the analyses involving microstructure data (39 participants: mean age: 22.5 years, SD 4.2, range: 18-38 years; 29 female).

5.2.2 The oddity task and incidental recognition memory task.

See *Chapter 3,* for a detailed description of the oddity and memory tasks and for diagrams of the paradigms. In short, the oddity task included 96 scene, face and size trials. The oddity blocks were followed by a 5-minute pause after which the participants were asked to perform a memory task that was a "surprise test" inasmuch as they knew there was an additional part of the study, but they did not know its nature. The memory task consisted of 48 "old" (shown during the oddity task) scenes, 48 "old" faces, 48 "new" (not shown in the oddity task) scenes and 48 "new" faces.

The percentage of correct oddity trial responses was used as a measure of oddity task performance. RT was measured in ms. To analyse the memory task data, individual results from the oddity and memory tasks were combined, allowing the identification of matching trials (old trials) that appeared in the oddity and the memory tasks, and non-matching trials (new trials), which appeared in the memory task only. The former data were used to calculate the number of hits and the hit rate (old trials correctly identified as old), and misses (old trials incorrectly identified as new). The latter data was used to calculate correct rejections (new trials correctly identified as new) and the number of false alarms and the false alarm rate (new trials incorrectly identified as old).

The scene and face memory performances were compared, to understand if memorability of the stimuli differed between conditions. The hit and false alarm rates were inspected, and then the hits were split by confidence level to see if confidence in memory of the conditions differed (a similar comparison of confidence of hit rates across stimulus types has been done by Michalowski et al. (2014)). To test whether performance in the oddity task influenced memory performance, the hit rates for oddity-incorrect and oddity-correct trials in the scene and face conditions, were compared. Finally, d' scores were calculated by

the Psycho package for R (Makowski, 2018), and were tested for correlations with scene and face oddity performance.

5.2.3 MRI scanning protocol and microstructure measurement.

5.2.3.1 Protocol.

Methods to obtain structural MRI data are outlined in *Chapter 4* (section 4.2.3).

Diffusion weighted data were acquired using the CHARMED protocol with the following parameters: phase encoding = A>P; slice thickness = 2 mm; TE = 73 ms; TR = 4100 ms; 203 gradient directions and 4 shells (maximum b-value: 4000 s/mm^2); FOV = 220 mm x 220 mm. A reference acquisition with the opposite phase encoding direction was acquired for blip-up blip-down correction, with 33 directions and 2 shells (maximum b-value: 1200 s/mm^2).

qMT sensitive data was acquired through an optimized 3D MT-weighted fast spoiled-gradient recalled-echo sequence (Cercignani & Alexander, 2006) with the following parameters: TR = 32 ms, TE = 2.46 ms, flip angle = 5°, Gaussian MT pulses, duration t = 12.8 ms, bandwidth = 330 Hz/Px, FOV = 240 mm x 240 mm, slice thickness = 2 mm. 11 MT-weighted scans had the following off-resonance irradiation frequencies/saturation pulse amplitudes: 1000 Hz/332°, 1000 Hz/333°, 12060 Hz/628°, 47180 Hz/628°, 56360 Hz/332°, 2750 Hz/628°, 1000 Hz/628°, 1000 Hz/628°, 2768 Hz/628°, 2790 Hz/628°, 2890 Hz/628°. Data for two B1 maps were collected through two four-shot spin-echo echo-planar imaging sequences with the following parameters: TR = 5000 ms, TE = 1.83 ms, flip angle = 8°, matrix = 64 × 64. Data for two B0 maps were collected through gradient recalled acquisitions with the following parameters: TE = 4.92 ms/ 7.38 ms; TR = 330 ms; FOV = 240 mm; slice thickness = 2.5 mm.

5.2.3.2 Analysis of structural images.

Diffusion analysis pipelines were orchestrated by G. Parker of Cardiff University. Motion distortion correction was carried out using the Eddy tool in FSL (Andersson & Sotiropoulos, 2016; Jenkinson et al., 2012). The separate contribution of the free water compartment to the DTI data was identified and removed by a customized version of the Free Water Elimination algorithm (Pasternak et al., 2009).

Tensor fitting was carried out on the 1200 b-value shell. To estimate the diffusion tensor in the presence of physiologic noise and system-related artefacts, the Robust Diffusion Tensor

Estimation (RESTORE) algorithm was applied (Chang et al., 2005). This analysis resulted in FA, MD and RD maps.

Tractography analysis was applied to the 1400 b-value shell. To detect and eliminate signal artefacts, the Robust Estimation in Spherical Deconvolution by Outlier Rejection (RESDORE) algorithm was applied (Parker, 2014). Subsequently, peaks in the fODF in each voxel were extracted using the dRL technique (Dell'acqua et al., 2010). Whole-brain deterministic tractography was conducted in Explore DTI (version 4.8.3) (Leemans, 2009), using an fODF amplitude threshold of 0.05, step size of 0.5 mm and an angle threshold of 45°.

NODDI maps were created using the Accelerated Microstructure Imaging via Convex Optimization (AMICO) NODDI algorithm (Daducci et al., 2015) (description and pipelines available here[10]). For this, the co-registered and distortion-corrected 1200 and 2400 b-value shells were combined.

All shells were used for the CHARMED analysis, which was conducted using an in-house program coded in MATLAB (MATLAB, 2015) which calculated FR per voxel (De Santis et al., 2014).

The magnetization transfer-weighted images were co-registered (affine, 12 degrees of freedom), within each participant, to the image with the highest contrast, to correct for interscan motion, using Elastix (Klein et al., 2010). Modelling was then carried out by using two-pool pulsed-magnetization transfer approximation as described by Ramani et al. (2002), which also corrects for amplitude of B0 field inhomogeneities and produces MPF maps.

5.2.3.3 Tractography.

To generate three-dimensional streamlines that represented the fornix, the ILF and the PHC, 'way-point' ROIs were manually drawn onto whole-brain FA maps in the diffusion space of 18 subjects, using Explore DTI (Leemans et al., 2009). These 'way-point' ROIs allow the user to define Boolean AND and NOT gates with the aim of isolating the relevant streamlines. The resultant tracts were used to train in-house automated tractography software (written by G. Parker of Cardiff University), which was then applied to the entire dataset.

Protocols for the manual construction of the tract streamlines are described below. NOT

[10] https://github.com/daducci/AMICO/blob/master/doc/demos/NODDI_01.md

gates were added until no spurious fibres remained. To generate the images shown here for illustration (Figure 23), the same methods were used to extract streamlines from an example dataset (available here[11]; Leemans et al., 2009).

A protocol based upon Hodgetts et al. (2015) was used to isolate fornix streamlines. One AND and six NOT gates (if required) were used (note that, in this case, the AND gate placed on the transverse plane used by Hodgetts et al. was not used, as it did not appear to be required). The AND gate encompassed the body of the fornix, selected from a coronal view. This was approximately five voxels back from the anterior commissure, as identified on the sagittal plane. NOT gates were placed as follows: two on the transverse plane to intersect the corpus callosum and corticospinal tracts; two on the sagittal plane to intersect the anterior commissure and corpus callosum; and two on the coronal plane to intersect fibres travelling posteriorly towards the occipital cortex, or anteriorly towards the frontal cortex.

The protocol of Wakana et al. (2007) was used to isolate ILF streamlines. One 'seed', one AND and 4 NOT gates (if required) were used in each. In the sagittal plane, the coronal cross-hair was placed just posterior to the cingulum bundle. In the coronal plane, a 'seed' was drawn around the entire left/right cortex (for extraction of the left and right ILF, respectively). The AND gate was placed encompassing the temporal lobe, on the furthest posterior coronal slice in which a connection could not be seen between the temporal and frontal lobes. NOT gates were placed as follows: one on the transverse plane to intersect fibres reaching the parietal lobe; two on the sagittal plane to intersect fibres that crossed the midline; and one on the coronal plane to intersect fibres extending into the frontal cortex.

[11] https://www.exploredti.com/exampledataset.htm

The protocols of Jones et al. (2013) and Sibilia et al. (2017) were used to isolate streamlines representing the PHC (note that Jones et al. refer to this as the 'restricted PHC'). Two AND gates and one NOT gate were used. For the first AND gate, the corpus callosum was identified on a midline sagittal plane. The transverse plane cross-hair was placed approximately four slices above the bottom of the curve of the posterior corpus callosum and the AND gate was placed on the transverse plane, encompassing the cross section of the cingulum (Jones et al. 2013). The transverse plane was then moved to around four slices below the curve of the posterior corpus callosum and a second AND gate was placed on the transverse plane, encompassing a lower cross section of the cingulum (Jones et al. 2013). A NOT gate was placed on the sagittal plane transecting, and extending above, the posterior portion of the corpus callosum, to exclude any streamlines of the cingulum that curved forward (Sibilia et al., 2017). These steps were carried out bilaterally, to extract the left and right PHC.

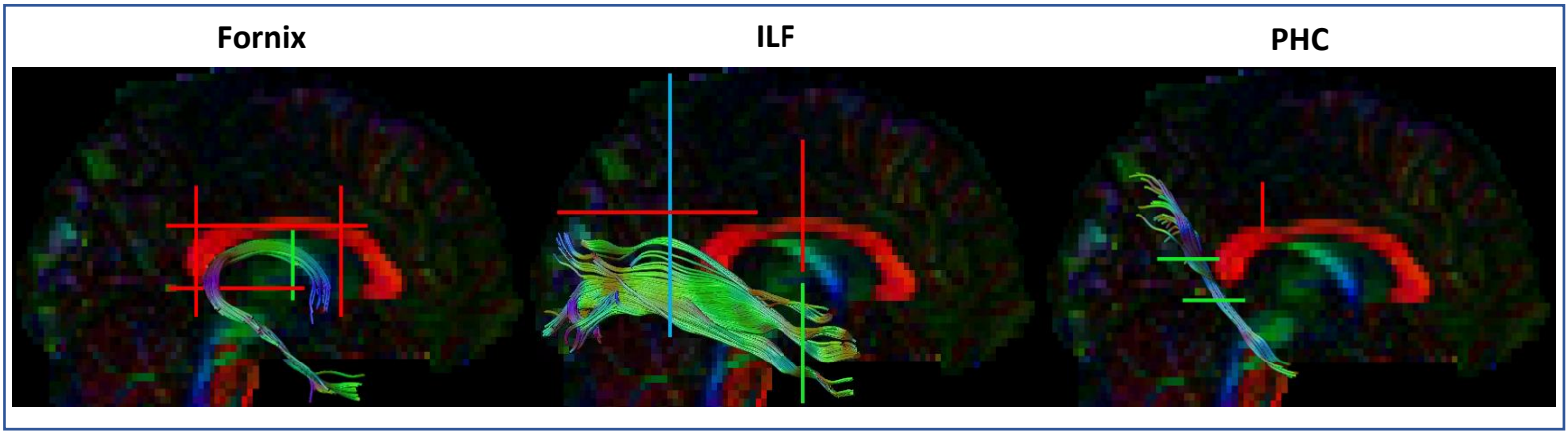

Figure 23. Construction of tract streamlines.

Sagittal views of the fornix (left), ILF (middle) and PHC (right) streamlines constructed in an example dataset. Right ILF and PHC tracts are shown, though they were extracted bilaterally. Colours on the brain map and the streamlines indicate diffusion along the gradient directions (left-right: red; top-bottom: blue; front-back: green). Example locations of the Boolean gates are represented by coloured lines (NOT: red, AND: green, SEED: blue).

The resultant tracts were used to train the in-house automated tractography software that was then applied to the entire dataset. Streamlines produced by the automated tractography software were visually inspected, and spurious fibres were removed using additional NOT gates.

5.2.4 Tract microstructure data reduction.

FA, MD, RD, FR, MPF, ICVF and OD values for the voxels encompassed in the tract streamlines were extracted and averaged for each tract. This resulted in seven microstructure metrics for three tracts for 39 participant datasets.

Redundancies in dMRI-derived microstructure measures can be exploited by dimensionality reduction, to collate data in a biologically interpretable way and to reduce the risk of false positive errors arising from multiple statistical comparisons (Chamberland et al., 2019). Therefore, microstructure data were reduced through PCA, which has been shown to be effective in capturing age-sensitive, biologically informative features from previous microstructure datasets (Chamberland et al., 2019; Geeraert et al., 2020). The tract microstructure data were combined in a single table. Correlations between the microstructure measures were explored. The Bartlett test was used to assess the appropriateness for PCA. The *prcmp* function in R (R Core Team, 2019) was then used to apply PCA to centred and scaled data (converted to z-scores). Sampling adequacy of the PCA results was tested using the Kaiser-Meyer-Olkin (KMO) test (from the R 'Psych' package; Revelle, (2020)). Components were retained depending on the amount of cumulative variation they explained and on inspection of the scree plot. Following data reduction, participant scores in two principal components (PCs) were used for analysis.

5.2.5 MEG analysis and creation of time- and trial- averaged ROI data, and trial-averaged VS data, for testing correlations with behavioural performance.

A detailed description of MEG data preprocessing, frequency analysis and source analysis, using Fieldtrip (Oostenveld et al., 2011), can be found in *Chapter 4*. In that analysis, power between conditions was stastically compared. In the current Chapter, the confirmatory analyses included the trial-averaged change in oscillatory powers for all three oddity task conditions measured relative to the fixation condition, as well as power differences between scene or face conditions compared to the size condition. The aim of the former was to understand how brain oscillatory activity during a task (compared with at rest) related to performance in that task. The fixation periods lasted 5 s, but to match the length of the task conditions (2 seconds), data from the period from one second to three seconds after the start of the fixation period was analysed. This was done to include a fixation period sufficiently distanced from the task trials to minimise the risk of including any carried-over task-dependent processes. Oscillatory power differences were averaged within PMN ROIs (HPC, PCC, mPFC and IPL) and the AIN ROI (FG). The additional FG VSs was constructed using the same techniques described in *Chapter 4*, using the left and right FG ROIs of the AAL atlas. Confirmatory analyses included inspecting the relationships between HPC theta and gamma power and scene oddity accuracy, and the relationship between FG gamma power and face oddity accuracy (controlling for MEG trial numbers, see below section 5.2.6).

In addition, averaged delta (1-4 Hz), alpha (8-12 Hz) and beta (13-30 Hz) HPC power, and broadband (1-90 Hz) HPC time-frequency data of the scene and face oddity tasks (both also contrasted with the fixation period) were tested for partial correlations with scene and face accuracy data (controlling for MEG trial numbers). This allowed investigation into whether the correlation between hippocampal theta and scene accuracy was specific to the theta range or to the right or left hemisphere. It also allowed exploration of the temporal dynamics of this relationship.

Lastly, the t-maps produced from statistically comparing oscillatory power between the conditions (scene>size, face>size, scene>face; described in *Chapter 4*) were also tested for partial correlations with scene and face oddity performance (controlling for MEG trial numbers). As it is akin to source-source subtraction (so MTL signals would have been less influenced from stronger more shallow sources, such as those from the occipital cortex), it may help to localize deep sources (see *Chapter 3* and Quraan et al., (2011)).

5.2.6 Statistical analysis.

Statistical analyses were carried out using Fieldtrip for MATLAB (MATLAB, 2015; Oostenveld et al., 2011), or using Rstudio (R Core Team, 2018; RStudio Team, 2015). Outliers were defined as being further than three times the SD from the mean and were removed per variable. The number of values entering each statistical test (N) is reported through degrees of freedom with the test statistics, or noted in results tables.

Pearson's correlation tests were applied to understand relationships between tract microstructure, oscillatory activity and behaviour. In cases where variable data did not have a normal distribution, the data was transformed to de-skew the distribution. To make the brain-behaviour correlations across conditions, tracts or ROIs comparable, it was important that the same, ideally parametric, tests could be applied to all and if one variable was transformed, the same was applied to the other variables within that modality.

To compare correlations, differences between correlation coefficients were tested using the Pearson and Filson's test (Pearson, 1897), with the package 'Cocor' for R (Diedenhofen & Musch, 2015).

Since the results of Hodgetts et al. (2015) showed correlations between fornix MD and scene oddity accuracy, and ILF MD and face oddity accuracy, and revealed trends between fornix FA and scene oddity accuracy, and ILF FA and face oddity accuracy, there were

directed hypotheses about correlations between microstructure and oddity task performance. Therefore, the contribution of FA and MD values to microstructure PCA components, prescribed the hypotheses of how the components of the tracts would relate to oddity task performance, supporting the use of one-tailed statistical tests.

Partial correlations were used for correlation analyses involving MEG data so that MEG trial numbers in each condition could be controlled for. MEG trials in which the participant did not respond were not included in the MEG analysis, but were regarded as incorrect in the behavioural data. Since an aim of this study was to capture predominantly perceptual processes, and since participants had a long time in which to respond (8 s) and on average, took around 5s, there was a risk that trials not answered within 8 s would contain off-task thoughts, such as those pertaining to mind-wandering or exhaustion. Therefore, trials without responses were not included in the MEG analysis. However, missed trials could not be removed from the behaviour analysis without artificially inflating performance scores of participants with missing trials, because of the high likelihood that missing trials would have been answered incorrectly. Although this is a small proportion of excluded MEG trials (MEG trials were also removed due to length criteria and noise during data-cleaning), there was still an association between the number of MEG trials and oddity performance. Therefore, partialling-out the variance from MEG trial numbers was performed to adjust for its potential biasing of performance-MEG data correlations. Importantly, tests for correlations between the MEG data and the number of MEG trials produced no significant results (these are reported in *Appendix 2A)*.

Multiple-comparisons correction was not carried out considering the number of tests in total, which may have resulted in false negatives from overly strict correction. For the microstructure-behavioural correlation tests, the alpha level was Bonferroni-corrected by dividing by the number of statistical comparisons involving each individual DTI measure (0.05/3 oddity accuracy measures = 0.017; Hodgetts et al. 2015). This rule was also used for the oscillatory power-behavioural correlation tests and oscillatory power-microstructure correlation tests inasmuch as the alpha level was Bonferroni-corrected by dividing by the number of statistical comparisons involving each individual DTI measure or oscillatory variable. Similarly, when comparing correlation coefficients, the alpha level was Bonferroni-corrected by dividing by the number of statistical comparisons relating to a variable (0.05/2 = 0.025). For the tests involving memory performance, the alpha level was Bonferroni-corrected according the to the number of conditions (0.05/2 = 0.025).

Some of the hypotheses in this project were that specific phenomena should *not* occur. For example, it was hypothesized that ILF microstructure should not relate to scene oddity performance, a hypothesis that cannot be supported using inferential statistics. Therefore, for analyses that pertain to this kind of hypotheses, inferential statistics are accompanied by BFs from equivalent Bayesian tests. BFs were calculated using the BayesFactor package in R (Morey & Rouder, 2018), and were reported as BF_{10} (evidence of the alternative model over the null model).

Exploratory analyses were included to ask whether correlations found between structure, function and oddity performance, in the confirmatory analyses, were specific to the tract or ROI. Therefore, despite the fact that a whole-brain search should require multiple comparison correction, the traditional alpha level of 0.05 was retained so that the relative importance of the tract or ROI investigated in the confirmatory analyses, was not exaggerated by the use of a stricter alpha threshold in the exploratory analyses. In light of this leniency, the results obtained from exploratory analysis were interpreted only as complementary to the confirmatory analyses or for consideration for future investigations.

Additionally, exploratory searches for correlations between scene and face oddity accuracy and whole-brain t-maps of theta/low gamma/high gamma power differences between conditions were carried out using, partial correlation tests, with Monte Carlo sampling and 5000 permutations. These controlled for the trial numbers of each condition. Both the alpha and cluster alpha thresholds were set at the traditional alpha level of 0.05.

Plots were drawn using several R packages. Visualization of the correlation matrices was achieved using *ggcorrplot* (Kassambara, 2019). For the PCA results, *stats* (R Core Team, 2019) and *ggplot2* (Wickham, 2016) were used. To visualize correlation plots, with histograms *ggstatsplot* (Patil, 2021) was used.

5.3 Results.

5.3.1 Further examination of the oddity behavioural data.

Performance across the conditions was well matched, with similar mean and SD values (see *Chapter 4* and summary statistics in Table 4). RT across conditions was not as well matched (scene RT > face RT > size RT; see *Chapter 4*).

The scene performance data had a right skew. To reduce the skew, so that parametric tests could be used while keeping the conditions matched, all accuracy data was squared (McDonald, 2014). This resulted in a coefficient of skewness of less than 1 for the scene performance data but did not cause the coefficients of skewness of the face and size performance data to exceed +/-1. These transformed accuracy values were used for subsequent parametric tests and (except when stated otherwise) the terms 'scene accuracy', 'face accuracy' and 'size accuracy' in the results section of this chapter refer to the transformed conditions.

	Scene Accuracy, untransformed (%)	Face Accuracy, untransformed (%)	Size Accuracy, untransformed (%)	Scene Accuracy, squared	Face Accuracy, squared	Size Accuracy, squared
Mean	60.87	60.78	61.35	3754.64	3768.77	3927.25
SD	7.08	8.74	12.97	807.59	1062.13	1580.89
Minimum	38.95	39.58	29.17	1516.90	1566.84	850.70
Maximum	70.53	80.21	89.58	4973.96	6433.38	8025.17
Skew	-1.12	-0.08	-0.16	-0.84	0.40	0.42

Table 4. Descriptive statistics of the transformed oddity task performance results.

SD: Standard Deviation.

Pearson's correlation tests revealed significant correlations between scene and face accuracy ($r = 0.317$, $p = 0.046$) and between scene and size accuracy ($r = 0.343$, $p = 0.030$), but not between face and size accuracy ($r = 0.179$, $p = 0.270$). There were also significant correlations between scene and face RT ($r = 0.691$ $p < 0.001$), scene and size RT ($r = 0.645$, $p < 0.001$), and face and size RT ($r = 0.682$, $p < 0.001$). However, there were no significant

correlations between condition accuracies and condition RTs (all p-values >0.05). The lack of correlations between accuracy and RT indicated that there were no clear speed-accuracy trade-offs so creating integrated measures, such as inverse efficiency scores would not be appropriate (Bruyer & Brysbaert, 2011; Townsend & Ashby, 1978). Therefore, accuracy and RT were inspected separately. A graphical summary is shown in Figure 24.

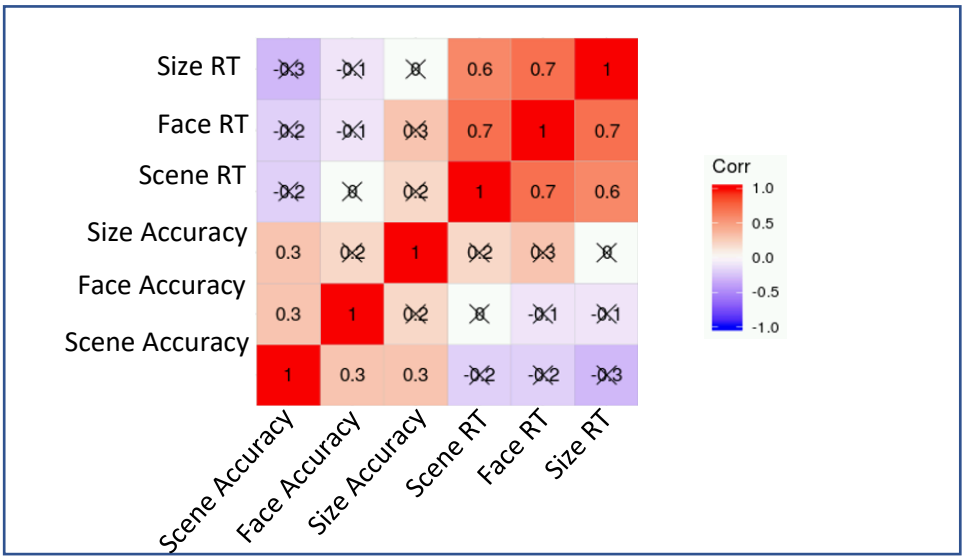

Figure 24. Graphical summary of the Pearson's correlation statistics between oddity performance and RT within and between the scene face and size conditions.

Numbers and box-colours represent r values, according to the key on the right. Crossed-out boxes represent relationships whose corresponding p-values were above the traditional alpha level of 0.05. Note that this is not Bonferroni-corrected, as this is a hypothesis-free exploration of the data.

RT: Reaction Time.

5.3.2 Tract microstructure.

The microstructure measures were averaged over each tract streamlines construction, resulting in seven measures each for the fornix, ILF and PHC, for each participant. Details of the microstructure measures across the group are shown in Table 5.

	Fornix		**ILF**		**PHC**	
	Group mean	**SD**	**Group mean**	**SD**	**Group mean**	**SD**
FA	0.72	0.03	0.78	0.03	0.64	0.05

MD	0.09 $x10^{-2}$	0.03 $x10^{-3}$	0.07 $x10^{-2}$	0.01 $x10^{-3}$	0.07 $x10^{-2}$	0.002 $x10^{-3}$
RD	0.07 $x10^{-2}$	0.03 $x10^{-3}$	0.05 $x10^{-2}$	0.01 $x10^{-3}$	0.06 $x10^{-2}$	0.002 $x10^{-3}$
FR	0.24	0.01	0.33	0.02	0.25	0.02
MPF	0.08	0.01	0.14	0.01	0.12	0.01
ICVF	0.56	0.03	0.52	0.02	0.48	0.02
OD	0.15	0.01	0.17	0.01	0.21	0.03

Table 5. Group means and SDs for each microstructure value, for each tract.

Microstructure values are averaged over tract streamlines for each participant. Means and SDs of microstructure values, across the group, for the three tracts of interest are shown.

FA: Fractional Anisotropy. FR: Restricted Fraction. ICVF: Intracellular Volume Fraction. ILF: Inferior Longitudinal Fasciculus. MD: Mean Diffusivity. MPF: Molecular Proton Fraction. OD: Orientation Dispersion. PHC: Parahippocampal Cingulum. RD: Radial Diffusivity. SD: Standard Deviation.

The results from the PCA (KMO: 0.66, sphericity: $p<0.0001$) showed that 94% of the microstructure data variance was accounted for by the first two principal components, PC1 and PC2. PC1 accounted for 56% of the variance with MD and RD providing the major negative contributions, while FR and MPF provided the major positive contributions (Table 6; Figure 25B). This is similar to the first component found in Chamberland et al. (2019), and therefore PC1 was interpreted as positively relating to a 'restriction' property of the fibre (the proclivity for water movement along the fibres as opposed to other dispersed directions). It was hypothesized that tract PC1 would relate positively to oddity performance. PC2 accounted for 38% of the variance, with FA and ICVF providing the major negative contributions, while OD provided a major positive contribution (Table 6). Since OD is lower in tracts known to have more fibre coherency and higher in tracts known to have more fibre fanning and crossing (Zhang et al., 2012), and FA can be influenced by how coherently fibres within a voxel are organised (Pierpaoli et al., 1996; Jones et al., 2013), PC2 was interpreted as negatively relating to a 'coherence' property of the fibre (the dispersion of modelled fibre orientations). It was hypothesized that PC2 would relate negatively to oddity performance. The relative differences between the scores of the tracts are illustrated in Figure 25C.

	PC1	PC2
FA	0.16	-0.56
MD	-0.48	-0.17
RD	-0.50	0.01
FR	0.42	-0.32
MPF	0.48	0.12
OD	0.16	0.55
ICVF	-0.23	-0.48

Table 6. PCA microstructure measure weightings.

FA: Fractional Anisotropy. FR: Restricted Fraction. ICVF: Intracellular Volume Fraction. MD: Mean Diffusivity. MPF: Molecular Proton Fraction. OD: Orientation Dispersion. PC: Principal Component. RD: Radial Diffusivity.

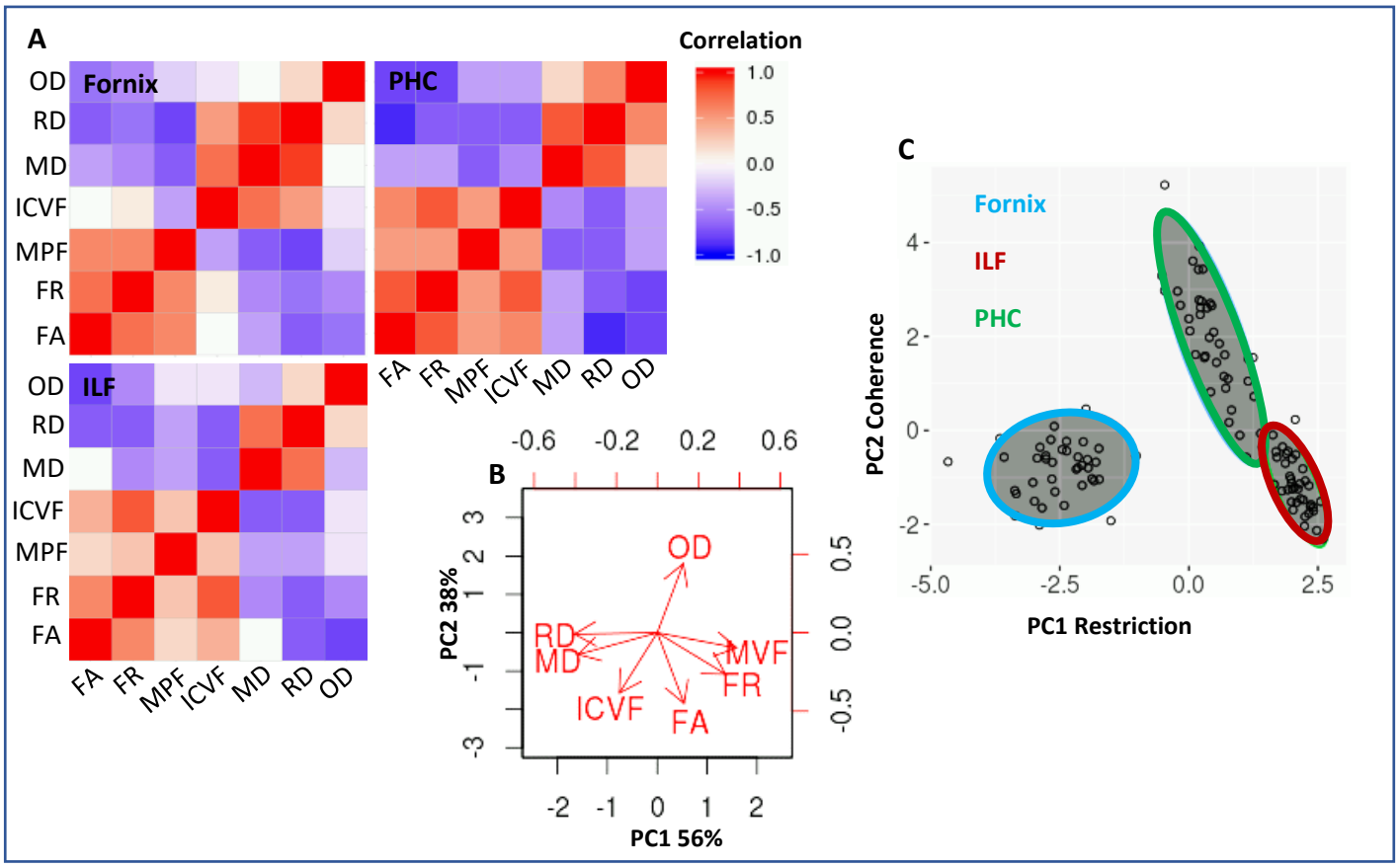

Figure 25. Redundancy between tract diffusion values and results from PCA.

A) Pearson's correlations within the microstructure data from each tract suggest that the values give overlapping information (generated using ggcorrplot, Alboukadel, 2019). Colour denotes r value according to the key. B) Biplot illustrating the influence of each of the measures on PC1 and PC2, which account for 56% and 38% of the variance, respectively. C) Tract component scores for each participant, illustrating the differing properties of the tracts.

FA: Fractional Anisotropy. FR: Restricted Fraction. ICVF: Intracellular Volume Fraction. ILF: Inferior Longitudinal Fasciculus. MD: Mean Diffusivity. MPF: Molecular Proton Fraction. OD: Orientation Dispersion. PC: Principal Component. PHC: Parahippocampal Cingulum. RD: Radial Diffusivity.

5.3.3 Associations between structure, function and oddity task performance.

5.3.3.1 Correlations between oddity accuracy and tract microstructure.

As predicted, there was a significant positive correlation between face oddity accuracy and ILF PC1 and a significant negative correlation between face oddity accuracy and ILF PC2 (Figure 26), which were supported by BFs indicating weak evidence in favour of the alternative models over the null models. Moreover, neither ILF component measure correlated with scene or size oddity accuracy (Table 7).

It was predicted that there would be a positive correlation between fornix PC1 and scene oddity accuracy. Although this trend did not surpass the experiment-wise alpha level (Figure 26), the resulting BF indicated weak evidence in favour of the alternative model over the null model. In addition, neither fornix microstructure component correlated with face or size oddity accuracy. Contrary to the hypothesis, fornix PC2 did not negatively correlate with scene oddity accuracy (Table 7).

It was hypothesized that PHC microstructure would not relate to any oddity task performance. Indeed, all of the correlations surpassed the experiment-wise alpha level (Table 7). However, for the correlations between face oddity accuracy and PHC components, the BFs indicated weak evidence in favour of the alternative over the null models. For the correlations between scene and size oddity accuracy and PHC components, the BFs indicated evidence in favour of the null models.

		Scene Accuracy	Face Accuracy	Size Accuracy
Fornix	PC1	r = 0.321 p = 0.023 BF_{10} = 2.05	r = 0.243 p = 0.068 BF_{10} = 0.94	r = -0.035 p = 0.585 BF_{10} = 0.36
	PC2	r = 0.057 p = 0.635 BF_{10} = 0.38	r = -0.090 p = 0.292 BF_{10} = 1.27	r = 0.088 p = 0.702 BF_{10} = 0.40
ILF	PC1	r = 0.100 p = 0.272 BF_{10} = 0.42	r = 0.349 p = 0.014* BF_{10} = 2.84	r = -0.037 p = 0.589 BF_{10} = 0.36

PHC	PC2	r = -0.119 p = 0.236 BF_{10} = 0.45	r = -0.340 p = 0.017* BF_{10} = 2.58	r = 0.170 p = 0.849 BF_{10} = 0.57
	PC1	r = 0.053 p = 0.372 BF_{10} = 0.37	r = 0.294 p = 0.034 BF_{10} = 1.52	r = 0.180 p = 0.136 BF_{10} = 0.61
	PC2	r = -0.03 p = 0.427 BF_{10} = 0.36	r = -0.258 p = 0.057 BF_{10} = 1.07	r = -0.106 p = 0.260 BF_{10} = 0.43

Table 7. Correlation tests between oddity task performance and Fornix, ILF and PHC microstructure components.

One-tailed Pearson's correlation tests, and undirected Bayesian correlation tests, between fornix, ILF and PHC microstructure, and oddity accuracy.
*Highlights p≤0.017. *Highlights a $BF_{10} \geq 3$. N=39.

ILF: Inferior Longitudinal Fasciculus. PC: Principal Component. PHC: Parahippocampal Cingulum.

There was partial support for dissociability of the correlations. The coefficient of the correlation between fornix PC1 and scene oddity accuracy was significantly larger than that of the correlations between fornix PC1 and size oddity accuracy ($z_{(36)}$ = 2.019, p = 0.022). However, it was not larger than that of the correlations between fornix PC1 and face oddity accuracy ($z_{(36)}$ = 0.442, p = 0.329). Similarly, the correlation coefficient between ILF PC1 and face oddity accuracy was significantly larger than that of the correlation between ILF PC1 and size oddity accuracy ($z_{(36)}$ = 1.991, p = 0.023), but was not larger than that of the correlation between ILF PC1 and scene oddity accuracy ($z_{(36)}$ = 1.390, p = 0.082). Also, coefficient of the correlation between fornix PC1 and scene oddity accuracy was not significantly larger than that of the correlation between PHC PC1 and scene oddity accuracy ($z_{(36)}$ = 1.454, p = 0.146).

Multiple linear regression was also used to assess whether fornix microstructure was specific in its relationship with scene oddity accuracy or whether ILF and PHC microstructure also contributed. A model with fornix PC1, PHC PC1, ILF PC1 did not significantly predict scene oddity accuracy (adjusted R^2 = 0.029, p = 0.267) but fornix PC1 was an independent predictor (p = 0.031, one-tailed).

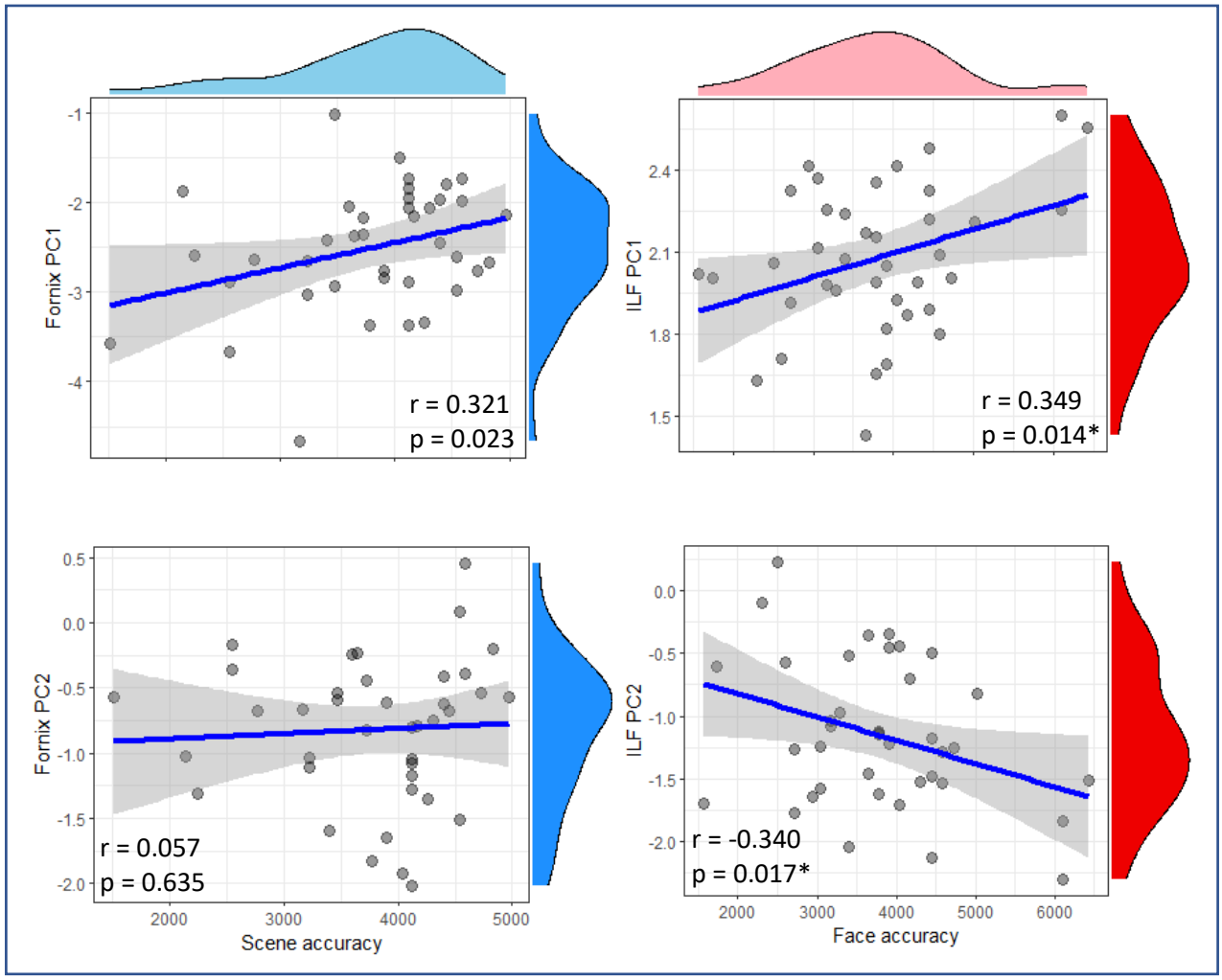

Figure 26. Scatterplots showing the relationship between fornix and ILF microstructure, and scene and face oddity performance.

The mid-blue histograms show the distribution of the fornix PC1 data (top) and fornix PC2 data (bottom). The red histograms show the distributions of the ILF PC1 data (top) and ILF PC2 data (bottom). The light blue histogram shows the distribution of the scene accuracy data and the light pink histogram shows the face accuracy data. The blue lines are the regression lines and surrounding shaded areas represent the 95% confidence interval. Note that the accuracy data has been transformed to normal. *Highlights p≤0.017.

ILF: Inferior Longitudinal Fasciculus. PC: Principal Component.

5.3.3.2 Investigating relationships between oddity RT and tract microstructure.

There were no significant correlations between fornix or ILF microstructure and oddity RTs (Table 8). However, the BF indicated weak evidence in favour of a correlation between face RT and ILF PC1.

		Scene RT	Face RT	Size RT
Fornix	PC1	r = -0.059 p = 0.362 BF_{10} = 0.37	r = -0.111 p = 0.250 BF_{10} = 0.43	r = 0.020 p = 0.547 BF_{10} = 0.36
	PC2	r = -0.194 p = 0.882 BF_{10} = 0.66	r = 0.148 p = 0.816 BF_{10} = 0.51	r = 0.020 p = 0.548 BF_{10} = 0.36
ILF	PC1	r = -0.171 p = 0.150 BF_{10} = 0.57	r = -0.319 p = 0.024 BF_{10} = 1.99	r = -0.020 p = 0.453 BF_{10} = 0.36
	PC2	r = -0.030 p = 0.573 BF_{10} = 0.36	r = 0.189 p = 0.125 BF_{10} = 0.64	r = 0.011 p = 0.473 BF_{10} = 0.36
PHC	PC1	r = 0.011 p = 0.528 BF_{10} = 0.36	r = -0.199 p = 0.113 BF_{10} = 0.68	r = -0.038 p = 0.410 BF_{10} = 0.36
	PC2	r = 0.097 p = 0.278 BF_{10} = 0.42	r = 0.238 p = 0.073 BF_{10} = 0.91	r = 0.001 p = 0.498 BF_{10} = 0.36

Table 8. Relationships between oddity RT and microstructure components of the fornix and the ILF.

One-way Pearson's correlation tests, and undirected Bayesian correlation tests, between fornix, ILF and PHC microstructure, and oddity RT.
*Highlights p≤0.017. *Highlights a $BF_{10} \geq 3$. N=39.

ILF: Inferior Longitudinal Fasciculus. PC: Principal Component. PHC: Parahippocampal Cingulum. RT: Reaction Time.

5.3.3.3 Inspecting the relationships between oddity performance and theta and gamma power in the HPC ROI.

It was hypothesized that scene task HPC theta (4-8 Hz) power difference (between task and fixation) would be correlated with scene task accuracy. This trend was apparent. The p-value of the correlation exceeded the experiment-wise alpha level, but the BF indicated evidence in favour of the alternative model. As predicted, significant correlations were not found between face task HPC theta difference and face accuracy, or between size task HPC theta difference and size oddity accuracy. Furthermore, the BFs indicated evidence in favour of the null models (Table 9).

Contradictory to the hypothesis, neither low (40-60 Hz) nor high (60-80 Hz) HPC gamma power difference (between task and fixation) in the scene task correlated with scene oddity accuracy. Significant correlations were also not found between face task HPC gamma difference and face oddity accuracy, or between size task HPC gamma difference and size oddity accuracy (Table 9). Scatter plots showing the relationships between HPC theta, and scene and face oddity accuracy, are shown in Figure 27.

	Scene accuracy	**Face accuracy**	**Size accuracy**
HPC theta power difference (task vs fixation) (N=40)	r = -0.374 p = 0.019 BF_{10} = 4.24*	r = 0.084 p = 0.612 BF_{10} = 0.40	r = 0.051 p = 0.756 BF_{10} = 0.37
HPC low gamma power difference (task vs fixation) (N=38)	r = -0.054 p = 0.750 BF_{10} = 0.38	r = -0.182 p = 0.281 BF_{10} = 0.61	r = -0.025 p = 0.883 BF_{10} = 0.36
HPC high gamma power difference (task vs fixation) (N=38)	r = -0.034 p = 0.841 BF_{10} = 0.37	r = -0.301 p = 0.070 BF_{10} = 1.58	r = -0.097 p = 0.567 BF_{10} = 0.42

Table 9. Relationships between oddity accuracy and HPC theta, low gamma and high gamma power during task compared to fixation.

Partial correlation tests, and Bayesian correlation tests, between HPC theta and gamma power (task vs fixation) and oddity accuracy.
*Highlights p≤0.017. *Highlights a $BF_{10} \geq 3$. N differs in each row due to outlier deletion.

HPC: Hippocampal Complex.

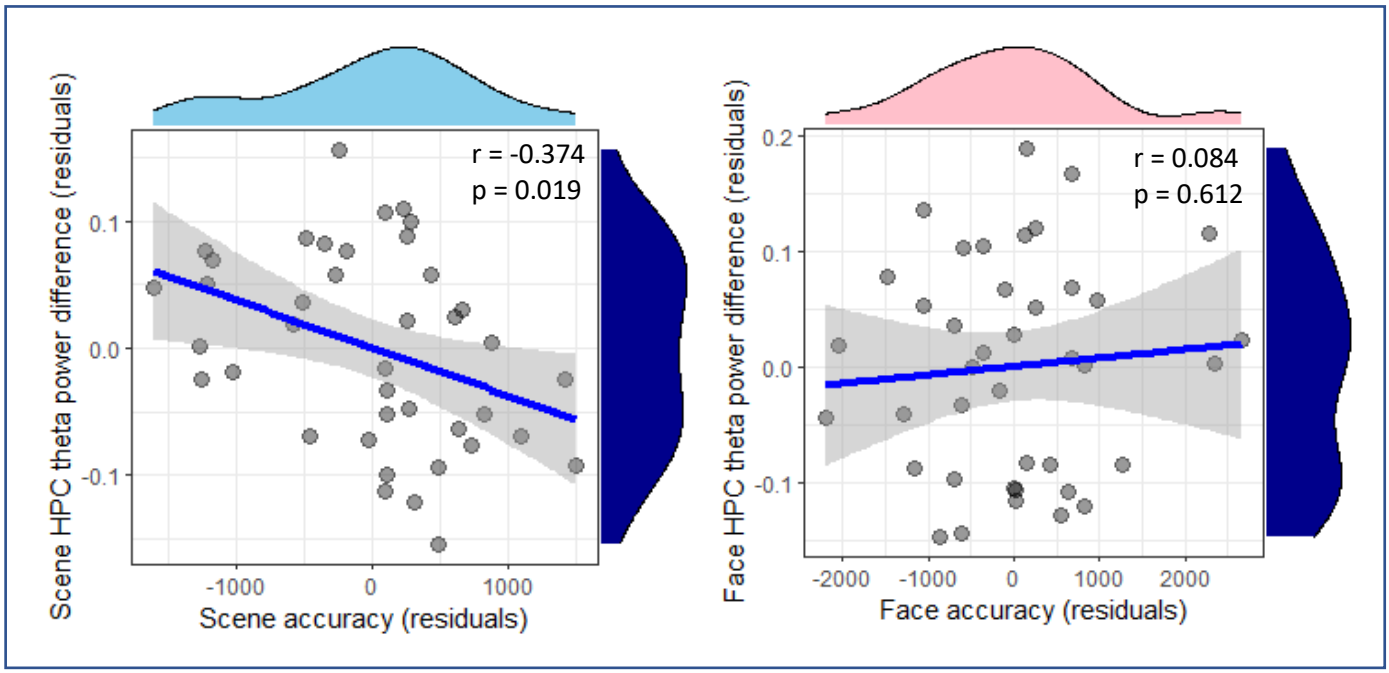

Figure 27. Relationships between scene and face oddity task accuracy and HPC theta power difference between task and fixation, with MEG trial number partialled out.

The light blue histogram shows the distribution of the residuals of the scene accuracy data, and the light pink histogram shows the distributions of the residuals of the face accuracy data. The dark blue histograms show the distributions of the residuals of the HPC theta difference for scene vs fixation (left) and face vs fixation (right). The blue lines are the regression lines and surrounding shaded areas represent the 95% confidence interval. Note that the accuracy data was transformed to normal.

HPC: Hippocampal Complex.

HPC theta power difference, between scene and size, in the scene task did not correlate with scene oddity accuracy. Significant correlations were also not found between face task HPC theta difference (between face and size) and face oddity accuracy (Table 10).

There was, however, weak evidence for a trend between scene oddity accuracy and HPC high gamma power difference, between scene and size, but the p-value of the correlation exceeded the experiment-wise alpha level (Table 10).

	Scene accuracy	Face accuracy
HPC theta power difference (scene/face vs size)	r = 0.071 p = 0.667 BF_{10} = 0.38	r = -0.008 p = 0.962 BF_{10} = 0.35
HPC low gamma power difference (scene/face vs size)	r = 0.110 p = 0.504 BF_{10} = 0.43	r = -0.047 p = 0.778 BF_{10} = 0.37
HPC high gamma power difference (scene/face vs size)	r = 0.338 p = 0.035 BF_{10} = 2.62	r = -0.015 p = 0.929 BF_{10} = 0.35

Table 10. Relationships between oddity accuracy and HPC theta, low gamma and high gamma power during scene or face tasks compared to size task.

Partial correlation tests, and Bayesian correlation tests, between HPC theta and gamma power (scene/face vs size) and oddity accuracy.
*Highlights p≤0.017. *Highlights a $BF_{10} \geq 3$. N=40.

HPC: Hippocampal Complex.

There was partial support for dissociability of the correlations. The coefficient of the correlation between the scene HPC theta power difference (compared with fixation) and scene oddity accuracy was significantly stronger than that of the correlation between face HPC theta power difference (compared with fixation) and face oddity accuracy ($z_{(37)}$ = -2.607, p = 0.009). However, the p-value for the test between the coefficient of the correlation between the scene HPC theta power difference (compared with fixation) and scene oddity, and that of the correlation between size HPC theta power difference and size oddity accuracy, exceeded the experiment-wise alpha level ($z_{(37)}$ = -2.204, p = 0.028).

The coefficient of the correlation between the scene HPC high gamma power difference (compared with size) and scene oddity was not significantly larger than that of the correlation between face HPC high gamma power difference (compared with size) and face oddity accuracy ($z_{(37)}$ = 1.859, p = 0.063).

5.3.3.4 Investigating three-part relationships between scene oddity performance, HPC theta power and fornix microstructure.

It was hypothesized that there would be a three part-relationship between HPC oscillatory activity, fornix microstructure and scene task accuracy. Correlations were found between HPC theta difference (compared with fixation) in the scene task and scene accuracy, and between fornix PC1 and scene accuracy but fornix PC1 did not significantly correlate with HPC theta difference in the scene task (Table 11).

However, there was a negative correlation between fornix PC2 and scene HPC theta difference (compared to fixation) and the corresponding the BF indicated evidence in favour of the alternative model (Table 11). In line with the hypothesis, this correlation coefficient was significantly stronger than those of the correlations between ILF PC2 and scene HPC theta power difference ($z_{(36)}$ = -2.585, p = 0.010), and between PHC PC2 and scene HPC theta power difference ($z_{(36)}$ = --2.335, p = 0.020). However, this correlation coefficient was not stronger than those of the correlations between fornix PC2 and face HPC theta power difference ($z_{(36)}$ = -1.661, p = 0.097) or size HPC theta power difference ($z_{(36)}$ = -0.636, p = 0.548). Indeed, there was weak evidence supporting trends between fornix PC2 and face and size HPC theta difference (compared to fixation).

As predicted, there were no significant correlations between ILF or PHC microstructure and theta power differences in any of the conditions (Statistics shown in *Appendix 2B).*

		Scene HPC theta power difference	Face HPC theta power difference	Size HPC theta power difference
Fornix	PC1	r = -0.162 p = 0.331 BF_{10} = 0.55	r = -0.295 p = 0.072 BF_{10} = 1.56	r = -0.193 p = 0.246 BF_{10} = 0.65
	PC2	r = -0.389 p = 0.016 * BF_{10} = 4.89 *	r = -0.277 p = 0.093 BF_{10} = 1.28	r = -0.355 p = 0.029 BF_{10} = 2.91

Table 11. Relationships between HPC theta power difference (compared to fixation), and fornix microstructure.

Partial correlation tests, and Bayesian correlation tests, between HPC theta power (task vs fixation) and tract microstructure
*Highlights p≤0.017. *Highlights a $BF_{10} \geq 3$. N=39.

HPC: Hippocampal Complex. PC: Principal Component.

5.3.3.5 *Investigating three-part relationships between face oddity performance, FG gamma power and ILF microstructure.*

Contradictory to the hypothesis, neither low nor high FG gamma power difference (compared with fixation), during the face task, significantly correlated with face task accuracy. Similarly, were there no significant correlations between high or low FG gamma power difference (compared with fixation) during the face task, and either of the ILF components (Table 12).

	Scene accuracy	Face accuracy	Size accuracy	ILF PC1	ILF PC2
FG low gamma power difference (task vs fixation)	r = -0.035 p = 0.832 BF_{10} = 0.36	r = -0.225 p = 0.169 BF_{10} = 0.83	r = -0.002 p = 0.992 BF_{10} = 0.35	r = -0.185 p = 0.266 BF_{10} = 0.62	r = 0.223 p = 0.178 BF_{10} = 0.81
FG high gamma power difference (task vs fixation)	r = 0.032 p = 0.848 BF_{10} = 0.36	r = -0.232 p = 0.156 BF_{10} = 0.88	r = -0.039 p = 0.817 BF_{10} = 0.36	r = -0.289 p = 0.078 BF_{10} = 1.44	r = 0.159 p = 0.340 BF_{10} = 0.54

Table 12. Relationships between low and high FG gamma power (task vs fixation), oddity accuracy and ILF microstructure.

Partial correlation tests, and Bayesian correlation tests, between FG gamma power difference (task vs fixation) and oddity accuracy (N=40), and between FG gamma power difference and ILF microstructure (N=39).
*Highlights p≤0.017. *Highlights a $BF_{10} \geq 3$.

FG: Fusiform Gyrus. ILF: Inferior Longitudinal Fasciculus.

Contradictory to the hypothesis, neither low nor high FG gamma power difference (compared with size), during the face task, significantly correlated with face task accuracy (Table 13).

	Scene accuracy	Face accuracy
FG low gamma power difference (scene/face vs size)	r = 0.089 p = 0.591 BF_{10} = 0.40	r = 0.051 p = 0.760 BF_{10} = 0.37
FG high gamma power difference (scene/face vs size)	r = 0.314 p = 0.052 BF_{10} = 1.95	r = 0.013 p = 0.940 BF_{10} = 0.35

Table 13. Relationships between low and high FG gamma power (task vs size) and oddity accuracy.

Partial correlation tests, and Bayesian correlation tests, between FG gamma power difference (scene/face vs size) and oddity accuracy.
*Highlights p≤0.017. *Highlights a $BF_{10} \geq 3$. N=40.

FG: Fusiform Gyrus.

A graphical summary of the main results is shown in Figure 28.

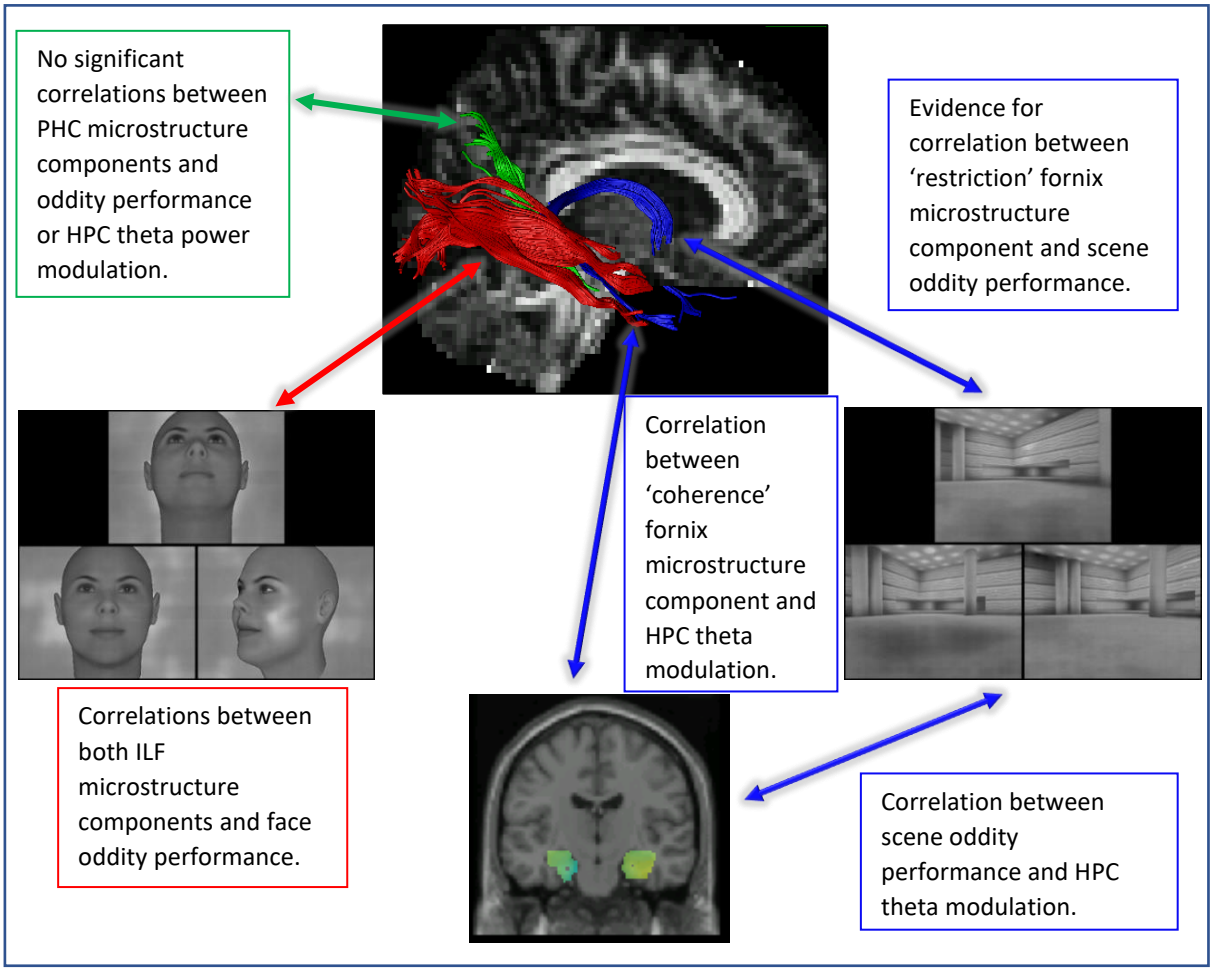

Figure 28. Graphical summary of findings of correlations between structure, function and behaviour.

No associations were found between PHC (green tract) microstructure and oddity performance or between PHC microstructure and HPC oscillatory power differences, between scene task and fixation (green arrow). There were correlations between ILF (red tract) microstructure and face oddity performance (red arrow). There was evidence for correlations between fornix (blue tract) PC1 and scene oddity performance, between fornix PC2 and HPC theta power difference between scene and fixation, and between scene oddity performance and theta power difference between scene and fixation (blue arrows).

(The brain image was made using ExploreDTI and an example dataset (Leemans et al., 2009)).

HPC: Hippocampal Complex. ILF: Inferior Longitudinal Fasciculus. PHC: Parahippocampal Cingulum.

5.3.4 Exploratory searches for associations between structure, function and oddity accuracy.

5.3.4.1 Investigating relationships between other PMN ROIs and whole-brain power modulations, task accuracy and tract microstructure.

An exploratory examination of the relationships between theta power differences (compared with fixation) in other PMN ROI data and task accuracy revealed no further significant correlations. However, there was a negative trend between scene PCC theta power difference and scene oddity accuracy (Table 14). Although the p-value of this trend exceeded the experiment-wise alpha level, the correlation coefficient was significantly stronger than that of the correlation between face PCC theta difference and face oddity accuracy ($z_{(37)}$ = -2.618, p = 0.009), and it was also significantly stronger than that of the correlation between size PCC theta difference and size oddity accuracy ($z_{(37)}$ = -2.348, p = 0.019). Similarly, there was a negative trend between scene PCC low gamma power difference and scene oddity accuracy, but this correlation coefficient was not significantly stronger than those of the correlations between face PCC low gamma difference and face oddity accuracy, or size PCC low gamma difference and size oddity accuracy (p values >0.05).

	Scene accuracy	**Face accuracy**	**Size accuracy**
mPFC theta power difference (task vs fixation) (N=40)	r = 0.057 p = 0.731	r = 0.173 p = 0.292	r = 0.179 p = 0.275
PCC theta power difference (task vs fixation) (N=40)	r = -0.337 p = 0.036	r = 0.139 p = 0.423	r = 0.069 p = 0.675
IPL theta power difference (task vs fixation) (N=40)	r = -0.138 p = 0.401	r = 0.192 p = 0.245	r = -0.046 p = 0.779
mPFC low gamma power difference (task vs fixation) (N=37)	r = -0.092 p = 0.603	r = -0.004 p = 0.982	r = -0.065 p = 0.717
PCC low gamma power difference (task vs fixation) (N=37)	r = -0.343 p = 0.046	r = -0.124 p = 0.486	r = -0.292 p = 0.094
IPL low gamma power difference (task vs fixation) (N=35)	r = -0.185 p = 0.296	r = 0.147 p = 0.407	r = -0.309 p = 0.075
mPFC high gamma power difference (task vs fixation) (N=35)	r = 0.066 p = 0.702	r = -0.156 p = 0.362	r = -0.257 p = 0.130

PCC high gamma power difference (task vs fixation) (N=35)	r = -0.050 p = 0.772	r = 0.020 p = 0.910	r = -0.163 p = 0.344
IPL high gamma power difference (task vs fixation) (N=35)	r = 0.001 p = 0.997	r = -0.155 p = 0.366	r = -0.085 p = 0.621

Table 14. Correlation tests between PMN ROI theta and gamma power, and oddity accuracy.

Partial correlation tests between PMN ROI theta power (task vs fixation) and oddity accuracy.
No significant correlations were found. N values shown on each row and differed due to outlier removal.

IPL: Inferior Parietal Lobule. mPFC: Medial Prefrontal Cortex. PCC: Posterior Cingulate Cortex.

There were no significant correlations between scene mPFC, PCC or IPL theta power and fornix microstructure (Table 15).

	Fornix	
	PC1	***PC2***
Scene mPFC theta	r = 0.002 p = 0.992	r = -0.169 p = 0.310
Scene PCC theta	r = -0.254 p = 0.123	r = -0.208 p = 0.211
Scene IPL theta	r = 0.006 p = 0.972	r = -0.325 p = 0.047

Table 15. Correlation tests between PMN ROI theta and gamma power, and fornix microstructure.

Partial correlation tests between PMN ROI theta power (scene vs fixation) and tract microstructure.

IPL: Inferior Parietal Lobule. mPFC: Medial Prefrontal Cortex. PC: Principal Component. PCC: Posterior Cingulate Cortex.

5.3.4.2 Whole-brain search for negative theta power modulations and scene oddity accuracy correlations.

To see if the negative correlation between theta power and scene oddity accuracy was specific to the HPC, a one-sided whole-brain search for negative correlations between theta power difference (compared with fixation) and scene task accuracy was carried out (while controlling for the number of MEG trials in each condition). In accordance with the result of the confirmatory correlation analysis focusing on the HPC ROI, a large cluster where theta power difference in the scene task negatively correlated with scene oddity accuracy was

revealed (cluster p = 0.048). This encompassed several posteromedial areas, including bilateral MTL, bilateral inferior temporal lobe, precuneus and the PCC (Figure 29). No significant clusters were found for equivalent partial correlation tests between theta power

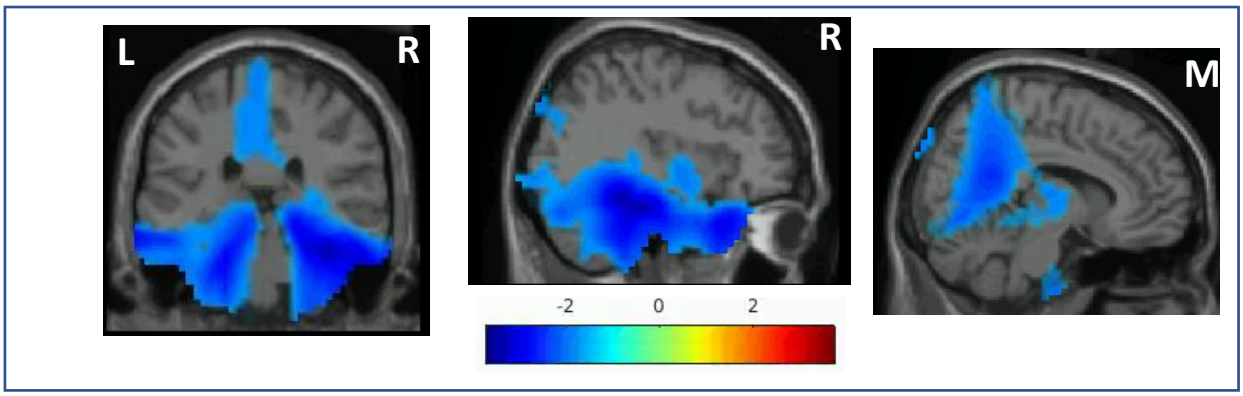

Figure 29. Relationships between theta power difference (compared with fixation) and scene accuracy.

Negative relationships were found in bilateral medial and inferior temporal lobes, the right hippocampus and the PCC. Colours represent t-values, and the scale is shown below the middle image (alpha threshold = 0.05). L = left. R = right. M = mid-line.

differences during face or size conditions, and face and size oddity accuracy.

5.3.4.3 Investigating relationships between task accuracy and differences between scene and face whole-brain theta and gamma oscillatory power.

Source-source subtraction can aid localization of oscillatory activity from deep sources in MEG (see *Chapter 2*). Therefore, associations between whole-brain power t-map differences between the conditions (see *Chapter 4*), and scene and face oddity accuracies, were also explored (while controlling for the number of MEG trials in each condition).

Partial correlation tests between scene oddity accuracy and scene vs size theta/low gamma t-maps (controlling for scene and size trial numbers) revealed no significant clusters. However, partial correlations tests between scene oddity accuracy and scene vs size high gamma t-maps (controlling for scene and size trial numbers) revealed one large positive cluster spanning multiple medial areas including bilateral MTL, portions of the cerebellum, PMC, inferior occipital areas and superior frontal cortex areas (cluster p = 0.039) (Figure 30). Partial correlation tests between face oddity accuracy and face vs size theta/low gamma/high gamma t-maps (controlling for face and size trial numbers) revealed no significant clusters.

A partial correlation test between scene oddity accuracy and scene vs face theta t-maps (controlling for scene and face trial numbers) revealed one large positive cluster spanning

several medial areas including portions of the cerebellum, PCC, middle cingulate cortex, thalamus and caudate (cluster p = 0.020) (Figure 30). The equivalent test for correlations with face oddity accuracy revealed no significant clusters.

Partial correlations tests between scene or face oddity accuracy and scene vs face low gamma t-maps (controlling for scene and face trial numbers) revealed no significant clusters.

A partial correlation test between scene oddity accuracy and scene vs face high gamma t-maps (controlling for scene and face trial numbers) revealed one large positive cluster which included posterior right MTL, the PCC, the occipital lobe, right inferior parietal cortex and the right precuneus (cluster p = 0.048) (Figure 30). The equivalent test for correlations with face oddity accuracy revealed no significant clusters.

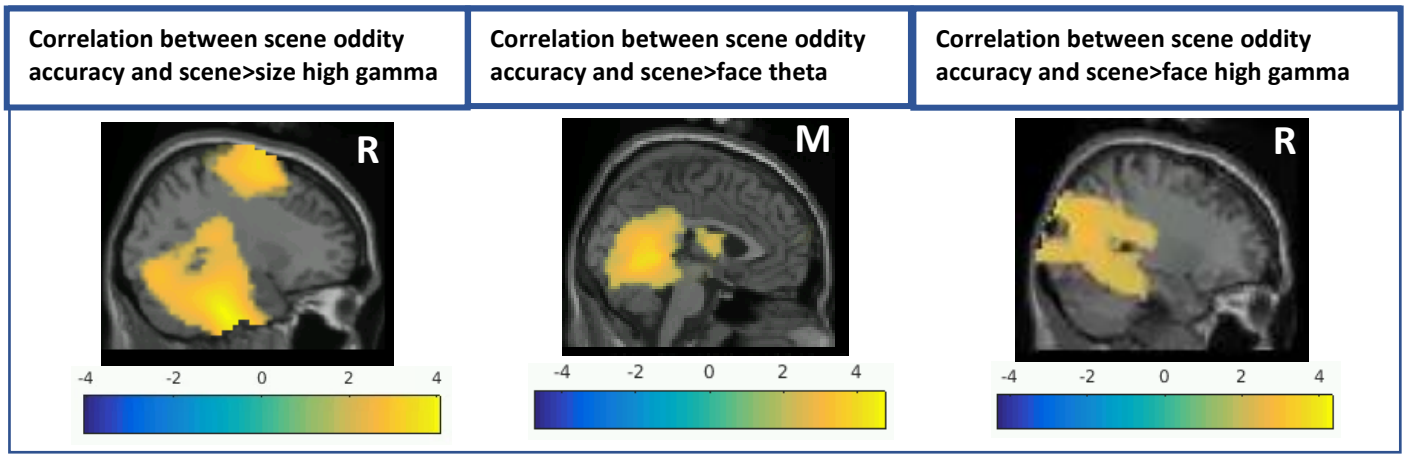

Figure 30. Relationships between scene oddity accuracy and oscillatory power differences between conditions.

Left: Positive relationships were found between scene oddity accuracy and scene vs size high gamma in several medial areas such including portions of the cerebellum, bilateral MTL, inferior occipital areas, PMC areas and the superior frontal cortex. Middle: Positive relationships were found between scene oddity accuracy and scene vs face theta in several medial areas including portions of cerebellum, PCC, middle cingulate cortex and midbrain. Right: Positive relationships were found between scene oddity accuracy and scene vs face high gamma in portions of the right MTL, PCC, occipital lobe, and the right precuneus. Colours represent t-values from correlation tests according to the keys shown below the images (alpha threshold = 0.05). M = midline. R = right.

5.3.4.4 Investigating the frequency specificity and timing of the correlation between scene HPC theta power modulation and scene oddity accuracy.

To understand whether scene oddity accuracy related to scene HPC power difference (compared to fixation) in the theta band only, scene HPC power difference (compared to fixation) was also calculated for the frequency bands surrounding theta and gamma, and

partial correlations between these values and scene oddity accuracy were tested (controlling for MEG trial numbers). These tests revealed that scene HPC delta power difference negatively correlated with scene oddity accuracy (Table 16). There were no significant correlations between scene HPC power difference and scene oddity accuracy in the alpha or beta bands.

	Scene accuracy
HPC delta power difference (task vs fixation)	r = -0.401 p = 0.012*
HPC alpha power difference (task vs fixation)	r = -0.233 p = 0.154
HPC beta power difference (task vs fixation)	r = -0.033 p = 0.843

Table 16. Relationships between scene HPC ROI power difference in surrounding frequency bands and scene oddity accuracy.

Partial correlation tests between HPC oscillatory power difference (task vs fixation) and scene oddity accuracy.
*Highlights p≤ 0.017. N=40.

HPC: Hippocampal Complex.

To further understand the laterality, timing and frequency-spread of this relationship between HPC theta/delta power and oddity accuracy, and how they compare in the scene and face tasks, HPC time-frequency data of the scene and face tasks (contrasted with the fixation period) were tested for partial correlations with scene and face oddity accuracy data, respectively (controlling for MEG trial numbers).

In the right HPC scene data, there was a negative cluster, spanning the lower frequencies and encompassing theta and delta, which commenced at around 0.4 s and continued for the rest of the time period (cluster p = 0.002). Equivalent partial correlation tests between time-frequency comparison of the right HPC virtual sensor during the face task and fixation period and face oddity accuracy data (controlling for MEG face trial numbers) revealed no significant clusters (Figure 31).

The left HPC scene data also contained a negative cluster, spanning the lower frequencies and encompassing theta and delta, which commenced at around 0.5 s and continued for the rest of the time-period (cluster p = 0.0062). Equivalent partial correlation tests between time-frequency comparison of the left HPC virtual sensor during the face task and fixation

period and face oddity accuracy data (controlling for MEG face trial numbers) revealed a negative cluster, spanning low to high gamma ranges, which commenced at around 1.4 s and continued to the end of the time period (cluster p = 0.027) (Figure 31).

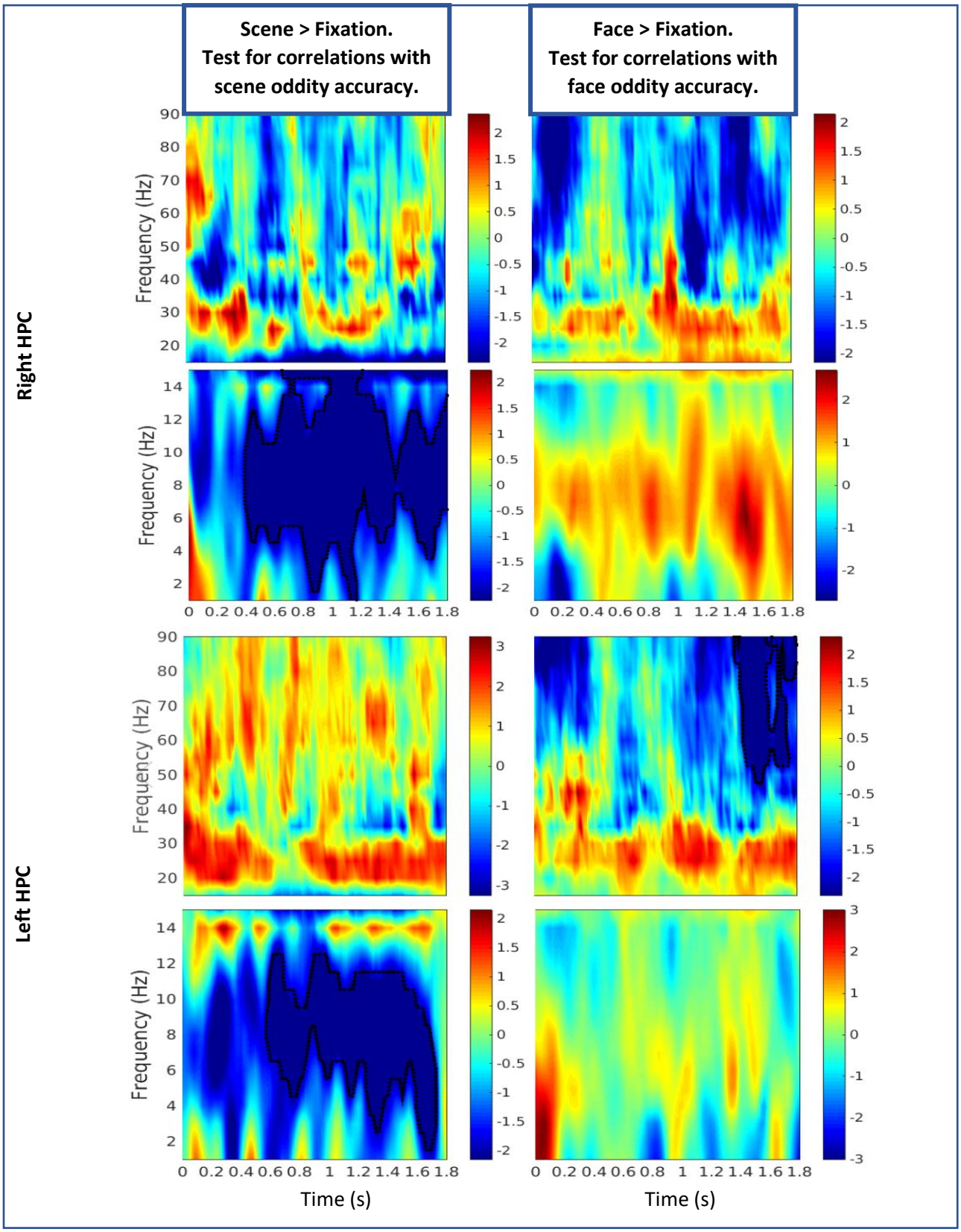

Figure 31. Whole time frequency search for correlations between right and left HPC theta power difference (compared with fixation) and scene and face oddity accuracy.

Colours represent t-values, according the to the key presented next to each spectrogram. Dotted lines outline significant clusters (alpha threshold = 0.05).

HPC: Hippocampal Complex.

5.3.5 Incidental memory behavioural data.

Overall, memory performance was poor. The mean of scene hit rate was 0.63 (SD = 0.140), with a mean false alarm rate of 0.45 (SD = 0.140). The mean of face hit rate was 0.55 (SD = 0.156), with a false alarm rate of 0.44 (SD = 0.140). The mean d' scores for scenes and faces were 0.49 (SD = 0.452) and 0.28 (SD = 0.287), respectively, and were both above the chance level of 0 ($t_{(39)}$ = 9.197, p >0.001; $t_{(39)}$ = 6.197, p >0.001). The d' scores for scenes were significantly larger than those for faces ($t_{(39)}$ = 2.635, p = 0.012; BF_{10} = 3.49), and the two did not correlate significantly ($t_{(38)}$ = 1.001, r = 0.161, p = 0.320; BF_{10} = 0.32).

However, assessing recognition performance without confidence may not reveal if the confidence with which items were remembered differed across the stimuli. To assess whether the difference in memory performance for scenes and faces was reflected in the confidence of hit responses, the proportions of high confidence hit responses ("It's definitely new", rather than "I think it's new") were compared between the conditions. On average, 50% of the scene hits, and 26% of the face hits were answered with high confidence (Figure 32). These were significantly different ($t_{(39)}$ = 7.101, p<0.001; BF_{10} = 846112).

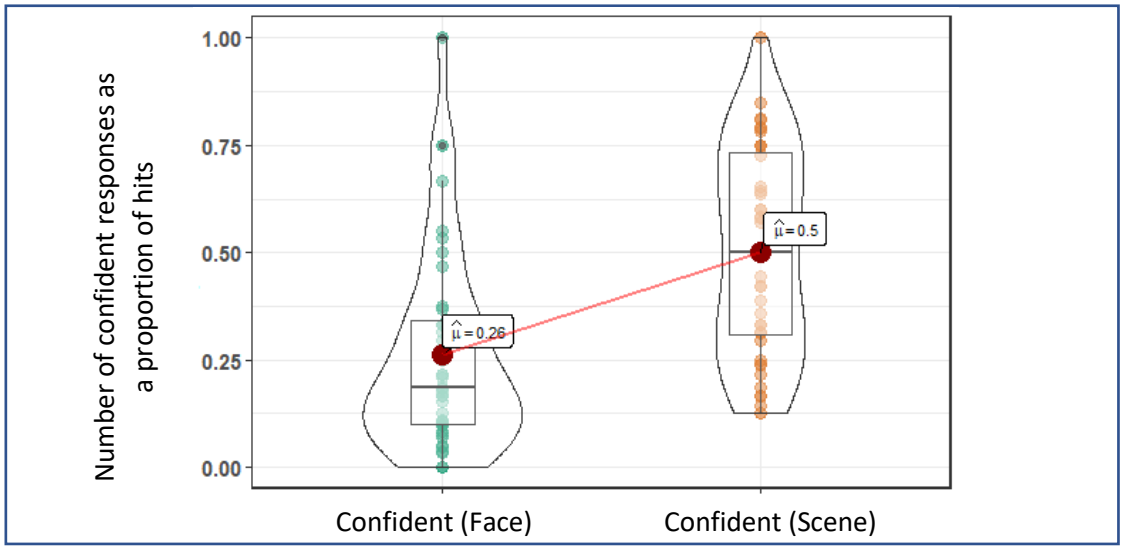

Figure 32. Confident scene and face hits, as proportions of all scene and face hits.

Density plots of confident scene and face hit responses, as proportions of all scene and face hits, averaged over the group. Red dots/μ = mean. Boxplots indicate the median and upper and lower quartiles.

5.3.5.1 Associations between oddity performance and memory performance.

A two-way RM ANOVA was constructed to test whether scenes and faces differed in terms of the proportions of hit responses for stimuli answered correctly or incorrectly in the

oddity task (the 'condition' factor had two levels, scene and face, the 'hits' factor had two levels, oddity-correct and oddity-incorrect, and the dependant variable was the proportion of hits in the memory task). There was a simple main effect of condition (more hit responses for scenes than for faces; $F_{(1,39)} = 10.067$, $p = 0.003$) but there was no main effect of oddity task accuracy ($F_{(1,39)} = 2.653$, $p = 0.111$), indicating that stimuli answered correctly in the oddity task were not more, or less, likely to be recognised as previously-seen than stimuli answered incorrectly (Figure 33).

Also, there was no significant interaction between condition and oddity accuracy ($F_{(1,39)} < 0.001$, $p = 0.993$).

Bayesian RM ANOVA also supported these results. A model based on the alternative hypothesis that condition influenced hit rate was supported with the highest BF ($BF_{10} = 278.65$, compared to the null). The model based on the alternative hypothesis that oddity accuracy influenced hit rate was not supported ($BF_{10} = 0.29$).

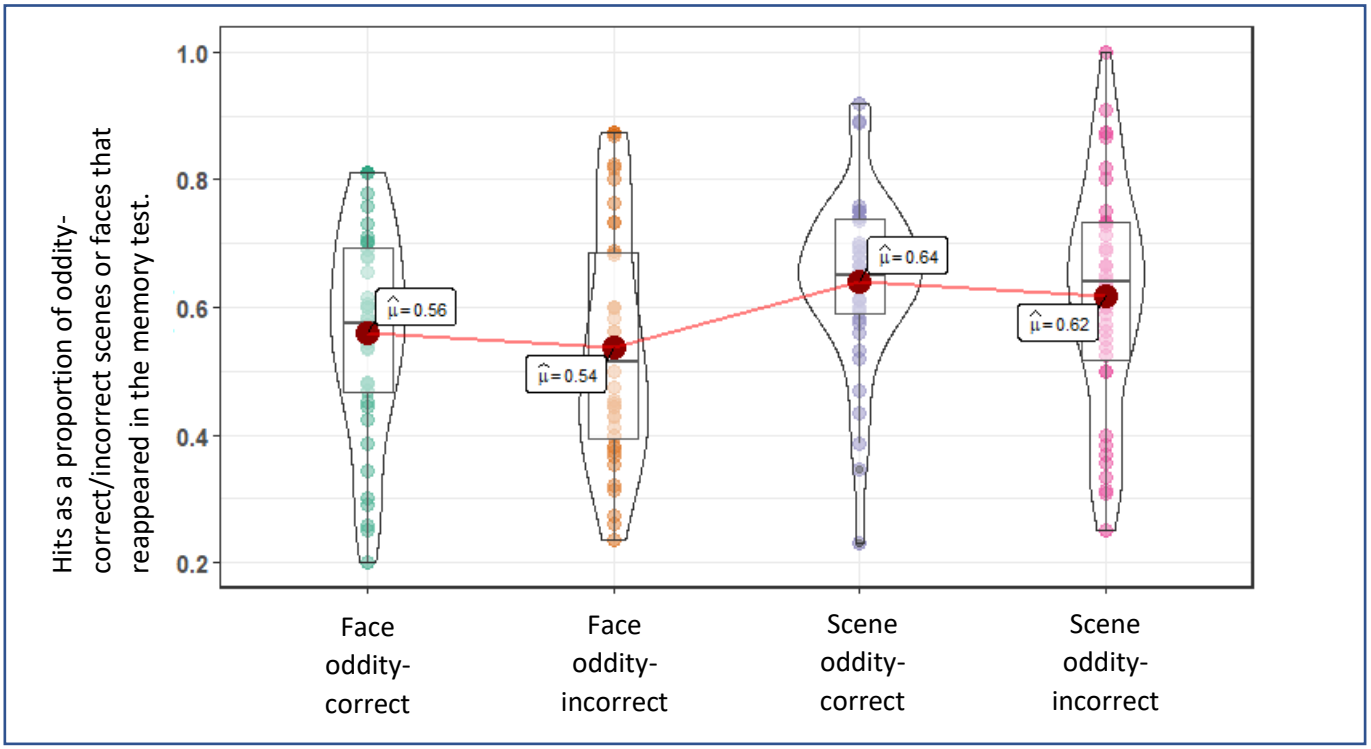

Figure 33. Proportion of hit responses in oddity-correct trials and oddity-incorrect trials.

Density plots of oddity-correct and oddity-incorrect scene and face hit responses, as proportions of all old oddity-correct and oddity-incorrect scene and face trials, averaged over the group.
Red dots/μ = mean. Boxplots indicate the median and upper and lower quartiles.

A correlation test revealed a positive trend between scene oddity accuracy and scene d', but the p-value exceeded the experiment-wise alpha threshold ($t_{(38)}$ = 2.157, r = 0.330, p = 0.037), and the BF indicated weak evidence in favour of the alternative model over the null model (BF_{10} = 2.37). There was also a positive trend between face oddity accuracy and face d', but the p-value exceeded the traditional alpha level ($t_{(38)}$ = 1.913, r = 0.290 p = 0.063), and the BF indicated only weak evidence in favour of the alternative model over the null model (BF_{10} = 1.61; Figure 34).

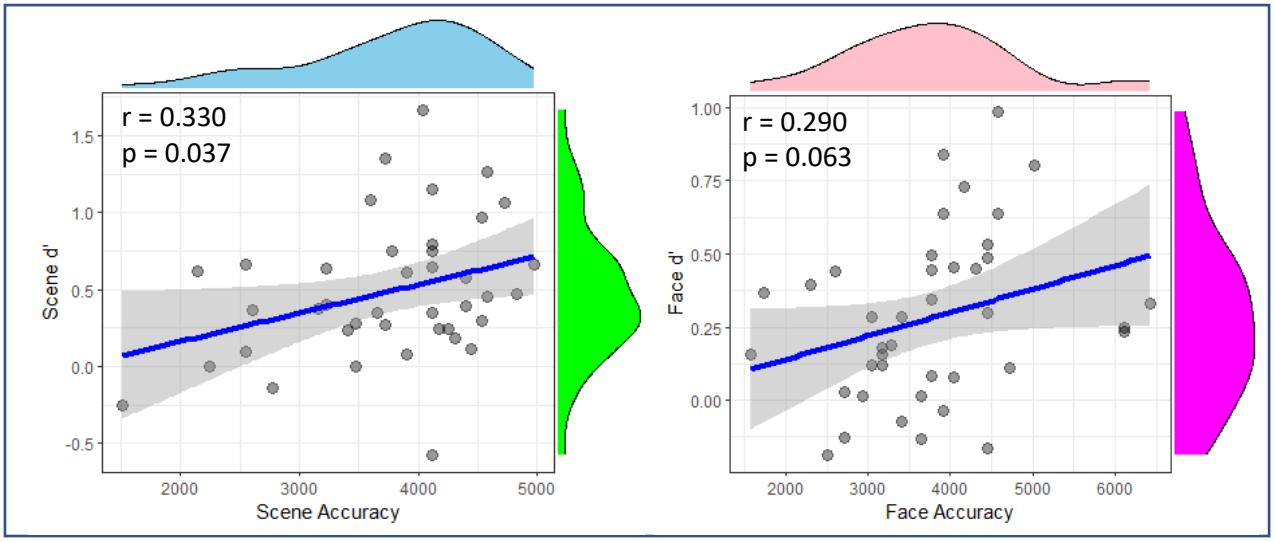

Figure 34. Relationships between oddity and memory performance for scenes and faces.

The light blue histogram shows the distribution of the scene accuracy data, and the light pink histogram shows the distribution of the face accuracy data. The green histogram shows the distribution of the scene d' data and the dark pink histogram shows the distribution of the face d' data. The blue lines are the regression lines and surrounding shaded areas represent the 95% confidence interval.

5.3.5.2 Testing whether correlations between tract microstructure and HPC theta power modulation, and oddity accuracy, carry over to memory performance.

One-way correlations between tract microstructure scores and d' scores were carried out to investigate whether fornix and ILF microstructure measures correlated with scene and face memory performance, respectively, as they did with scene and face oddity accuracy, respectively. There were no significant correlations between scene d' and either fornix PC1 ($t_{(37)}$ = 0.840, r = 0.137, p = 0.203; BF_{10} = 0.28) or fornix PC2 ($t_{(37)}$ = -0.709, r = =0.116, p = 0.242; BF_{10} = 0.25). Similarly, there were no significant correlations between face d' and ILF PC1 ($t_{(37)}$ = -0.450, r = -0.074, p = 0.673; BF_{10} = 0.22) or ILF PC2 ($t_{(37)}$ = 0.187, r =0.031, p = 0.574; BF_{10} = 0.20).

In addition, partial correlation tests were carried out between HPC theta power difference (compared with fixation) during the scene oddity task and scene memory performance (while controlling for the number of scene MEG trials) and between HPC theta power

difference (compared with fixation) during the face oddity task and face memory performance (while controlling for the number of face MEG trials). There were no significant correlations between scene HPC theta power difference and scene d' ($t_{(36)}$ = 0.995, r =0.161, p = 0.326; BF_{10} = 0.54) or between face HPC theta power difference and face d' ($t_{(36)}$ = -1.671, r =-0.264, p = 0.103; BF_{10} = 1.17).

5.4 Discussion

This experiment aimed to test relationships between structure and function in components of the PMN, and performance in a complex scene processing task, and to contrast these with relationships between structure and function in components of the AIN and performance in a complex face processing task. This project expanded upon the work of Hodgetts et al. (2015) by harnessing the added oscillatory and temporal information provided by MEG and the more biologically specific representation of tract structure provided by combining DTI measures with those obtained using higher-order microstructure models. Here, scene processing in the HPC, connected to the PMN by the fornix, was the focus of the research, and it was contrasted with aspects of face processing in the FG, which is connected to AIN regions by the ILF. These results provided support for the PM-view: the 'restriction' property of the fornix, and the 'restriction' and 'coherence' properties of the ILF were evidenced to be related to complex perceptual processing for scenes and faces, respectively. Furthermore, HPC theta power difference between the scene task and fixation correlated with scene oddity performance, and the 'coherence' property of the fornix. These relationships were unique to the fornix and were not also the case for PHC microstructure, a tract which also connects areas of the PMN. Furthermore, relationships between structure, function and oddity performance were not carried over to memory performance, indicating that the processes measured were not purely reflections of incidental encoding. Contrary to the hypotheses, there was not a three-part relationship between fornix microstructure, HPC theta power difference between the scene task and fixation, and scene oddity accuracy. In addition, gamma power in the FFA did not relate to face oddity performance or ILF microstructure.

5.4.1 Reduction of tract microstructure measures produced biologically interpretable components.

Tract microstructure data were reduced to two main components. These were biologically interpretable and were similar to those described in previous studies which also reduced tract microstructure data through PCA (Chamberland et al., 2019; Geeraert et al., 2020). PC1 was most influenced negatively by MD, RD and positively by FR and MPF. It was interpreted as positively relating to a 'restriction' property of the fibre (the proclivity for water movement along the fibres as opposed to other dispersed directions). It shares similarities to the first component reported in Chamberland et al. (2019), which was negatively influenced by RD and positively influenced by another measure of fibre density,

and they also interpreted this component as reflecting 'restriction'. It is also similar to the second component reported in Geeraert et al. (2020) which they named 'myelin and axonal packing' because it was influenced positively by FA and negatively by RD and MD.

PC2 was most influenced positively by OD and negatively by FA. It was interpreted as negatively relating to a 'coherence' property of the fibre (the dispersion of modelled fibre orientations). It was similar to the first component reported in Geeraert et al. (2020) which they named 'tissue complexity' because it was influenced positively by FA and negatively by OD. However, the term 'coherence' was used here to clarify the hypothesis that increased coherency, and therefore increased FA, would reflect a beneficial tract property. The term 'complexity' is ambiguous in its expected relationship with performance. Although there are slight differences in the resulting components across studies (as would be expected as there is variation in the microstructure measures and tracts included), common biologically interpretable properties are revealed supporting the usefulness of microstructure data reduction across studies.

5.4.2 Partially dissociable correlations between fornix microstructure and scene task performance, and ILF microstructure and face task performance.

In line with the results of Hodgetts et al. (2015), there was weak evidence of a correlation between the fornix microstructure component relating to restriction, and scene oddity performance. Although the p-value did not surpass the experiment-wise alpha level, the resulting BF indicated weak evidence in favour of the alternative model over the null. Similarly, the ILF microstructure components relating to restriction, PC1, and coherence, PC2, correlated with face oddity performance and both BFs indicated weak evidence in favour of the alternative model over the null. Moreover, the coefficient of the correlation between fornix PC1 and scene oddity performance was significantly larger than that of the correlation between fornix PC1 and size oddity performance; and the coefficients of the correlations between ILF components and face oddity performance were larger than those of correlations between ILF components and size oddity performance. These distinctions are important because the scene and face oddity tasks require the construction of a view invariant internal model, whereas the size task does not.

However, the correlations were not dissociable as would be predicted by the PM-view. The coefficient of the correlation between fornix PC1 and scene oddity performance was not significantly larger than that of the correlation between fornix PC1 and face oddity

performance; and the coefficients of the correlation between the ILF PC1 and face oddity performance were not significantly larger than that of the correlation between ILF PC1 and scene oddity performance. This may be due to a lack of power as Hodgetts et al. (2015) found a significant difference between the correlations between ILF MD and face oddity performance and ILF MD and scene oddity performance, and in the current work, the BFs for the correlations between ILF components and scene oddity performance indicated evidence in favour of the null. Although, Hodgetts et al. (2015) did not find a significant difference between the correlations between fornix MD and scene oddity performance and fornix MD and face oddity performance, it approached significance. Moreover, Postans et al. (2014) conducted a similar experiment comparing associations between fornix microstructure and scene and face complex processing and did find a significant difference between the coefficients of correlations between fornix microstructure and scene performance, and fornix microstructure and face performance. These studies reported larger effect sizes than those found in the current study. Since the current participant population was larger than these previous studies but comparable in demographics, it may be that differences in the methods (for example natural versus virtual stimuli or tract microstructure measurement) reduced the tract-behaviour correlations, possibly thereby reducing power.

It was also of interest to understand whether associations between scene oddity performance and PMN tract microstructure were specific to the fornix, or also related to microstructure of the PHC, since both these tracts connect areas of the hippocampal–diencephalic–cingulate loop (Bubb et al., 2017). The hypothesis that the fornix would be uniquely important was partially supported by the results. Scene oddity performance did not correlate with PHC microstructure, but the coefficient of the correlation between fornix PC1 and scene oddity accuracy was not significantly larger than that of the correlation between PHC PC1 and scene oddity accuracy.

Conversely, in a one-tailed multiple linear regression including fornix PC1, ILF PC1 and PHC PC1, and designed to predict scene oddity accuracy, only fornix PC1 significantly contributed. Together, these results cannot rule-out associations between ILF and PHC microstructure and scene oddity performance, but they indicate that fornix microstructure may have an independent relationship with scene oddity performance, distinct from that between scene oddity performance and ILF or PHC microstructure.

5.4.3 HPC theta power correlated with scene oddity performance.

It was hypothesized that there would be an oscillatory change in the HPC ROI that would be related to scene task performance, and it was proposed that signals from this location would largely originate from the hippocampus because the reduction of hippocampal BOLD was previously found to relate to scene oddity performance (Hodgetts et al., 2015). Indeed, there was evidence that reduction of HPC theta power during the scene task correlated with scene oddity performance and not face or size oddity performance, indicating the importance of decreased HPC theta for successful complex perception of scenes. This aligns with the common understanding of the importance of the theta rhythm in hippocampal processing (Colgin, 2016) and with two previous MEG studies which found decreased hippocampal theta power during novel scene imagery (Barry et al., 2019; Monk et al., 2020). The underlying cognitive processes reflected by decreased theta power are not clear. However, commonalities between these two previous studies and the current project include: the novelty of the scene stimuli (every scene in the current work was trial unique); the requirement for internal processing (internal rotation of the scenes is required to identify the odd image and internal novel scene construction was required in the tasks of Barry et al. 2019 and Monk et al. 2020); and the lack of instruction to encode. Relatedly, decreased hippocampal theta has been reported in rats when they experience novelty in their environment (Jeewajee et al., 2008), and it is suggested that decreased theta contributes to the generation of the MTL-P300 (Jeewajee et al., 2008), a commonly reported evoked signature of novelty (Nieuwenhuis et al., 2011).

Exploration of bilateral HPC time-frequency data, indicated that the association between scene oddity performance and theta power decrease commenced with a delay after stimulus onset, and continued for much of the trial time, suggesting that this beneficial process was not transient. This pattern was similar for the right and left HPC.

Theta power has also previously been related to performance in MEG navigation studies, specifically theta power negatively related to time taken to find the hidden platform in a virtual Morris water maze suggesting that higher theta power was associated with better performance (Cornwell et al., 2008; Y. Pu et al., 2020). Moreover, invasive recording in rats using the radial arm maze, has shown increased theta preceding correct versus incorrect spatial decisions (Belchior et al., 2014). Although these associations between theta power change and performance are in the opposite direction to that reported here, they support

the hypothesis that modulation of hippocampal theta reflects beneficial hippocampal processes.

To assess the specificity of the frequency effect, tests of correlations between scene oddity performance and HPC power in frequency bands surrounding theta, delta and alpha, were also carried out as part of the exploratory analyses. The effect was largely specific to the theta band inasmuch as no significant correlation was found between scene oddity performance and HPC alpha power. However, a negative association was found with averaged HPC delta, and the correlation test with HPC time-frequency data shows that the negative cluster encompasses delta frequencies for some of the time period. Frequencies associated with navigation, such as theta, in humans have been reported to be shifted to lower frequencies to those reported in animals (Watrous et al., 2013), which may be because human studies involve participants exploring virtual environments without any physical movement (Bohbot et al., 2017). Similar to the current results, invasive recordings from humans navigating virtual environments have shown modulation of both delta and theta in response to what was viewed in the environment (Watrous et al., 2011). Invasive recordings in humans during virtual navigation has indicated differing roles for theta and delta oscillations: posterior hippocampal theta (around 8Hz) was associated with movement speed and delta (around 3Hz) was more prominent in the anterior hippocampus and was not modulated by movement speed (Goyal et al., 2020). However, the current results provide no evidence of functional differences between delta and theta modulations during spatial processing, and there was no movement.

Decreases in low frequency power have been shown to accompany increases in power in higher frequencies (Scheeringa et al., 2011). However, there was no equivalent positive correlation between scene oddity performance and HPC power difference between scene and fixation, in either of the gamma frequencies. Interestingly, Barry et al. (2019), who identified a MEG-measured decrease in hippocampal theta in response to novel scene imagery, also reported no equivalent change in higher frequencies. It may be the case that increased power in higher frequencies did occur but were undetected, because accurate localization of higher frequency signals from deep sources with MEG is more challenging because of the decreased SNR of MEG recordings due to source-sensor distance and muscle artefacts (Muthukumaraswamy, 2013). Deep source localization of MEG signals is improved when stronger signals related to visual processing are cancelled out by contrasting two visually similar tasks, rather than contrasting a task to a baseline (Mills et al., 2012; Quraan et al., 2011). This may have meant that oddity performance – power

modulation correlations were missed in the confirmatory analyses that comprised task vs fixation comparisons. Indeed, the exploratory test of correlations between t-maps of the difference between scene and size high gamma power, and scene oddity accuracy revealed a positive cluster which included bilateral MTL areas. Similarly, the exploratory test of correlations between t-maps of the difference between scene and face high gamma power, and scene oddity accuracy, revealed a positive cluster which included areas of the right MTL. Together, the results could indicate that optimal complex scene processing in the hippocampus, entails increased high gamma power in conjunction with decreased theta/delta power. However, further confirmatory investigation of the relationship between scene oddity performance and hippocampal gamma, ideally with invasive recording, would be required to test this.

It is important to note that the correlation between scene oddity performance and decreased scene HPC theta/delta was not a phenomenon occurring across all lower frequencies as there was no equivalent correlation with scene HPC alpha. However, it remains unclear whether the reduction in theta/delta power reflects one process which causes a wide-spread power reduction, or two simultaneous processes, and, if the latter, whether these processes took place in the same MTL structure.

Decreases in low frequency power, including decreases in theta (Fellner et al., 2016), have been associated with increased BOLD signal (Scheeringa et al., 2011). This highlights a discrepancy between the current results and those of Hodgetts et al. (2015), as they found an association between the extent of decreased hippocampal BOLD and scene oddity performance. It could be that this decrease in hippocampal BOLD, and the decrease in HPC theta found in the current study, reflect different aspects of the same hippocampal process, and that the unexpected relationship between the two stems from the complexity of the relationship between the BOLD response and hippocampal neuronal activity. Alternatively, it could be that the two modalities have measured different processes. One clear difference between fMRI and MEG measurements is the temporal information: each give blurred representations of multiple simultaneous processes over time, but on different scales. Whereas Hodgetts et al. (2015) averaged BOLD data over 6 s trials, in this study, oscillatory power in the first 2 s was examined, before a more in-depth look of this time-period with time-frequency analysis. Considering the complexity of the oddity task, it is imaginable that several processes take place within 2 s, and likely more, in 6 s.

5.4.4 Is the HPC theta result reflective of hippocampal processing?

Although hippocampal activity is fundamental to this test of PMN functioning in complex scene perception, and functional results have been interpreted in relation to hippocampus-related literature, it is uncertain whether recordings in this study reflect hippocampal signals. Indeed, the HPC ROI is made from hippocampal and parahippocampal AAL atlas ROIs (because deep source localization is inaccurate and these areas have been analysed together in previous MEG research (Pu et al., 2017)), so it may be that theta decreases in the parahippocampus or PrC, rather than the hippocampus, actually correlated with scene oddity performance. However, it is unlikely that PrC signals contribute to the HPC power measures, considering the previous fMRI work which has identified scene oddity task related BOLD modulations in the hippocampus and not PrC (Hodgetts et al., 2015), and considering the challenge involved in measuring PrC activity with MEG.

Furthermore, the trend between fornix PC2 and HPC theta, found in the current study, may indicate that these signals originate from the hippocampus rather than the parahippocampal cortex because the fornix is the major connecting tract of the hippocampus (Bubb et al., 2017). Relatedly, Hodgetts et al. (2015) did not find any correlations between fornix microstructure and parahippocampal cortex BOLD. On the other hand, both the hippocampus and parahippocampal cortex have been shown to engage during the scene oddity task (Hodgetts et al., 2016) and both areas may have displayed a decrease in theta power in this study. Future work could address this localization uncertainty using invasive electrophysiological recording, comparing oscillatory local field potential recordings between the hippocampus and parahippocampal areas.

5.4.5 HPC theta and fornix microstructure 'restriction' component related to scene oddity accuracy, but not to each other.

Although it was expected that there would be a three-part relationship linking fornix structure, HPC theta and scene oddity performance, the results suggest there are separate correlated groups of related variables: fornix PC1 and scene oddity accuracy; scene HPC theta power difference and scene oddity accuracy; and fornix PC2 and scene HPC theta power difference. Interestingly, this suggests a dissociation in the importance of the fornix restriction property and the fornix coherence property in PMN functioning. Fornix 'coherency' was indicated to relate positively with scene HPC theta (negative correlation between fornix PC2 and theta power), suggesting that this property may aid theta

oscillations in this circuit. Although this result clashes with the finding that scene HPC theta negatively relates to oddity performance, it fits well with literature showing the importance of connectivity via the fornix for hippocampal theta rhythms (Benear et al., 2020). On the other hand, a reduction in fibre coherence could be interpreted as an increase in fibre complexity and it is possible that fornix fibre complexity correlates with reductions in theta power during scene oddity task completion. This would then be complementary to the finding that scene HPC theta negatively relates to scene oddity performance. An invasive animal electrophysiological and histological study measuring theta power modulations and fornix fibre shapes, would be beneficial in validating these suggestions.

Hodgetts et al. (2015) also found this dissociation: while fornix MD correlated with scene oddity performance, fornix FA correlated with hippocampal BOLD difference between the scene task and baseline. They suggest that some but not all aspects of hippocampally related scene processing are mediated by the fornix, based on three relevant findings: non-fornical hippocampal pathways are also important for spatial processing (Dumont et al., 2015); fornix lesions, impairing spatial memory, disrupt hippocampal plasticity changes instead of neuronal activity (Fletcher et al., 2006); and that the fornix may aid functions not attributable to the hippocampus (Whishaw & Jarrard, 1995).

However, neither hippocampal theta power nor BOLD reflect the full orchestra of hippocampal functioning and fornix 'restriction' may mediate optimal hippocampal processes that went unmeasured, or that the relationships between structure and function are more complex than the current analysis was able to reveal. For example, there are correlations between MEG-measured spontaneous signal complexity (Lempel–Ziv's Complexity) and white-matter microstructure in several tracts (Fernández et al., 2011) and, signal complexity has been shown to be reduced in cases of mild cognitive impairment, where it correlates with hippocampal volume (Shumbayawonda et al., 2020). Alternatively, fornix microstructure, as well as relating to hippocampal activity, may also influence functional connectivity between the hippocampus and more distant brain areas, which was not measured here. For example, correlations have been found between functional connectivity of the hippocampus and DMN areas, fornix microstructure and cognitive ability, in patients with AD (Wang et al., 2020).

The dissociation may also come about because of the different types of individual variation being measured. On the one hand, structure is a static trait (although structure can change with learning (X. Wang et al., 2014), we assume changes are minimal in the time period

between the MEG and MRI scan), whereas the functional measures reflect state traits: magnitude of oscillatory differences between two tasks, or between task and baseline. For example, the relationship between fornix PC2 and HPC scene theta power difference between scene and fixation, implies that fornix 'coherence' related positively with scene HPC theta power, even though average HPC theta power is lower in the scene task versus the fixation. Therefore, it could be that fornix 'coherence' correlates with the general propensity for an individual to generate theta rhythms in the HPC regardless of the current state. It is possible to measure more static individual differences in functional data, which is not reliant on task state, in the form of RS-connectivity. Previous work has shown correlations between tract microstructure and RS-connectivity (Messaritaki et al., 2020) and between RS-connectivity and behaviour (Wegman & Janzen, 2011). *Chapter 6* describes an investigation into relationships between: RS-connectivity of the hippocampus and PCC to other PMN areas; tract microstructure; and oddity task performance.

5.4.6 Exploratory analyses results indicate that oscillatory power differences in other PMN areas are associated with scene oddity performance.

The PM-view suggests that the hippocampus is important for complex scene processing due to its role in creating view-invariant internal spatiotemporal models (Graham et al., 2010; Murray et al., 2017). However, other areas of the PMN are also thought to aid spatial processing (Clark et al., 2018; Hodgetts et al., 2016). Therefore, associations between theta and power changes between task and fixation in the mPFC, PCC and IPL, and scene oddity performance were also explored. The results of this exploratory analysis suggested PCC theta power negatively correlated with scene oddity performance, and did not correlate with face or size oddity performance. Similarly, a whole-brain search for negative associations between theta power difference between the scene task and fixation, and oddity performance, revealed a large cluster which included bilateral MTL, PCC and precuneus. Similarly, whole-brain searches for correlations between scene oddity performance and high gamma power difference between the scene and size conditions, and between the scene and face conditions, both revealed positive clusters which included PMC areas. Although it is important not to over-interpret results from exploratory analyses, these results mirror results from an fMRI study that found increased PCC/precuneus BOLD modulation during a scene oddity task versus face or object oddity tasks (Costigan et al., 2019). It is suggested that the role of the PCC is to aid scene processing by receiving spatial representation information from parietal areas and passing information to the parahippocampus and hippocampus, thereby providing the spatial component of

spatiotemporal representations (Rolls, 2019). In line with this finding, *Chapter 4* revealed significant oscillatory changes in the PCC/precuneus in the scene and face conditions comparison.

5.4.7 FG gamma did not relate to face oddity performance or ILF microstructure.

In contrast to the hypothesis, and the findings of Hodgetts et al. (2015), no significant correlations were found between FG gamma power difference (in either gamma band) between the face task and fixation, and face oddity performance, or ILF microstructure. There are several possibilities for these findings. First, although gamma power has been shown to positively correlate with BOLD, it is not the only contributor (Ekstrom, 2010). Therefore, the process reflected by FFA BOLD in Hodgetts et al. (2015) may not have been the same process that was reflected by increased gamma power during face oddity task completion (seen in *Chapter 4*). Another possibility is that the signal recorded in this study did not reflect face processing areas, as the FFA is located in the FG but the FG is large and may contain multiple functionally-distinct areas. Also, the face processing network has been shown to be right-lateralized (Bukowski et al., 2013; Hildesheim et al., 2020) and combining bilateral FG signals may have obscured a correlation between right FG power and face oddity performance (see *Chapter 8* for further discussion). Lastly, the PrC has been shown to be more engaged when participants view highly similar faces, than the FFA, which is more engaged when participants view faces with more differences (Mundy et al., 2012). This was interpreted as meaning that the FFA is more sensitive to individual features rather than the whole face (Mundy et al., 2012), which would explain why activity in the FG did not correlate in the current study, in which aggregate face processing was necessary.

5.4.8 Evidence that the oddity performance effects are not purely reflections of incidental encoding.

Although there were positive trends between scene and face oddity performance, and memory performance (d' scores), the associations found between fornix structure, HPC oscillatory power and task performance were exclusive to the oddity task. Furthermore, there were no significant differences between the proportion of incorrect scene or face oddity trials and correct scene or face oddity trials, that were subsequently remembered. In line with the hypothesis, the results suggest that there are processes involved in complex scene and face perception which are distinct from processes involved in incidental encoding. This aligns well with the results of previous fMRI studies which found that

modulations of hippocampal BOLD that were associated with scene oddity task completion, were not modulated by subsequent memory (Hodgetts et al., 2016; Lee et al., 2013).

Similarly, it is also important to ensure that differences between structural and functional correlates of scene and face oddity performance were not facilitated by differences in the memorability of the scene and face stimuli. However, the hit rate and the proportion of confident hits were larger for the scene trials than face trials, indicating that the scene stimuli were more confidently memorable than face stimuli. This may be because face features are always consistent (they all include eyes, nose, etc.) whereas scene features could vary between scenes (they could include doors, stairs, pillars, blocks, etc.) and the varying objects may aid incidental encoding. This differs from the results of Hodgetts et al. (2016) who found no differences between memory of different stimulus types, including scenes and faces. The discrepancy between this and the current findings may be due to the use of naturalistic versus computer generated scenes and faces. Regardless, due to the lack of correlations between fornix and ILF microstructure, and HPC theta, and scene and face memory performance, it seems unlikely that the difference in memorability explains the dissociations between structure, function, and performance in the oddity task for scenes and faces.

5.4.9 Limitations.

There are limitations of this study that warrant further thought. First, the issue caused by the discrepancy in how unanswered trials were treated in the MEG (excluded) and behavioural (classed as incorrect) data, which has already been described, was addressed by using partial correlations (controlling for MEG trial numbers). The reasoning behind this discrepancy was because inclusion of unanswered trials in the MEG data processing may have reduced sensitivity to task relevant signals as it is not clear if the participant was attempting the trial or was distracted. However, in the behavioural data, if unanswered trials are removed then, when calculating the percentage of correct responses, scores of participants who missed trials would be inflated, as we can assume that either prolonged trial attempts or distraction would likely result in an incorrect answer. Importantly, there were no correlations between MEG-measure task oscillatory power differences and MEG trial numbers. Nevertheless, future work could reduce the risk of unanswered trials by removing the time-to-respond restraint, or by reducing participant fatigue by splitting the MEG scan into multiple sessions. However, any such changes would increase inter-trial variability and experiment time, in an already long experiment.

Unlike Hodgetts et al. (2015), MEG oscillatory power analyses were not confined to correct oddity trials only, as it was important to have as many trials as possible in the MEG analysis to aid deep source localization. Therefore, while one may conclude from the results of Hodgetts et al. (2015) that the propensity for an individual to display reduced hippocampal BOLD would mean that that individual would be better at complex scene processing, the equivalent conclusion cannot be drawn from the current project. For example, here, it is not possible to clarify whether the correlation between HPC theta power during scene oddity task and scene oddity performance, reflects a difference in theta power between correct and incorrect trials, or whether an individual's general HPC theta power during scene oddity trials related to that individual's performance. Supporting the former, Lee et al. (2013) found differences in hippocampal BOLD during correct versus incorrect scenes. However, if scene HPC theta power simply reflected the proportion of correct and incorrect trials in an individual, then fornix PC2, which correlated with scene HPC theta, should have also correlated with scene oddity performance. Furthermore, it's important to note that restricting analysis to correct oddity trials only is also not without its flaws. It may create a difference in SNR for each participant's data which directly relates to their performance. One solution could be to increase the trial number and difficulty (to achieve an equal number of correct and incorrect answers, a design similar to that of Lee et al. 2013) and compare the correlation between oddity accuracy and HPC theta in the incorrect trials, with the correlation between oddity accuracy and HPC theta in the correct trials. An alternative could be to use RT as a measure of performance as this would mean that analysis could be limited to correct trials and trial number would not directly relate to the performance measure. However, the RT values here do not represent performance well as participants were told to aim for accuracy over speed. It also would not have been the solution for this experiment because participants were not instructed to answer as quickly as they could as this may have increased the number of trials lasting shorter than the required 2 s. Furthermore, this is not a good solution for this challenging task as faster RTs may lead to reduced accuracy (Palmer et al., 2005).

Regarding the microstructure data reduction, the aim of reducing several microstructure measures was to create more biologically interpretable variables than FA and MD alone, while not increasing the number of tests, but it cannot be claimed that the true anatomical meanings of the 'restriction' and 'coherence' components are known. Future work could use such a technique in combination with histology of tissue cultures to assess whether components of multiple MRI-derived microstructure data capture histology-measured

anatomical features more accurately than the raw MRI-derived measures. Reassuringly, however, the similarities of the resulting components across studies (Chamberland et al., 2019; Geeraert et al., 2020) means that this is a useful technique in non-invasively comparing the behavioural and functional influences of tract structure properties, even if the underlying anatomy being represented is unclear.

5.5 Conclusions

Implications of the PM-view include: the PMN and AIN networks should aid behaviours in different modalities; network areas, including MTL areas, should be involved in processes across memory and perception; and that the behavioural performance of those modalities should be related to the structural and functional properties of the respective networks (Graham et al., 2010; Murray et al., 2017). This chapter further tested these assumptions by expanding on the work of Hodgetts et al. (2015) with the use of multiple microstructures measures of the fornix ILF and PHC, reduced into biologically interpretable components, and by measuring functional correlates of complex scene and face processing, utilizing the added temporal and oscillatory information provided by MEG. Confirming the results of the previous study, there was evidence for correlations between fornix and ILF microstructure and scene and face oddity performance, respectively. Furthermore, fornix microstructure components, reflecting the properties of restriction and coherence, appear to have different influences on PMN functioning. Fornix restriction was associated with scene oddity performance while fornix coherence was associated with scene HPC theta. Fornix restriction and scene HPC theta independently related to scene oddity performance. These structural and functional oddity correlates did not relate to memory performance in a follow-up surprise memory test, showing that the results did not reflect incidental encoding. Results from exploratory analysis indicated that the association between scene oddity task performance and HPC theta decrease was prolonged throughout the 2 s time period and extended to include delta frequencies. Further exploratory whole-brain analyses implicated the importance of other PMN areas, particularly the PCC/precuneus areas in scene oddity performance. In conclusion, this experiment provides evidence for dissociable roles of MTL-connecting tracts in complex scene and face complex perceptual processing, and for the role of oscillatory modulation in the PMN structures in complex scene perceptual processing.

Chapter 6: Examining relationships between RS-connectivity, structure and oddity performance in the PMN and AIN.

6.1 Introduction

6.1.1 Background.

It is widely accepted that brain areas display functional connectivity during taskless periods, bringing about 'RS-connectivity' or RS networks (Fox & Raichle, 2007). In this context, connectivity is defined as a statistical dependency between measures of brain regions' activity over time. For example, correlation or coherence are commonly used (Fox & Raichle, 2007; van Diessen et al., 2015). RS networks have been found to be consistent across individuals inasmuch as brain areas show higher connectivity with other brain areas that share behavioural functions (Fox & Raichle, 2007; Kahn et al., 2008; Kong et al., 2017; O'Neil et al., 2014), but they can also be seen to be different in different individuals inasmuch as there is evidence of inter-individual differences in spatial topography and in connectivity strength indices between areas (Wens et al., 2014). Regarding the former, RS functional connectivity has been demonstrated between PMN areas, as part of networks supporting navigation (Ramanoël et al., 2019), recollection and future imagining (Gilmore et al., 2018). These areas include the hippocampus, the parahippocampal cortex, the PCC; the RSC; and the IPL. Conversely, intrinsic connectivity between areas of the AIN has been demonstrated as part of semantic (Jackson et al., 2016), object (Konkle & Caramazza, 2017) and face (O'Neil et al., 2014) processing networks, and the areas involved include the FFA, the OFA, the inferior temporal gyrus, the PrC and the anterior temporal lobe.

The hippocampus and the PCC (often regarded to spatially overlap with the RSC (Burles et al., 2018; Natu et al., 2019)) may be particularly important regions in widespread PMN communication. The hippocampus is known to be an important region in episodic memory (Benoit & Schacter, 2015), spatial memory (Baldassano et al., 2016) and scene perception (Hodgetts et al., 2016) networks. The PCC is highly connected with other areas of the DMN (Huijbers et al., 2012), and is proposed to play a key role in functional connectivity across the DMN (Fransson & Marrelec, 2008).

Studies examining mild cognitive impairment (MCI) or AD, both thought to be diseases of the PMN (Ranganath & Ritchey, 2012; Yu et al., 2016), have highlighted the PCC (Bai et al., 2009; Liang et al., 2008) and the hippocampus (Allen et al., 2007) as key structures in the pathophysiology. Studies comparing RS-fMRI patterns in Alzheimer's patients and healthy controls have revealed reduced connectivity between the hippocampus and various cortical areas, including the mPFC, the inferior temporal gyrus, the superior temporal gyrus, the caudate nucleus and the PCC (Z. Wang et al., 2014; Xue et al., 2019). Similarly, RS-fMRI connectivity between the PCC and other brain areas such as the middle occipital gyrus, the hippocampus and the FG, has also been shown to be reduced in Alzheimer's patients (Yokoi et al., 2018). In MCI patients, there is evidence of reduced PCC-temporal cortex connectivity, which may be associated with the level of cognitive impairment (Bai et al., 2009). Also, in mesial temporal lobe epilepsy patients, increased RS-fMRI connectivity between the affected hippocampus and the PCC, was associated with better pre-surgical memory but worse post-surgical memory (McCormick et al., 2013). Together, these results illustrate a relationship between increased hippocampal and PCC connectivity and improved PMN network functioning.

Moreover, studies examining individual differences in healthy adults have identified associations between hippocampal RS-fMRI connectivity with other PMN areas, or PCC RS-fMRI connectivity with other PMN areas, and performance in tasks requiring PMN-related behaviours. For example, RS-fMRI connectivity between the hippocampus and the RSC has been found to be stronger in good navigators versus poor navigators (Sulpizio et al., 2016) and was positively associated with memory of places as measured by d' (Collins & Dickerson, 2019). For another example, RS-fMRI connectivity between the parahippocampal cortex and areas of the DMN including the PCC and mPFC, was found to be associated with path integration ability in navigation (Izen et al., 2018). However, behaviours in these studies rely on memory processes so it is unclear whether similar relationships exist between RS-connectivity of the hippocampus and PCC and scene perception performance.

This study aims to investigate such relationships and to contrast them with associations between RS-connectivity within the AIN network and face perception. Associations, between RS PMN connectivity and PMN-related behaviours have previously been dissociated from associations between RS AIN connectivity and AIN-related behaviours. For example, hippocampal-RSC and FFA-PrC connectivity, post encoding task, were found to be

correlated with place and face memory task performance, respectively (Collins & Dickerson, 2019).

The FFA and the PrC, along with the OFA, the superior temporal sulcus and the amygdala, are among the face-selective areas that show functional connectivity at rest (O'Neil et al., 2014). RS-connectivity between the FFA and the OFA has been associated with several measures of face processing performance including: famous face recognition; the face inversion effect (the extent of performance improvement when assessing upright versus upside-down faces); and the whole-part effect (the extent of performance improvement when assessing whole faces versus parts of faces) (Zhu et al., 2011).

The hippocampus and the PCC, and the FFA and the OFA, have previously been found to show activity modulation during completion of the scene and face perceptual oddity tasks, respectively. Hippocampal and PMC (includes the PCC, the precuneus and the RSC) BOLD have been found to be modulated during the scene oddity task (Hodgetts, Voets, et al., 2017), and the magnitude of the hippocampal BOLD modulation correlated with task performance (Hodgetts et al., 2015). This was complemented by the findings of *Chapter 4*, in which reduced theta power in the MTL and the PCC was found during the scene oddity task versus the face oddity task or control. Conversely, during the face oddity task, as compared to control, FFA BOLD has been found to increase (Hodgetts et al., 2015), which is complemented by the findings of *Chapter 4*, which showed modulated theta/gamma power in the FG and the IOC. However, it is unclear whether communication between these areas dissociably supports complex scene and face processing. Therefore, this study tested whether individual differences in RS-connectivity patterns of PMN and AIN regions dissociably correlate with scene and face oddity task performance, respectively.

The discussed studies used fMRI, which benefits from high spatial resolution, whereas the current work used MEG. MEG recording is more temporally resolved than fMRI and allows for direct measurement of synchronised electrophysiological activity. Although RS-MEG recordings can be compromised by field-spread, the use of constrained source-localization and robust connectivity measures mean that true functional connections can be characterized with reduced influence from arbitrary connectivity caused by field-spread (van Diessen et al., 2015). Therefore, RS-MEG can unveil a rich and reliable picture of connectivity across the brain within multiple frequency bands. It is becoming clear that oscillations of different frequencies can have different topographical spread (Hillebrand et al., 2012; Hillebrand et al., 2016), leading to different RS networks displaying oscillatory

coupling in different frequencies (Samogin et al., 2020). Although functional correlations within the PMN and AIN are likely to occur over multiple frequency ranges, it may be that behaviourally relevant RS-connectivity patterns, within the two networks, lie in different frequency ranges.

In this study, RS-connectivity patterns in the theta (4-8 Hz), alpha (8-12 Hz) and beta (12-30 Hz) bands were examined. Functional connectivity in lower ranges, such as alpha and theta, have been associated with long-range connectivity (Ganzetti & Mantini, 2013; Jones et al., 2000), and alpha connectivity is higher in intra-network versus inter-network connections within DMN and visual networks (Samogin et al., 2020). These results suggest that alpha connectivity may be important in both the PMN and AIN. However, RS-connectivity within the PMN in theta may be specifically important in complex scene processing. Multiple studies have associated hippocampal functioning with theta oscillations (Buzsaki, 2002; Colgin, 2016), which are thought to be a platform for hippocampal-cortical interactions, in support of scene processing and episodic memory (Buzsaki & Moser, 2013; Karakaş, 2020), and RS theta oscillations have been identified in the PMC, which includes the PCC (Foster & Parvizi, 2012). However, in a study inspecting RS-connectivity in AD patients versus healthy controls, in frequency ranges from delta (1-4 Hz) to high gamma (50-90 Hz), connectivity was found to be specifically reduced in the alpha and beta bands only (Koelewijn et al., 2017). Therefore, behaviourally relevant RS interactions between PMN regions were hypothesized to occur primarily in the theta range, but alpha and beta bands were also inspected.

Alpha oscillations may be specifically important for AIN processing. Frontotemporal dementia is associated with decreased alpha power in diffuse areas including the orbitofrontal and temporal cortices (Nishida et al., 2011), areas which are part of the AIN. Also, alpha coherence between the FFA and several cortical areas has been found to be reduced in adolescents with autism spectrum disorder (Khan et al., 2013), a condition that is associated with impaired face identification (Weigelt et al., 2012).

Since functional connections must be supported by structural connections, and whole-brain changes in structure with age have been associated with changes in RS intra/inter-network connectivity (Betzel et al., 2014), there may also be relationships between microstructure of the tracts connecting the PMN and AIN, and RS-connectivity. Associations have been found between fornix microstructure and: RS-fMRI connectivity between the hippocampus and the thalamus in healthy older adults (Kehoe et al., 2015); average connectivity strength

of the hippocampus to whole-brain ROIs in Alzheimer's and MCI patients (Wang et al., 2020); and increased connectivity between the hippocampus and several medial brain areas during an episodic memory task (Ly et al., 2016). Fornix microstructure may influence connectivity within the theta band specifically, as hippocampal theta rhythms stem from the septum/diagonal band of Broca (Leao et al., 2015) and the supramammillary area (Pan & McNaughton, 2004), which are connected to the hippocampus through the fornix (Swanson & Cowan, 1979). Furthermore, low frequency stimulation of the fornix, and not the mammillothalamic tract, has been found to modulate the theta rhythm in the thalamus, indicating that the hippocampus modulates thalamic activity through this tract (Tsanov et al., 2011). Therefore, there may be a correlation between the strength of RS theta amplitude correlation between the hippocampus and PMN areas, such as the thalamus, and fornix microstructure in healthy adults, but this has not been tested. Additionally, it unclear whether fornix microstructure would relate to the strength of RS theta amplitude correlation between the hippocampus and PCC. If fornix microstructure does influence hippocampal theta connectivity, then theta hippocampus-PCC connectivity may also be expected to be influenced. However, there is evidence for both hippocampus-generated, and hippocampus-independent theta rhythms in the PCC (Colom et al., 1988; Talk et al., 2004).

The ILF connects the ventral visual pathway, including the inferior occipital visual areas and the inferior temporal and temporal pole areas (Herbet et al., 2018), and RS-connectivity in the alpha band has been associated with bottom-up processing, originating from areas such as visual areas in the occipital lobe (Hillebrand et al., 2016). Therefore, individual differences in ILF microstructure could be related to RS alpha connectivity between areas of the ventral visual stream, which overlaps with the AIN.

6.1.2 Aims and hypotheses.

The aims of the experiment in this chapter were to test relationships between individual differences in oddity task performance, tract microstructure and RS-connectivity. RS-MEG scans were recorded between the perceptual oddity task and a subsequent unforeseen memory task (see *Chapters 4 and 5*). First, connectivity strengths between the hippocampus, and the PCC, with PMN ROIs were tested. To do this, amplitude-amplitude correlations were measured within the PMN network, created by selecting the AAL atlas ROIs that were included in the areas examined in *Chapter 4* (HPC, mPFC, IPL, and PCC). In addition, the precuneus and thalamus regions were also inspected as the precuneus

showed frequency power modulation during the scene oddity task in *Chapter 4*, and connectivity between the hippocampus and thalamus has been associated with fornix microstructure previously (Kehoe et al., 2015). The averages of the coefficients of the bilateral hippocampus-PMN ROIs and bilateral PCC-PMN ROIs correlations – for the theta, alpha and beta frequency bands – were calculated to create hippocampus and PCC 'connectivity strengths'. It was hypothesized that hippocampus and PCC connectivity strengths, specifically in the theta band, would correlate with scene oddity performance and fornix microstructure.

Second, amplitude-amplitude correlations between specific ROIs were inspected. The connection between hippocampus and the PCC (hippocampus-PCC) was inspected because the hippocampus and PCC are well-connected brain areas important for PMN-related behaviours such as episodic memory (Bubb et al., 2017; Hagmann et al., 2008; Lega et al., 2017; Natu et al., 2019), and hippocampus-PCC RS-connectivity has been shown to relate to PMN functioning (McCormick et al., 2013; Natu et al., 2019). Also, the connection between the hippocampus and the thalamus (hippocampus-thalamus) was inspected because hippocampus-thalamus RS-connectivity has been shown to relate to fornix microstructure (Kehoe et al., 2015). The AIN connections examined were between the FG and the IOC (FG-IOC) which contain the FFA (Kanwisher & Yovel, 2006) and the OFA (Pitcher et al., 2011)[12], respectively. RS-connectivity between these areas has been associated with face processing performance (Zhu et al., 2011).

Following the theme of this thesis, relationships between PMN structure, function and behaviour were contrasted with relationships between AIN measures of structure, function and behaviour. Regarding the PMN, it was hypothesized that hippocampus and PCC strengths would correlate with scene oddity performance and not face or size oddity performance. It was then tested if specific PMN ROI connections, hippocampus-PCC RS-connectivity and hippocampus-thalamus RS-connectivity, correlated with scene oddity performance and not face or size oddity performance. Also, RS-connectivity measures that correlated with scene oddity performance were predicted to also correlate with fornix microstructure, and not ILF microstructure. Regarding the AIN, it was hypothesized that FG-

[12] The OFA and FFA are functionally defined regions, usually residing in or close to the inferior occipital cortex and on the middle fusiform gyrus, respectively (for reviews see Pitcher et al., 2011 and Kanwisher & Yovel, 2006).

IOC connectivity would correlate with face oddity performance, and not scene or size oddity performance, and ILF microstructure, and not fornix microstructure.

It was further hypothesized that relationships between behaviour, microstructure and RS-connectivity might differ for different frequency bands. Theta connectivity within the PMN was predicted to correlate with scene oddity performance and fornix microstructure, more strongly than connectivity in the alpha and beta ranges. Conversely, the connectivity of the AIN within the alpha band was predicted to correlate with face oddity performance and ILF microstructure, more strongly than connectivity in the theta and beta bands.

The focus of this chapter was to examine network properties that relate to perception specifically. RS recording took place after oddity task completion so, although memory for the oddity scene and face stimuli was poor (see *Chapter 5*), these data may contain signatures of stimulus encoding. Therefore, partial correlations were used when scene and face oddity performance were examined, and the scene and face d' scores from the subsequent memory test, were controlled for.

It was of interest to understand whether PC1 and PC2 component scores unequally related to RS-connectivity. Results of a recent study, which aimed to uncover relationships between individual differences in white-matter structure and RS-connectivity by combining MEG and microstructure scanning (Messaritaki et al., 2020), might predict stronger correlations between PC1 components scores and RS-connectivity than PC2 component scores. In this work, the authors' microstructurally informed algorithms were constructed using multiple microstructure measures, to predict functional connectivity in multiple frequency bands and they found that their myelin measure was a better predictor of functional connectivity properties in the theta, alpha and beta bands, than FA. In the current study, the microstructure data were reduced to two components. PC1 was more influenced by MPF (a measure of myelin) and PC2 was more influenced by FA (see *Chapter 5*). Therefore, it was predicted that RS-connectivity between the PMN and AIN ROIs would specifically relate to the PC1 scores of the fornix and the ILF, respectively.

Lastly, it was hypothesized that PMN RS-connectivity patterns which correlated with scene oddity performance, would not also correlate with PHC microstructure. This was because, despite the PHC supporting PMN connections, PHC microstructure was not found to relate to scene oddity performance (*Chapter 5*).

6.2 Methods

Descriptions of the oddity task paradigm and resulting behavioural data can be found in *Chapters 4 and 5*. Descriptions of the isolation of fornix, ILF and PHC streamlines, and assessments of their microstructure, can be found in *Chapter 5*. The RS-MEG recording and analyses are outlined below.

6.2.1 Participants.

The 40 participants are the same as those of the experiments described in *Chapters 4* and *5*.

6.2.2 RS-MEG recording and connectivity analysis.

6.2.2.1 RS-MEG recording.

The five-minute RS-MEG recording occurred immediately after the oddity task blocks and before the memory task. Subjects were asked to keep still and keep their eyes fixated on a small black dot, displayed at the centre of a grey screen. As in *Chapters 4 and 5* the recordings were performed using a 275-channel axial gradiometer CTF system, located inside a magnetically shielded room and the data were acquired continuously, with a sampling rate of 1200 Hz. Head movement was monitored, head-shape was mapped, and MEG-MRI co-registration was conducted, using the methods detailed in *Chapter 4*.

6.2.2.2 RS-MEG data pre-processing.

Previously (*Chapter 4*), muscle artefacts were removed as part of manual inspection of trial data. As RS-data is treated as continuous data, an automatic artefact detection approach was used (Fieldtrip function: ft_artifact_zvalue, described here[13]). This process involves: calculating the Hilbert envelope of the data of each channel, over time; calculating the mean and SD of the data of each channel; applying z-transformation to the data of each channel; and lastly, averaging the z-values per timepoint. Then, as each timepoint is expressed as a deviation from the mean over time and channels, a threshold can be applied to identify samples containing artefactual data. The threshold values used ranged between 4 and 10, depending on each individual's data, with the aim of effectively removing muscle artefacts while keeping as much data as possible. The original data were then

[13] https://www.fieldtriptoolbox.org/tutorial/automatic_artifact_rejection/#iii-z-transforming-the-filtered-data-and-averaging-it-over-channels

downsampled (250 Hz) and decomposed into 100 components using ICA (using Fieldtrip's fast ICA) (Oostenveld et al., 2011). Components relating to eye-movement and heart rate were removed from the original data. Lastly, the data was visually inspected to ensure the efficacy of the previous steps.

6.2.2.3 RS-MEG connectivity analysis.

Amplitude envelope correlations across the whole brain were calculated using an ROI-based approach (Hillebrand et al., 2012), which has previously been used as part of published work (Koelewijn et al., 2019; Messaritaki et al., 2020; Routley et al., 2017). Theta and alpha frequency bands were isolated by applying bandpass filters of 4-8 Hz and 8-12 Hz, respectively, and source localization was carried out using LCMV beamforming. Each participant's data was warped to MNI space and segregated into the 90 AAL ROIs. For each frequency band, a time-series was assigned to each ROI, by constructing VSs for each voxel and taking a representative VS (the one with the greatest power change during the recording) within each ROI. To reduce source leakage between ROI VSs (which would result in spurious signal correlations) a symmetric orthogonalization procedure was carried out which involves removing zero-lag correlations (Colclough et al., 2015).

To calculate amplitude coupling between ROI VSs, the amplitude envelopes of these orthogonalized VS time-series data were extracted through calculating the Hilbert transforms, and were then down-sampled to 1 Hz and had edge artefacts removed. Correlation matrices (90x90) for each participant were constructed by calculating correlations across the envelopes. Lastly, the coefficients were Z-transformed using Fisher's transform. Higher and lower Z-values were taken as indicators of higher and lower connectivity, respectively.

6.2.2.4 Assessing Connectivity measures within the PMN and AIN.

From the whole-brain data (90x90), a PMN network was constructed including ROIs thought to have major roles in the PMN network, resulting in a 22x22 matrix (Figure 35). This included the same AAL ROIs examined in *Chapter 4* (bilateral hippocampus and parahippocampal regions, frontal medial orbital, bilateral middle frontal, and bilateral superior medial frontal regions, the inferior parietal gyrus, the angular gyrus the supramarginal gyrus, bilateral PCC regions) and bilateral thalamus and precuneus regions. To measures the strengths of the hippocampus and PCC connections to the other PMN ROIs, Z-values along the rows of the PMN matrix were summed, for the hippocampus and

PCC columns, creating the 'connection strength' scores (Routley et al., 2017). The bilateral scores were averaged, and this was done separately for each frequency band.

Specific connectivities between the hippocampus and PCC, and between the hippocampus and the thalamus were also inspected. Z-transformed correlation coefficients between the bilateral hippocampus and PCC ROIs, and the bilateral hippocampus and thalamus, were both averaged for each individual for the three frequency bands. These PMN connectivity scores were contrasted with connectivity scores (calculated in the same way) between two ROIs hypothesized to play a role in the AIN: the FG and IOC.

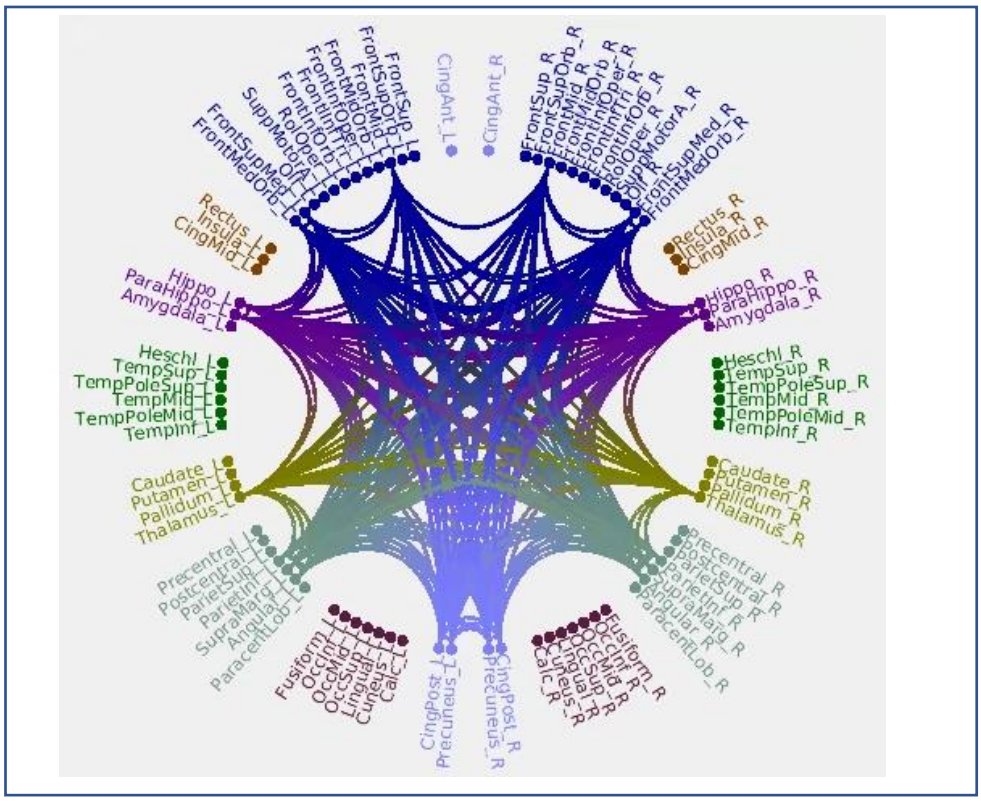

Figure 35. The defined PMN network on a circular network plot.

Connectivity between nodes that are considered members of the PMN is shown. Each line is associated with a coefficient for each frequency band, for each participant. Lines and ROIs are colour coded according to location of the node. From top to bottom (or anterior to posterior brain): dark blue denotes frontal lobe areas; brown denotes deep frontal areas; purple denotes MTL areas; green denotes lateral temporal lobe areas; yellow denotes midbrain areas; grey denotes parietal lobe areas; maroon denotes occipital lobe areas; and pale blue denotes posteromedial areas. To save space, abbreviated labels are used and a translation into full names is included in the *Appendix 3A*. Note that '_L' and '_R' refers to left and right hemisphere, respectively.

6.2.3 Statistical analysis: testing correlations between oddity performance, RS-connectivity and tract microstructure.

Statistical analyses were carried out using MATLAB (MATLAB, 2015), or using Rstudio (R Core Team, 2019; RStudio Team, 2020). Pearson's correlation tests were applied, to elucidate relationships between RS-connectivity, task performance and tract microstructure. The transformed-to-normal scene, face and size oddity accuracy scores, scene and face d' memory scores, and tract microstructure component scores, described in *Chapters 4 and 5*, were used. The RS-MEG measures were tested for outliers, defined as being further than three times the SD from the mean. The number of values entering each statistical test (N) is noted in results.

First, partial correlations between RS-connectivity scores and scene and face oddity accuracy scores, controlling for scene and face d' scores, were carried out. Correlations between the RS-connectivity scores and size oddity accuracy (the control task) were calculated, as incidental encoding of the circles was assumed not to occur. The alpha value was Bonferroni-corrected to 0.006 to account for the number of oddity conditions and frequency bands (0.05/9, for 3 frequency bands and 3 oddity task conditions).

Second, Pearson's correlations between fornix, ILF and PHC microstructure scores, and RS-connectivity scores were computed. All scatterplots were constructed using ggscatterstats for R (Patil, 2021). The alpha value was Bonferroni-corrected to 0.006 to account for the number of tracts and frequency bands (0.05/9, for 3 frequency bands and 3 tracts).

When comparing correlation coefficients (methods described in section 5.2.6), the alpha value was Bonferroni-corrected for the number of tests within each section, to 0.025 (0.05/2).

Parametric correlation statistics were accompanied by Bayesian correlation tests. BFs were calculated using the BayesFactor package in R (Morey & Rouder, 2018), and were reported as BF_{10} (evidence of the alternative model over the null model).

It was hypothesized that behaviour–RS-connectivity and structure–RS-connectivity would share similar correlations, indicating a functional mediator, explaining the structure-behaviour correlations found in *Chapter 5.* However, no such common correlations were identified. Therefore, additional exploratory analyses were carried out. For these, partial correlations between scene/face oddity accuracy and the whole-brain Z coefficient data

(controlling for scene/face d' scores) were tested. Also, correlations between fornix and ILF microstructure component scores and the whole-brain Z coefficient data were carried out. Previous similar studies, testing whole-brain RS-connectivity effects, have used a conservative ranking procedure with the aim of reducing the impact of noise (e.g. Koelewijn et al., 2019). For this, each connection within each participant's data is ranked and these rank maps are then averaged across the group. Those connections in the top 20% of the average rank map are considered valid and reproducible. However, this method produces few remaining theta connections (e.g. see Dima et al. (2020)). As this was an exploratory analysis, to allow for a widespread search while eliminating the least reproducible connections, a lower threshold was used resulting in selection of the top 40% of connections. Regression analyses were carried out, testing predictions of the remaining RS connections, with either the behaviour or tract microstructure measures. For the former, both oddity accuracy and d' scores were included as predictors in the same models so that the independent contribution of oddity accuracy data to RS-connectivity could be assessed. Each test comprised 5000 permutations. For each section, the alpha value was Bonferroni-corrected to 0.0083 to account for the tests involving the oddity task and tract microstructure in three frequency bands (0.05/6, for one oddity measure, one tract, and three frequency bands). The p-values of the correlations that did not surpass this threshold were then FDR corrected and accepted at the traditional 0.05 level.

6.3 Results

6.3.1 Investigating relationships between hippocampus and PCC connectivity strengths and oddity performance.

As predicted, there was a significant partial correlation between PCC theta connectivity strength and scene oddity accuracy (controlling for scene d') and the corresponding BF indicated evidence against the null (Table 17; Figure 36). However, only a trend for a partial correlation between hippocampus connectivity strength and scene oddity accuracy was apparent, and this did not reach significance. As expected, there were no significant correlations between either hippocampus or PCC connectivity strength, in any frequency band, with face oddity accuracy (controlling for face d') or size oddity accuracy (statistics shown in *Appendix 3B*).

The correlation coefficient between theta PCC connectivity and scene oddity accuracy was significantly larger than that of the correlation between theta PCC connectivity and face oddity accuracy ($z_{(37)} = 4.284$, $p<0.001$).

		Scene Accuracy	Face Accuracy
Hippocampus connectivity strength	theta	r = 0.280 p = 0.084 BF_{10} = 1.27	r = -0.224 p = 0.170 BF_{10} = 0.84
	alpha	r = -0.004 p = 0.979 BF_{10} = 0.36	r = -0.169 p = 0.303 BF_{10} = 0.56
	beta	r = 0.075 p = 0.649 BF_{10} = 0.39	r = - 0.007 p = 0.968 BF_{10} = 0.35
PCC connectivity strength	theta	r = 0.429 p = 0.006* BF_{10} = 9.06*	r = -0.282 p = 0.082 BF_{10} = 1.39
	alpha	r = -0.028 p = 0.864 BF_{10} = 0.36	r = -0.065 p = 0.695 BF_{10} = 0.38
	beta	r = 0.119 p = 0.471 BF_{10} = 0.45	r = 0.010 p = 0.953 BF_{10} = 0.35

Table 17.Partial correlation tests between oddity task performance and Hippocampus and PCC connectivity strengths.

Partial correlation tests between Hippocampus and PCC PMN connectivity strengths, in theta, alpha and beta bands, and oddity accuracy. Subsequent scene and face memory scores (d') were controlled-for.
*Highlights p≤0.006. *Highlights a $BF_{10} \geq 3$. N=40.

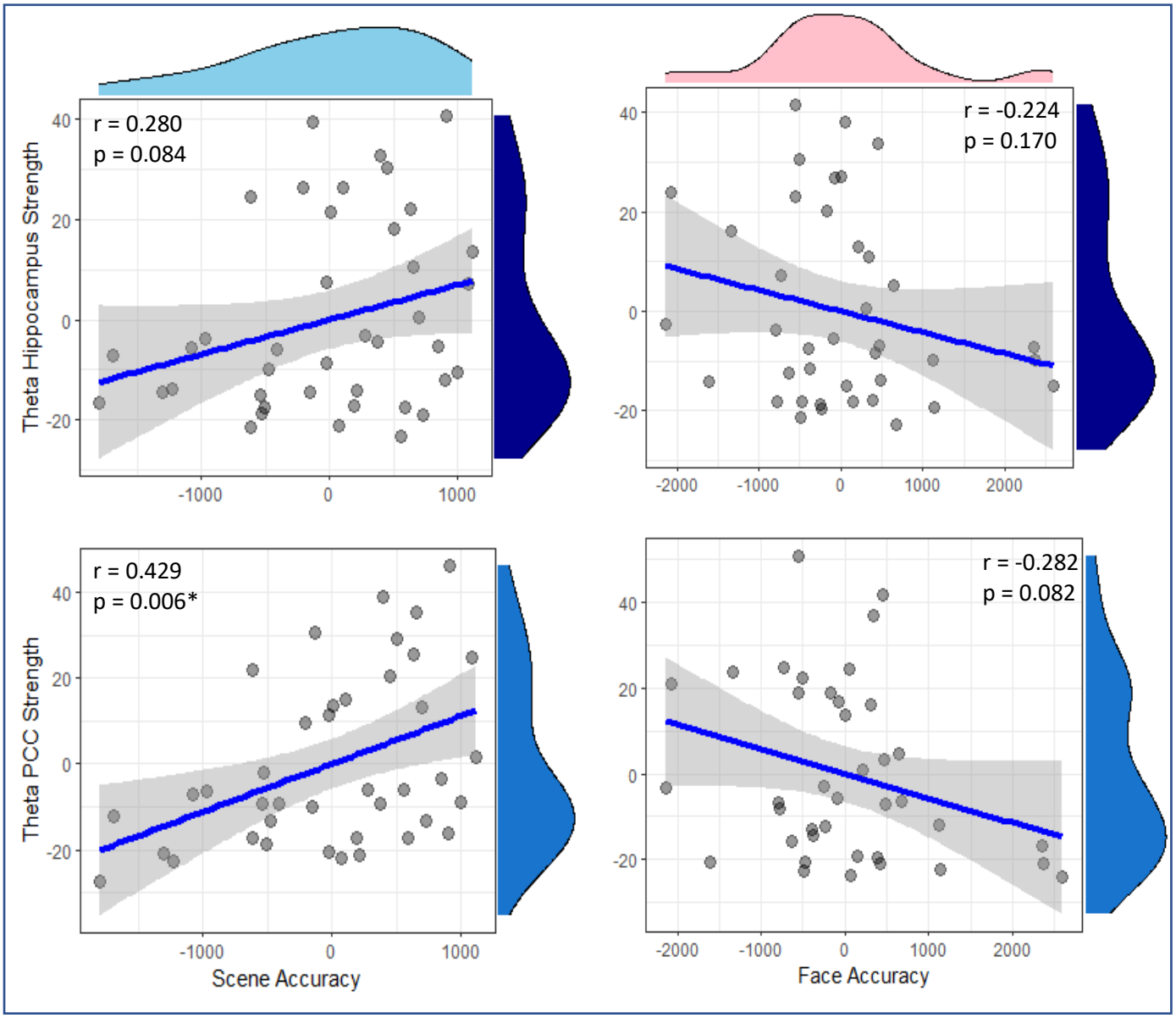

Figure 36. Scatterplots showing the relationships between scene and face oddity performance and hippocampus and PCC connectivity strengths.

The light blue histogram shows the distributions of the scene accuracy data and the light pink histogram shows the face accuracy data. The darker(top) and lighter (bottom) blue histograms show the distributions of the theta hippocampus and PCC connectivity strength scores, respectively. Note that these data are the residuals after controlling for scene d' scores (two left scatterplots) and for face d' scores (two right scatterplots). The blue lines are the regression lines and the surrounding shaded areas represent the 95% confidence interval. Note that the accuracy data was transformed to normal. *Highlights p≤0.006.

PCC: Posterior Cingulate Cortex.

6.3.2 Investigating relationships between Hippocampus-PCC connectivity and scene processing with FG-IOC connectivity and face processing.

There were no significant partial correlations between RS hippocampus-PCC or hippocampus-thalamus connectivity and scene or face oddity accuracy (controlling for scene and face d'). The BFs indicated only weak evidence in favour of a positive relationship between scene oddity accuracy and theta hippocampus-PCC connectivity, and a negative relationship between face oddity accuracy and theta hippocampus-PCC connectivity (Table 18; Figure 37). There were also no significant correlations between hippocampus-PCC theta connectivity, or hippocampus-thalamus connectivity, and size oddity accuracy (statistics shown in *Appendix 3C*).

		Scene Accuracy	Face Accuracy
Hippocampus-PCC	theta	r = 0.252 p = 0.121 BF_{10} = 1.07	r = -0.251 p = 0.123 BF_{10} = 1.01
	alpha	r = -0.081 p = 0.624 BF_{10} = 0.38	r = -0.239 p = 0.146 BF_{10} = 0.87
	beta	r = 0.083 p = 0.616 BF_{10} = 0.39	r = -0.030 p = 0.857 BF_{10} = 0.36
Hippocampus - Thalamus	theta	r = 0.151 p = 0.389 BF_{10} = 0.51	r = -0.257 p = 0.114 BF_{10} = 1.08
	alpha	r = 0.023 p = 0.888 BF_{10} = 0.36	r = -0.001 p = 0.997 BF_{10} = 0.36
	beta	r = 0.146 p = 0.375 BF_{10} = 0.50	r = -0.040 p = 0.810 BF_{10} = 0.36

Table 18. Partial correlation tests between oddity task performance and hippocampus-PCC and hippocampus-thalamus connectivity scores.

Partial correlation tests between Hippocampus and PCC PMN connectivity strengths, in theta, alpha and beta bands, and oddity accuracy. Scene and face memory scores (d') were controlled-for. N=40.

PCC: Posterior Cingulate Cortex.

Contrary to the hypothesis, FG-IOC connectivity, in any of the frequency bands, did not significantly correlate with face oddity accuracy or scene oddity accuracy (Table 19).

		Scene Accuracy	Face Accuracy
FG-IOC	theta	r = 0.122 p = 0.459 BF_{10} = 0.56	r = -0.110 p = 0.505 BF_{10} = 0.42
	alpha	r = -0.075 p = 0.651 BF_{10} = 0.38	r = 0.087 p = 0.599 BF_{10} = 0.41
	beta	r = -0.142 p = 0.387 BF_{10} = 0.49	r = 0.013 p = 0.936 BF_{10} = 0.35

Table 19. Partial correlation tests between oddity task performance and FG-IOG connectivity scores.

Partial correlation tests between FG-IOC connectivity scores, in theta, alpha and beta bands, and oddity accuracy. Scene and face memory scores (d') were controlled-for.
N=40.

FG: Fusiform Gyrus. IOC: Inferior Occipital Cortex.

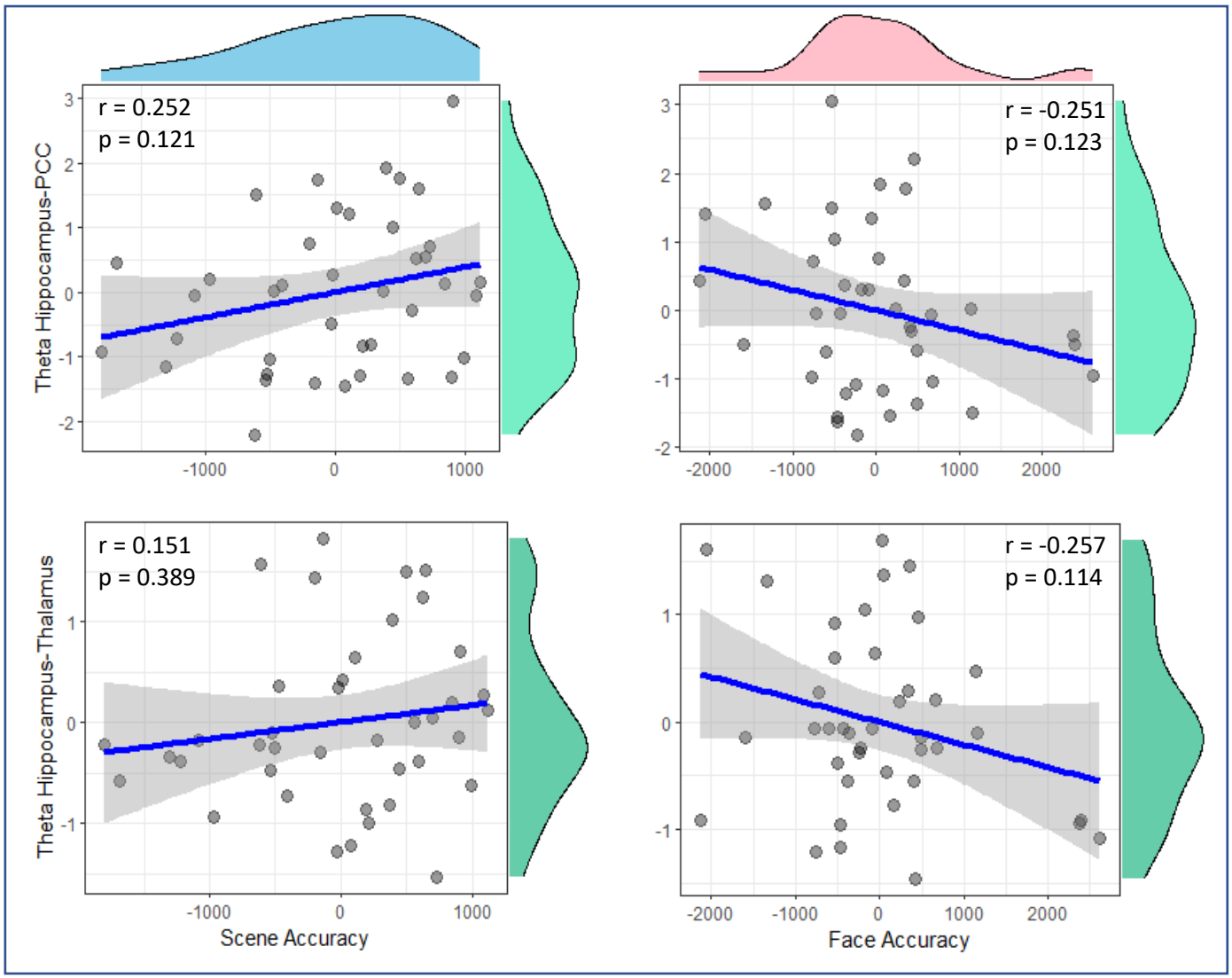

Figure 37. Scatterplots showing the non-significant relationships between scene and face oddity accuracy and theta hippocampus-PCC and hippocampus-thalamus connectivity.

The light blue histogram shows the distributions of the scene accuracy data and the light pink histogram shows the face accuracy data. The lighter (top) and darker (bottom) green histograms show the distributions of the theta hippocampus-PCC and hippocampus-thalamus connectivity scores, respectively. Note that these data are the residuals after controlling for scene d' scores (two left scatterplots) and for face d' scores (two right scatterplots). The blue lines are the regression lines and surrounding shaded areas represent the 95% confidence interval. There were no significant correlations between theta hippocampus-PCC or hippocampus-thalamus connectivity and scene or face oddity accuracy. However, the coefficient of the correlation between theta hippocampus-PCC and scene oddity accuracy was significantly different to that of the correlation between theta hippocampus-PCC and face oddity accuracy. Note that the accuracy data was transformed to normal.

PCC: Posterior Cingulate Cortex.

6.3.3 Investigating relationships between RS-connectivity and tract microstructure.

Contrary to the hypotheses, there were no significant correlations between hippocampus-PCC connectivity, hippocampus-thalamus connectivity, and fornix microstructure components. Unexpectedly, there was a correlation between ILF PC2 and alpha hippocampus-thalamus connectivity (Table 20). However, the coefficient of the correlation between alpha hippocampus-thalamus connectivity and ILF PC2 was not significantly stronger than that of the correlation between alpha hippocampus-thalamus connectivity and fornix PC2 ($z_{(36)}$ = -1.795, p = 0.073).

		Fornix		**ILF**	
		PC1	**PC2**	**PC1**	**PC2**
Hippocampus-PCC	theta	r = 0.124 p = 0.450 BF_{10} = 0.46	r = 0.092 p = 0.579 BF_{10} = 0.41	r = 0.145 p = 0.379 BF_{10} = 0.50	r = -0.228 p = 0.162 BF_{10} = 0.84
	alpha	r = 0.023 p = 0.891 BF_{10} = 0.36	r =-0.023 p = 0.889 BF_{10} = 0.36	r = 0.169 p = 0.303 BF_{10} = 0.57	r = -0.292 p = 0.071 BF_{10} = 1.49
	beta	r = 0.011 p = 0.945 BF_{10} = 0.36	r = 0.178 p = 0.279 BF_{10} = 0.60	r = 0.252 p = 0.122 BF_{10} = 1.02	r = -0.293 p = 0.070 BF_{10} = 1.50
Hippocampus-Thalamus	theta	r = -1.500 p = 0.143 BF_{10} = 0.92	r = -0.035 p = 0.830 BF_{10} = 0.36	r = -0.026 p = 0.875 BF_{10} = 0.36	r = -0.289 p = 0.074 BF_{10} = 1.45
	alpha	r = -0.010 p = 0.547 BF_{10} = 0.42	r = -0.151 p = 0.358 BF_{10} = 0.52	r = 0.226 p = 0.167 BF_{10} = 0.82	r = -0.462 p = 0.003* BF_{10} = 16.7*
	beta	r = 0.076 p = 0.644 BF_{10} = 0.39	r = 0.014 p = 0.934 BF_{10} = 0.36	r = 0.567 p = 0.094 BF_{10} = 0.41	r = -0.300 p = 0.063 BF_{10} = 1.62

Table 20. Correlation tests between hippocampus-PCC and hippocampus-thalamus connectivity, and fornix and ILF microstructure components.

*Highlights p≤0.006. *Highlights a BF_{10} ≥ 3. N=39.

ILF: Inferior Longitudinal Fasciculus. PC: Principal Component. PCC: Posterior Cingulate Cortex.

All correlations between hippocampus or PCC connectivity strength in any of the frequency bands, and fornix and ILF microstructure exceeded the experiment-wise alpha level (Table 21). However, there were trends between ILF PC2 and theta/alpha/beta hippocampus connectivity strength and alpha/beta PCC connectivity strength which were supported by BFs indicating evidence against the null.

		Fornix		ILF	
		PC1	**PC2**	**PC1**	**PC2**
hippocampus connectivity strength	Theta	r = 0.074 p = 0.653 BF_{10} = 0.39	r = -0.016 p = 0.921 BF_{10} = 0.36	r = 0.152 p = 0.356 BF_{10} = 0.52	r = -0.381 p = 0.017 BF_{10} = 4.37*
	Alpha	r = 0.005 p = 0.978 BF_{10} = 0.36	r = -0.069 p = 0.677 BF_{10} = 0.38	r = 0.246 p = 0.131 BF_{10} = 0.97	r = -0.367 p = 0.022 BF_{10} = 3.60*
	Beta	r = 0.124 p = 0.450 BF_{10} = 0.46	r = 0.111 p = 0.503 BF_{10} = 0.43	r = 0.328 p = 0.041 BF_{10} = 2.21	r = -0.408 p = 0.010 BF_{10} = 6.63*
PCC connectivity Strength	Theta	r = -0.057 p = 0.732 BF_{10} = 0.38	r = 0.077 p = 0.640 BF_{10} = 0.39	r = 0.103 p = 0.533 BF_{10} = 0.42	r = -0.263 p = 0.105 BF_{10} = 1.13
	Alpha	r = -0.047 p = 0.776 BF_{10} = 0.37	r = -0.051 p = 0.756 BF_{10} = 0.37	r = 0.209 p = 0.202 BF_{10} = 0.73	r = -0.364 p = 0.022 BF_{10} = 3.50*
	Beta	r = 0.027 p = 0.869 BF_{10} = 0.36	r = 0.099 p = 0.547 BF_{10} = 0.42	r = 0.247 p = 0.130 BF_{10} = 0.97	r = -0.329 p = 0.041 BF_{10} = 2.23

Table 21. Correlation tests between hippocampus and PCC connectivity strengths, and fornix and ILF microstructure components.

*Highlights p≤0.006. *Highlights a $BF_{10} \geq 3$. N=39.

ILF: Inferior Longitudinal Fasciculus. PC: Principal Component. PCC: Posterior Cingulate Cortex.

In line with the hypotheses, there were significant correlations between ILF PC2 and FG-IOC connectivity in the theta, alpha and beta bands (Table 22). There were also trends between ILF PC1 and FG-IOC connectivity in the alpha and beta bands which were supported by BFs indicating evidence against the null. Also, there were no significant correlations between FG-IOC connectivity and fornix microstructure.

		Fornix		**ILF**	
		PC1	PC2	PC1	PC2
FG-IOC	theta	r = 0.168 p = 0.306 BF_{10} = 0.56	r = -0.044 p = 0.791 BF_{10} = 0.37	r = 0.347 p = 0.031 BF_{10} = 2.76	r = -0.467 p = 0.003* BF_{10} = 18.36*
	alpha	r = 0.126 p = 0.441 BF_{10} = 0.46	r = 0.001 p = 0.950 BF_{10} = 0.36	r = 0.405 p = 0.011 BF_{10} = 6.27*	r = -0.44 p = 0.005* BF_{10} = 11.84*
	beta	r = 0.198 p = 0.226 BF_{10} = 0.68	r = 0.129 p = 0.436 BF_{10} =0.47	r = 0.354 p = 0.027 BF_{10} = 3.03*	r = -0.435 p = 0.006* BF_{10} = 10.24*

Table 22. Correlation tests between FG-IOC and fornix and ILF microstructure components.

*Highlights p≤0.006. *Highlights a $BF_{10} \geq 3$. N=39.

ILF: Inferior Longitudinal Fasciculus. PC: Principal Component. FG: Fusiform Gyrus. IOC: Inferior Occipital Cortex.

As predicted, the coefficient of the correlation between alpha FG-IOC connectivity and ILF PC2 was significantly larger than that of the correlation between alpha FG-IOC connectivity and fornix PC2 ($z_{(36)}$ = -2.620, p = 0.009). Similarly, the coefficient of the correlation between theta FG-IOC connectivity and ILF PC1 was significantly larger than that of the correlation between theta FG-IOC connectivity and fornix PC2 ($z_{(36)}$ = -2.451, p = 0.014; Figure 38).

There were no significant correlations between PHC microstructure scores and any ROI connectivity scores (statistics shown in *Appendix 3D*).

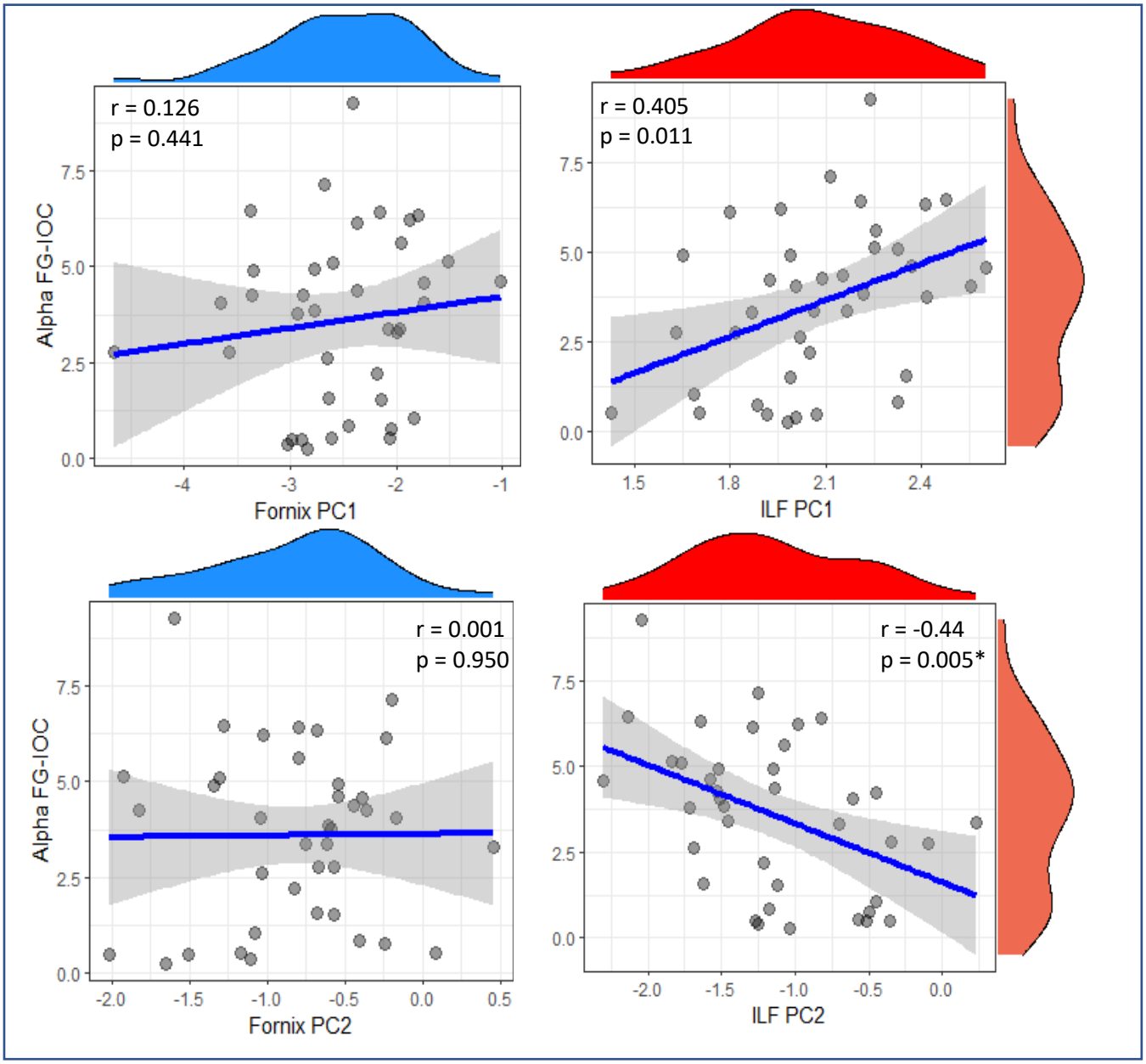

Figure 38. Scatterplots showing the relationship between Fornix and ILF microstructure component scores and alpha FG-IOC connectivity scores.

The blue histograms show the distributions of the fornix PC1 (top) and fornix PC2 (bottom) data. The red histograms show distributions of the ILF PC1 (top) and ILF PC2 (bottom) data. The lighter red histograms show the distribution of the alpha FG-IOC connectivity scores. The blue lines are the regression lines and the surrounding shaded areas represent the 95% confidence interval. *Highlights p≤0.006.

ILF: Inferior Longitudinal Fasciculus. PC: Principal Component. FG: Fusiform Gyrus. IOC: Inferior Occipital Cortex.

6.3.4 Whole-brain exploratory search for relationships between RS-connectivity, oddity performance and tract microstructure.

Exploratory analyses, searching for correlations between whole-brain RS-connectivity and scene oddity accuracy, and whole-brain RS-connectivity and fornix microstructure revealed one common connection in the theta band (Figure 39). Scene accuracy correlated with connectivity between the left angular gyrus and the left Heschl's gyrus. Fornix PC1 correlated with connectivity between the left angular gyrus and left hippocampus. There were no significant correlations between RS-connectivity and fornix PC2. There were no significant correlations between RS-connectivity and scene oddity accuracy or fornix microstructure in the alpha or beta bands.

	Theta	Alpha	Beta
Top 40% connections	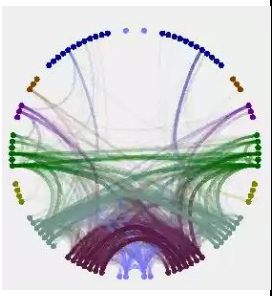 connections = 599	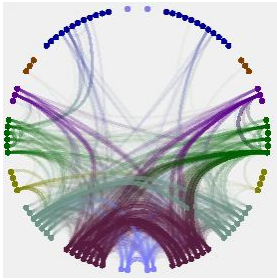 connections = 845	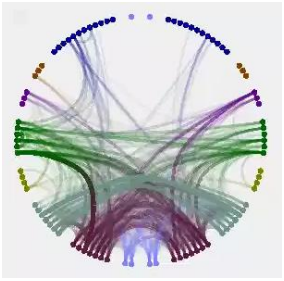 connections = 861
Scene Accuracy	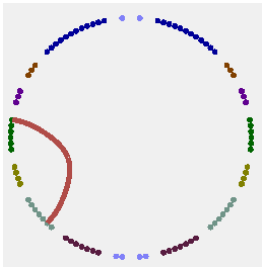 p value = 0.014 (FDR corrected)	X	X
Fornix PC1	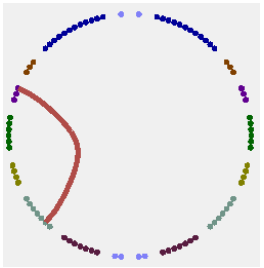 p value = 0.029 (FDR corrected)	X	X
Fornix PC2	X	X	X

Figure 39. Exploratory search for correlations between whole-brain RS-connectivity and scene oddity performance and fornix microstructure.

Coloured dots represent AAL atlas ROIs, with frontal regions located at the top of the circle and posterior and occipital regions located at the bottom of the circle. The top row shows the top 40% strongest connections for each of the frequency bands and the lines are colours by the regions they connect (see *Appendix 3A* for region names).
For the remaining rows, lines between ROIs indicate RS connectivities that correlated with the behaviour or structure measure. Red and blue lines indicate positive and negative correlations, respectively. Opacity and width of the lines indicate relative strength of the correlations within that test.

Alpha = 0.0083, FDR corrected p-value threshold = 0.05. N = 39. 'X' indicates no significant correlations.

PC: Principal Component.

Exploratory analysis, searching for correlations between whole-brain RS-connectivity and face oddity accuracy, and whole-brain RS-connectivity and ILF microstructure revealed no common connections within any frequency band (Figure 40). Face accuracy correlated with connectivity between the posterior and middle cingulum in the beta band. ILF PC1 correlated with multiple ROI-ROI connectivities in the alpha band. Most of these connectivities were between occipital areas but there were connections between: the occipital and temporal lobes; the parietal and temporal lobes; the PMC and the frontal lobe; and the parietal lobe and the MTL. ILF PC2 correlated with multiple ROI-ROI connectivities within the theta band. These connectivities were between several posterior areas including occipital, parietal, temporal and PMC areas.

	Theta	Alpha	Beta
Face Accuracy	X	X	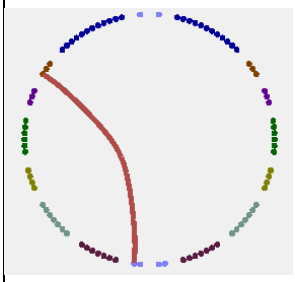 p value < 0.001
ILF PC1	X	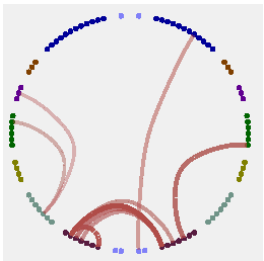 p values < 0.010	X

ILF PC2	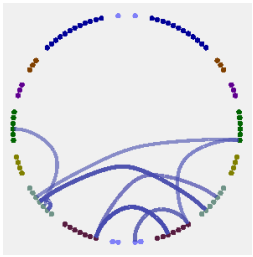 p values < 0.034	X	X

Figure 40. Exploratory search for correlations between whole-brain RS-connectivity and face oddity performance and ILF microstructure.

Coloured dots represent AAL atlas ROIs, with frontal regions located at the top of the circle and posterior and occipital regions located at the bottom of the circle (see *Appendix 3A* for region names). Lines between ROIs indicate RS connectivities that correlated with the behaviour or structure measure. Red and blue lines indicate positive and negative correlations, respectively. Opacity and width of the lines indicate relative strength of the correlations within that test.

Alpha = 0.0083, FDR corrected p-value threshold = 0.05. N = 39. 'X' indicates no significant correlations.

ILF: Inferior Longitudinal Fasciculus. PC: Principal Component.

6.4 Discussion

This study aimed to investigate correlations between inter-individual differences in RS-connectivity and task performance in a complex perceptual task, and between inter-individual differences in RS-connectivity and white-matter tract microstructure. It was hypothesized that dissociable relationships would be found for two networks. Specifically, RS connectivity patterns of the hippocampus and PCC, with other PMN ROIs, were predicted to correlate with scene oddity performance and not face oddity performance, and also to correlate with fornix microstructure and not ILF microstructure. The results provided partial support for this, as the strength of PCC connectivity to other PMN areas, in the theta band, correlated with scene oddity accuracy and not face or size oddity accuracy, but no correlations were found between fornix microstructure and any measures of RS-connectivity. Moreover, tests to see whether scene oddity performance and fornix microstructure related to specific RS connectivities, between the hippocampus and PCC, and between the hippocampus and thalamus, revealed no evidence to support these. Regarding the AIN, FG-IOC connectivity was predicted to correlate with face oddity performance and ILF microstructure. There was no evidence of correlations between face oddity accuracy and RS-connectivity, but ILF microstructure correlated with FG-IOC RS-connectivity.

6.4.1 The importance of widespread RS-connectivity of the PCC.

The PCC is a highly connected area within the DMN, a network which has been noted to be more active at rest than during task engagement (Leech & Sharp, 2014; Raichle, 2015), and is thought to be a key member of the PMN, which highly overlaps with the DMN (Ranganath & Ritchey, 2012). Both functional (Lord et al., 2017) and structural (Hagmann et al., 2008) mapping has identified the PCC as a major hub of the brain, and there are direct structural connections between the PCC and the mPFC, and the PCC and the MTL (Greicius et al., 2009). Along with the hippocampus, the PCC is an important area in the pathophysiology of AD (Lee et al., 2020; Liang et al., 2008), a disease thought to affect the PMN (Ranganath & Ritchey, 2012), and RS-connectivity of the PCC has been shown to be reduced, and correlate with cognitive impairment, in MCI (Bai et al., 2009). The current results extend the importance of PCC RS-connectivity in PMN processing to healthy adults. Moreover, RS-connectivity of the PCC correlated only with scene oddity performance and not face or size oddity performance, thus supporting the PM-view, which states that the

PMN carries out spatiotemporal processing (Murray et al., 2017; Ranganath & Ritchey, 2012).

It is unclear whether connectivity of the PCC reflects its direct involvement in scene processing, or simply its large influence on PMN communication. The PCC could play a role in internal processing, generating internal representations (Leech & Smallwood, 2019), a process that is thought to be necessary for solving the oddity task (Barense et al., 2010). The connectivity of the PCC with both the DMN and PMN may also result in its pivotal role in internal scene presentations, specifically. Additionally, since the PCC is a major network hub (Hagmann et al., 2008), it has been suggested that it regulates network dynamics (Leech & Smallwood, 2019). In this view, the PCC may activate and deactivate networks (such as the DMN and PMN) depending on the current task demands, such as reducing activity in task-irrelevant areas during sensory processing, to balance the brain's activity (Hellyer et al., 2017; Leech & Smallwood, 2019).

The suggested role of the PCC in regulating network-wide activity would explain the apparent lack of importance of RS hippocampal connectivity in scene oddity performance. Although this seems to contradict studies showing the engagement of the hippocampus in this task (Barense et al., 2010; Graham et al., 2010; Hodgetts et al., 2015) and also contradicts the EAM, which suggests that the hippocampus is crucial for spatiotemporal processing (Murray et al., 2017, 2018), these studies inspect the task-state and this single area rather than a network, and the PCC is proposed to have more of a role in mediating whole-brain network information flow than the hippocampus (Lee et al., 2020; Leech & Sharp, 2014).

Similarly, the suggested role of the PCC in regulating PMN-wide activity would explain why the microstructure measures of neither the fornix nor the PHC correlated with theta RS-connectivity strength of the PCC to the other PMN ROIs. There is evidence that the fornix supports hippocampal theta (Rawlins et al., 1979; Swanson & Cowan, 1979), which has been shown to influence PCC theta (Colom et al., 1988), and that connections between the PCC and MTL have been shown to run along the PHC bundle (Greicius et al., 2009). However, study of the direct pathway between the hippocampus and PCC may not reflect the role of the PCC within the PMN as well as studying all PCC-PMN connections. Indeed, PCC connections are supported by multiple white-matter routes (Greicius et al., 2009). Moreover, hippocampally-independent theta rhythms have been measured in the PCC. Therefore, the theta amplitude correlations between the PCC and other PMN areas may

not be limited by the characteristics of the direct structural connection with the hippocampus.

The current results share similarities with a study investigating structural and functional connections in MCI (Gilligan et al., 2019), which found altered fornix and PHC microstructure and reduced functional connectivity between the hippocampus and DMN areas, but no correlation between the two. This, together with the current results, may mean that fornix/PHC microstructure and RS-connectivity independently relate to PMN functioning. On the other hand, both studies used network-wide functional measures (average connection strength was used here while Gilligan et al. used graph theory measures), but the structure of a small number of individual tracts was assessed. If microstructure measures of multiple PCC structural connections were collectively scored in a similar way, it might be that structure and function correlations would be revealed.

The aim of this study was to investigate correlations between RS-connectivity patterns and scene perceptual performance, specifically. As it has been argued that MTL activity during oddity tasks are actually reflections of encoding processes (Suzuki, 2009), and because there was a weak relationship between scene oddity accuracy and scene d' (*Chapter 5*), it was important to control for potential incidental encoding activity that may have occurred during the RS period. This means that the correlation between theta PCC connectivity strength within the PMN and scene accuracy is independent of encoding processes. The importance of RS PCC connectivity outside of mnemonic processes has also been shown in a study investigating scene construction impairments in AD (Irish et al., 2015), which asked patients to imagine fictitious scenes. Using voxel-based morphometry as a measure of structure quality, the authors found an association between PCC structure and scene construction performance in both patients and healthy controls. However, this is not to say that RS-connectivity of the PCC within the PMN is not related to memory processes. Indeed, previous work has already identified relationships between PCC RS-connectivity patterns and memory functioning (Greicius et al., 2004; Natu et al., 2019). Instead, we can conclude that RS-connectivity patterns of the PCC may reflect a role in spatiotemporal processing across memory, perception and imagining, echoing the predictions of the PM-view.

6.4.2 The relationship between ILF microstructure and RS-connectivity measures.

There was partial support for the hypothesis that ILF microstructure measures would specifically correlate with FG-IOC RS-connectivity. There were significant correlations

between FG-IOC RS-connectivity in the theta, alpha and beta bands, and ILF PC2, and not fornix or PHC PC2. Moreover, there were trends between ILF PC1 and FG-IOC RS-connectivity in the alpha and beta bands, which were supported by BFs over 3. The FG and IOC are connected through the ILF (Herbet et al., 2018) but a correlation between their RS-connectivity and ILF microstructure had not been demonstrated in healthy adults before. This adds to the evidence that RS-connectivity relates to the underlying brain structure (Betzel et al., 2014; Messaritaki et al., 2020).

However, since FG-IOC connectivity did not relate to face oddity performance, it is unclear whether there is a behavioural consequence of this correlation between structure and function. Furthermore, ILF microstructure may not specifically relate to connectivity within the AIN as ILF PC2 also correlated with alpha hippocampus-thalamus connectivity, and there were trends between ILF PC2 and hippocampus, and between ILF PC2 and PCC, connectivity strengths, supported by BFs above 3. There are several possible reasons for correlations between ILF PC2 and widespread alpha RS-connectivity: RS-connectivity patterns between areas connected by the ILF may also influence connections elsewhere in the brain; as the thalamus may influence occipital alpha (Minami et al., 2020), there may be a mechanism by which thalamic alpha influences both functional visual pathway communication and ILF tract structure; or given that the ILF is a large tract, the average microstructure of this tract may be more representative of an individual's average white-matter properties across the whole brain, than the fornix or PHC. Expanding the last point, this would mean that ILF microstructure measures are more likely to be closely related to microstructure measures of other tracts, and therefore to relate to RS-connectivity patterns between brain areas that the ILP does not connect. Lastly, there is a risk that measures of RS-connectivity patterns of deep brain areas measures may be inaccurate (see *Limitations* section 6.4.5) so RS-connectivity strength of the hippocampus, for example, may not actually represent hippocampal connectivity, but rather connectivity from another region (poor localization) or noise. Therefore, ILF microstructure may correlate with functional connectivities of areas it anatomically connects, but these functional signals have been mis-localized. Future work, which controls for voxel numbers within compared tracts and invasively records deep brain activity, would provide insight into the validity of these suggestions.

6.4.3 Partial dissociability between connectivity frequencies between the networks.

It is has been demonstrated that intra- and inter-network connectivity in different frequency bands are unequal across RS networks (Hillebrand et al., 2012). It was hypothesized that behaviourally and structurally relevant connectivity between the PMN and AIN ROIs would be primarily in the theta and alpha bands, respectively. The results provide support for this, as scene oddity accuracy correlated with PCC connectivity strength only in the theta band. Moreover, the exploratory analyses, which searched for correlations between scene oddity accuracy and whole-brain RS-connectivity strength and between fornix microstructure and whole-brain RS-connectivity strength, only revealed significant correlations with connectivities in the theta band. These findings appear to contradict the RS-MEG study that showed reduced connectivity in AD specifically in the alpha and beta bands (Koelewijn et al., 2017). However, it may be that optimal PMN functionality relies on functional connections in multiple bands, but that only theta connectivity relates to individual differences in behaviour in healthy adults.

The reason for the specific importance of RS theta amplitude correlations in scene processing performance remains unclear. It was hypothesized that PMN theta connectivity would be relevant because hippocampal processing is important in scene oddity task completion (Barense et al., 2007; Hodgetts et al., 2015; Hodgetts, Voets, et al., 2017) and hippocampal processing has been associated with theta rhythms (Buzsaki, 2002). Although hippocampus-PCC RS-connectivity did not relate to oddity task performance, PCC communication with the hippocampus may still influence PCC connectivity strength to other PMN areas. On the other hand, there are hippocampus-dependent theta rhythms in the PCC (Talk et al., 2004).

Regardless of the underlying mechanism, the finding of the importance of PCC theta aligns with the results of a study assessing RS oscillatory peaks of the PMC, an area with includes the PCC (Foster & Parvizi, 2012). RS spectral power of the PMC was found to peak in the theta range, a pattern that was distinguishable from nearby occipital tissue which displayed spectral power peaks in the alpha range.

There was less support for the specific importance of connectivity in the alpha band within the AIN. ILF microstructure was found to relate to alpha RS FG-IOC and alpha RS hippocampus-thalamus, but it also correlated with RS FG-IOC connectivities in the theta

and beta ranges. Furthermore, no RS-connectivities correlated with face oddity performance. The exploratory analyses indicated relationships between ILF PC1 and whole-brain alpha RS connectivities, but ILF PC2 and face oddity accuracy related to whole-brain RS connectivities in the theta and beta bands, respectively. Therefore, further assessment of functional connections between face processing regions is necessary to understand whether there is a dominant oscillatory frequency binding these areas.

6.4.4 The evidence for three-part relationships between structure, function and behaviour.

Since brain white-matter microstructure can predict functional connectivity between brain areas at rest (Messaritaki et al., 2020), and there is evidence of relationships between white-matter microstructure and behaviour (e.g. Hodgetts et al. 2015), and RS-connectivity and behaviour (e.g. Sulpizio et al. 2016), it was hypothesized that three-part relationships between structure, function and behaviour would be found for the PMN and AIN networks. Specifically, it was predicted that RS-connectivity of the hippocampus with the PCC or thalamus would correlate with both scene oddity performance and fornix microstructure (which was evidenced to relate to scene oddity performance in *Chapter 5*). Similarly, it was predicted that RS-connectivity between the FG and IOC would correlate with both face oddity performance and ILF microstructure (which was evidenced to correlate with face oddity performance in *Chapter 5*). However, the results suggest that, in the case of PMN functioning, fornix microstructure and RS PCC theta connectivity strength independently relate to scene oddity performance. This aligns with the results of *Chapter 5,* which indicated that fornix PC1 and HPC theta change between scene oddity and fixation independently correlated with scene oddity task performance, and of Hodgetts et al. (2015), which also showed that fornix MD and hippocampal BOLD decrease between scene oddity task and baseline independently correlated with scene oddity performance.

However, the results from the exploratory analyses could incite further investigation into the angular gyrus. Theta RS-connectivity between the left angular gyrus and left hippocampus correlated with fornix PC1, and theta RS-connectivity between the left angular gyrus and the left lateral temporal cortex (Heschl's gyrus) correlated with scene oddity accuracy. Moreover, the angular gyrus is part of the IPL, an area which displayed modulated oscillatory power during scene oddity task completion in *Chapter 4*. Therefore, the angular gyrus appears to be a common factor in PMN structure, function and behaviour.

6.4.5 Limitations.

The challenge of measuring deep source activity may explain why no relationships were found between hippocampus RS and scene oddity performance, or between any RS-connectivity patterns and fornix microstructure. Measuring signals from deep brain structures such as the hippocampus and thalamus is challenging in MEG (Hillebrand & Barnes, 2002). Hippocampal signals have been shown to be measurable with MEG when source subtraction techniques are used, as in *Chapter 4*, to reduce the overshadowing of weak deep MTL signals by stronger visual signals (Quraan et al., 2011). However, since RS is taskless, source activity from different conditions cannot be contrasted to cancel-out stronger signals, making measuring RS-connectivity between deep sources with MEG challenging. The challenge of measuring deep brain RS-connectivity is illustrated in three studies (Dima et al., 2020; Godfrey & Singh, 2020; Koelewijn et al., 2019) that measured amplitude-amplitude coupling across AAL ROIs and used a ranking procedure to isolate the top 20% strongest connections. Hippocampus connections did not surpass this threshold in any frequency band studied, in any of the studies, indicating either that the strengths of hippocampal connections are highly variable across participants, or that they are consistently weak, both of which could be caused by a low SNR. The field would benefit from a re-evaluation of the relationships between RS-connectivity of the hippocampus and fornix microstructure or scene processing performance, with the use of a technique which can better measure deep brain sources. Several fMRI studies have shown correlations between RS hippocampal connectivity with structure or behaviour (Kehoe et al., 2015; Sulpizio et al., 2016; Wegman & Janzen, 2011), but fMRI does not allow the measurement of electrophysiological oscillatory activity, and results of the current study indicated the specific importance of PMN connectivity within the theta band. Invasive electrophysiological recording may allow further understanding into whether fornix microstructure relates to hippocampal RS-connectivity in the theta band specifically.

ILF microstructure, and FFA BOLD modulation, have previously been shown to relate to face oddity performance (Hodgetts et al., 2015), and the present study showed an association between FG-IOC RS-connectivity and ILF microstructure, so the lack of evidence for a correlation between FG-IOC RS-connectivity and face oddity performance, was unexpected. However, the ILF is a large tract with multiple subcomponents (Catani et al., 2003), and the FG has multiple functional roles (Weiner & Zilles, 2016), so it is possible that a non-face-sensitive network was inspected. This is because the choice of the representative VS for each area was based on the voxel with the largest activity change

during the recording, rather than functional activations of the areas. The VSs could have been reflecting activity from brain areas that do not have roles in face processing. Therefore, while I aimed to measure RS-connectivity between two face areas, and individual differences in this connectivity could have no association with face processing performance, it is also possible that RS-connectivity between two areas not primarily associated with face processing, but still connected via the ILF, was measured. Previous studies inspecting the OFA and FFA have used fMRI and run functional localizer scans to ensure that face specific areas are being inspected (Kanwisher et al., 1997; Pitcher et al., 2011). However, a similar method in MEG would be challenging because the face localizing task and RS recording would have to take place within the same session, otherwise mapping exact brain locations from two recordings with different head localization measures, would incite source localization errors. A future MEG study, hoping to localize RS-connectivity between face specific areas could produce VSs from these areas using a PCA technique to reduce the signal data (see *Chapter 4* and Seymour et al., 2014) and then investigate for correlations between the resulting components and face processing ability.

RS-connectivity patterns were thought to portray an individual 'trait' inasmuch as RS patterns are less variable over time than in-task activity patterns. However, true RS patterns of the participants may not have been captured as the scan took place after the oddity task, because it was anticipated that beginning a long MEG session with inactivity in a dimly lit room may increase the chances that participants were fatigued before the end of the session. It also created a minimum time between the oddity and memory tasks. Lingering oddity task processes may have influenced the scan. For example, the PMN and AIN may have been more active. Therefore, the correlation between PCC theta connectivity strength and scene oddity performance may be interpreted as a relationship between scene processing ability and connectivity between PMN areas post-scene-processing, rather than connectivity between PMN areas during rest. Future work could compare RS patterns before and after the oddity task to characterize influences of carry-over effects.

Lastly, it should be noted that amplitude-amplitude oscillation correlations are only one measure of functional connectivity, and further correlations between RS-connectivity, behaviour and structure may have been identified if another functional connectivity method was used. For example, other methods include oscillation-based coupling, such as phase-coherence between different brain areas (Marquetand et al., 2019) or entropy-based coupling, in which brain areas can be functionally coupled through correlations in irregular activity over time (Godfrey & Singh, 2020). The amplitude-amplitude correlation

method was used because it has been demonstrated to be one of the most reliable measures of RS-MEG connectivity (Colclough et al., 2015), but this field may benefit from future work that combines functional connectivity measures from different methods to better portray functional correlations within the PMN and AIN.

6.5 Conclusion

This study aimed to investigate correlations between inter-individual differences in RS-connectivity and task performance in a complex perceptual task, and between inter-individual differences in RS-connectivity and tract microstructure. In line with the hypotheses, theta RS-connectivity strength between the PCC and other PMN areas correlated with scene oddity performance and not face or size oddity performance, demonstrating the importance of theta PCC connectivity in spatiotemporal processing. The confirmatory analyses revealed no correlations between RS-connectivity and fornix microstructure, suggesting that theta RS-connectivity within the PMN and fornix microstructure independently relate to scene processing performance. However, exploratory whole-brain analyses indicated theta connectivity of the angular gyrus as a common element in correlations between RS-connectivity and scene oddity accuracy, and RS-connectivity and fornix microstructure, suggesting that it may act as a mediating factor between structure and behaviour. Confirmation of this would need further investigation. Regarding the AIN, and contradicting the predictions, no RS-connectivity patterns correlated with face oddity performance. However, there were RS-connectivity patterns, such as alpha FG-IOC, that did correlate with ILF microstructure, which aligned with the hypotheses. Overall, the results demonstrate the behavioural relevance of PMN RS-connectivity in the theta band, particularly between the PCC and other PMN areas.

Chapter 7: Examining relationships between structure and object-in-sequence memory performance in the PMN and AIN.

7.1 Introduction

7.1.1 Background.

Space and time are often combined in episodic memory (Eichenbaum, 2017a) and the PMN is thought to conduct concurrent spatiotemporal processing (Murray et al., 2017; Ranganath & Ritchey, 2012). Up to this point, this thesis has assessed the role of the PMN, specifically the hippocampus and fornix, in spatial processing but the role of the PMN in temporal processing has not been similarly addressed. PMN areas, in particular components of the extended hippocampal network that are connected via the fornix, have been shown to be critical for episodic memory (Aggleton & Brown, 1999), specifically through contributions to the processing of space and time (Buzsaki & Moser, 2013; Ranganath & Hsieh, 2016). Inter-individual differences in fornix microstructure in healthy individuals have been shown to be correlated with recollection of episodic information (Rudebeck et al., 2009), spatial-temporal information in autobiographical memories (Hodgetts, Postans, et al., 2017), spatial perception (Hodgetts et al., 2015) and spatial learning (Hodgetts et al., 2020). To date, however, the contribution of the fornix to temporal sequence memory has not been investigated in healthy humans, and animal and human lesion studies have provided inconclusive results (Charles et al., 2004; Hunsaker & Kesner, 2009).

Work by Hsieh et al. (Hsieh et al., 2014; Hsieh & Ranganath, 2015) involving object-in-sequence memory, has shown that the hippocampus holds object-in-sequence information. In these studies, participants learned several different object sequences, by answering semantic questions on the objects. They then underwent fMRI, during which they again answered semantic questions on the objects presented in these sequences. Activation pattern similarity matrices showed that the hippocampus responded to object-in-sequence information. Other PMN areas, the mPFC, RSC, parahippocampal cortex and angular gyrus, responded to sequence position regardless of which objects were presented in that sequence position. Conversely, the PrC, an important region in the AIN, responded to the objects regardless of where they were positioned in the sequence.

These findings suggest that the temporal context of events may arise through processing of object-in-sequence information in the hippocampus, complementing the purely contextual processing functions of other PMN areas, and aggregate object processing in the AIN. Therefore, microstructure of the fornix, the main connecting tract of the hippocampus, may determine the effectiveness of communication between the hippocampus in support of temporal processing, and relate to interindividual differences in temporal memory.

Previous animal research examining contributions of the fornix to temporal sequence memory has produced inconclusive results. For example, rats with dorsal fornix transections (thought to be the major output of the hippocampal CA1 sub-region) were found to be unimpaired in the temporal processing component of an object recognition task, but they displayed poor novel object detection (Hunsaker & Kesner, 2009). The authors suggested that preservation of the direct perforant pathway between CA1 and the entorhinal cortex may have allowed temporal information still to be effectively communicated. By contrast, complete transection of the fornix in monkeys has been shown to result in poor between-session recency memory in a delayed matching-to-sample task, while sparing object novelty detection (Charles et al., 2004). This task required the selection of an item seen in the preceding sequence as opposed to an item seen elsewhere during the task. Similarly, impaired temporal order memory but intact content memory has been described in a human fornix lesion case, a finding attributed to disrupted fronto-hippocampal communication (Yasuno et al., 1999).

There are multiple possible mechanisms by which the hippocampus and connected regions could support the temporal ordering of information. Items within events may be temporally ordered through serial inter-item associations or item-position coding (Cohn-Sheehy & Ranganath, 2017; Long & Kahana, 2019). The hippocampus may also support representation of temporal associations within groups of objects without specific serial orders (Cohn-Sheehy & Ranganath, 2017). For example, the hippocampus has been reported to hold information about temporal community structures (Schapiro et al., 2016), in which transition probabilities within communities are equal and therefore items are temporally linked but not in any specific order. Both mechanisms may be related to sequence boundary effects, where memory for event order within events is enhanced compared with memory for event order across contextual boundaries (DuBrow & Davachi, 2013). Hippocampal activity has also been reported to alter at sequence boundaries (Schapiro et al., 2016). The hippocampus thus appears to be important for memory of objects grouped by their temporal proximity, either with specific serial orders (object-

position binding) or without specific orders. It may be that an extended-hippocampal network, supported by the fornix, is also important for these functions.

7.1.2 Aims and hypotheses.

To investigate the role of the fornix in object-in-sequence memory, an adaptation of the behavioural task of Hsieh et al. (2014) was used. Participants were exposed to two types of object sequences: fixed sequences (objects always appeared in fixed temporal positions) and random sequences (objects appeared in random temporal positions). During the 'Learning Phase', they answered semantic questions about objects, which were presented in their associated sequences. In the 'Retrieval Phase' they also answered semantic questions about the objects, which were again presented in their associated sequences, and novel object sequences were also included. As in Hsieh et al. (2014), the time taken to answer the semantic questions (RT) was used as a measure of implicit learning of object structures. This differs from previous chapters of this thesis where accuracy was the focus, because semantic decision accuracy was not of interest, and measuring RT can reveal individual differences in retrieval even if accuracy levels are at ceiling level (the task was designed to be easy). Average response RTs for novel, random and fixed sequences were contrasted, with the assumption that response RTs to objects learned in randomly ordered sequences would be shorter than response RTs to novel objects, and that response RTs to objects learned in fixed ordered sequences would be shorter than response RTs to objects learned in randomly ordered sequences. These measures of object-in-sequence memory were called 'RT Enhancement novel-random' and 'RT Enhancement random-fixed', respectively. The aims of this study were threefold: to assess the role of hippocampal communication in temporal memory, by testing for associations between fornix microstructure and performance in the object-in-sequence memory task; to investigate whether this fornix pathway is specific to particular forms of temporal memory, by comparing the correlations with the two RT enhancement measures; and to investigate whether this fornix-supported pathway supports temporal memory retrieval independent of a contribution to learning.

There was thus a hypothesis that fornix microstructure would relate to measures of object-in-sequence retrieval, but the nature of the temporal memory was unclear. Considering that Hsieh et al. (2014) identified bound item-position information in the hippocampus, it could be predicted that inter-individual differences in fornix microstructure would be correlated with RT Enhancement random-fixed, indicating fornix contributions to bound

object-position memory. On the other hand, Hsieh et al. (2014/15) also found evidence for temporal context memory for random sequences, revealed as a gradual reduction in response RT across serial positions, indicating that memory of the object sequence facilitated anticipation of upcoming objects. This behavioural pattern indicates memory akin to temporal community structures. If individual differences in communication via the fornix related to this form of temporal memory, then fornix microstructure may relate to RT Enhancement novel-random.

It was unclear whether individual variation in the fornix-supported pathway would relate equally to temporal sequence learning and retrieval. While some microstructure studies have found associations between fornix microstructure and retrieval (Hayek et al., 2020; Hodgetts, Postans, et al., 2017), others have found associations between fornix microstructure and encoding (Green et al., 2016; Hodgetts et al., 2020). Additionally, hippocampal BOLD has been shown to increase during learning and retrieval of non-spatial sequences of faces (Ross et al., 2009), which aligns with the understanding that networks involved in successful encoding and retrieval heavily overlap (Rugg et al., 2008). Bridging encoding and retrieval processes together, a test of adaptability to changes in temporal structure over short delays in fornix-transected monkeys, has indicated that the fornix is crucial to the processes of updating internal models of temporal structure (Kwok et al., 2015). Together, these results suggest that individual differences in fornix microstructure would correlate with measures of temporal sequence learning to the same degree as measures of temporal sequence retrieval, or they might even imply that any apparent relationship between fornix microstructure and retrieval performance is actually just a reflection of encoding ability. However, functional connectivity within the PMN and AIN, and the hippocampus, has been found to differ in encoding and retrieval states (Cooper & Ritchey, 2019). Cooper and Ritchey (2019) examined fMRI-measured functional connectivity during encoding and retrieval of associations between objects, and the colour, spatial properties, and emotional properties of those objects. They found that while the connectivity patterns of the PMN and AIN networks indicated that they functioned somewhat separately from each other during encoding, whole network (all regions together) modularity decreased during retrieval, indicating increased connectivity between the networks, and between the network areas and the hippocampus, during this state. These results may indicate differing levels of influence of connecting white-matter properties on network functioning, within the learning and retrieval phases. Therefore, in addition to examining RT in retrieval responses during the retrieval phase, the accuracy of

sequence reconstruction during the learning phase was tested. This measure of retrieval, assessed intermittently during learning, was intended to indirectly reflect learning performance. It was thus possible to test whether correlations between fornix microstructure and retrieval measures, were independent of learning performance.

To test if the fornix had a specific role in temporal sequence memory, correlations between temporal sequence memory measures and microstructure properties of the ILF and PHC were also tested. The ILF is an important tract of the AIN (Catani et al., 2003; Latini, 2015) and studies have reported correlations between ILF microstructural properties and performance of tasks involving production of semantic content in autobiographical memory (Hodgetts, Postans, et al., 2017) and object recognition (Ortibus et al., 2012). Therefore, while the ILF may support performance in this study through supporting semantic/object processing, performance in semantic/object processing was not directly assessed so it was anticipated that relationships between ILF microstructure and the RT enhancement measures would be weaker than those between fornix microstructure and the RT enhancement measures, or not apparent. Conversely, the PHC, along with the fornix, is an important pathway within the hippocampal–diencephalic–cingulate loop, connecting parahippocampal areas to other areas of the PMN, including the RSC (Bubb et al., 2017). Therefore, it may have been expected that PHC microstructural properties would be associated with temporal sequence memory measures. However, areas connected through the PHC have been shown to hold temporal sequence position knowledge only, irrespective of objects (Hsieh & Ranganath, 2015), and the current experiment's tasks probed object-in-sequence memory. Therefore, since the fornix is the primary white-matter connection of the hippocampus, and the RT enhancement measures would not capture position-only information, it was anticipated that relationships between PHC microstructure and the RT enhancement measures would be weaker than those between fornix microstructure and the RT enhancement measures, or not apparent.

As with the previous microstructure analysis within this thesis, inter-individual differences in tract properties were scored by reducing multiple MRI-derived microstructure measures, through PCA, to biologically interpretable components, and extracting individuals' tract scores from those components. Also, similar to the previous analysis, tract FA, MD and RD were calculated from the DTI model and ICVF and OD were calculated from the NODDI model. However, the current experimental MRI protocol did not include CHARMED or qMT imaging, so FR and MPF values could not be extracted. With the aim of creating comparable components across the datasets, AxD was additionally calculated from the DTI

model. This way, the number of measures entering the PCA were similar (6 in the current study, 7 previously). Also, AxD and FR are correlated in areas of single fibre populations (De Santis et al., 2014), so it was predicted to provide some information similar to that provided by FR.

7.2 Methods

7.2.1 Participants.

Fifty-one female volunteers (mean age: 20.1 years, SD 1.1, range: 19-24 years), with no reported neurological pathology, were recruited. Participants underwent behavioural testing followed by a diffusion MRI scan, on the same day[14].

7.2.2 The Object-in-sequence memory task.

The temporal sequencing task, which was adapted from Hsieh et al. (2014), comprised two phases, a learning phase immediately followed by a retrieval phase. In these, participants were asked to make semantic decisions on objects, including man-made objects, animals, fruits and vegetables, that were presented in sequences of five objects. Both phases included fixed and random sequence types. Fixed sequences contained consistent objects that always appeared in a consistent order: one of these contained unique objects and another two shared identical objects in serial positions 2 and 3. Two random sequences contained unique objects, but these were presented in a different order in every repetition. The retrieval phase additionally included novel sequences, which contained novel and trial-unique objects upon every repetition. Examples of the sequences are shown in Figure 41.

[14] This was a previously collected dataset and I analysed the data subsequently.

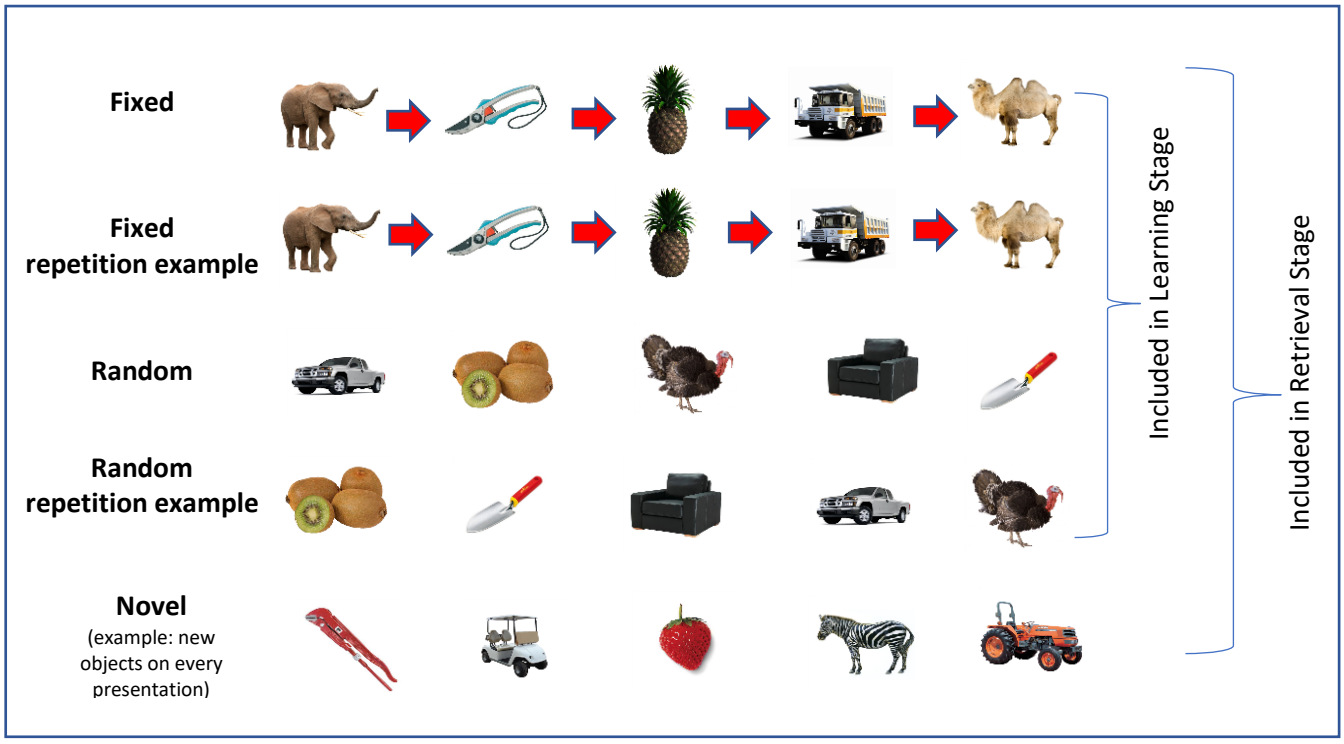

Figure 41. Examples of sequence types.

The task comprised two phases, a learning phase immediately followed by a retrieval phase. The learning phase included cycles in which participants answered semantic questions on the objects presented in the sequences, and reconstructed the sequences. In the retrieval phase, participants only answered semantic questions on the objects presented in the sequences. Both phases included object sequences that were either consistently ordered, "fixed", or randomly ordered, "random". Fixed sequences contained consistent objects that always appeared in a consistent order: one of these contained unique objects and another two shared identical objects in serial positions 2 and 3 (in this study, the two fixed sequence types were analysed together so this detail is not illustrated in this figure). Two random sequences contained unique objects, but these were presented in a different order in every repetition. Sequences of novel objects, "novel", were additionally included in the retrieval stage. Repetition examples are included to illustrate that fixed sequences had consistent object order across repetitions whereas random sequences did not.

Learning phase.

The learning phase included two study-test cycles. In each study cycle, the three fixed and the two random sequences were each presented three times. One of five semantic yes/no questions e.g. "Is the presented item readily edible?" (more example questions shown in *Appendix 4A*) was presented at the beginning of each cycle, and participants answered this question for each object presented within the cycle. Participants were instructed to answer as quickly and accurately as possible[15]. The order of sequences was semi-randomised to

[15] Note that this contrasts with the oddity task described in previous chapters of the thesis, where participants were told to focus on answering correctly rather than quickly. In the current task, RT was the measure of interest, and the semantic questions were not designed to be challenging or to reveal individual differences in semantic decision-making accuracy.

ensure that identical sequences were not presented consecutively and that all sequences had been presented before showing repeats (see Figure 42 for more detail and presentations timings).

In each of the test cycles in the learning phase, participants were shown all classes of sequences again. Again, the order of sequences was semi-randomised. Participants were explicitly tested on how well they had learned each of the fixed sequences, three times. They were shown all the objects from a sequence simultaneously and these were labelled 1 to 5, with five boxes underneath each of the numbers. Participants were asked to reconstruct the order in which they were presented in that sequence, using keys 1 to 5 along the top of the keyboard. The correct order was then displayed. For the random sequence trials, participants simply placed the objects in a random order and then another random order was displayed, which required no response. Answers were regarded as correct if objects were placed in the correct temporal position. The fraction of answers that were correct was expressed as a percentage. There were two study-test cycles within the learning phase. Accuracy over all the reconstruction tests was averaged to give a "Learning Score". Note that this score is actually comprised of explicit measures of sequence retrieval, assessed intermittently during the learning phase, with the aim of reflecting learning performance, but does not directly measure learning.

Retrieval phase.

Each of the five blocks was preceded by the presentation of a yes/no semantic question (different from those used in the learning phase). Each sequence was presented three times within each block. The presentation times were the same as those in the Learning phase, except that the sequences were run seamlessly: sequence boundaries were not highlighted by a longer fixation screen.

Response RTs were recorded to measure the extent to which individuals utilized object sequence knowledge to facilitate semantic judgments. This should be reflected as a reduction in average response RT of the fixed sequences compared to the random sequences, "RT Enhancement random-fixed", and a reduction in average response RT of the random sequences compared to novel sequences, "RT Enhancement novel-random". Initially, the RT differences between responses to positions 3 and 4 of the overlapping fixed sequences were to be included to examine sequence separation. However, response RTs to position 3 and 4 were not found to be significantly different (see *Appendix 4B*).

Averaged sequence RT scores were calculated for each sequence by computing the mean of the RTs to decisions on objects presented in positions 2-5. Response RTs to position 1 were removed at this stage, as it was assumed these RTs would be influenced more strongly by the inability to predict the first object, than by individual differences in object-in-sequence knowledge.

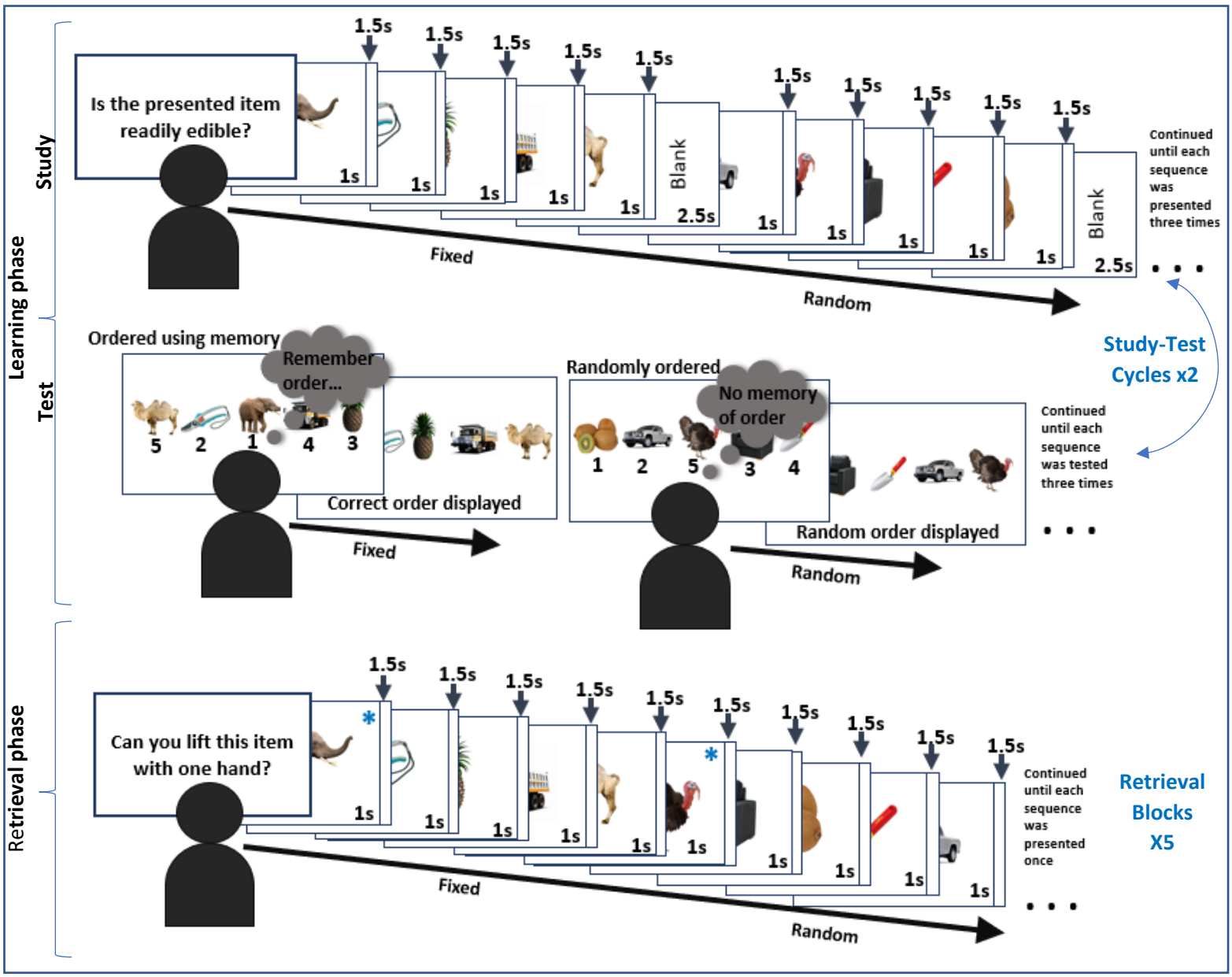

Figure 42. Layout of the temporal sequence memory task.

To aid understanding, only examples of the fixed and random sequences are shown. Note that the retrieval phase additionally included novel object sequences. The task comprised a "learning" phase followed by a "retrieval" phase. The Learning phase comprised study-test cycles. In the study part, participants learned the object sequences by answering semantic questions about the objects presented in their sequences. Each object was displayed for 1 s and was followed by a blank fixation screen lasting 1.5 s. Participants could respond any time between object onset and the end of this fixation screen. Additionally, the sequences were separated by a longer blank fixation screen lasting 2.5 s. In the test part, participants were asked to re-order randomly ordered objects from the sequences. Note that the random sequence cannot be reordered correctly, and participants randomly ordered the objects before being shown another random order. The sequences were shown three times within the test and study parts, and there were two test-study cycles. The Retrieval phase comprised five blocks, which was similar to the study part of the Learning phase, but all the sequences were shown seamlessly (without longer fixation screens). Again, participants answered semantic questions about each object displayed.
Blue asterisks have been added for illustrative purposes, on some images in the Retrieval phase, to denote the image in position 1 of a sequence.

7.2.3 MRI scanning protocol and microstructure measurement.

7.2.3.1 Protocol.

Structural and diffusion MRI data were collected using a Siemens Prisma GE 3T MRI system with a 32-channel head coil. DWI data were acquired using a dual-shell HARDI (Tuch et al., 2002) protocol with the following parameters: slices = 80, TR = 9400 ms, TE = 67 ms, FOV = 256 mm x 256 mm, voxel dimensions = 2 x 2 x 2 mm. Gradients were applied along 90 isotropic directions with b-values of 1200 s/mm^2 and 2400 s/mm^2. Six non-diffusion-weighted images were also acquired with a b-value of 0 s/mm^2.

T1-weighted anatomical images were obtained using an MPRAGE sequence with the following parameters: slices = 176, TR = 2250.0 ms, FOV = 256 mm x 256 mm, matrix size = 256 mm x 256 mm, flip angle = 9^o, TE = 3.06 ms, slice thickness = 1 mm.

7.2.3.2 Analysis of structural images.

The T1 MPRAGE files underwent alignment to their respective DWI images, cropping, skull removal with the FSL brain extraction tool (BET), and downsampling to a voxel size of 1.5 x 1.5 x 1.5 mm.

Subject motion and echo planar imaging distortions were corrected by co-registering the DWIs to their respective T1 images using Explore DTI (Leemans et al., 2009). Tensor fitting was carried out on the 1200 b-value shell, tractography analysis was applied to the 1400 b-value shell, AMICO NODDI was applied to the dual-shell data, using the same methods described in *Chapter 5* (section 5.2.3.2.).

ICVF and OD values were extracted from NODDI maps. DTI Modelling was used to extract measures, FA, MD, RD and AxD. Although MD is an average of RD and AxD, all are included, as they have been associated with different tissue properties, and have been previously included together in a similar study using PCA to reduce microstructure data (Geeraert et al., 2020).

7.2.3.3 Tractography.

To generate three-dimensional streamlines that represented the fornix, the ILF and the PHC, 'way-point' ROIs were manually drawn onto whole-brain FA maps in the diffusion space of

18 subjects, using Explore DTI (Leemans, 2009). These 'way-point' ROIs allow the user to define Boolean AND and NOT gates with the aim of isolating the relevant streamlines. The resultant tracts were used to train in-house automated tractography software (written by Greg Parker of Cardiff University), that was then applied to the entire dataset. Afterwards, streamlines produced by the automated tractography software were visually inspected and spurious fibres were removed using additional NOT gates. The protocols for the manual construction of the tract streamlines are the same as those described in *Chapter 5*.

7.2.4 Tract microstructure data reduction.

FA, MD, RD, AxD, ICVF and OD values for the voxels encompassed in the tract streamlines were extracted and averaged for each tract. This resulted in six microstructure metrics for three tracts for all 51 participants. Reduction of the microstructure data, through PCA, was carried out using the same methods as those described in *Chapter 5*.

7.2.5 Statistical analysis.

For assumption testing, tract microstructure-behaviour correlations and figure generation, R (R Core Team, 2019) and RStudio (RStudio Team, 2020) were used. Where appropriate, parametric tests were applied to raw values or transformed-to-normal values. Tests used, and applied transformations, are outlined alongside the results.

To inspect position response RT effects for fixed, novel and random sequences, RM ANOVA, with sphericity correction if necessary, was applied.

To assess the unique contribution of fornix microstructure, compared with ILF and PHC microstructure, to the behavioural indexes of sequence memory, both individual tract microstructure-behaviour correlations, and a multiple linear regression model, were tested. The latter allowed assessment of whether the fornix microstructure predicted RT Enhancement random-fixed independently from contributions of PHC and ILF microstructure data, and independently from Learning Score.

Similar to the methods of *Chapter 5* and Hodgetts et al. (2015), p-values were Bonferroni-corrected by dividing the traditional 0.05 alpha level by the number of correlation tests for each microstructure component. Therefore, the experiment-wise threshold used was 0.017, this being 0.05/3 behavioural measures (Learning Score, RT Enhancement random-fixed and RT Enhancement novel-random). When comparing correlation coefficients

(methods described in *Chapter 5* section 5.2.6), the alpha value was Bonferroni-corrected for the number of tests within each section, to 0.025 (0.05/2).

Some of the hypotheses in this project were that specific phenomena should *not* occur. Therefore, confirmatory correlation tests between structure, function and behaviour were carried out with both inferential statistics and equivalent Bayesian tests. BFs were calculated using BayesFactor package in R (Morey & Rouder, 2018), and were reported as BF_{10} (evidence of the alternative model over the null model).

Outliers were identified in the microstructure component data, and in the behavioural measures that were used for correlation testing with microstructure component data. Participant datasets containing outlying values (>3 SDs from the mean) in either the contrasted behaviour conditions or the microstructure PCA score data were identified in each analysis stage and removed.

Plots were drawn using several R packages. Visualization of the correlation matrices was achieved using *ggcorrplot* (Kassambara, 2019). For the PCA results, *stats* (R Core Team, 2019) and *ggplot2* (Wickham, 2016) were used. To visualize correlation plots, with histograms, and to test and visualize regression results, *ggstatsplot* (Patil, 2021) was used.

7.3 Results

7.3.1 Object-in-sequence memory behavioural data.

7.3.1.1 Learning phase: Learning Scores.

Results from the reconstruction tests of the learning phase showed that fixed sequences were learned reasonably well. The mean and mode of the scores from the last repeat of the second cycle (the 6th reconstruction of a sequence) were 90.39% and 100% respectively. The Learning Scores, created by averaging the reconstruction results across Study-Test cycles, were thought to reflect individual differences in the rate of initial learning (Table 23).

	Learning Score
Mean	80.81
SD	16.90
Minimum	25.83
Maximum	100
Skew	-0.69

Table 23. Learning Score.

Each participant had a learning score, which was an average of their reconstruction scores across Study-Test cycles.

7.3.1.2 Retrieval Phase.

7.3.1.3 Average response RTs differed between sequence types.

Sequence position RT effects are described in detail in the *Appendix 4B*. The averaged response RTs to positions 2-5 of the three sequence types, novel, random and fixed were compared (Table 24; Figure 43). Response RTs to position 1 were not included in the average calculation because it was anticipated that these would be influenced by sequence boundary effects, which are not the focus of this experiment. RMANOVA revealed a significant difference between the means of the conditions ($F_{(2, 100)}$ = 147.8, p <0.001, ω2 = 0.230). Post hoc testing (with Bonferroni correction) revealed that, as expected, the averaged RTs of the novel sequences were larger than those of the random sequences (mean difference = 90.55, p <0.001), which in turn were larger than those of the fixed sequences (mean difference = 21.97, p = 0.003).

RM ANOVA revealed that, unlike the finding of Hsieh et al. (2014), response RTs for positions 3 and 4 of the overlapping fixed sequences did not significantly differ (see *Appendix 4B*). Therefore, the response RTs of the overlapping fixed sequences were not independently included in subsequent analyses but averaged, with the other fixed sequence.

	Novel	Random	Fixed	RT Enhancement novel-random	RT Enhancement random-fixed
Mean	685.23	594.69	572.71	90.55	21.97
SD	87.03	82.33	96.64	42.91	44.90
Minimum	509.00	432.28	290.17	13.30	-47.14
Maximum	908.61	856.40	792.10	216.48	192.75
Skew	-0.01	0.44	-0.38	0.32	1.56

Table 24. Average RT of sequence-types, and contrasted sequence-types values.

Average RT values (in ms) were made from averaging RTs for positions 2-5. RT Enhancement novel-random and RT Enhancement random-fixed scores were made by subtracting the averaged RTs of random from novel, and fixed from random, respectively.

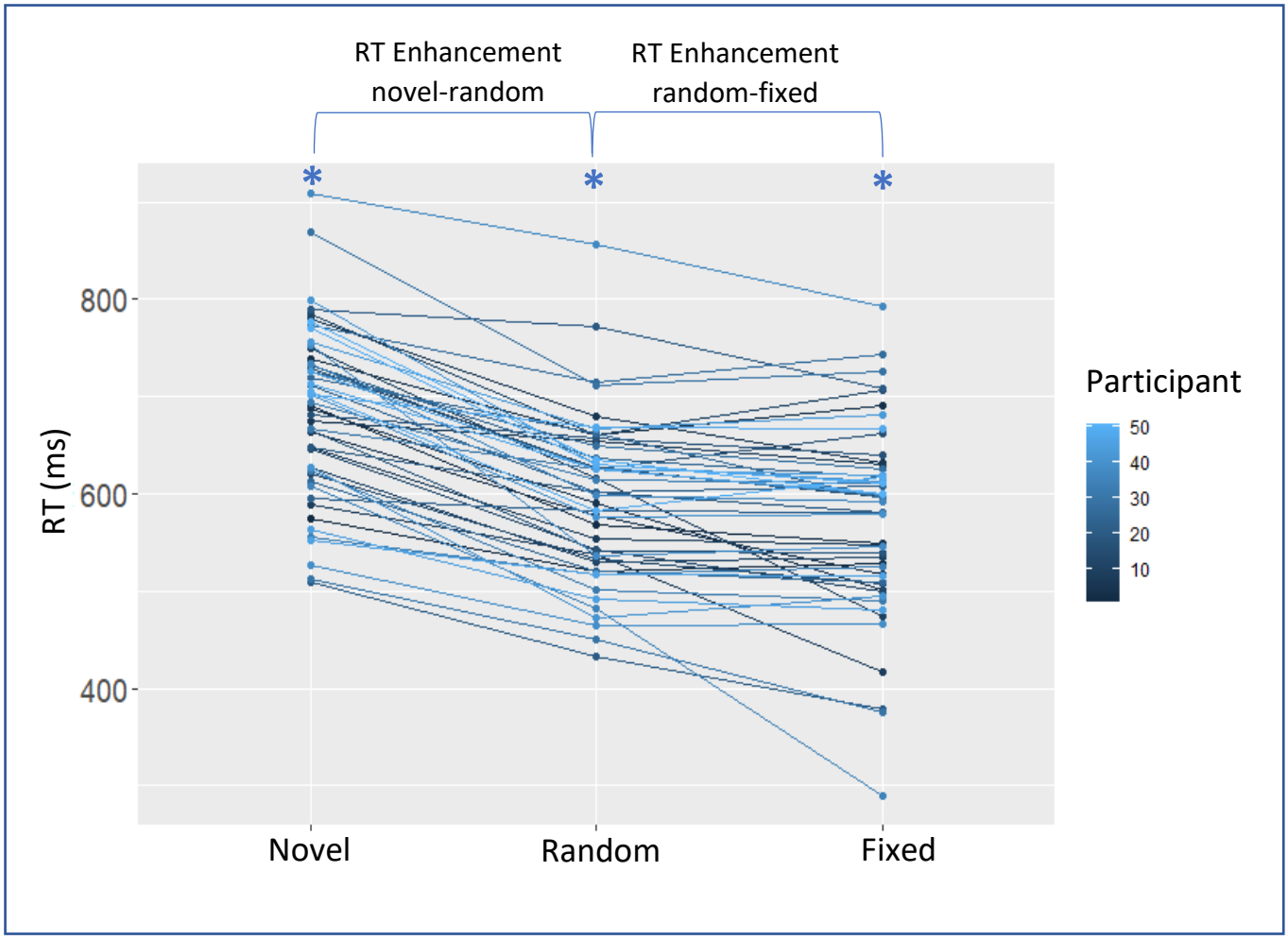

Figure 43. Participant averaged response RTs, for each condition.

Individual participant averaged response RTs, for positions 2-5, for the novel, random and fixed sequences scores are plotted. The asterisks indicate that the group average RTs of each sequence type were significantly different from each other (p-values ≤ 0.003). The behavioural indexes of sequence memory, RT Enhancement novel-random and RT Enhancement random-fixed are the differences between novel and random averaged RTs and between the random and fixed averaged RTs, respectively.

7.3.2 Tract microstructure.

Mean along-tract, bilaterally averaged tract microstructure metrics are shown in Table 25. The Pearson correlation values shown in Figure 44A highlight the shared variance in this data.

	Fornix		ILF		PHC	
	Group mean	**SD**	**Group mean**	**SD**	**Group mean**	**SD**
FA	0.40	0.01	0.44	0.02	0.35	0.03
MD	0.09×10^{-2}	0.03×10^{-3}	0.07×10^{-2}	0.01×10^{-3}	0.07×10^{-2}	0.01×10^{-3}
RD	0.07×10^{-2}	0.03×10^{-3}	0.05×10^{-2}	0.02×10^{-3}	0.06×10^{-2}	0.02×10^{-3}
AxD	0.14×10^{-2}	0.07×10^{-3}	0.11×10^{-2}	0.02×10^{-3}	0.10×10^{-2}	0.02×10^{-3}
ICVF	0.45	0.03	0.46	0.03	0.46	0.03
OD	0.15	0.01	0.19	0.02	0.24	0.02

Table 25. Group means and SDs for each microstructure value, for each tract.

Microstructure values are averaged over tract streamlines for each participant. Means and SDs of microstructure values, across the group, for the three tracts of interest are shown.

AxD: Axial Diffusivity. FA: Fractional Anisotropy. ICVF: Intracellular Volume Fraction. ILF: Inferior Longitudinal Fasciculus. MD: Mean Diffusivity. OD: Orientation Dispersion. PHC: Parahippocampal Cingulum. RD: Radial Diffusivity.

The results from the PCA (overall KMO: 0.63, sphericity: $p < 0.001$) showed that 93% of the microstructure data variability was accounted for by the first two principal components, PC1 and PC2. PC1 accounted for 59% of the variance, and MD, RD and AxD provided major negative contributions (Table 26; Figure 44B). It was similar to the first component found in Chamberland et al. (2019) and the second component of Geeraert et al. (2020). Therefore, PC1 was interpreted as positively relating to a 'restriction' property of the fibres (presumed to relate to myelin density and axonal packing). PC2 accounted for 34% of the variance, and FA and ICVF provided the major negative contributions, while OD provided a major positive contribution (Table 26; Figure 44B). Since OD is lower in tracts known to have more fibre coherency and higher in tracts known to have more fibre fanning and crossing (Zhang et al., 2012), and FA can be influenced by how coherently fibres within a voxel are organised (Jones, Knosche, et al., 2013; Pierpaoli et al., 1996), PC2 was interpreted as negatively relating to a 'coherence' property of the fibres (the dispersion of modelled fibre orientations). The relative differences between the scores of the tracts are illustrated in Figure 44C.

	PC1	PC2
FA	-0.027	-0.674
MD	-0.527	0.046
AxD	-0.521	-0.126
RD	-0.495	0.222
ICVF	-0.255	-5.02
OD	0.375	0.476

Table 26. PCA Loadings.

AxD: Axial Diffusivity. FA: Fractional Anisotropy. ICVF: Intracellular Volume Fraction. ILF: Inferior Longitudinal Fasciculus. MD: Mean Diffusivity. OD: Orientation Dispersion. PC: Principal Component. RD: Radial Diffusivity.

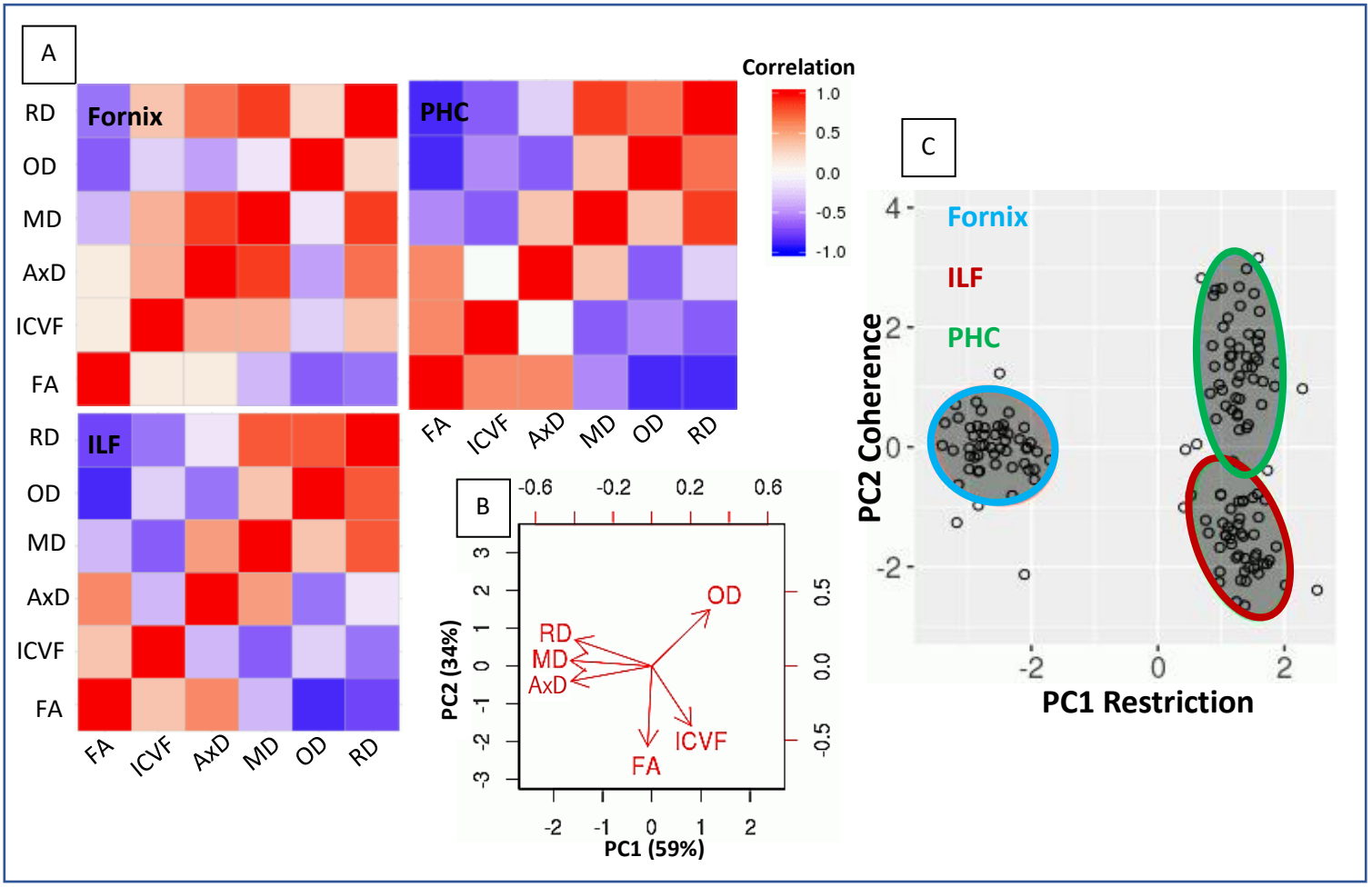

Figure 44. Redundancy between tract diffusion values and results from PCA.

A) Pearson's correlations within the microstructure data from each tract suggest that the values give overlapping information. Colour denotes r value. B) Biplot illustrating the influence of each of the measures on PC1 and PC2, which account for 59% and 34% of the variance, respectively. C) Tract component scores for each participant, illustrating the differing properties of the tracts.

AxD: Axial Diffusivity. FA: Fractional Anisotropy. ICVF: Intracellular Volume Fraction. ILF: Inferior Longitudinal Fasciculus. MD: Mean Diffusivity. OD: Orientation Dispersion. PC: Principal Component. PHC: Parahippocampal Cingulum. RD: Radial Diffusivity.

7.3.3 Associations between object-in-sequence memory performance and structure

7.3.3.1 Correlations between Learning Score and tract microstructure.

The BF indicated only weak evidence for a correlation between Learning Score and fornix PC1, and this did not survive the experiment-wise alpha threshold ($t_{(48)}$ = 2.087 , r = 0.289, p = 0.042). There were also no significant correlations between Learning Score and ILF or PHC microstructure.

There were no significant correlations between Learning Score and fornix PC2, PHC PC2 and ILF PC2 and no BFs indicated evidence in favour of the alternative over the null model (Table 27).

		Learning Score
Fornix	PC1	r = 0.0289 p = 0.042 BF_{10} = 2.05
	PC2	r = -0.052 p = 0.724 BF_{10} = 0.34
ILF	PC1	r = 0.153 p = 0.293 BF_{10} = 0.53
	PC2	r = -0.026 p = 0.831 BF_{10} = 0.33
PHC	PC1	r = 0.139 p = 0.341 BF_{10} = 0.48
	PC2	r = -0.103 p = 0.482 BF_{10} = 0.40

Table 27. Correlation tests between Learning Score and Fornix, ILF and PHC microstructure components.

N=49. ILF: Inferior Longitudinal Fasciculus. PC: Principal Component. PHC: Parahippocampal Cingulum.

7.3.3.2 Correlations between RT Enhancement scores and tract microstructure.

RT Enhancement random-fixed had a right skew (>1), so a constant (of the most negative value, sign-flipped and rounded up) was added to each value, and the square root was then

calculated (McDonald, 2014). Unless stated otherwise, 'RT Enhancement random-fixed' refers to the transformed data.

There were no significant correlations between RT Enhancement random-fixed, or RT Enhancement novel-random, and fornix, ILF or PHC PC1. The BFs indicated evidence in favour of the nulls (Table 28).

There was a significant correlation between RT Enhancement random-fixed and fornix PC2 ($t_{(46)}$ = 2.473, r = 0.343, p = 0.017), and the resulting BF indicated evidence in favour of the alternative model. Also, there were no significant correlations between RT Enhancement random-fixed and ILF or PHC PC2, and the resulting BFs indicated evidence in favour of the null (Table 28).

		RT Enhancement random-fixed	RT Enhancement novel-random
Fornix	PC1	r = 0.029 p = 0.847 BF_{10} = 0.33	r = -0.175 p = 0.233 BF_{10} = 0.61
	PC2	r = 0.346 p = 0.017* BF_{10} = 4.16*	r = -0.235 p = 0.108 BF_{10} = 1.03
ILF	PC1	r = 0.030 p = 0.839 BF_{10} = 0.33	r = 0.015 p = 0.918 BF_{10} = 0.33
	PC2	r = 0.361 p = 0.720 BF_{10} = 0.34	r = -0.059 p = 0.691 BF_{10} = 0.35
PHC	PC1	r = -0.014 p = 0.923 BF_{10} = 0.33	r = 0.032 p = 0.313 BF_{10} = 0.33
	PC2	r = 0.116 p = 0.433 BF_{10} = 0.43	r = -0.229 p = 0.117 BF_{10} = 0.98

Table 28. Correlation tests between RT Enhancement random-fixed, and RT Enhancement novel-random, and fornix, ILF and PHC microstructure components.

*Highlights p≤0.017. *Highlights a logBF_{10} ≥ 3. N=48.

ILF: Inferior Longitudinal Fasciculus. PC: Principal Component. PHC: Parahippocampal Cingulum.

There were no significant correlations between RT Enhancement novel-random and fornix, ILF or PHC PC2.

However, the coefficient of the correlation between RT Enhancement random-fixed and fornix PC2 was not significantly larger than those of the correlations between RT Enhancement random-fixed and ILF PC2 ($z_{(45)}$ = 1.671, p = 0.095), or PHC PC2 ($z_{(45)}$ = 1.308, p = 0.191).

Partial correlations between RT Enhancement random-fixed and tract microstructure component scores were then carried out so that individual differences in the rate of initial sequence learning, Learning Score, could be controlled-for. In line with the hypothesis, the only significant partial correlation was between RT Enhancement random-fixed and fornix PC2 ($t_{(45)}$ = 2.638, r = 0.369, p = 0.012) and the resulting BF indicated evidence in favour of the alternative model (Table 29; Figure 45).

		RT Enhancement random-fixed
Fornix	PC1	r = -0.050 p = 0.740 BF_{10} = 0.34
	PC2	r = 0.369 p = 0.012* BF_{10} = 6.11*
ILF	PC1	r = -0.016 p = 0.916 BF_{10} = 0.33
	PC2	r = 0.057 p = 0.708 BF_{10} = 0.35
PHC	PC1	r = -0.057 p = 0.707 BF_{10} = 0.035
	PC2	r = 0.146 p = 0.332 BF_{10} = 0.50

Table 29. Partial correlation tests between RT Enhancement random-fixed and fornix, ILF and PHC microstructure components, controlling for initial sequence learning.

*Highlights p≤0.017. *Highlights a logBF_{10} ≥ 3. N=47.

ILF: Inferior Longitudinal Fasciculus. PC: Principal Component. PHC: Parahippocampal Cingulum.

Multiple linear regression was used to assess whether fornix microstructure was specific in its relationship with RT Enhancement random-fixed or whether ILF and PHC microstructure also contributed, and to see if this correlation was separate to any associations with

Learning Score. A model with fornix PC2, PHC PC2, ILF PC2 and Learning Score predicted RT Enhancement random-fixed (adjusted $R^2 = 0.124$, $p = 0.047$). Significant predictors included fornix PC1 ($p = 0.020$) and Learning Score ($p = 0.046$). Detailed statistics are shown in Figure 45B.

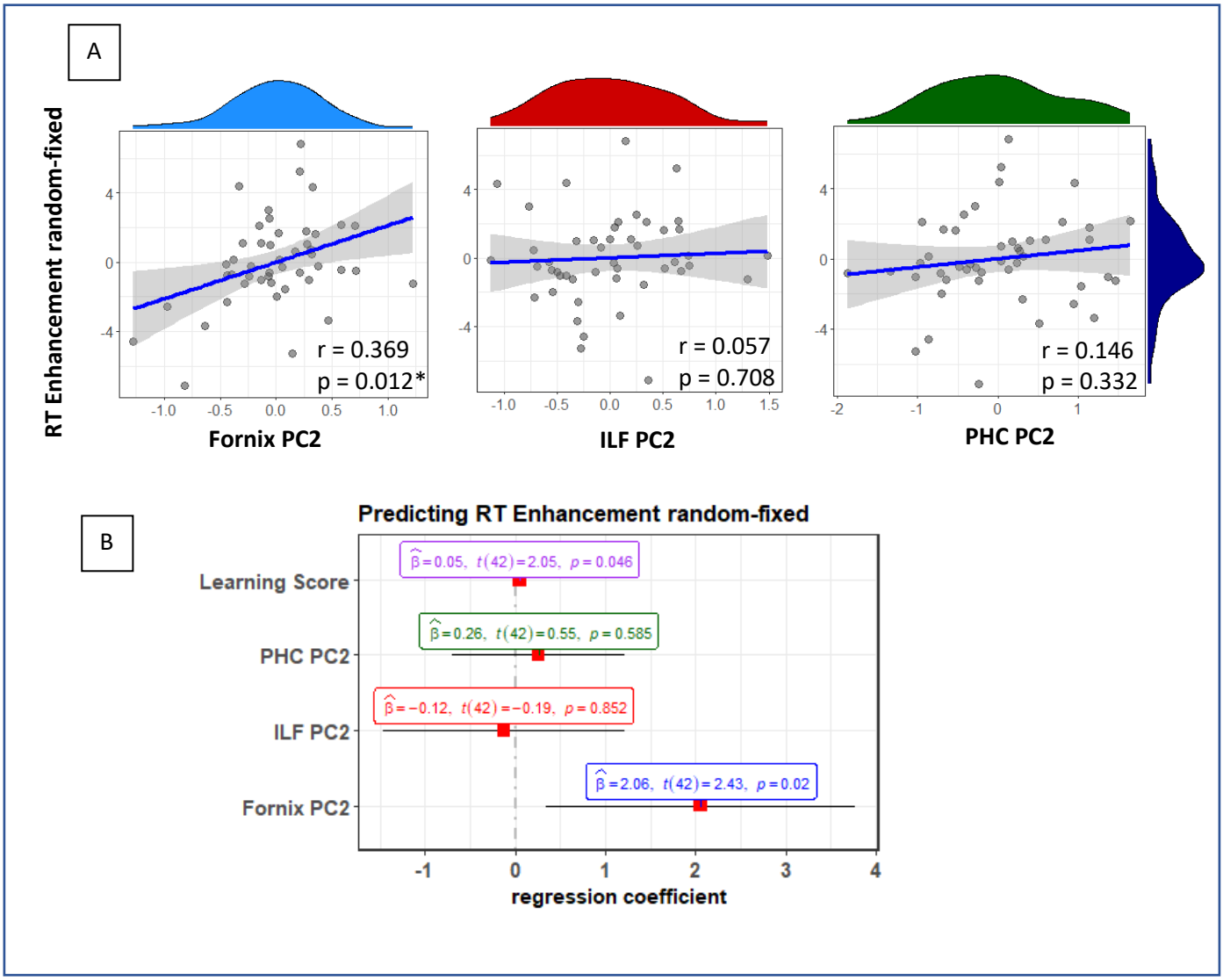

Figure 45. Associations between tract PC2 microstructure scores and RT Enhancement random-fixed, controlling for Learning Score.

A) Scatter plots showing the partial correlations between microstructure and RT Enhancement random-fixed residual scores. The mid-blue histogram shows the distribution of the fornix PC2 data. The green and red histograms show the distributions of the PHC PC2 data and ILF PC2 data, respectively. The dark blue histogram shows the distribution of RT Enhancement random-fixed. The blue lines are the regression lines and surrounding shaded areas represent the 95% confidence interval.
B) Multiple Linear Regression results. The model was built to predict RT Enhancement random-fixed with tract PC2 scores and Learning Score. Fornix PC2 and Learning Score were significant predictors (at the 0.05 level).

ILF: Inferior Longitudinal Fasciculus. PC: Principal Component. PHC: Parahippocampal Cingulum.

7.4 Discussion

The AIN and PMN have been linked to representations of object and position information, respectively (Hsieh & Ranganath, 2015; Murray et al., 2017), and the hippocampus is thought to hold conjoined object-time information in the form of recency memory (Jenkins & Ranganath, 2016), temporal community structure (Schapiro et al., 2016) and object-position binding (Hsieh et al., 2014). To investigate whether network structure relates to individual differences in object-in-sequence memory, the current study combined a microstructure reduction technique with an implicit object sequence memory task adapted from Hsieh et al. (2014/15). Associations between inter-individual differences in fornix, ILF and PHC microstructure and in object-in-sequence memory, were investigated.

Due to its key role in connecting the hippocampus, it was hypothesized that the fornix would have a specific role in memory for objects in temporal sequences. Considering the results of Hsieh et al. (2014), who found that the hippocampus held object-in-position information, it was proposed that there might be correlations between fornix microstructure and differences in RTs in the retrieval of random sequences compared with fixed sequences. Furthermore, we tested whether fornix microstructure correlated with fixed sequence retrieval independently of the participants' learning of fixed sequences. Additionally, it was predicted that these correlations would be specific to fornix microstructure because, although the PHC also connects areas of the PMN, it is not the major tract providing connections for the hippocampus. These hypotheses were supported by a significant correlation between RT Enhancement random-fixed and fornix PC2 and a significant partial correlation between RT Enhancement random-fixed and fornix PC2 when Learning score was controlled for. Although the RT Enhancement random-fixed - fornix PC2 correlation coefficient was not found to be significantly stronger than those of the correlations between RT Enhancement random-fixed and ILF or PHC PC2, fornix PC2 and Learning score were the only significant predictors of RT Enhancement random-fixed in a multilinear regression model.

Since Hsieh et al. (2014) also found evidence of broader context learning in the case of random sequences, and the hippocampus has also been shown to hold information about temporal community structure (Schapiro et al., 2016), it could have been predicted that fornix microstructure would also correlate with RT differences between novel sequences and random sequences (RT Enhancement novel-random). However, no significant

correlations were found between fornix microstructure scores and RT Enhancement novel-random.

7.4.1 The role of the fornix pathway in object-in-temporal-sequence retrieval in healthy adults.

The fornix may facilitate communication between the hippocampus and multiple areas, supporting bound temporal memory. Indeed Hsieh et al. (2014/2015) demonstrated that temporal context information is stored in multiple cortical areas, including the mPFC, RSC and angular gyrus, while the PrC and caudate were shown to hold object information. For example, fornix supported hippocampal-mPFC communication may allow complementary temporal order processes, with the working memory functions of the PFC (Naya et al., 2017) facilitating current goals, and context processing in the hippocampus supporting more fine-tuned sequencing. This suggestion aligns with the following evidence: PFC activity is predictive of coarse temporal memory (Jenkins & Ranganath, 2010); mPFC activity reduces at sequence boundaries (Schapiro et al., 2013); mPFC-hippocampus communication is elevated during sequence boundaries (Schapiro et al., 2016); and the fornix indirectly supports connections between the hippocampus and the mPFC (Bubb et al., 2017). In addition, the fornix directly connects the hippocampus to the thalamus (Bubb et al., 2017). Not only is the thalamus thought to support mPFC-hippocampal processing by synchronising the theta oscillations of these two areas (Ketz et al., 2015), but lesions to the rat thalamus have been shown to impair temporal order memory of odour sequences (Wolff et al., 2006). Although the exact dependencies of these hippocampal communications on the fornix pathway are unclear, the results show the importance of fornix-supported communication in temporal memory, and that this differs between different healthy young adult individuals in a behaviourally relevant way.

The current results specifically indicate a role of this fornix-supported pathway in object-sequence-retrieval that is independent of object-in-sequence learning. The multilinear regression model that was predicting RT Enhancement random-fixed and included Learning Score, showed fornix PC2 to be an independent predictor. These results suggest that the relationship between fornix PC2 and object-in-sequence retrieval cannot be attributed to an influence of fornix PC2 on encoding. Assessment of functional connectivity within the PMN and the AIN, and the hippocampus, during encoding and retrieval, found increased network connections between these networks, and between these networks and the hippocampus, during retrieval (Cooper & Ritchey, 2019). These results, and those of the

current study, together indicate that although many brain areas are involved in both encoding and retrieval (Rugg et al., 2008), PMN network communication during encoding may differ from PMN network communication during retrieval, so that inter-individual differences in fornix coherence may relate more strongly to individual differences in retrieval performance. Furthermore, a subiculum-connected hippocampal circuit, as opposed to a CA1-entorhinal, hippocampal circuit has been shown to be selectively involved in retrieval over memory formation (Roy et al., 2017), and subiculum volume has been associated with fornix microstructure, independent of age, in healthy adults (Hartopp et al., 2018). Therefore, it may be that while this fornix pathway supports both encoding and retrieval, that healthy adults only display correlations between fornix microstructure and retrieval associations.

However, there was a positive trend between fornix PC1 (reflecting the property of restriction) and Learning Score that did not survive the experiment-wise alpha threshold (and the BF only indicated weak evidence in favour). It is possible that limitations in this measure of encoding could have weakened this association. Learning Score was made by averaging the scores from the reconstruction tests in the study-test cycles of the learning phase, so a higher score could reflect both faster learning and better over-all learning. Distinguishing between these is not possible. Hodgetts et al. (2020), who found a correlation between fornix microstructure and navigational learning, fitted a power curve to the RT as it reduced during a repeated navigation task, so that learning rate could be isolated. Then, correlations between microstructure measures and the slopes for each participant were tested. It may be that a similar correlation would have been revealed in the current study, if average RTs of the learned sequences during the repeats within the learning phase were examined. Unfortunately, so that objects would be learned rather than answers to semantic questions, the question asked was different in the first and second study-test cycle. This meant that there was not a smooth decrease in RT from the first exposure of a sequence to the sixth exposure. There was an increase in RT for the fourth exposure, coinciding with the question change. However, RTs to the fourth exposure were generally lower than RTs to the initial exposure, so future work could re-examine associations between fornix microstructure and object-in-structure learning by using the same learning-phase paradigm as used here, but by fitting power slopes to RT data and adding more repetitions with more questions, with the aim of smoothing-out question-change-related RT increases.

Additionally, it is important to note that object-position binding may also benefit from communication between the hippocampus and other brain areas, mediated by extra-fornix/PHC routes. For example, the entorhinal cortex also holds a type of time-cell (Heys & Dombeck, 2018), and activity in this region has been associated with object-position binding, which suggests that hippocampal-entorhinal cortex interactions aid the production of temporal representations (Rolls & Mills, 2019). Multiple alternative routes exist within the parahippocampal regions and between the parahippocampal regions and the hippocampus (Bubb et al., 2017). The use of high-resolution diffusion scans may uncover the relationships between structure and object-in-sequence encoding performance in other smaller pathways such as these, which were not included in the present study.

7.4.2 The correlation between fornix PC2 and RT Enhancement random-fixed was positive.

FA contributed negatively to, and OD contributed positively to, the second major component resulting from our tract microstructure reduction, and therefore a decrease in PC2 was interpreted as representing an increase in tract fibre coherence. In line with the hypothesis, fornix PC2 significantly correlated with RT Enhancement random-fixed but the direction of this correlation was positive, suggesting that increased temporal memory performance, requiring object-position binding relates to decreased fornix coherence. The equivalent PC2 from the dataset in the study in *Chapter 5*, was also positively and negatively contributed-to, by OD and FA, respectively. This was predicted to negatively correlate with performance because of previous work showing positive relationships between spatial processing and fornix FA (Postans et al., 2014). Although no equivalent previous research was available to support a directional hypothesis in the case of the current study, it was still anticipated that lower PC2 scores would equate to a beneficial tract property.

There are several possible interpretations for the positive relationship between fornix PC2 and RT Enhancement random-fixed. First, increased fornix coherence could impair sequence position learning. Second, there may be fibres that perpendicularly cross the fornix, whose structural properties relate to object-position binding memory. Third, increased fornix OD may represent a positive tract property linking greater fibre complexity, rather than decreased coherence, with greater retrieval performance. Fourth, the fornix pathway may not support object-position retrieval, but temporal community structure retrieval instead. The first suggestion lacks plausibility, since there is no clear

reason why better communication ability in the fornix, aligned to increased fornix coherence, would impair this memory-based behaviour. The second explanation can also be refuted as the fornix is largely free from crossing fibres (Acosta-Cabronero & Nestor, 2014).

The third explanation is more plausible and calls for further investigation. A positive correlation between white matter OD and reading skill, and a negative correlation between FA and reading skill, has been shown in children (Huber et al., 2019), but cognitive performance or functioning is often negatively associated with increased white matter OD in adults (Coad et al., 2020; Ota et al., 2018; Wen et al., 2019). That said, adult pre-commissural fornix has been shown to have higher OD than the post-commissural fornix, which the authors suggested could be the result of the larger number of pre-commissural target sites (Coad et al., 2020). Therefore, an increase in OD could mirror an increase in fornix target site connections.

The fourth explanation, that the fornix pathway supports learning of objects in temporal community structures over ordered temporal sequences, is suggested because RT Enhancement random-fixed was calculated by subtracting the average RT of the fixed sequences from the average RT of the random sequences. Consequently, smaller values may indicate a better ability to retrieve groups of objects without object-position associations. Therefore, this result may reflect a positive correlation between fornix fibre coherence and memory for temporal community structures. Indeed, as well as finding hippocampal signals coding object-position binding, Hsieh et al. (2014) also found evidence for processing that generally relates objects to sequences, in the hippocampus. When hippocampal fMRI multivariate pattern representations for identical items with identical positions, in different overlapping sequences, were compared, pattern similarity was higher for repetitions for the item within one sequence than the presentation of the same item as part of the other sequence. This result suggests that hippocampal signals also represented the sequence context. Considering this suggestion that the fornix pathway supports learning of objects in temporal community structures, one might have expected correlations between fornix microstructure and RT Enhancement novel-random, as this could have reflected temporal community structure retrieval. However, RT Enhancement novel-random likely also reflects object (without context) memory.

A future study, which includes contextless objects, could investigate the validity of the third and fourth explanations. This could include a measure of response RTs to objects shown

repeatedly, randomly, and in isolation, between sequences (the surrounding sequences must be displayed in a random order so that these do not become a context for the isolated objects). Then, average response RT of the object-in-isolation condition could be compared with the average response RT of the random sequences to create a measure of object-in-random-community-structure retrieval, which is not influenced by pure object retrieval. In the interim, it can be concluded that fornix microstructure relates to temporal sequence memory in healthy adults, but the exact nature of the temporal memory needs further investigation.

7.4.3 Reduction of tract microstructure measures produced biologically interpretable components.

The two major components resulting from microstructure PCA, PC1 and PC2, were influenced most by MD, RD and AxD; and FA and OD, respectively. Therefore, these components were considered to capture the properties of fibre restriction and coherence. PCA allowed reduction of the DTI and NODDI data in a way that was biologically interpretable. The PCA components reported in this study share similarities with those reported in previous studies (Chamberland et al., 2019; Geeraert et al., 2020), which found correlations between microstructure components and age in children, and those reported in *Chapter 5*. PC1 is similar to the first component reported in Chamberland et al. (2019), which was negatively influenced by RD and positively influenced by a measure of fibre density, and they also interpreted this component as reflecting 'diffusion restriction'. It is also similar to the second component reported in Geeraert et al. (2020), which they named 'myelin and axonal packing' because it was influenced positively by ICVF and negatively by RD and MD. PC2 was similar to the first component reported in Geeraert et al. (2020), which they named 'tissue complexity' because it was influenced positively by FA and negatively by OD. However, the term 'coherence' was used in the present study to clarify the hypothesis that increased coherency, and therefore increased FA, would reflect a beneficial tract property. Although, there are slight differences in the resulting components across studies, common biologically-interpretable properties are revealed supporting the usefulness of microstructure data reduction.

The results indicate unequal importance of the two components to behavioural performance. There was an association between RT Enhancement random-fixed and fornix PC2 but not fornix PC1. There may be multiple reasons for inter-individual differences in tract coherence in the young, healthy adult population. For example, studies have reported

fornix microstructure differences induced by learning (Hofstetter et al., 2013), or associated with different polygenic risk scores (Braskie et al., 2011). Although the exact nature of this coherence/complexity property is unclear, the current work shows the usefulness of examining FA and OD in young, healthy adult populations, as they revealed inter-individual differences, and indicated the importance of fornix fibre coherence.

Although it is important not to over-interpret trends, it is noteworthy that there was evidence for a correlation between fornix PC1 and Learning Score, and evidence against a correlation between fornix PC2 and Learning Score. This is mirrored in other studies. Hodgetts et al. (2020) found significant correlations between navigational learning and fornix MD, but not fornix FA. The authors suggest that finding correlations with MD is more likely because it is more 'tract representative' than FA because MD varies less than FA along the tract. However, in Hodgetts et al. (2017), episodic detail in retrieval was found to correlate more strongly with fornix FA than with fornix MD. The dissociation found in the current study indicates different behavioural implications of the fornix properties on behaviour. Our understanding of the importance of fornix microstructure properties in learning and retrieval of temporal sequences may benefit from future work testing dissociable correlations between fornix restriction and learning, and between fornix coherence and retrieval.

7.4.4 Limitations.

A limitation with the current design is that behavioural RT measurements are an indirect measurement of memory processes. This behavioural task was previously combined with multivariate analysis of fMRI data (Hsieh et al., 2014), so information about brain processes relating to object-position retrieval could be assessed more directly. Indeed, while the finding of no significant RT difference between positions 3 and 4 in the overlapping sequences may indicate very good sequence knowledge (such that there were no substantial differences between RTs of overlapping objects and non-overlapping objects), it may also indicate poor sequence knowledge, such that each object is equally unpredictable, leading to equal RTs in each position. Although this is unlikely, given the overall performance on the last recall test of the learning phase, it cannot be ruled out. This contrasts with the study of Hsieh et al. (2014), in which it was possible to test multivariate classification in the fMRI data relating to objects in positions 2 and 3 in the two overlapping sequences, for each individual.

The indirect measurement of memory processes, through RT differences, also meant that there was no object-without-context memory measure. Hsieh et al. (2015), from which this behavioural task was adapted, were able to isolate fMRI signals holding pure object information, originating from the PrC, using multivariate analysis of brain signals produced during objects from various sequences (learned and novel). Without such a measure, it was not possible to test a double dissociability of the fornix and ILF roles in object-in-sequence and object-without-context memory. It may have been that ILF microstructure measures would have correlated with object-without-context memory performance. The ILF is an important tract of the AIN, connecting the ventro-anterior temporal lobe (including the PrC) with the occipital lobe (Catani et al., 2003; Latini, 2015), and studies have reported correlations between ILF microstructural properties and performance of tasks involving face processing (Hodgetts et al., 2015), production of semantic content in autobiographical memory (Hodgetts, Postans, et al., 2017), and in object recognition (Ortibus et al., 2012). An object-without-context memory measure could have been created by measuring average response RT differences between repeated isolated objects (described above) and the novel sequences. Furthermore, as discussed above, the lack of an object-without-context memory measure meant that the influence of isolated object memory of RT Enhancement novel-random could not be removed. It could be that fornix microstructure does not support isolated object memory and that variation from this in the RT Enhancement novel-random measure diminished a correlation between fornix microstructure and object-in-random-sequence memory.

A further suggestion for future work could be to include assessment of processing times. Machine-learning analysis techniques, in combination with more temporally sensitive, electrophysiological imaging, such as MEG, can allow classification over time. Therefore, in addition to measuring behavioural RTs, individual differences in the latency at which classifiers perform above chance when classifying imaging data trials from different sequence representations conditions, could be used to assess processing speed. With or without this, future work combining behavioural data, tract microstructure measures and multivariate pattern analysis of oscillatory signals might further reveal relationships between network structure, speed of processing and behavioural performance.

7.5 Conclusion

This study used an object-in-sequence memory task to assess the influence of the microstructure of the fornix, a principal connecting tract of the hippocampus, on temporal

order memory. Our results indicate that inter-individual variation in fornix microstructure, and perhaps specifically individual differences in fornix fibre coherence (PC2), was related to retrieval of object-in-sequence performance. Importantly, the relationship between fornix PC2 and RT Enhancement random-fixed was independent of contribution from Learning Score, indicating that the relationship was not mediated by an influence of fornix PC2 on encoding. The relationship between fornix PC2 and RT Enhancement random-fixed was rather complex, however, as the correlation was positive. Further research is needed to understand whether this positive correlation indicates an importance of fornix complexity (rather than coherence) for object-position binding, or whether it indicates that increased fornix coherence relates to reduced RT differences between random and fixed, which could reflect temporal community structure memory. Microstructure measures of the PHC and ILF did not correlate with measures of object-in-sequence retrieval, suggesting a specific role of the hippocampus and a fornix-supported pathway. Consequently, this study augments prior work by providing evidence of a selective relationship between fornix microstructure and object-in-sequence memory in healthy young adults.

Chapter 8: General Discussion.

8.1 Thesis rationale and overview.

This thesis examined functional and structural properties of spatial processing networks with the aim of investigating and expanding upon the PM-view, which is encompassed by two memory models, the EAM (Murray et al., 2017, 2018) and the PMAT framework (Ranganath & Ritchey, 2012; Ritchey et al., 2015). By combining networks defined by these models, *Chapter 1* described two networks with distinct functions. The PMN was proposed to conduct sequencing and separation to create models for spatiotemporal navigation, and it incorporates areas associated with scene processing and episodic memory (Hodgetts et al., 2016; Nasr et al., 2013; Rugg & Vilberg, 2013) such as: the hippocampus; the parahippocampal cortex; the RSC; the PCC; the IPL and the mPFC. The AIN was proposed to conduct aggregate processing to create models for identification and meaning, and it incorporates areas associated with semantic memory, object processing and face processing (Haxby et al., 2000; Ishai et al., 2000; Jefferies, 2013) such as: the PrC; the inferior temporal cortex, the orbitofrontal cortex; the amygdala; and the temporal pole.

Evaluation of the PM-view was done through considering the implications of the view and the two memory models: the PMN and AIN should aid behaviours in different modalities across perception and memory; network areas, including MTL areas, should be involved in complex visual perceptual tasks; and the behavioural performance in tasks involving those modalities should be related to the structural and functional properties of the respective networks (Graham et al., 2010; Murray et al., 2017). Therefore, this thesis evaluated the networks' functions from two approaches, one task requiring complex visual perceptual processing and the other implicitly testing memory of object sequences. To assess network roles, correlations between inter-individual differences in task performance, tract microstructure and functional correlates of network activity were investigated. An advantage of examining individual differences in healthy adults, unlike examining patients with lesions, is that it allows assessment of normally functioning networks.

Specifically, this thesis focused on the role of the PMN by studying: MEG-measured oscillatory modulations, particularly within the MTL, during complex scene perception; associations between these oscillatory modulations and fornix microstructure; and associations between fornix microstructure and behavioural performance in tasks requiring complex scene perception and temporal sequencing memory. A comparison was made

between microstructure-behaviour associations of the fornix and the PHC, as these primarily connect different areas of the PMN, the hippocampus and parahippocampal cortex, respectively. As hippocampal processes were hypothesized to be specifically important for the spatiotemporal tasks chosen, it was hypothesized that fornix microstructure would relate more strongly than PHC microstructure would, to performance in these tasks. Functions of the PMN were also compared with functions of the AIN by studying MEG-measured oscillatory modulation in areas of the AIN during complex face perception, and by studying associations between ILF microstructure and behavioural performance in complex face perception.

8.2 Discussion of the main findings.

8.2.1 There was evidence for correlations between fornix microstructure measures and performance in two tasks measuring spatiotemporal processing.

Since study of the role of the PMN and, particularly the role of the hippocampus in the PMN, was the major aim of this thesis, studying the fornix was a major focus. The PM-view, particularly the EAM, places importance in a 'medial' extended hippocampal network (Murray et al., 2017). The prediction was that individual differences in fornix microstructure should relate to individual differences in performance of tasks requiring spatiotemporal processing, in healthy adults. Indeed fornix microstructure had already been shown to relate to recollection of episodic information (Rudebeck et al., 2009), spatiotemporal information in autobiographical memories (Hodgetts, Postans, et al., 2017), spatial learning (Hodgetts et al., 2020), and complex scene perception (Hodgetts et al., 2015; Postans et al., 2014).

Two shortcomings in this prior literature were identified. The first concerned the role of the fornix in complex scene perception. Although fornix microstructure had been related to complex scene pereption in two studies (Hodgetts et al., 2015; Postans et al., 2014), these focused on the microstructure values FA and MD, so the underlying anatomical properties important for the task were indecipherable, perhaps explaining why they obtained differing results (with Postans et al. finding correlations between scene task performance and both fornix FA and MD, and Hodgetts et al. only identifying a correlation between scene task performance and fornix MD). Additionally, the timing in the paradigm of Postans et al. (2014) meant that mnemonic processes were required to undertake the task, because there were delays between the display of different images to discriminate between, and a

further delay before the response period. Lastly, since neither study tested correlations between fornix microstructure and performance in a subsequent unexpected retrieval task, probing incidental encoding, it was unclear whether the fornix-supported pathway was contributing to perceptual processes *per se* or whether it was facilitating incidental memory processes, which in turn supported task performance (Kim et al., 2011). *Chapter 5* addressed these issues with an experiment involving an oddity task with trial-unique scene, face and size trials, and the assessment of multiple microstructure measures of the fornix. The results provided evidence in favour of a positive correlation between fornix restriction property and scene oddity performance. Although, the p-value just surpassed the experiment-wise alpha level, the resulting BF indicated weak evidence in favour of the alternative model over the null, a result that aligns with those of Hodgetts et al. (2015) and Postans et al. (2014). In this thesis, MD negatively influenced the fornix restriction measure (PC1) and both Hodgetts et al. (2015) and Postans at al. (2014) found significant negative correlations between scene discrimination accuracy and fornix MD. However, Postans et al. (2014) also found a significant positive correlation with fornix FA (albeit with a higher p-value) and Hodgetts et al. (2015) identified a positive trend with fornix FA. This pattern may emerge because MD needs a smaller sample size to detect a statistically significant effect than FA (De Santis et al., 2014). However, considering the current results, it is also possible that the difference came about because the anatomical properties represented by FA and MD are overlapping but not the same (i.e. that they are both influenced by restriction and coherence properties but to differing extents) and that all these studies together highlight the specific importance of the fornix restriction in complex scene perception. Moreover, in line with Hodgetts et al. (2015) and Postans et al. (2014) fornix microstructure properties did not correlate with face task performance, showing the specificity of this network to scene stimuli over face stimuli.

Importantly, despite there being some evidence for a positive correlation between oddity scene task performance and subsequent scene retrieval performance, as measured by d', there was no correlation between fornix microstructure and scene retrieval performance. This implied that scene retrieval performance did not mediate the relationship between fornix microstructure and scene task performance. Therefore, the results indicate that the fornix pathway has a role in complex scene perception that is not purely to facilitate incidental memory processes. This aligns with the study of Lee et al. (2013), which reported significantly larger hippocampal BOLD responses for correct versus incorrect oddity scene trials, independent of subsequent memory. Additionally, using multivariate analysis, they

found that classification of hippocampal BOLD signals on trials into correct and incorrect trials performed above chance level. Together, their results indicate that the hippocampus has a role in complex scene perception that is not mediated by incidental encoding. Importantly, neither the results of Lee et al. (2013), nor the current results, dismiss the role of the extended hippocampal network in memory, suggesting instead that this pathway supports both perceptual and mnemonic functions. Indeed, Lee et al. (2013) also found that classification of hippocampal BOLD signals of trials into 'subsequently remembered' and 'forgotten' performed above chance level. It could be that the two processes rely on internal spatiotemporal representations. It could be that hippocampus-supported internal spatiotemporal representations are required for both memory and perception (Graham et al., 2010; Murray et al., 2017), and that representations constructed online for perceptual processes can become encoded when additional mnemonic processes are incited.

The second shortcoming in the literature concerned the lack of a study testing the role of the fornix in temporal sequence memory in healthy humans. The hippocampus has been shown to hold conjoined object-in-sequence information (Hsieh et al., 2014) but investigations into fornix involvement have provided contradictory results, with one animal study suggesting that transection impairs object memory but spares temporal memory (Hunsaker & Kesner, 2009), and animal and patient studies suggesting that transection impairs temporal memory and spares object memory (Charles et al., 2004; Yasuno et al., 1999). The current results indicate that inter-individual variation in fornix microstructure, and perhaps specifically individual differences in fornix fibre coherence, are related to object-in-sequence retrieval performance. The fornix was predicted to be important, as the hippocampus is the only area to have been found to hold object-in-sequence information, other PMN areas such as the RSC and mPFC having been found to hold ordinal sequence position information only (Hsieh & Ranganath, 2015; Reeders et al., 2021). Furthermore, although the fornix pathway is likely important for encoding (Green et al., 2016), the current project found an independent correlation between fornix microstructure and sequence retrieval, indicating that the contribution of this pathway to retrieval is not purely mediated by an encoding process. Interestingly, fornix PC2 was thought to negatively relate to fibre coherence, but it positively correlated with RT Enhancement random-learned. In this behavioural measure, larger values were taken to mean better object-position retrieval. Therefore, although there was no specific hypothesis about the direction of the correlation between fornix PC2 and temporal sequence retrieval, as there was between tract PC2 and oddity task performance (see *Chapter 5*), the positive relationship between

fornix PC2 and RT Enhancement random-learned was unanticipated. As discussed in *Chapter 7,* it remains unclear whether decreased coherence, perhaps implying increased complexity (Chamberland et al., 2019), can be a beneficial tract property with respect to object-position binding, or whether increased fornix coherence relates to performance of behaviour akin to temporal community structure memory (Schapiro et al., 2013), rather than object-position binding. Regardless of the exact temporal memory mechanism, the results support the importance of this pathway in temporal memory.

In the current project, associations between behaviour and fornix microstructure were contrasted with associations between behaviour and PHC microstructure, a tract supporting PMN communication but not primarily to and from the hippocampus (Bubb et al., 2017; Bubb et al., 2018). The absence of any significant correlations between PHC microstructure and tasks requiring spatiotemporal processing supports the specific importance of the hippocampus in these tasks. Regarding the scene oddity task, it has been proposed that the hippocampus is of particular importance in the creation of view invariant scene models (Barense et al., 2010), whereas the parahippocampal cortex, connected primarily through the PHC (Bubb et al., 2017), has been shown to conduct view-specific scene processing (Epstein et al., 2003). However, this is not to say that the PHC does not contribute to spatiotemporal processes. Its connections include the parahippocampal cortex, RSC and PCC, areas already shown to play roles in spatial (Baldassano et al., 2016; Burles et al., 2018; Clark et al., 2018; Epstein et al., 2007) and temporal (Hsieh & Ranganath, 2015; M. Pu et al., 2020) processing. Furthermore, PHC microstructure differs between healthy adults and MCI patients (Metzler-Baddeley et al., 2012), a disease affecting the PMN. Despite these, animal lesion work has demonstrated that fornix lesions cause more severe impairments to spatial processing behaviours than cingulum lesions (Bubb et al., 2018), and memory performance and PHC microstructure only correlates in human MCI patients, not healthy controls, whereas fornix microstructure has been found to correlate with memory performance in both groups (Metzler-Baddeley et al., 2012; Rudebeck et al., 2009). These findings suggest that the structure of the fornix has a larger influence on performance in healthy individuals and structure of the PHC, being a minor pathway of communication between the hippocampus and other PMN structures, only influences behaviour when the fornix pathway is damaged, perhaps as a result of compensatory re-routing (Bubb et al., 2017).

Additionally, in this project, associations between PMN related behaviour and fornix microstructure were contrasted with associations between AIN related behaviour and ILF

microstructure. This was because the ILF connects the ventral visual stream, allowing communication between visual occipital areas and AIN areas such as the PrC and temporal pole (Catani et al., 2003; Herbet et al., 2018). The AIN has been proposed to conduct aggregate item processing for identification, as areas of this network and the ILF have been found to be important for object processing (Lee & Rudebeck, 2010; Ortibus et al., 2012), familiarity (Haskins et al., 2008), semantic memory (Devereux et al., 2018; Ripolles et al., 2017) and face processing (Collins & Olson, 2014; Hodgetts et al., 2015). In line with the hypotheses and previous work (Hodgetts et al., 2015), ILF microstructure correlated with face oddity performance and not scene oddity performance or temporal sequence memory.

BOLD modulation in the PrC and FFA during face oddity task completion has been found to correlate with task performance (Hodgetts et al., 2015) and RS-connectivity between these areas been found to relate to patterns of face recognition (O'Neil et al., 2014). Therefore, it may be that its connection between these areas is particularly important in the case of complex face perception.

8.2.2 Oscillatory activity of the PMN related to complex scene perception.

Previous fMRI work has found hippocampal BOLD modulations during scene oddity task completion (Barense et al., 2010; Hodgetts et al., 2015; Lee et al., 2008). One of these found BOLD deactivations to correlate with performance (Hodgetts et al., 2015), but relating deactivations to underlying neuronal processes is challenging, especially in MTL areas, where the relationship between BOLD and oscillatory activity is unclear (Ekstrom et al., 2009). Oscillatory activity of the PMN has previously been recorded during recollection (Herweg et al., 2016), navigation (Pu et al., 2017) and novel scene imagery (Barry et al., 2019; Monk et al., 2020), but not during complex scene perception.

In *Chapter 4*, whole-brain theta (4-8 Hz) power analyses revealed power modulations in the MTL and in other posteromedial areas that are specific to complex scene perceptual processing. Whole-brain gamma power analyses revealed power modulations in high gamma (60-80 Hz) in the inferior parietal cortex and the precuneus that were specific to complex scene processing. Together, the pattern of areas with modulated oscillatory activity, is strikingly similar to the scene network revealed by Hodgetts et al. (2016) who measured whole-brain BOLD modulations during a scene one-back recognition task. The current work complements this past research by extending the involvement of these network areas into perceptual processes, and adds an understanding of the underlying

neuronal activity through characterization of oscillatory power modulations. Moreover, *Chapter 5* showed that theta power decrease in the MTL ROI correlated with scene oddity performance and not with face oddity performance, showing similarities with the results of Hodgetts et al. (2015). Importantly, MTL theta power did not correlate with subsequent scene memory performance, showing that the relationships between MTL theta and oddity performance was unlikely to be purely mediated by incidental encoding processes.

Theta rhythms are known to be important in hippocampal processes (Buzsaki, 2002), and increases in low frequency oscillations have been associated with decreased BOLD (Fellner et al., 2016), so considering the hippocampal BOLD decrease reported in Hodgetts et al. (2015), it could have been assumed that MTL theta power would increase during the scene oddity task. However, it may be the case that MTL theta power decreases during novel scene processing. The MTL theta power decrease reported in *Chapter 4* is echoed in two previous MEG studies which found decreased hippocampal theta power during novel scene imagery (Barry et al., 2019; Monk et al., 2020). Furthermore, hippocampal theta has been shown to be lower in novel spatial environments than in familiar environments, whereas gamma shows the opposite pattern (Park et al., 2014). Regarding the apparent conflict with the previous BOLD results, theta in the MTL has been shown to be positively related to BOLD (Ekstrom et al., 2009), and the results of a recent preprint study (Hill et al., 2021), which combined fMRI with invasive electrophysiological recording during a free recall task, have further supported unique relationships between BOLD and oscillatory patterns in the MTL. In this study, gamma and BOLD subsequent memory effects (encoding-related activity that predicts subsequent recall) related positively across the cortex but related negatively in the hippocampus. Therefore, shifts in power from low frequency to high frequency within the MTL may be associated with both novel scene processing and reduced BOLD.

It was expected that phase-coherence between the hippocampus and the mPFC, and PAC in the mPFC, would increase during the scene oddity task. However, no evidence to support these hypotheses was found. Rather, mPFC PAC was found to reduce in the scene task versus the control, which contradicts previous studies, which reported theta coherence between the MTL and the mPFC during spatial memory retrieval (Kaplan et al., 2014) and increased mPFC theta-gamma PAC during correct versus incorrect trials of a Y-maze working memory task (Li et al., 2012). It may be that complex novel scene processing is reflected by different patterns of network communication or inter-frequency interactions that were not assessed here. Further work could explore communication between the hippocampus and the parietal cortex, and the mPFC and the parietal cortex. Exploratory

analysis in *Chapter 4* indicated that phase-coherence (in the theta and alpha bands) between the hippocampus and the IPL was increased during the scene oddity task in comparison with the face or size oddity tasks, and previous work has shown increased coupling between the phase of theta rhythms in the mPFC and gamma amplitude in the medial parietal cortex during spatial memory retrieval (Kaplan et al., 2014).

Regarding RS PMN connectivity, theta connectivity strength between the PCC and other PMN areas was associated with scene oddity performance while hippocampus-PMN connectivity strength was not (*Chapter 6*). This was a partial correlation, controlling for subsequent memory performance, so it is unlikely that the perceptual benefit of increased PCC-PMN connectivity was a reflection of the benefits of PCC-PMN connectivity in incidental encoding. The findings of *Chapter 5* suggest a specific importance of the MTL compared with the PCC during the scene oddity task (MTL theta correlated with oddity performance, whereas the correlation test between PCC theta and scene oddity performance was exploratory and gave a larger, non-significant p-value). Comparison of the results in these two chapters may indicate that flexibility within the PMN is advantageous. Although the assessments of network function differ between the chapters (*Chapter 6* assessed amplitude correlations between multiple areas, whereas *Chapter 5* assessed oscillatory power in ROIs including a combined MTL ROI), it may be that PCC connectivity best reflects PMN quality at rest, while task related engagement of hippocampal processes best reflects PMN quality during the behaviour. Supporting this suggestion, the PCC is proposed to have more of a role in mediating whole-brain network information flow than the hippocampus (Lee et al., 2020; Leech & Sharp, 2014). Future work comparing connectivity between the hippocampus, the PCC and other PMN ROIs during perceptual processing and rest, using the same functional analysis methods in each, would help to validate this suggestion.

Regarding the AIN, whole-brain gamma power analyses revealed power modulations in low gamma (40-60 Hz) in the right inferior occipital and fusiform areas that were specific to complex face processing. These results concurred with Hodgetts et al. (2015) who found increased FFA BOLD during face oddity task completion, and also with MEG studies examining face processing, which found increased gamma power in the same locations (Gao et al., 2013; Uono et al., 2017). Although the PrC is thought to be of particular importance in creating view-invariant internal face representations (Barense et al., 2010), and the ILF was proposed to be important in complex face perception because of its connections to the PrC, the current project found no oscillatory activity within the MTL that

was specific to the face task over the scene task. Indeed, it was anticipated that measuring PrC activity with MEG would not be possible, and that therefore it would be likely that the MTL signals relating to the scene oddity task would have originated from the hippocampus or the parahippocampal cortex but not from the PrC. The inability to measure PrC activity with MEG may also explain why no RS-connectivity patterns correlated with face oddity performance. It could be the case that RS-connectivity between the FFA and the PrC would have related to face oddity performance as it has been shown to do in other face processing tasks when measured with fMRI (Collins & Dickerson, 2019; O'Neil et al., 2014).

8.2.3 Tract microstructure was reduced to biologically interpretable and replicable components.

Whereas multiple studies have assessed correlations between behavioural performance and tract microstructure measures separately, and mostly only used FA and MD derived from DTI (Coad et al., 2017; Hodgetts et al., 2015; Metzler-Baddeley et al., 2011; Postans et al., 2014), this thesis took advantage of PCA-based reduction of multiple microstructure measures (Chamberland et al., 2019; Geeraert et al., 2020) and then tested correlations between the microstructure component scores and behavioural measures. This method is comparatively novel and has only been carried out in the context of childhood development (Chamberland et al., 2019; Geeraert et al., 2020), rather than for studying individual differences in adults.

In this thesis, PCA-based reduction of microstructure data was carried out on fornix, PHC and ILF data across two studies. Despite these studies having different groups of adult participants, different diffusion-weighted MRI protocols, and a different collection of microstructure measures, the final components were similar. The experiment in *Chapter 5* included: FA, MD and RD from the DTI model; FR from CHARMED; ICVF and OD from NODDI; and MPF from qMT. The experiment in *Chapter 7* included FA, MD, RD and AxD from the DTI model, and ICVF and OD from NODDI. Biplots, illustrating the weightings of the microstructure measures on two components for each experiment (Figure 46), show how similar the resulting components were across the experiments. PC1 was interpreted as positively relating to the property of restriction and, as it is assumed that increased axon density and myelin proportion contribute to restricting water diffusion, it was predicted to correlate positively with behavioural performance. In both studies, PC1 was negatively influenced by MD and RD, which are both negatively related to myelin density (Seehaus et al., 2015). PC1, from the study in *Chapter 5*, was also positively influenced by MPF, which is

positively related to myelin proportion (Turati et al., 2015), and FR, which is interpreted as relating to axon density (De Santis et al., 2016). PC2 was interpreted as negatively relating to the property of fibre coherence. In both studies it was negatively influenced by FA and positively influenced by OD. OD is lower in tracts known to have more fibre coherency and higher in tracts known to have more fibre fanning and crossing (Zhang et al., 2012), and FA can be influenced by the extent of coherent organisation of fibres within a voxel (Jones, Knosche, et al., 2013; Seehaus et al., 2015). Since many studies have found tract FA to positively relate to performance (Coad et al., 2017; Postans et al., 2014; Schlaffke et al., 2017), or to be reduced in disease (Agosta et al., 2010; Chen et al., 2019; Kantarci, 2014), it was assumed that fibre coherence was a beneficial property, so this component was predicted to negatively relate to behavioural performance. With regard to OD, it should be noted that an increased value could be interpreted as increased fibre complexity (Chamberland et al., 2019; Geeraert et al., 2020), a property that increases during normal childhood development (Chang et al., 2015). Indeed, a positive relationship between white matter OD and reading skill has been shown in children (Huber et al., 2019). However, cognitive performance or functioning is often negatively associated with increased white matter OD in adults (Coad et al., 2020; Ota et al., 2018; Wen et al., 2019).

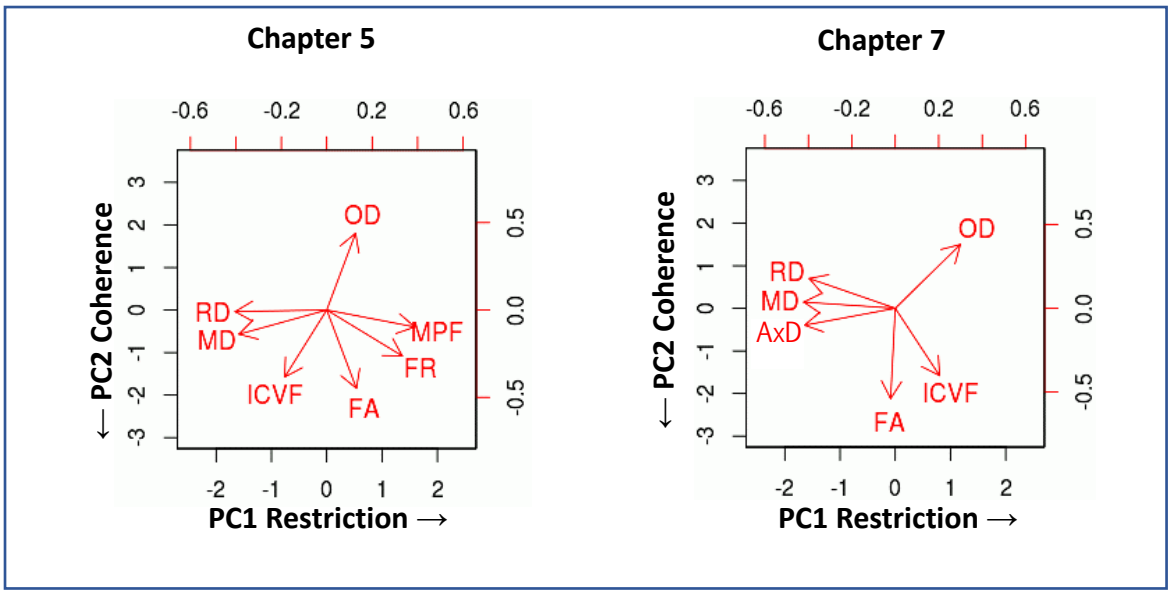

Figure 46. Biplots from PCA-based microstructure data reduction for two experiments.

AxD: Axial Diffusivity. FA: Fractional Anisotropy. FR: Restricted Fraction. ICVF: Intracellular Volume Fraction. ILF: Inferior Longitudinal Fasciculus. MD: Mean Diffusivity. MPF: Molecular Proton Fraction. OD: Orientation Dispersion. PC: Principal Component. PHC: Parahippocampal Cingulum. RD: Radial Diffusivity.

This method allowed for further interpretation of the underlying biology influencing structure-performance relationships. For example, Postans et al. (2014) found correlations between fornix FA and MD, and complex scene perception performance, but since both FA and MD are influenced by fibre density, myelination, and fibre dispersion (Beaulieu, 2002; De Santis et al., 2014), interpreting which of these particular fornix properties is specifically influential is unfeasible. *Chapter 5* revealed that the fornix microstructure component relating to restriction, and not the component relating to coherence, correlated with complex scene perception performance, suggesting that fornix myelination or fibre density may be more related to this behaviour than fornix fibre dispersion.

The influences of AxD and ICVF on the PCA components warrant further thought. AxD measures the diffusion in the greatest direction, considered to be the diffusion path parallel to the fibres in a voxel, and decreases and increases in AxD have been associated with traumatic damage (Song et al., 2003) and axonal degeneration in AD (Mayo et al., 2018), respectively. Assuming a lack of axon damage, its meaning in a healthy population is unclear. AxD has previously been found to positively correlate with FR and negatively correlate with RD (De Santis et al., 2014). The correlation matrix between all microstructure measures within the tracts, shown in *Chapter 7*, indicates positive relationships between AxD and FA, and negative relationships between AxD and RD, in the ILF and PHC data, but these relationships are not the same for the fornix data, in which there was a positive relationship between AxD and RD. It may be that there are properties of the fornix, such as its curvature, that results in different sensitivities of the microstructure data for this tract. For example, it has been shown that correlations between AxD and FR are stronger in single fibre populations than in multiple fibre populations because of the reduction in variation in fibre orientations (De Santis et al., 2014). Analogous to the current PC1 component, an experiment examining fornix microstructure and memory scores in participants with mild cognitive impairment, found fornix MD, RD and AxD to all negatively correlate with memory performance, indicating that they represent shared properties of the fornix (Mielke et al., 2012).

It was anticipated that FR from CHARMED and ICVF from NODDI would be strongly related to each other, and contribute to the PCA components similarly, because they are both sensitive to the volume fraction of intracellular components of a voxel, and thought to represent axon density. However, they did not show a similar contribution to PCA components in *Chapter 5* (see their positions on the biplot, Figure 46). From examination of the relationships between individual microstructure data within each of the tracts, it seems

that this difference is driven by fornix data. In the ILF and PHC data, positive relationships exist among FA, FR, MPF and ICVF, as expected, but in the fornix, ICVF does not positively relate to FA, FR or MPF, instead showing positive relationships with MD and RD. The dissimilarity between FR and ICVF in the fornix may stem from differences in the assumptions from the models, as NODDI relies on the tortuosity assumption whereas the CHARMED model does not. The tortuosity assumption imposes a connection between the volume fraction and MD, which might mean that measures of ICVF are exaggerated in some tissue types (Lampinen et al., 2017). In a comparison between NODDI estimates and estimates from a model that did not rely on the tortuosity assumption, Lampinen et al. (2016), using tissue simulations, found that for cases with high anisotropy, volume fraction estimates of the two models were similar but they differed when anisotropy was low, and NODDI overestimated the restricted fraction. Since fornix FA and MD were lower and higher, respectively, than FA and MD of the other tracts recorded here, a pattern that is also seen in other studies (De Santis et al., 2014; Hodgetts et al., 2015; Pievani et al., 2010), it may be that fornix ICVF is less accurate than fornix FR while ILF/PHC FR and ICVF are similarly accurate. Due to this weakness of NODDI, it has been suggested that FR from CHARMED should be used when examining white-matter abnormalities (De Santis et al., 2019). However, no suggestions have been made about the appropriateness of the use of NODDI when studying different brain tracts. This field would benefit from direct comparison of accuracies of NODDI estimations in different brain tracts, ideally in conjunction with histological data.

By studying correlation matrices between raw microstructure measures of the tracts, different relationships between those of the fornix, compared with those of the ILF and PHC, were apparent. Moreover, when participant tract data was presented as PC1 and PC2 scores, the fornix cluster was distant from those of ILF and PHC, which overlapped. The fornix may have one or more properties that set it apart from the other tracts (e.g., its curvature). There is a risk that the proximity of the fornix to the ventricles means that values from this tract are inaccurate due to signal contamination despite the use of a ‘Free Water Elimination’ algorithm (Pasternak et al., 2009). Indeed, fornix microstructure data were omitted from a study by De Santis et al. (2014) because the low FA, low myelin water fraction and high MD values of this tract compared with the other tracts they studied led the authors to conclude that there had been contamination from CSF. However, in the current data, although fornix MPF was lower than ILF or PHC MPF, the FA and MD values of the fornix did not differ from those of the ILF and PHC to same degree as fornix values

differed from those of the ILF in De Santis et al. (e.g. fornix MD was almost double ILF MD in their study). Therefore, in this project, the difference in fornix microstructure from the other tracts is likely driven more by true differences in underlying anatomy than noise in MRI measurements.

Regardless of the reason, the difference in fornix microstructure from the other tracts may mean that the component scores from the PCA-based data reduction of all tract data may be less accurate at portraying each tract than if data reduction was carried out on the microstructure measures of each tract separately. Therefore, it was important for the correlations between behaviour/functional values and raw tract microstructure values to also be presented in the *Appendices 2C* and *4C,* so that if relationships between individual tract microstructure values and behaviour/functional values did not carry over to microstructure component data, they could be identified.

To summarize, the results presented in this thesis support the use of this PCA-based microstructure data reduction technique for collections of tracts, including the fornix, but also highlight the importance in examining the raw microstructure data.

8.3 Findings inspiring further thought.

8.3.1 No three-part structure-function-behaviour relationships were identified but the angular gyrus may be important in linking these in the PMN.

It was anticipated that the analyses of the oddity experiment would reveal three-part relationships between structure, function and behaviour in the PMN and the AIN. However, although there was evidence that fornix PC1 and HPC theta power related to scene oddity performance, they did not correlate with each other. Furthermore, PCC-PMN theta RS-connectivity also correlated with scene oddity performance but not fornix PC1. However, there was a correlation between fornix PC2 and HPC theta power, but fornix PC2 did not relate to scene oddity performance. These results may indicate that these functional and structural measures of PMN functioning independently contribute to performance in PMN related behaviours, in healthy adults. Indeed, Hodgetts et al. (2015) also found no correlation between fornix microstructure and hippocampal BOLD. Also, correlations between PMC/MTL RS-connectivity and fornix microstructure have been found in MCI patients and not healthy controls (Berron et al., 2020). Exploratory RS-connectivity analysis in *Chapter 6* revealed that the angular gyrus has a potentially important role in connecting structure, functional and behaviour. Theta RS-connectivity between the left angular gyrus

and left hippocampus correlated with fornix PC1, and theta RS-connectivity between the left angular gyrus and the left lateral temporal cortex correlated with scene oddity accuracy. This parallels the exploratory analysis in *Chapter 4* which suggested increased HPC- left IPL phase-coherence during scene oddity task completion. As part of the 'contextual integration model', the left angular gyrus has been proposed to be crucial in integrating and representing multimodal contextual details (Ramanan et al., 2018). In this model, interactions between the left angular gyrus and the MTL allow for richer representations, conjoined with perceptual-sensory and saliency information, over representations constructed in MTL alone. It may be that scene representations, built though MTL-left angular gyrus interactions, partly supported by fornix fibres (the fornix does not directly connect the angular gyrus), are beneficial to complex scene perception. Future work could specifically test correlations between MTL-left angular gyrus connectivity, during perceptual processing and during rest, with scene oddity performance and fornix microstructure.

There was no in-task functional imaging in conjunction with the temporal sequencing task, so three-part relationships were not tested here. However, since angular gyrus processes has been shown to aid temporal sequence memory (Hsieh & Ranganath, 2015), it would greatly benefit investigation of the PMN and the PM-view if the future study suggested above (testing correlations between MTL-left angular gyrus connectivity, during task and during rest, with scene oddity performance and fornix microstructure) also included a temporal sequence memory task.

8.3.2 Properties of the PMN and AIN were not fully dissociable.

When correlations between structure, function and behaviour were compared between the networks, some correlations were found to be dissociable and others were not. To exemplify the former, the coefficient of the correlation between the scene HPC theta power difference (compared with fixation) and scene oddity accuracy was significantly stronger than that of the correlation between face HPC theta power difference and face oddity accuracy. Similarly, the correlation coefficient between theta PCC RS-connectivity strength and scene oddity accuracy was significantly larger than that of the correlation between theta PCC connectivity and face oddity accuracy.

However, the coefficient of the correlation between fornix microstructure and scene oddity performance was not significantly greater than that of the correlation between fornix microstructure and face oddity performance. Furthermore, the coefficient of the

correlation between ILF microstructure and face oddity performance was not significantly larger than that of the correlation between ILF microstructure and scene oddity performance. These results differ from those of Hodgetts et al. (2015), which did find dissociable relationships within structure and function measures of the PMN and AIN. Similarly, regarding the temporal sequence memory experiment, the coefficient of the correlation between RT Enhancement random-fixed and fornix PC2 was not significantly larger than that of the correlation between RT Enhancement random-fixed and ILF PC2.

Despite the lack of dissociability between these correlations of structure and function, multilinear regression analyses provided some evidence of unique contributions of fornix microstructure, over the ILF and PHC, to predictions of PMN-related task performance. In *Chapter 5,* the regression results showed that fornix PC1 predicted scene oddity performance independently of ILF/PHC PC1, while in *Chapter 7*, the regression results showed that fornix PC2 predicted RT Enhancement random-fixed independently of ILF/PHC PC2.

Together, the results portray distinct inequalities in the importance of network structure and function properties, between the networks, but not complete separability. It is possible that the dissociable correlations found in Hodgetts et al. (2015) could not be reproduced because of the differences in experimental methods, for example, in how microstructure properties were measured or because the oddity task used in the current project was more difficult. Equally possible is that dissociable correlations would have been found with a larger sample size. Regardless, further studies are required to determine the extent of dissociability of structure, function and behaviour correlations in the PMN and the AIN.

8.4 Limitations and considerations.

8.4.1 Considerations of measuring functional activity from ROIs.

There are several aspects of the methods used to characterize the functional signals of ROIs that warrant further discussion. These can be characterized by two themes, the fact that multiple brain areas are known to be functionally heterogenous but were assessed collectively, and that differences in assessing ROI activity between the chapters could make cross-chapter comparisons flawed. To exemplify this, methods used to explore MTL and PCC signals are discussed.

Since theta power modulations associated with spatial processing have been identified in the hippocampus and in parahippocampal areas (Pu et al., 2017; Pu, Cornwell, et al., 2018), and differentiating activity within these locations with MEG is challenging (Stephen et al., 2005), it is not possible to be sure that theta power modulations found during the scene oddity task (*Chapter 4*) in a cluster that appeared to cover the hippocampus and parahippocampus, really show that both brain areas were active, or whether activity from one produced source spread effects. However, it seems likely that both areas were engaged, as BOLD modulations in both areas have previously been found during the scene oddity task (Hodgetts et al., 2015; Hodgetts, Voets, et al., 2017). Additionally, due to the challenge of separating MTL sources, a HPC ROI was constructed by combining AAL ROIs for hippocampal and parahippocampal areas (see methods of *Chapter 4*), and time-averaged theta power modulations of the voxels within this ROI were averaged for each participant, to create the MTL theta measure. This creates an uncertainty as to whether theta power modulations in the hippocampus or parahippocampal cortex, or both, correlated with scene oddity performance. However, it is likely that, while both areas contributed to the behaviour, only hippocampal signals correlated with performance, as the hippocampus has been shown to be specifically important when view-invariant scene representations are required (Barense et al., 2010). Moreover, significant and insignificant correlations between scene oddity performance and hippocampal BOLD, and parahippocampal BOLD, have previously been reported (Hodgetts et al., 2015). Nevertheless, further work investigating the influence of hippocampal and parahippocampal oscillatory activity on complex scene perception would be helpful, and would perhaps be best characterized by using invasive electrophysiological techniques.

Moreover, not all components of the hippocampus are likely to be equally involved in complex scene perception. The anterior hippocampus has been proposed to be specifically important for creation of internal scene representations (Zeidman & Maguire, 2016), and theta modulation during novel scene imagery has been reported specifically in the anterior hippocampus (Monk et al., 2020). In agreement, high field fMRI work has indicated the specific engagement of the anteromedial subiculum during scene oddity task completion (Hodgetts, Voets, et al., 2017). Such precise localization of source signals is challenging with MEG, so it was not attempted in the current work. Alternatively, the medial and lateral aspects of the fornix, connecting to the posterior and anterior portions of the hippocampus respectively, can be separately characterized using DWI techniques (Christiansen et al., 2017). Future work could attempt further investigations into the role of the anterior

hippocampus by testing for stronger correlations between lateral fornix microstructure and scene oddity performance than between medial fornix microstructure and scene oddity performance.

On a similar theme, functional heterogeneity and homogeneity of the PMC requires further examination. The PCC ROI may have multiple functions. For example, dorsal PCC locations are more associated with spatial recall than are ventral locations, which are more associated with spatial encoding (Burles et al., 2018). It may be that dorsal and ventral PCC were differently engaged within the scene oddity task. Similarly, some studies do not specifically distinguish between the PCC and RSC (Burles et al., 2018; Natu et al., 2019) and the RSC falls within the precuneus ROI of the AAL atlas, so it was not independently explored in this project either. Therefore, future work may benefit from splitting the PCC ROI and including the RSC separately to either the PCC or the precuneus. On the other hand, the PMC has been assessed as a whole (Shine et al., 2015), and the precuneus and the PCC were reported to display similar interactions between APOE-ε4 group scene oddity BOLD modulations and those of controls, so similarities between these brain areas may mean that grouped ROI analysis is still useful in understanding network functionality.

The construction methods of MTL VSs differ between analyses in this project. In *Chapter 4,* left and right HPC VSs were made by combining AAL ROIs for the hippocampus and the parahippocampal areas and creating single VSs (one left, one right) using a PCA reduction technique (Seymour et al., 2017). In *Chapter 6*, separate VSs were created for the hippocampus and the parahippocampal cortex, and single VSs were created by identifying the voxel with the largest signal variation. There are two reasons for these methodological differences. The first is the aim to use methods consistent with those used in the literature, so that the current work could be easily compared with other studies. The VS method in *Chapter 4* was the PCA reduction technique used by Seymour et al. (2017) and since the PAC analysis method also used by Seymour et al. was subsequently conducted, it was important to keep the creation of the VSs comparable. On the other hand, multiple RS MEG studies have tested amplitude-amplitude correlations between AAL ROIs and several of them created the VSs by identifying the voxel with the largest variation (Dima et al., 2020; Godfrey & Singh, 2020; Routley et al., 2017).

Additionally, the reason why the hippocampal and parahippocampal signals could be assessed separately within RS analysis is because part of the RS MEG analysis methods

removes the zero lag between the ROIs so that the risk of artificial connectivity from source spread is reduced (Dima et al., 2020; Godfrey & Singh, 2020; Routley et al., 2017).

8.4.2 Hemispheric differences may exist but were not tested.

Hemispheric lateralization may be present in the AIN and PMN, but this was not explicitly tested in the current project. For example, time-frequency spectrograms of the right and left HPC VSs were exploratively examined but not directly compared. This was because there was not a hypothesis regarding left or right lateralization for PMN functioning, or specifically, left or right hemispheric dominance for hippocampal engagement, in complex scene processing. Concurrently, Hodgetts et al. (2017) identified BOLD modulation in the bilateral subiculum for the scene oddity condition over face or object conditions.

Some findings have indicated that the right hippocampus is more sensitive to spatial memory, while the left is more sensitive to temporal sequence memory (Abrahams et al., 1997; Iglói et al., 2010). Characteristics of the theta rhythm may also differ between the hippocampi (Miller et al., 2018). However, MTL lateralization is not immediately obvious from the current project's results. In *Chapter 4*, whole-brain power comparisons showed decreased theta power in the left MTL in the scene-vs-size comparison, but showed decreased theta power in the right MTL in the scene-vs-face comparison, suggesting that MTL theta modulation occurs bilaterally during complex scene processing, perhaps with differing levels of strength. Regarding the time-frequency analysis of the VSs, although the right HPC displayed a brief increase in beta2 power, both the left and right HPC displayed reduced low theta/delta power near the end of the time window in the scene-vs-size comparison. Moreover, exploratory correlation tests in *Chapter 5*, revealed correlations between the decrease in HPC theta power in the scene-vs-fixation comparison and scene oddity accuracy, for both left and right HPC VSs.

On the other hand, the face processing network is generally agreed to be right-lateralized in adults (Bukowski et al., 2013; Cohen et al., 2019; Hildesheim et al., 2020; Sergent et al., 1992). Although not specifically tested, the results of this project also indicate right-lateralization of oscillatory power modulation during the face oddity task. Gamma power (both higher and lower bands) was found to be higher in the face condition versus the scene and size oddity conditions, in an area including the right FG and right IOC. However, the results of Hodgetts et al. (2015) provide only weak evidence of right-lateralization. There was no report of a significantly stronger correlation between right FFA/PrC BOLD and face oddity performance than between left FFA/PrC BOLD and face oddity performance. In

addition, although they found a numerically stronger correlation between right ILF MD and face oddity performance than between left ILF MD and face oddity performance, there was no significant difference between these correlation coefficients. Together, this inconclusive evidence incites the need for further research into right lateralization in complex face processing. While it would have been possible to inspect left and right ILF tracts in the current project, it was avoided because this would have increased the number of behaviour-microstructure tests far beyond the number of hypotheses. Due to the use of the microstructure PCA reduction techniques, splitting the ILF by hemisphere would have necessitated also splitting the fornix and the PHC, otherwise the PCA analysis would have been biased towards ILF values. Therefore, the number of behaviour-microstructure correlation tests would double because of only one hypothesis.

8.4.3 Microstructure components are useful for comparing tract properties, but the underlying biology is still undetermined.

Although the two microstructure components resulting from the two studies in this thesis allowed some understanding of how different microstructure properties influence behaviour, the results cannot provide an understanding of the true underlying anatomical properties. For example, it is inferred that PC1 represents restriction, mediated by myelin proportion and axon density, but these two anatomical properties cannot be distinguished here, or in previous studies using similar methods (Chamberland et al., 2019; Geeraert et al., 2020). It is unclear whether it would be possible to separate these properties using this data reduction method for two reasons. First, although FR and MPF are thought to be sensitive to axon sensitive and myelin proportion, respectively, it is unclear how dissociable those sensitivities are. For example, CHARMED is thought to be more sensitive than DTI measures, because the variation in the size of the restricted water pool was thought to reflect the proportion of axons in a voxel, making it a marker of axon density. However, it has been noted that the part of the calculation of FR is normalization according to the total, extra and intracellular, water content, meaning that variation in myelin and total water context can influence resulting FR values (De Santis et al., 2019). Unlike FA, MD (Seehaus et al., 2015), ICVF and OD (Sato et al., 2017), FR has not been validated histologically (De Santis et al., 2019). Second, while damage to axons and myelin may be separable in disease states (Song et al., 2003), in healthy brains there is a relationship between axon diameter and myelin thickness (Waxman, 1980), so it might be expected that axon density and myelin proportion would correlate within a healthy brain. Therefore, even if MPF and FR dissociably characterize myelin and axon density, correlations between these anatomical

properties would lead to correlations between these microstructure values, resulting in their similar contribution to PCA components.

Although future work would benefit from validation of FR from CHARMED, and even though NODDI has undergone histological validation (Wang et al., 2019), FR from CHARMED may be the more appropriate option when studying fornix data. As mentioned above, ICVF values of the fornix were difficult to interpret, and it may be that they were not accurate for this tract. Future work could aim to provide a better understanding of the underlying anatomy influencing fornix ICVF data, making individual differences in fornix ICVF more understandable.

In this thesis, varimax rotation was not applied to resulting principal components (the same methods as Chamberland et al. (2019) were used), but it was used in Geeraert et al., (2020). Varimax rotation is used to maximize the variance of components by minimizing the number of variables loading highly onto multiple components (Reinard, 2006). This can make interpretation of the meaning of the components clearer, as it can mean that the tract properties to which the components are related have less overlap, or are even separated. Without varimax rotation, there is a risk that fibre coherence, for example, is represented more by PC2, but still represented to a smaller extent in PC1. Varimax rotation may have resulted in no fibre coherence representation in PC1. In the case of Geeraert et al. (2019) it was particularly important to apply varimax rotation because their second and third components were very similar in the fact that myelin relating measures loaded onto both components. The third component also had an axon-diameter-sensitive measure, so the use of varimax allowed the researchers to interpret PC3 as sensitive to axon diameter, assuming that myelin sensitive measures were mostly loaded onto PC2. However, in the current project, and in Chamberland et al. (2019), this was less of a concern because the properties represented by the two resulting components did not appear to overlap to the same extent as seen in Geeraert et al., (2020). Furthermore, the primary goal of this thesis was to test tract microstructure and behaviour associations and a secondary goal was to ask whether different properties appear to be more influential, with the aim of explaining why previous work found relationships with FA and not MD, or vice versa. Future researchers using PCA-based data reduction of multiple microstructure measures may decide whether to apply varimax rotation after assessing the interpretability of the components or choose to present data with and without varimax rotation to see if it improves interpretation.

A further important point concerning the microstructure components revealed in the experiments of *Chapters 5 and 7* is that they are comparable, but not identical. This is crucial when considering the relative influence of fornix microstructure properties on behaviour/function. For instance, the findings that the fornix restriction measure correlated with complex scene perception performance (*Chapter 5*) while the fornix coherence measure correlated with object in temporal structure retrieval (*Chapter 7*) are interesting but we cannot conclude that fornix restriction and coherence are differentially influential in the contexts of perception and memory because the findings come from two different studies with different participant cohorts and collections of microstructure measures. These findings should be considered early steps in the understanding of how different white-matter properties influence different behaviours supported by single networks. Ideally, this work should be followed by a study assessing individual differences in performances of tasks requiring spatiotemporal processing in a range of contexts, from retrieval to learning and perception to future imaginings.

It is also important to consider the limitations of tractography itself. Virtual streamlines, which we consider to represent tracts, are created from estimations of the directionality of diffusion of water molecules in the brain, and not the tissue itself, which means that characterization of fibres is limited by the limitations of this MRI technique. For example, the magnetic gradient amplitudes influence the resolution, determining the minimum diameter fibre that can be detected (McNab et al., 2013). Strengths of the current methods include the use of prior understanding of tract anatomy and the placing of streamline ROIs according to previous studies, allowing some assurance that the streamlines captured fibres which were comparable across studies. In addition, although the automated software allowed an appropriate initial carving of each tract, each participant's streamlines differ in shape, and so were then pruned to remove any spurious streamlines. However, it is challenging to assess the specificity and sensitivity of the tractography methods used, for each participant, without the knowledge of the true underlying anatomy (Schilling et al., 2020).

8.4.4 The demographics of the experiment samples.

There are three aspects of the participant pool demographics that warrant discussion: sample size, participant sex and participant age.

Despite the experiments in *Chapters 4/5/6 and 7* having sample sizes comparable to, or larger than, other studies that revealed similar structure-behaviour (Geeraert et al., 2020;

Hodgetts et al., 2015) / structure-function (Hodgetts et al., 2015; Shin et al., 2019) / function-behaviour (Pu et al., 2017; Y. Pu et al., 2020)[16] correlations, some results in this project indicate that the experiments may have benefited from increased sample size. The sample size of the oddity-MEG-diffusion study was based on the sample size and effect sizes reported in Hodgetts et al. (2015), which included 30 participants. Individual differences studies, such as that of Hodgetts et al. (2015) and the present project, require larger samples than do group comparisons such as comparisons of healthy controls vs disease patients, as the effect sizes are usually weaker in individual differences studies (Dubois & Adolphs, 2016). Some correlations in this chapter had alpha values below the traditional threshold of 0.05, but not below the corrected experiment-wise alpha, and the corresponding BF indicated weak evidence in favour of the alternative model. For example, the correlation between the fornix restriction measure and scene oddity performance fits this description, suggesting that this result would have produced a lower p-value if the sample were larger. Moreover, Geeraert et al. (2020) suggested that they would have found relationships between white-matter properties and reading skill if their sample had been larger, stating that p-values less than 0.1 suggested that effects would have been found with increased sample size.

None of the hypotheses of this project was sex-specific. Key papers of interest studying complex perception (e.g. Hodgetts et al., 2015) and temporal sequence memory (e.g. Hsieh et al. 2014) did not study differences between males and females, so there were no predictions that structure, function and behaviour correlations would differ between them. However, the bias towards female participants in the two experiments of this project must be acknowledged. Most participants in the oddity task experiment were female and all the participants in the temporal sequence memory experiment were female. Therefore, there is a risk that the results of this project pertain specifically to females.

Gender-binary (Hyde et al., 2019) approaches have identified psychological differences between the sexes (Hyde et al., 2019; Ristori et al., 2020). For example, differences in spatial learning have been found in males vs females in a virtual navigation MEG study (Y. Pu et al., 2020). Task performance of the males was significantly higher than that of the females, and hippocampal theta decreased in power from the first to second training set, whereas no difference was found for females. Differences in hippocampal theta power modulation between the sexes was not tested in the current project and could have

[16] Sample sizes of example studies are as follows: Geeraert et al. (2020), 46; Hodgetts et al. (2015), 30; Shin et al. (2019), 10; Pu et al. (2017, 2020), 18.

influenced the correlations between MTL theta power and scene oddity performance. However, it should be noted that in Pu et al. (2020), the groups were tested at different times, for use in two difference studies (Pu et al., 2017; Y. Pu et al., 2020) and therefore it does not provide strong evidence that MTL theta differs between the sexes.

Although future work could aim to assess if the findings in this project can be replicated in male-dominated groups, it is unclear how useful this would be, when ignoring multiple aspects of gender (Hyde et al., 2019). It is not clear if brain differences noted between males and females are purely chromosome-based. Rather, it may be that brain differences are also based upon experience, genes and hormone effects on development (Ristori et al., 2020), all things that can influence an individual beyond relating to their sex. Therefore, it seems unlikely that humans can be easily categorized into two groups. Indeed, it is commonly argued that there are multiple genders (Hyde et al., 2019). Furthermore, it is unclear how useful it would be to separate participant pools when examining human aspects, such as spatial processing, which are not sex-specific.

The aims of this project were to study individual differences in young healthy adults. The age groups of the participant pools in the oddity experiment (mean: 22.4 years, SD 4.0, range: 18-38 years) and temporal sequence memory experiment (mean: 20.1 years, SD 1.1, range: 19-24 years) were largely comparable but not identically matched. In particular, the oddity experiment has a larger age range. Therefore, as suggested previously, one study (i.e. with one participant pool) investigating structure, function and behaviour correlations in the context of both mnemonic and perceptual tasks, with both spatial and temporal modalities, would be beneficial.

Revealing the underlying mechanisms behind individual differences in young healthy adults was not the primary interest of this project. It is possible that age contributed to differences in structure, function and behaviour, or even influenced the two networks unequally. Exploration of these ideas would be of great interest to the field of brain aging. Relatedly, microstructure measures of different tracts may not change equally with age. For example, in a study (Mårtensson et al., 2018) where DTI metrics of segments of the cingulum and inferior-fronto occipital fasciculus were compared between age groups, RD values of the anterior and posterior portions of the cingulum were lowest in the 28-40 age-group, and increased in the subsequent age groups. Conversely, for the PHC, RD appeared highest in the 19-27 age group and decreased in the subsequent age groups, and RD values

of the central inferior-fronto occipital fasciculus were low in the youngest group but was relatively stable across the other age groups.

It would have been possible to include participant age as a control variable in all tests of this project, but since the study of individual differences was primarily used as a method to examine networks, the mechanisms behind the healthy individual differences was not of interest, and beyond the scope of the investigation. Therefore, adding age correlation tests would have unnecessarily increased the chances of type 1 errors and made interpretation of results more complicated. However, understanding how age influences structure, function and behaviour correlations is important for the field generally. As discussed previously, correlations between PHC microstructure and behaviour have been revealed in MCI patients but not healthy controls (Metzler-Baddeley et al., 2012), perhaps due to compensatory mechanisms. It may be that age-related compensatory changes also result in changes in different structure-behaviour relationships over a life-time.

8.5 Final conclusions.

In conclusion, this project examined functional and structural properties of spatial processing networks in the brain with the aim of evaluating the PM-view that is encompassed by the EAM and PMAT models. Based upon the networks described by these models, the function of the PMN, thought to conduct spatiotemporal processing, was contrasted with the function of the AIN, thought to conduct aggregate item processing. To achieve this, individual differences in network structure, function and behaviour were characterized using multi-model imaging techniques, for the purposes of two experiments, probing perceptual processing and temporal sequence memory, respectively. Examination of MEG signals recorded during the perceptual oddity task revealed theta and gamma power modulation in PMN areas, including the MTL, during the scene oddity task. Of these, reduction of MTL theta correlated with scene oddity performance, indicating the importance of MTL areas in this perceptual task. In contrast, during rest, connectivity of the PCC to the rest of the PMN correlated with scene oddity performance. These results contrast with oscillatory patterns of the AIN during the face oddity task, where gamma-power increases were revealed in the FG and IOC. In terms of structure, tract microstructure data was successfully reduced into interpretable components that corresponded across two datasets. There was evidence of correlations between fornix microstructure and both scene oddity performance and temporal sequence memory, indicating the importance of hippocampal communication in both spatiotemporal-

perception and -mnemonic tasks. On the other hand, ILF microstructure correlated with face oddity performance only, and PHC microstructure did not correlate with any behaviour measures. Three-part relationships between structure, function and behaviour were hypothesized but not evidenced. However, exploratory RS analysis indicated correlations between angular gyrus connectivity within the theta band and both fornix microstructure and scene oddity performance. In general, the findings from this project provide evidence in support of the implications of the PM-view: areas of the PMN and AIN networks were found to be differently important for behaviours requiring different processing modalities; MTL areas were found to be involved in a complex visual perceptual task; and correlations were found between behavioural performance in tasks involving the network-specific modalities and structural/functional properties of the respective networks.

The results presented in this thesis weaken the conceptual and anatomical barriers between perception and memory, and instead reinforce the roles of MTL regions in supporting conjunctive representations as part of processing hierarchies. While supporting that individual brain areas play unique roles in cognitive functions, this thesis highlights the importance of large-scale network function by revealing individual differences in network properties and cognitive behaviours. The results also have implications in predictions of cognitive impairments from diseases affecting the MTL. These may be contributed to by diminished large-scale network communication with the MTL, as well as by MTL damage itself. Moreover, cognitive impairments would not be predicted to be restricted to memory but to include a range of behaviours that rely on the processing qualities of the damaged network.

Appendices

Appendix 1: Pertaining to Chapter 4. Number of MEG trials after cutting and cleaning.

A) Number of trials for each condition after 2 s cut. The last row contains the mean number of trials, in bold.

Participant number	Scene	Face	Size	Fixation
1	80	90	72	87
2	84	61	30	92
3	83	77	76	91
5	86	78	53	92
6	83	90	71	83
7	89	91	87	95
9	82	87	69	87
10	78	92	33	92
11	78	86	69	91
12	86	88	43	94
13	93	94	95	96
14	80	84	39	81
15	84	85	61	93
16	89	80	36	95
17	87	89	93	90
18	81	87	74	81
19	84	83	75	81
21	90	93	64	95
22	84	82	78	89
23	77	70	48	81
24	86	92	71	89
25	91	69	71	94
26	72	82	81	88
27	91	79	66	96
28	89	87	90	88
29	85	88	63	92
30	72	87	86	86
31	75	85	49	93
32	90	93	79	91
33	85	73	56	93
34	85	94	81	89
35	88	94	73	87
36	63	81	79	91
37	84	47	81	93
38	58	50	38	59

39	75	91	30	84
40	92	92	68	89
41	86	86	80	88
42	57	55	25	49
43	91	84	59	92
	82.3	**82.4**	**64.8**	**87.9**

B) Number of trials for each condition after 2.2 s cut. The last row contains the mean number of trials, in bold.

Participant number	Scene	Face	Size	Fixation
1	80	87	63	87
2	80	48	26	92
3	80	72	69	91
5	83	70	42	92
6	82	83	66	83
7	88	90	82	95
9	82	84	62	87
10	77	87	26	92
11	76	86	68	91
12	85	88	34	94
13	93	94	94	96
14	80	78	33	81
15	83	81	54	93
16	88	72	29	95
17	87	89	91	90
18	81	80	71	81
19	83	80	72	81
21	87	90	57	95
22	84	80	73	89
23	76	58	42	81
24	85	90	65	89
25	89	58	66	94
26	72	81	80	88
27	89	71	55	96
28	89	87	88	88
29	84	88	52	92
30	72	84	85	86
31	74	83	42	93
32	90	90	67	91
33	82	64	48	93
34	85	88	79	89
35	88	94	64	87
36	63	79	73	91
37	81	41	33	93

38	55	42	22	59
39	75	88	77	84
40	91	91	60	89
41	86	85	70	88
42	57	52	18	49
43	91	82	54	92
	81.3	**78.4**	**58.8**	**87.9**

C) PAC in the left and right HPC.

An exploratory search of PAC in the HPC VSs revealed no significant differences in the right or left HPC PAC between any of the conditions. However, an apparent increase in theta-gamma coupling, seen for the left HPC in the scene condition compared with the face condition, approached significance (cluster p-value = 0.09).

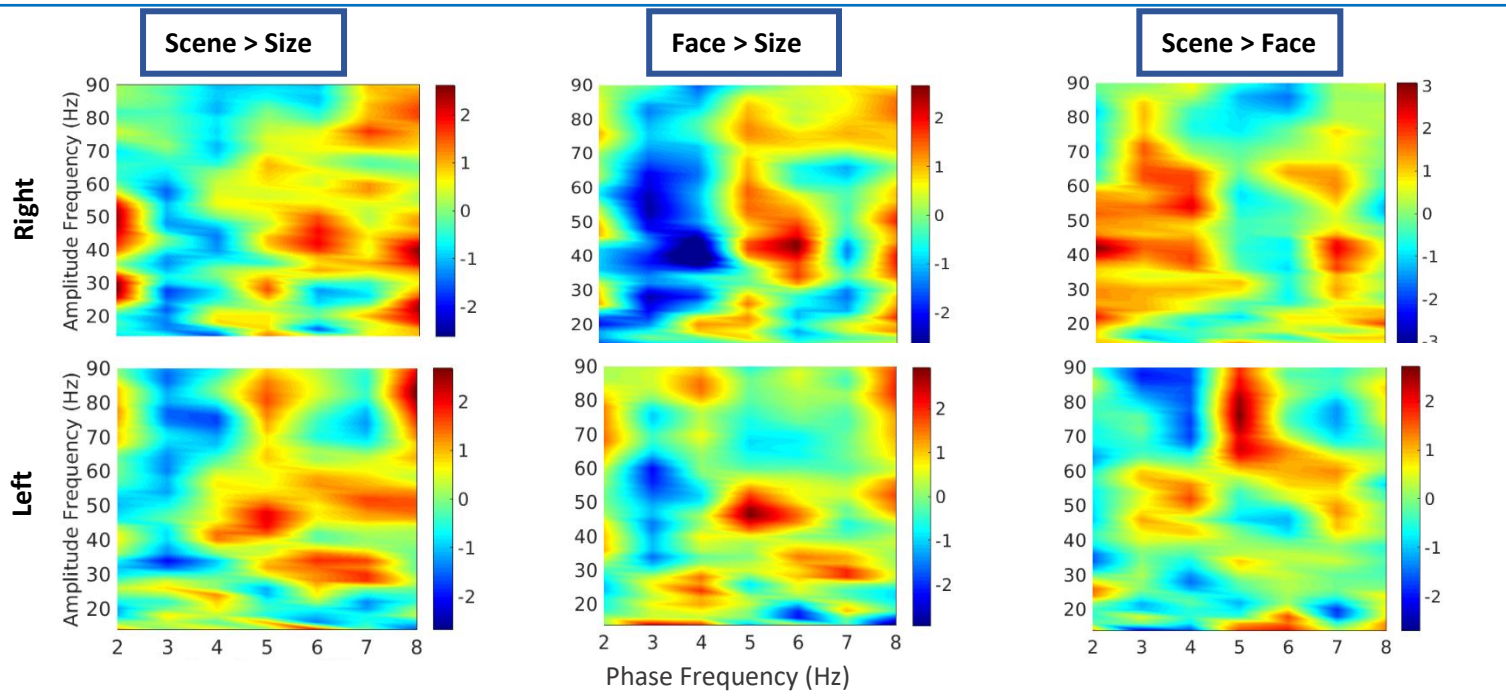

Appendix 1C Figure: PAC in the left and right HPC.
No significant differences in PAC between conditions were found for either the left or right HPC VSs. The colours represent t-values. The colour scale bar for each image is shown to the right of each image.

Appendix 2: Pertaining to Chapter 5. Correlation tests between: ROI power modulation and MEG trial numbers; HPC power modulation and ILF/PHC microstructure; and raw tract microstructure values and oddity accuracy.

A) Tables showing no significant correlations between number of trials in each condition and oscillatory power differences (between condition and fixation) in the ROIs. N=40.

Theta	Scene trial number		Face trial number		Size trial number	
	Pearson's r	p-value	Pearson's r	p-value	Pearson's r	p-value
HPC theta scene	0.091	0.575	0.044	0.789	0.132	0.417
HPC theta face	0.041	0.8	0.043	0.794	0.17	0.293
HPC theta size	0.194	0.23	0.154	0.344	0.204	0.208
PCC theta scene	0.212	0.189	0.196	0.226	0.16	0.325
PCC theta face	0.038	0.814	0.141	0.385	0.227	0.158
PCC theta size	0.257	0.109	0.17	0.294	0.193	0.232
mPFC theta scene	-0.069	0.674	-0.078	0.633	0.007	0.964
mPFC theta face	-0.16	0.325	-0.01	0.95	-0.048	0.768
mPFC theta size	-0.059	0.716	-0.126	0.44	-0.023	0.889
IPL theta scene	-0.076	0.641	-0.091	0.575	-0.108	0.508
IPL theta face	-0.046	0.777	-0.048	0.768	-0.029	0.86
IPL theta size	0.002	0.992	-0.045	0.783	-0.04	0.808

High gamma	Scene trial number		Face trial number		Size trial number	
	Pearson's r	p-value	Pearson's r	p-value	Pearson's r	p-value
HPC gamma scene	0.149	0.36	0.119	0.465	-0.018	0.912
HPC gamma face	-0.115	0.481	0.106	0.516	-0.118	0.469
HPC gamma size	-0.17	0.293	-0.165	0.309	-0.122	0.455
PCC gamma scene	0.051	0.756	0.109	0.504	-0.139	0.394
PCC gamma face	-0.136	0.404	0.123	0.45	-0.268	0.094
PCC gamma size	-0.012	0.942	-0.003	0.987	-0.188	0.246
mPFC gamma scene	0.138	0.396	0.14	0.388	0.021	0.897
mPFC gamma face	-0.067	0.68	0.183	0.259	-0.05	0.761
mPFC gamma size	-0.014	0.93	-0.11	0.501	-0.026	0.873
IPL gamma scene	0.233	0.148	0.161	0.321	0.141	0.385
IPL gamma face	0.02	0.901	0.076	0.643	-0.131	0.419
IPL gamma size	-0.017	0.918	-0.132	0.417	-0.046	0.78

Low gamma	Scene trial number		Face trial number		Size trial number	
	Pearson's r	p-value	Pearson's r	p-value	Pearson's r	p-value

HPC gamma scene	0.17	0.294	0.067	0.683	0.042	0.798
HPC gamma face	-0.192	0.234	-0.025	0.877	-0.203	0.209
HPC gamma size	-0.123	0.451	-0.226	0.161	-0.169	0.297
PCC gamma scene	0.019	0.909	0.019	0.907	-0.053	0.743
PCC gamma face	-0.16	0.324	-0.093	0.569	-0.202	0.211
PCC gamma size	-0.077	0.636	-0.164	0.312	-0.047	0.774
mPFC gamma scene	0.274	0.087	0.096	0.557	-0.051	0.753
mPFC gamma face	0.209	0.196	0.079	0.626	-0.141	0.385
mPFC gamma size	0.228	0.157	0.116	0.477	-0.023	0.887
IPL gamma scene	0.06	0.714	0.269	0.094	0.092	0.574
IPL gamma face	0.06	0.714	0.269	0.094	0.092	0.574
IPL gamma size	-0.006	0.968	0.099	0.543	0.007	0.968

B) Partial correlations between HPC theta power difference (compared to fixation), and ILF and PHC microstructure (controlling for trial number) N=39.

		Scene HPC theta power difference	Face HPC theta power difference	Size HPC theta power difference
ILF	PC1	r = -0.103 p = 0.538 BF_{10} = 0.42	r = -0.129 p = 0.440 BF_{10} = 0.47	r = -0.094 p = 0.573 BF_{10} = 0.41
	PC2	r = 0.065 p = 0.700 BF_{10} = 0.38	r = 0.167 p = 0.315 BF_{10} = 0.56	r = 0.038 p = 0.819 BF_{10} = 0.36
PHC	PC1	r = -0.004 p = 0.982 BF_{10} = 0.36	r = -0.051 p = 0.761 BF_{10} = 0.37	r = -0.163 p = 0.327 BF_{10} = 0.55
	PC2	r = 0.001 p = 0.998 BF_{10} = 0.36	r = 0.048 p = 0.773 BF_{10} = 0.37	r = 0.111 p = 0.507 BF_{10} = 0.43

C) Correlation matrix of the relationships between oddity accuracy scores and raw tract microstructure data.

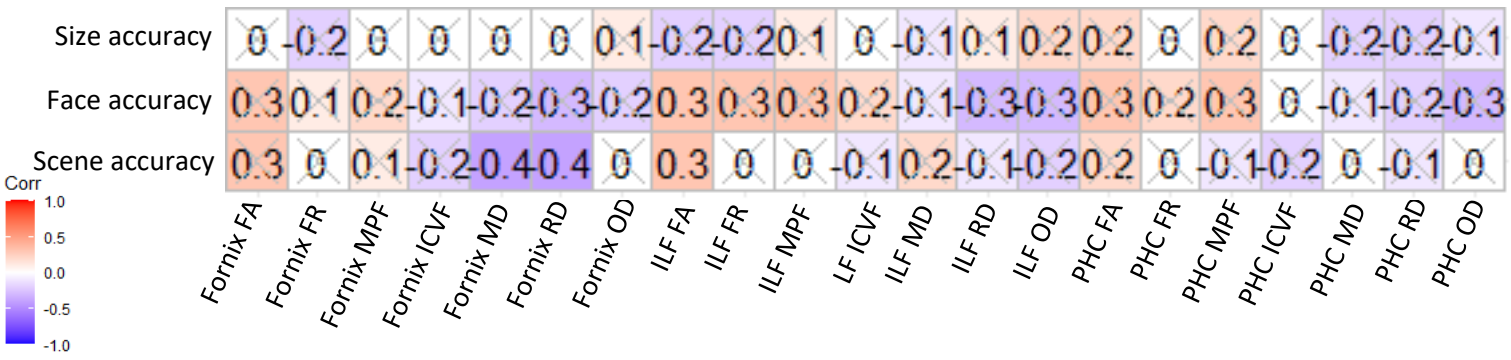

The correlation matrix shows that the relationships between the raw tract microstructure values and the behaviour scores follow similar patterns to the relationships between the tract PCA scores and behaviour scores (see main text). The values are correlation r values from Pearson tests. The colours represent r values, indicating positive or negative relationships, according to the key. Crossed-out values indicate the correlation tests that produced a p-value above 0.05. Significant correlations were found between: Face accuracy and ILF FA; Scene accuracy and fornix MD; Scene accuracy and fornix RD; and Scene accuracy and ILF FA. Note that no results from partial correlations are shown, whereas partial correlations were used in the main

Appendix 3: Pertaining to Chapter 6. AAL Atlas labels and correlation tests between: size oddity accuracy and connectivity values; and PHC microstructure and connectivity values.

3A) AAL ROI labels.

AAL Label	Atlas Colour	Region Name
Precentral_L'		Left Precental Gyrus
'Precentral_R'		Right Precental Gyrus
'Frontal_Sup_L'		Left Superior Dorsolateral Frontal Gyrus
'Frontal_Sup_R'		Right Superior Dorsolateral Frontal Gyrus
'Frontal_Sup_Orb_L'		Left Superior Orbital Frontal Gyrus
'Frontal_Sup_Orb_R'		Right Superior Orbital Frontal Gyrus
'Frontal_Mid_L'		Left Middle Frontal Gyrus
'Frontal_Mid_R'		Right Middle Frontal Gyrus
'Frontal_Mid_Orb_L'		Left Middle Orbital Frontal Gyrus
'Frontal_Mid_Orb_R'		Right Middle Orbital Frontal Gyrus
'Frontal_Inf_Oper_L'		Left Inferior Opercular Frontal Gyrus
'Frontal_Inf_Oper_R'		Right Inferior Opercular Frontal Gyrus
'Frontal_Inf_Tri_L'		Left Inferior Triangular Frontal Gyrus
'Frontal_Inf_Tri_R'		Right Inferior Triangular Frontal Gyrus
'Frontal_Inf_Orb_L'		Left Inferior Orbital Frontal Gyrus
'Frontal_Inf_Orb_R'		Right Inferior Orbital Frontal Gyrus
'Rolandic_Oper_L'		Left Rolandic Operculum
'Rolandic_Oper_R'		Right Rolandic Operculum
'Supp_Motor_Area_L'		Left Supplementary Motor Area
'Supp_Motor_Area_R'		Right Supplementary Motor Area
'Olfactory_L'		Left Olfactory Cortex
'Olfactory_R'		Right Olfactory Cortex
'Frontal_Sup_Medial_L'		Left Superior Medial Frontal Gyrus
'Frontal_Sup_Medial_R'		Right Superior Medial Frontal Gyrus
'Frontal_Med_Orb_L'		Left Medial Orbital Frontal Gyrus
'Frontal_Med_Orb_R'		Right Medial Orbital Frontal Gyrus
'Rectus_L'		Left Gyrus Rectus
'Rectus_R'		Right Gyrus Rectus
'Insula_L'		Left Insula
'Insula_R'		Right Insula
'Cingulum_Ant_L'		Left Anterior Cingulate
'Cingulum_Ant_R'		Right Anterior Cingulate
'Cingulum_Mid_L'		Left Middle Cingulate
'Cingulum_Mid_R'		Right Middle Cingulate
'Cingulum_Post_L'		Left Posterior Cingulate
'Cingulum_Post_R'		Right Posterior Cingulate
'Hippocampus_L'		Left Hippocampus

'Hippocampus_R'		Right Hippocampus
'ParaHippocampal_L'		Left Parahippocampal Gyrus
'ParaHippocampal_R'		Right Parahippocampal Gyrus
'Amygdala_L'		Left Amygdala
'Amygdala_R'		Right Amygdala
'Calcarine_L'		Left Calcarine Fissure
'Calcarine_R'		Right Calcarine Fissure
'Cuneus_L'		Left Cuneus
'Cuneus_R'		Right Cuneus
'Lingual_L'		Left Lingual Gyrus
'Lingual_R'		Right Lingual Gyrus
'Occipital_Sup_L'		Left Superior Occipital Gyrus
'Occipital_Sup_R'		Right Superior Occipital Gyrus
'Occipital_Mid_L'		Left Middle Occipital Gyrus
'Occipital_Mid_R'		Right Middle Occipital Gyrus
'Occipital_Inf_L'		Left Inferior Occipital Gyrus
'Occipital_Inf_R'		Right Inferior Occipital Gyrus
'Fusiform_L'		Left Fusiform Gyrus
'Fusiform_R'		Right Fusiform Gyrus
'Postcentral_L'		Left Post-Central Gyrus
'Postcentral_R'		Right Post-Central Gyrus
'Parietal_Sup_L'		Left Superior Parietal Gyrus
'Parietal_Sup_R'		Right Superior Parietal Gyrus
'Parietal_Inf_L'		Left Inferior Parietal Gyrus (Without Supramarginal and Angular Gyri)
'Parietal_Inf_R'		Right Inferior Parietal Gyrus (Without Supramarginal and Angular Gyri)
'SupraMarginal_L'		Left Supramarginal Gyrus
'SupraMarginal_R'		Right Supramarginal Gyrus
'Angular_L'		Left Angular Gyrus
'Angular_R'		Right Angular Gyrus
'Precuneus_L'		Left Precuneus
'Precuneus_R'		Right Precuneus
'Paracentral_Lobule_L'		Left Paracentral Lobule
Paracentral_Lobule_R'		Right Paracentral Lobule
'Caudate_L'		Left Caudate Nucleus
'Caudate_R'		Right Caudate Nucleus
'Putamen_L'		Left Putamen
'Putamen_R'		Right Putamen
Pallidum_L'		Left Pallidum
'Pallidum_R'		Right Pallidum
'Thalamus_L'		Left Thalamus
'Thalamus_R'		Right Thalamus
'Heschl_L'		Left Heschl Gyrus
'Heschl_R'		Right Heschl Gyrus
'Temporal_Sup_L'		Left Superior Temporal Gyrus

'Temporal_Sup_R'		Right Superior Temporal Gyrus
'Temporal_Pole_Sup_L'		Left Superior Gyrus Temporal Pole
'Temporal_Pole_Sup_R'		Right Superior Gyrus Temporal Pole
'Temporal_Mid_L'		Left Middle Temporal Gyrus
'Temporal_Mid_R'		Right Middle Temporal Gyrus
'Temporal_Pole_Mid_L'		Left Middle Gyrus Temporal Pole
'Temporal_Pole_Mid_R'		Right Middle Gyrus Temporal Pole
'Temporal_Inf_L'		Left Inferior Temporal Gyrus
'Temporal_Inf_R'		Right Inferior Temporal Gyrus

3B) Correlation tests between size oddity accuracy and hippocampal and PCC RS-connectivity strength. N=40.

		Size Accuracy
Hippocampus connectivity strength	Theta	r = 0.141 p = 0.387 BF_{10} = 0.49
	Alpha	r = -0.097 p = 0.551 BF_{10} = 0.41
	Beta	r = -0.057 p = 0.726 BF_{10} = 0.37
PCC connectivity Strength	Theta	r = 0.157 p = 0.332 BF_{10} = 0.53
	Alpha	r = -0.112 p = 0.490 BF_{10} = 0.43
	Beta	r = 0.203 p = 0.208 BF_{10} = 0.71

3C) Correlation tests between size oddity accuracy and hippocampal and PCC connectivity strength. N=40.

		Size Accuracy
Hippocampus-PCC	theta	r = 0.116 p = 0.478 BF_{10} = 0.44
	alpha	r = -0.188 p = 0.246 BF_{10} = 0.64
	beta	r = -0.017 p = 0.918 BF_{10} = 0.35
Hippocampus -	theta	r = 0.208 p = 0.197 BF_{10} = 0.73

	alpha	r = -0.147 p = 0.366 BF_{10} = 0.51
	beta	r = -0.187 p = 0.247 BF_{10} = 0.64

3D) Correlation tests between ROI RS-connectivity scores and PHC microstructure. N=39.

		PHC	
		PC1	**PC2**
hippocampus connectivity strength	Theta	r = 0.092 p = 0.579 BF_{10} = 0.41	r = -0.212 p = 0.195 BF_{10} = 0.75
	Alpha	r = 0.052 p = 0.753 BF_{10} = 0.37	r = -0.215 p = 0.189 BF_{10} = 0.76
	Beta	r = 0.176 p = 0.284 BF_{10} = 0.59	r = -0.298 p = 0.066 BF_{10} = 1.58
PCC connectivity Strength	Theta	r = -0.076 p = 0.644 BF_{10} = 0.39	r = -0.088 p = 0.595 BF_{10} = 0.40
	Alpha	r = -0.056 p = 0.735 BF_{10} = 0.37	r = -0.109 p = 0.509 BF_{10} = 0.43
	Beta	r = 0.003 p = 0.984 BF_{10} = 0.36	r = -0.192 p = 0.243 BF_{10} = 0.65
Hippocampus-PCC	theta	r = 0.054 p = 0.742 BF_{10} = 0.37	r = -0.168 p = 0.306 BF_{10} = 0.56
	alpha	r = -0.035 p = 0.833 BF_{10} = 0.36	r = -0.115 p = 0.486 BF_{10} = 0.44
	beta	r = 0.779 p = 0.046 BF_{10} = 0.37	r = 0.551 p = -0.099 BF_{10} = 0.42

Hippocampus-Thalamus	theta	r = -0.145 p = 0.377 BF_{10} = 0.50	r = -0.067 p = 0.686 BF_{10} = 0.38
	alpha	r = -0.021 p = 0.899 BF_{10} = 0.36	r = -0.261 p = 0.109 BF_{10} = 1.10
	beta	r = -0.026 p = 0.877 BF_{10} = 0.36	r = -0.152 p = 0.357 BF_{10} = 0.52
FG-IOC	theta	r = 0.046 p = 0.780 BF_{10} = 0.37	r = -0.230 p = 0.158 BF_{10} = 0.85
	alpha	r = 0.061 p = 0.714 BF_{10} = 0.38	r = -0.228 p = 0.164 BF_{10} = 0.84
	beta	r = 0.065 p = 0.692 BF_{10} = 0.38	r = -0.225 p = 0.168 BF_{10} = 0.82

Appendix 4: Pertaining to Chapter 7. Semantic question examples, sequence position RT effects, and correlation tests between retrieval performance and raw microstructure values.

A) Examples of semantic questions included in the Learning and Retrieval Phases.

Questions were presented before sequences of objects and participants were asked to answer 'yes' or 'no' with button presses. For each participant, they were randomly drawn at the beginning of the session.

Learning Phase Questions	'Does this item weigh more than a basketball?'
	'Is this item sold at Wal-Mart or a similar store?'
	'Does this item contain visible metal?'
	'Is the presented object living?'
	'Is the presented item readily edible?'
Retrieval Phase Questions	'Does this item fit in a shoebox or a similar sized box?'
	'Can you lift this item with one hand?'
	'Can you ride on/in it?'
	'Is this item bigger than the computer screen in front of you?'
	'Does this item require fuel/electrical power?'

B) Sequence Retrieval Position Effects

Repeated Measure (RM ANOVA) on the overlapping fixed sequences, with one factor with 5 levels for each position (and RT as the dependant variable), revealed significant RTs differences between the positions ($F_{(2.757,137.856)} = 10.68$, $p < 0.001$, $\omega^2 = 0.030$). However, only RT for the position 1 differed from the others (p-values <0.004), whereas RTs for the other positions, including positions 3 and 4, did not differ from each other (p-values >0.706).

Two-way RM ANOVA, with two factors, one with three levels for the fixed, random and novel sequence conditions, and another with five levels for the five positions (and RT as the dependant variable), revealed a significant difference between the means of the RTs for the conditions ($F_{(1.596, 79.817)} = 178.351$, $p<.001$, $\omega^2 = 0.246$). There was also a significant difference between the means of the RTs for the positions ($F_{(3.074, 153.716)} = 17.021$, $p<0.001$, $\omega^2 = 0.024$). There was no interaction between condition and position ($F_{(5.978, 298.881)} = 1.081$,

p = 0.374). Furthermore, position 1 RTs differed significantly from the subsequent four positions ($p \leq 0.001$), confirming the presumption that the inability to predict the first object would influence RT. Post-hoc testing with Bonferroni correction revealed that, as expected, the RTs for the positions in the novel sequences were larger than those for the random sequence (mean difference = 94.74 ms, $p<0.001$), which were larger than those for the fixed sequence (mean difference = 25.06 ms, $p<0.001$), indicating benefits of object sequence knowledge.

To further understand the condition and position RT differences, we then examined RTs of responses to each position in the novel, fixed and random conditions separately (illustrated in Appendix 4B Figure), by creating RM ANOVAs for each of the three sequence conditions, each with one factor with five levels for each position (and RT as the dependant variable). For each, RTs for position 1 were larger than those of the subsequent positions (novel $F_{(4, 200)} = 9.012$, $p<0.001$, $\omega^2 = 0.029$; fixed $F_{(2.289, 114.455)} = 9.230$, $p<0.001$, $\omega^2 = 0.020$; random $F_{(3.341, 167.026)} = 6.332$, $p<0.001$, $\omega^2 = 0.010$, respectively. Greenhouse-Geisser correction was applied to the last two). Post-hoc testing with Bonferroni correction revealed no significant differences between RTs for other positions (all p-values > 0.785).

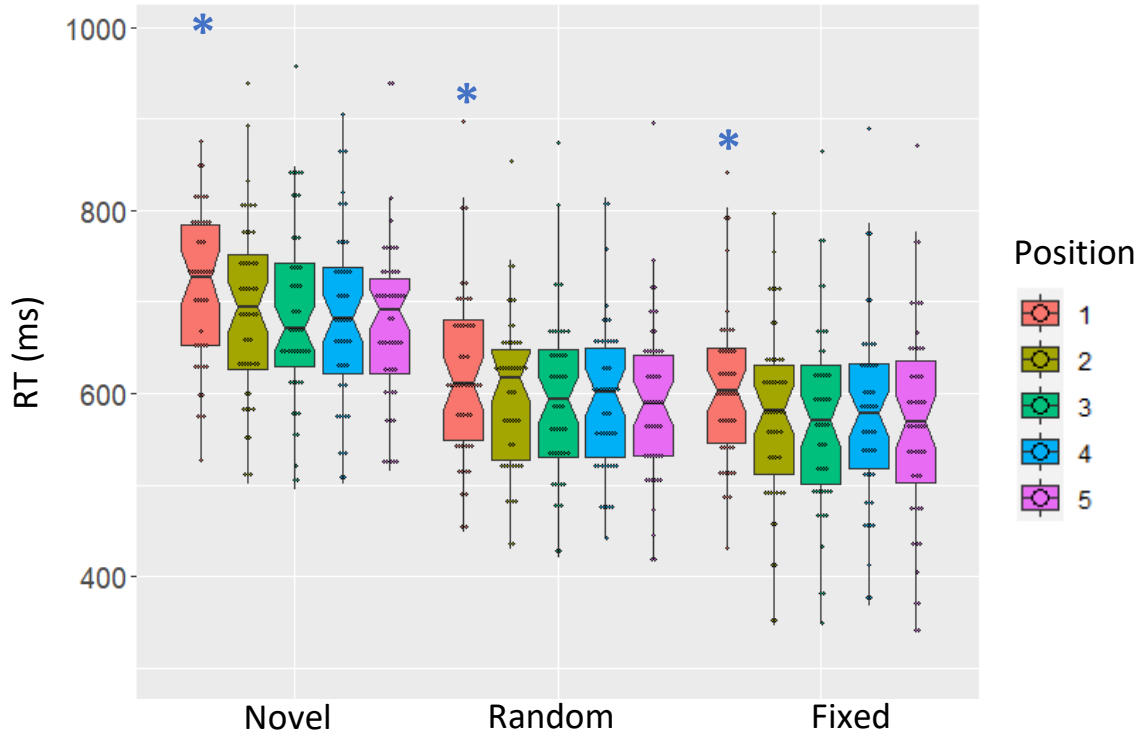

Appendix 4B Figure: RTs for each position for the conditions.
Box plots indicate the median (horizontal centred line) and the upper and lower quartiles (top and bottom edges of the box) of the RT data at each position of each sequence. The positions are colour-coded according to the key to the right. The blue asterisks reflect that the RTs of responses to objects in position 1 differed from those of the subsequence positions (Bonferroni-corrected p-values < 0.05), in all sequences (their vertical locations on the graph holds no meaning).
Note that the Y axis was limited, so that box plot notches could be seen easily, meaning that 5 high (these were from position 1 in Novel) and 5 low (these were from position 3-5 in fixed) values are not displayed.

C) Correlation matrix of the relationships between temporal sequence memory behaviour scores and raw tract microstructure data.

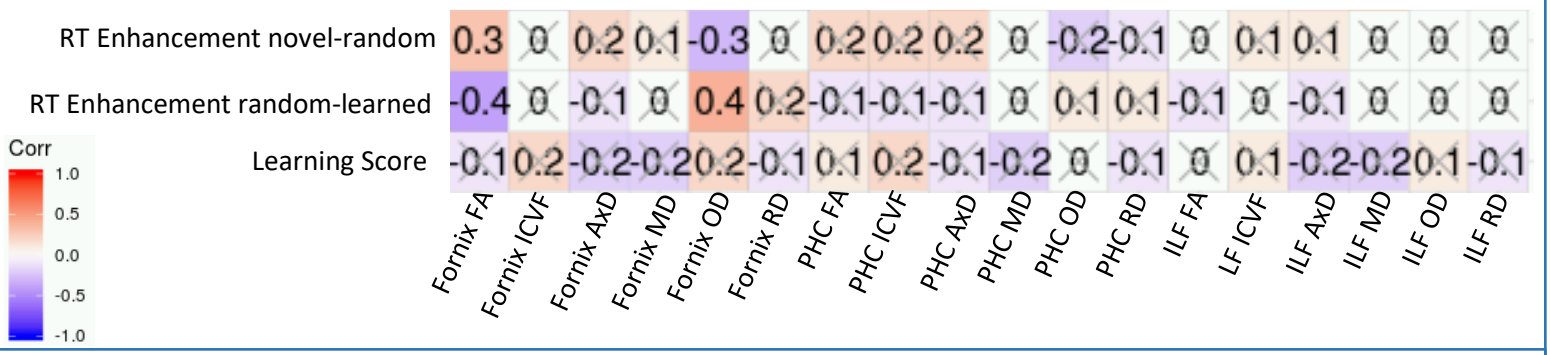

The correlation matrix shows that the relationships between the raw tract microstructure values and the behaviour scores follow similar patterns to the relationships between the tract PCA scores and behaviour scores (see main text). The values are correlation r values from Pearson tests. The colours represent r values, indicating positive or negative relationships, according to the key. Crossed-out values indicate correlation tests that produced a p-value above 0.05. Significant correlations were found between: RT Enhancement novel-random and fornix FA; RT Enhancement novel-random and fornix OD; RT Enhancement random-learned and fornix FA; and RT Enhancement random-learned and fornix OD. Note that no results from partial correlations are shown, whereas partial correlations were used in the main experiment.

References

Abdi, H., & Williams, L. J. (2010). Principal component analysis. *Wiley interdisciplinary reviews: computational statistics*, *2*(4), 433-459.

Abrahams, S., Pickering, A., Polkey, C. E., & Morris, R. G. (1997). Spatial memory deficits in patients with unilateral damage to the right hippocampal formation. *Neuropsychologia*, *35*(1), 11-24. https://doi.org/10.1016/s0028-3932(96)00051-6

Acosta-Cabronero, J., & Nestor, P. J. (2014). Diffusion tensor imaging in Alzheimer's disease: insights into the limbic-diencephalic network and methodological considerations. *Front Aging Neurosci*, *6*, 266. https://doi.org/10.3389/fnagi.2014.00266

Addis, D. R., Wong, A. T., & Schacter, D. L. (2007). Remembering the past and imagining the future: common and distinct neural substrates during event construction and elaboration. *Neuropsychologia*, *45*(7), 1363-1377. https://doi.org/10.1016/j.neuropsychologia.2006.10.016

Aggleton, J. P. (2012). Multiple anatomical systems embedded within the primate medial temporal lobe: implications for hippocampal function. *Neurosci Biobehav Rev*, *36*(7), 1579-1596. https://doi.org/10.1016/j.neubiorev.2011.09.005

Aggleton, J. P., & Brown, M. W. (1999). Episodic memory, amnesia, and the hippocampal-anterior thalamic axis. *Behav Brain Sci*, *22*(3), 425-444; discussion 444-489.

Aggleton, J. P., & Brown, M. W. (2005). Contrasting hippocampal and perirhinal cortex function using immediate early gene imaging. *Q J Exp Psychol B*, *58*(3-4), 218-233. https://doi.org/10.1080/02724990444000131

Aggleton, J. P., Neave, N., Nagle, S., & Hunt, P. R. (1995). A comparison of the effects of anterior thalamic, mamillary body and fornix lesions on reinforced spatial alternation. *Behav Brain Res*, *68*(1), 91-101. https://doi.org/10.1016/0166-4328(94)00163-a

Agosta, F., Henry, R. G., Migliaccio, R., Neuhaus, J., Miller, B. L., Dronkers, N. F., Brambati, S. M., Filippi, M., Ogar, J. M., Wilson, S. M., & Gorno-Tempini, M. L. (2010). Language networks in semantic dementia. *Brain*, *133*(Pt 1), 286-299. https://doi.org/10.1093/brain/awp233

Ahlfors, S. P., Han, J., Lin, F. H., Witzel, T., Belliveau, J. W., Hamalainen, M. S., & Halgren, E. (2010). Cancellation of EEG and MEG signals generated by extended and distributed sources. *Hum Brain Mapp*, *31*(1), 140-149. https://doi.org/10.1002/hbm.20851

Ahn, J. R., Lee, H. W., & Lee, I. (2019). Rhythmic Pruning of Perceptual Noise for Object Representation in the Hippocampus and Perirhinal Cortex in Rats. *Cell Rep*, *26*(9), 2362-2376.e2364. https://doi.org/10.1016/j.celrep.2019.02.010

Akhlaghpour, H., Wiskerke, J., Choi, J. Y., Taliaferro, J. P., Au, J., & Witten, I. B. (2016). Dissociated sequential activity and stimulus encoding in the dorsomedial striatum during spatial working memory. *Elife*, *5*. https://doi.org/10.7554/eLife.19507

Albrecht, D. G., & Hamilton, D. B. (1982). Striate cortex of monkey and cat: contrast response function. *J Neurophysiol*, *48*(1), 217-237. https://doi.org/10.1152/jn.1982.48.1.217

Alexander, A. L., Hurley, S. A., Samsonov, A. A., Adluru, N., Hosseinbor, A. P., Mossahebi, P., Tromp do, P. M., Zakszewski, E., & Field, A. S. (2011). Characterization of cerebral white matter properties using quantitative magnetic resonance imaging stains. *Brain Connect*, *1*(6), 423-446. https://doi.org/10.1089/brain.2011.0071

Allen, G., Barnard, H., McColl, R., Hester, A. L., Fields, J. A., Weiner, M. F., Ringe, W. K., Lipton, A. M., Brooker, M., McDonald, E., Rubin, C. D., & Cullum, C. M. (2007). Reduced hippocampal functional connectivity in Alzheimer disease. *Arch Neurol*, *64*(10), 1482-1487. https://doi.org/10.1001/archneur.64.10.1482

Alvarez, P., Lipton, P. A., Melrose, R., & Eichenbaum, H. (2001). Differential effects of damage within the hippocampal region on memory for a natural, nonspatial Odor-Odor Association. *Learn Mem*, *8*(2), 79-86. https://doi.org/10.1101/lm.38201

Amaro, E., Jr., & Barker, G. J. (2006). Study design in fMRI: basic principles. *Brain Cogn*, *60*(3), 220-232. https://doi.org/10.1016/j.bandc.2005.11.009

Aminoff, E. M., Kveraga, K., & Bar, M. (2013). The role of the parahippocampal cortex in cognition. *Trends Cogn Sci*, *17*(8), 379-390. https://doi.org/10.1016/j.tics.2013.06.009

Andelman, F., Hoofien, D., Goldberg, I., Aizenstein, O., & Neufeld, M. Y. (2010). Bilateral hippocampal lesion and a selective impairment of the ability for mental time travel. *Neurocase*, *16*(5), 426-435. https://doi.org/10.1080/13554791003623318

Anderson, K. L., Rajagovindan, R., Ghacibeh, G. A., Meador, K. J., & Ding, M. (2010). Theta oscillations mediate interaction between prefrontal cortex and medial temporal lobe in human memory. *Cereb Cortex*, *20*(7), 1604-1612. https://doi.org/10.1093/cercor/bhp223

Andersson, J. L. R., & Sotiropoulos, S. N. (2016). An integrated approach to correction for off-resonance effects and subject movement in diffusion MR imaging. *Neuroimage*, *125*, 1063-1078. https://doi.org/10.1016/j.neuroimage.2015.10.019

Assaf, Y., & Basser, P. J. (2005). Composite hindered and restricted model of diffusion (CHARMED) MR imaging of the human brain. *Neuroimage*, *27*(1), 48-58. https://doi.org/10.1016/j.neuroimage.2005.03.042

Attal, Y., & Schwartz, D. (2013). Assessment of subcortical source localization using deep brain activity imaging model with minimum norm operators: a MEG study. *PLoS One*, *8*(3), e59856. https://doi.org/10.1371/journal.pone.0059856

Auger, S. D., Mullally, S. L., & Maguire, E. A. (2012). Retrosplenial cortex codes for permanent landmarks. *PLoS One*, *7*(8), e43620. https://doi.org/10.1371/journal.pone.0043620

Auger, S. D., Zeidman, P., & Maguire, E. A. (2017). Efficacy of navigation may be influenced by retrosplenial cortex-mediated learning of landmark stability. *Neuropsychologia*, *104*, 102-112. https://doi.org/10.1016/j.neuropsychologia.2017.08.012

Avanaki, A. N. (2009). Exact global histogram specification optimized for structural similarity. *Optical review*, *16*(6), 613-621.

Axmacher, N., Henseler, M. M., Jensen, O., Weinreich, I., Elger, C. E., & Fell, J. (2010). Cross-frequency coupling supports multi-item working memory in the human hippocampus. *Proc Natl Acad Sci U S A*, *107*(7), 3228-3233. https://doi.org/10.1073/pnas.0911531107

Backus, A. R., Schoffelen, J. M., Szebényi, S., Hanslmayr, S., & Doeller, C. F. (2016). Hippocampal-Prefrontal Theta Oscillations Support Memory Integration. *Curr Biol*, *26*(4), 450-457. https://doi.org/10.1016/j.cub.2015.12.048

Baddeley, A. D., & Warrington, E. K. (1970). Amnesia and the distinction between long- and short-term memory. *Journal of Verbal Learning and Verbal Behavior*, *9*(2), 176-189. https://doi.org/https://doi.org/10.1016/S0022-5371(70)80048-2

Bai, F., Watson, D. R., Yu, H., Shi, Y., Yuan, Y., & Zhang, Z. (2009). Abnormal resting-state functional connectivity of posterior cingulate cortex in amnestic type mild cognitive impairment. *Brain Res*, *1302*, 167-174. https://doi.org/10.1016/j.brainres.2009.09.028

Baillet, S. (2017). Magnetoencephalography for brain electrophysiology and imaging. *Nat Neurosci*, *20*(3), 327-339. https://doi.org/10.1038/nn.4504

Baldassano, C., Esteva, A., Fei-Fei, L., & Beck, D. M. (2016). Two Distinct Scene-Processing Networks Connecting Vision and Memory. *eNeuro*, *3*(5). https://doi.org/10.1523/eneuro.0178-16.2016

Bang, J., Spina, S., & Miller, B. L. (2015). Frontotemporal dementia. *Lancet*, *386*(10004), 1672-1682. https://doi.org/10.1016/s0140-6736(15)00461-4

Banquet, J. P., Gaussier, P., Cuperlier, N., Hok, V., Save, E., Poucet, B., Quoy, M., & Wiener, S. I. (2021). Time as the fourth dimension in the hippocampus. *Prog Neurobiol*, *199*, 101920. https://doi.org/10.1016/j.pneurobio.2020.101920

Barense, M. D., Gaffan, D., & Graham, K. S. (2007). The human medial temporal lobe processes online representations of complex objects. *Neuropsychologia*, *45*(13), 2963-2974. https://doi.org/10.1016/j.neuropsychologia.2007.05.023

Barense, M. D., Henson, R. N., Lee, A. C., & Graham, K. S. (2010). Medial temporal lobe activity during complex discrimination of faces, objects, and scenes: Effects of viewpoint. *Hippocampus*, *20*(3), 389-401. https://doi.org/10.1002/hipo.20641

Barry, D. N., Barnes, G. R., Clark, I. A., & Maguire, E. A. (2019). The neural dynamics of novel scene imagery. *J Neurosci*. https://doi.org/10.1523/jneurosci.2497-18.2019

Beaulieu, C. (2002). The basis of anisotropic water diffusion in the nervous system - a technical review. *NMR Biomed*, *15*(7-8), 435-455. https://doi.org/10.1002/nbm.782

Becker, R., Van de Ville, D., & Kleinschmidt, A. (2018). Alpha Oscillations Reduce Temporal Long-Range Dependence in Spontaneous Human Brain Activity. *J Neurosci*, *38*(3), 755-764. https://doi.org/10.1523/jneurosci.0831-17.2017

Belchior, H., Lopes-Dos-Santos, V., Tort, A. B., & Ribeiro, S. (2014). Increase in hippocampal theta oscillations during spatial decision making. *Hippocampus*, *24*(6), 693-702. https://doi.org/10.1002/hipo.22260

Bellana, B., Liu, Z. X., Diamond, N. B., Grady, C. L., & Moscovitch, M. (2017). Similarities and differences in the default mode network across rest, retrieval, and future imagining. *Hum Brain Mapp*, *38*(3), 1155-1171. https://doi.org/10.1002/hbm.23445

Benear, S. L., Ngo, C. T., & Olson, I. R. (2020). Dissecting the Fornix in Basic Memory Processes and Neuropsychiatric Disease: A Review. *Brain Connect*, *10*(7), 331-354. https://doi.org/10.1089/brain.2020.0749

Benoit, R. G., & Schacter, D. L. (2015). Specifying the core network supporting episodic simulation and episodic memory by activation likelihood estimation. *Neuropsychologia*, *75*, 450-457. https://doi.org/10.1016/j.neuropsychologia.2015.06.034

Berke, J. D., Hetrick, V., Breck, J., & Greene, R. W. (2008). Transient 23-30 Hz oscillations in mouse hippocampus during exploration of novel environments. *Hippocampus*, *18*(5), 519-529. https://doi.org/10.1002/hipo.20435

Berron, D., van Westen, D., Ossenkoppele, R., Strandberg, O., & Hansson, O. (2020). Medial temporal lobe connectivity and its associations with cognition in early Alzheimer's disease. *Brain*, *143*(4), 1233-1248. https://doi.org/10.1093/brain/awaa068

Bertrand, O., & Tallon-Baudry, C. (2000). Oscillatory gamma activity in humans: a possible role for object representation. *Int J Psychophysiol*, *38*(3), 211-223.

Bestmann, S., Thilo, K. V., Sauner, D., Siebner, H. R., & Rothwell, J. C. (2002). Parietal magnetic stimulation delays visuomotor mental rotation at increased processing demands. *Neuroimage*, *17*(3), 1512-1520. https://doi.org/10.1006/nimg.2002.1266

Bett, D., Allison, E., Murdoch, L. H., Kaefer, K., Wood, E. R., & Dudchenko, P. A. (2012). The neural substrates of deliberative decision making: contrasting effects of hippocampus lesions on performance and vicarious trial-and-error behavior in a spatial memory task and a visual discrimination task. *Front Behav Neurosci*, *6*, 70. https://doi.org/10.3389/fnbeh.2012.00070

Betzel, R. F., Byrge, L., He, Y., Goñi, J., Zuo, X. N., & Sporns, O. (2014). Changes in structural and functional connectivity among resting-state networks across the human lifespan. *Neuroimage*, *102 Pt 2*, 345-357. https://doi.org/10.1016/j.neuroimage.2014.07.067

Bieniek, M. M., Frei, L. S., & Rousselet, G. A. (2013). Early ERPs to faces: aging, luminance, and individual differences. *Front Psychol*, *4*, 268. https://doi.org/10.3389/fpsyg.2013.00268

Blondin, F., & Lepage, M. (2008). An fMRI study on memory discriminability for complex visual scenes. *Hum Brain Mapp*, *29*(10), 1159-1169. https://doi.org/10.1002/hbm.20455

Bohbot, V. D., Copara, M. S., Gotman, J., & Ekstrom, A. D. (2017). Low-frequency theta oscillations in the human hippocampus during real-world and virtual navigation. *Nat Commun*, *8*, 14415. https://doi.org/10.1038/ncomms14415

Bonnefond, M., Kastner, S., & Jensen, O. (2017). Communication between Brain Areas Based on Nested Oscillations. *eNeuro*, *4*(2). https://doi.org/10.1523/eneuro.0153-16.2017

Boudewyn, M. A., Luck, S. J., Farrens, J. L., & Kappenman, E. S. (2018). How many trials does it take to get a significant ERP effect? It depends. *Psychophysiology*, *55*(6), e13049. https://doi.org/10.1111/psyp.13049

Boxer, A. L., Rankin, K. P., Miller, B. L., Schuff, N., Weiner, M., Gorno-Tempini, M. L., & Rosen, H. J. (2003). Cinguloparietal atrophy distinguishes Alzheimer disease from semantic dementia. *Arch Neurol*, *60*(7), 949-956. https://doi.org/10.1001/archneur.60.7.949

Bozoki, A. C., Korolev, I. O., Davis, N. C., Hoisington, L. A., & Berger, K. L. (2012). Disruption of limbic white matter pathways in mild cognitive impairment and Alzheimer's disease: a DTI/FDG-PET study. *Hum Brain Mapp*, *33*(8), 1792-1802. https://doi.org/10.1002/hbm.21320

Braskie, M. N., Jahanshad, N., Stein, J. L., Barysheva, M., McMahon, K. L., de Zubicaray, G. I., Martin, N. G., Wright, M. J., Ringman, J. M., Toga, A. W., & Thompson, P. M. (2011). Common Alzheimer's disease risk variant within the CLU gene affects white matter microstructure in young adults. *J Neurosci*, *31*(18), 6764-6770. https://doi.org/10.1523/jneurosci.5794-10.2011

Brown, M. W., & Aggleton, J. P. (2001). Recognition memory: what are the roles of the perirhinal cortex and hippocampus? *Nat Rev Neurosci*, *2*(1), 51-61. https://doi.org/10.1038/35049064

Bruyer, R., & Brysbaert, M. (2011). Combining speed and accuracy in cognitive psychology: Is the inverse efficiency score (IES) a better dependent variable than the mean reaction time (RT) and the percentage of errors (PE)? *Psychologica Belgica*, *51*(1), 5-13. https://doi.org/10.5334/pb-51-1-5

Brüers, S., & VanRullen, R. (2018). Alpha Power Modulates Perception Independently of Endogenous Factors. *Front Neurosci*, *12*, 279. https://doi.org/10.3389/fnins.2018.00279

Bubb, E. J., Kinnavane, L., & Aggleton, J. P. (2017). Hippocampal - diencephalic - cingulate networks for memory and emotion: An anatomical guide. *Brain Neurosci Adv*, *1*(1). https://doi.org/10.1177/2398212817723443

Bubb, E. J., Metzler-Baddeley, C., & Aggleton, J. P. (2018). The cingulum bundle: Anatomy, function, and dysfunction. *Neurosci Biobehav Rev*, *92*, 104-127. https://doi.org/10.1016/j.neubiorev.2018.05.008

Buckley, M. J., Booth, M. C., Rolls, E. T., & Gaffan, D. (2001). Selective perceptual impairments after perirhinal cortex ablation. *J Neurosci*, *21*(24), 9824-9836.

Budde, M. D., & Annese, J. (2013). Quantification of anisotropy and fiber orientation in human brain histological sections. *Front Integr Neurosci*, *7*, 3. https://doi.org/10.3389/fnint.2013.00003

Bukowski, H., Dricot, L., Hanseeuw, B., & Rossion, B. (2013). Cerebral lateralization of face-sensitive areas in left-handers: only the FFA does not get it right. *Cortex*, *49*(9), 2583-2589. https://doi.org/10.1016/j.cortex.2013.05.002

Burles, F., Umiltá, A., McFarlane, L. H., Potocki, K., & Iaria, G. (2018). Ventral-Dorsal Functional Contribution of the Posterior Cingulate Cortex in Human Spatial Orientation: A Meta-Analysis. *Front Hum Neurosci*, *12*, 190. https://doi.org/10.3389/fnhum.2018.00190

Burns, E. J., Tree, J. J., & Weidemann, C. T. (2014). Recognition memory in developmental prosopagnosia: electrophysiological evidence for abnormal routes to face recognition. *Front Hum Neurosci*, *8*, 622. https://doi.org/10.3389/fnhum.2014.00622

Bussey, T. J., & Saksida, L. M. (2007). Memory, perception, and the ventral visual-perirhinal-hippocampal stream: thinking outside of the boxes. *Hippocampus*, *17*(9), 898-908. https://doi.org/10.1002/hipo.20320

Buzsaki, G. (2002). Theta oscillations in the hippocampus. *Neuron*, *33*(3), 325-340.

Buzsaki, G., & Moser, E. I. (2013). Memory, navigation and theta rhythm in the hippocampal-entorhinal system. *Nat Neurosci*, *16*(2), 130-138. https://doi.org/10.1038/nn.3304

Buzsáki, G., & Draguhn, A. (2004). Neuronal oscillations in cortical networks. *Science*, *304*(5679), 1926-1929. https://doi.org/10.1126/science.1099745

Cabral-Calderin, Y., Schmidt-Samoa, C., & Wilke, M. (2015). Rhythmic gamma stimulation affects bistable perception. *J Cogn Neurosci*, *27*(7), 1298-1307. https://doi.org/10.1162/jocn_a_00781

Canolty, R. T., Edwards, E., Dalal, S. S., Soltani, M., Nagarajan, S. S., Kirsch, H. E., Berger, M. S., Barbaro, N. M., & Knight, R. T. (2006). High gamma power is phase-locked to theta oscillations in human neocortex. *Science*, *313*(5793), 1626-1628. https://doi.org/10.1126/science.1128115

Canolty, R. T., & Knight, R. T. (2010). The functional role of cross-frequency coupling. *Trends Cogn Sci*, *14*(11), 506-515. https://doi.org/10.1016/j.tics.2010.09.001

Cardin, J. A. (2016). Snapshots of the Brain in Action: Local Circuit Operations through the Lens of gamma Oscillations. *J Neurosci*, *36*(41), 10496-10504. https://doi.org/10.1523/jneurosci.1021-16.2016

Carr, M. F., Karlsson, M. P., & Frank, L. M. (2012). Transient slow gamma synchrony underlies hippocampal memory replay. *Neuron*, *75*(4), 700-713. https://doi.org/10.1016/j.neuron.2012.06.014

Carrera, E., & Tononi, G. (2014). Diaschisis: past, present, future. *Brain*, *137*(Pt 9), 2408-2422. https://doi.org/10.1093/brain/awu101

Catani, M., Jones, D. K., Donato, R., & Ffytche, D. H. (2003). Occipito-temporal connections in the human brain. *Brain*, *126*(Pt 9), 2093-2107. https://doi.org/10.1093/brain/awg203

Cercignani, M., & Alexander, D. C. (2006). Optimal acquisition schemes for in vivo quantitative magnetization transfer MRI. *Magn Reson Med*, *56*(4), 803-810. https://doi.org/10.1002/mrm.21003

Chadwick, M. J., Mullally, S. L., & Maguire, E. A. (2013). The hippocampus extrapolates beyond the view in scenes: an fMRI study of boundary extension. *Cortex*, *49*(8), 2067-2079. https://doi.org/10.1016/j.cortex.2012.11.010

Chamberland, M., Raven, E. P., Genc, S., Duffy, K., Descoteaux, M., Parker, G. D., Tax, C. M. W., & Jones, D. K. (2019). Dimensionality reduction of diffusion MRI measures for improved tractometry of the human brain. *Neuroimage*, *200*, 89-100. https://doi.org/10.1016/j.neuroimage.2019.06.020

Chan, A. M., Baker, J. M., Eskandar, E., Schomer, D., Ulbert, I., Marinkovic, K., Cash, S. S., & Halgren, E. (2011). First-pass selectivity for semantic categories in human anteroventral temporal lobe. *J Neurosci*, *31*(49), 18119-18129. https://doi.org/10.1523/jneurosci.3122-11.2011

Chang, L. C., Jones, D. K., & Pierpaoli, C. (2005). RESTORE: robust estimation of tensors by outlier rejection. *Magn Reson Med*, *53*(5), 1088-1095. https://doi.org/10.1002/mrm.20426

Chang, Y. S., Owen, J. P., Pojman, N. J., Thieu, T., Bukshpun, P., Wakahiro, M. L., Berman, J. I., Roberts, T. P., Nagarajan, S. S., Sherr, E. H., & Mukherjee, P. (2015). White Matter Changes of Neurite Density and Fiber Orientation Dispersion during Human Brain Maturation. *PLoS One*, *10*(6), e0123656. https://doi.org/10.1371/journal.pone.0123656

Chapeton, J. I., Haque, R., Wittig, J. H., Jr., Inati, S. K., & Zaghloul, K. A. (2019). Large-Scale Communication in the Human Brain Is Rhythmically Modulated through Alpha Coherence. *Curr Biol*. https://doi.org/10.1016/j.cub.2019.07.014

Charles, D. P., Gaffan, D., & Buckley, M. J. (2004). Impaired recency judgments and intact novelty judgments after fornix transection in monkeys. *J Neurosci*, *24*(8), 2037-2044. https://doi.org/10.1523/jneurosci.3796-03.2004

Chaumon, M., Puce, A., & George, N. (2021). Statistical power: Implications for planning MEG studies. *Neuroimage*, *233*, 117894. https://doi.org/10.1016/j.neuroimage.2021.117894

Chen, F., Wu, T., Luo, Y., Li, Z., Guan, Q., Meng, X., Tao, W., & Zhang, H. (2019). Amnestic mild cognitive impairment in Parkinson's disease: White matter structural changes and mechanisms. *PLoS One*, *14*(12), e0226175. https://doi.org/10.1371/journal.pone.0226175

Christiansen, K., Metzler-Baddeley, C., Parker, G. D., Muhlert, N., Jones, D. K., Aggleton, J. P., & Vann, S. D. (2017). Topographic separation of fornical fibers associated with the anterior and posterior hippocampus in the human brain: An MRI-diffusion study. *Brain Behav*, *7*(1), e00604. https://doi.org/10.1002/brb3.604

Ciaramelli, E., Rosenbaum, R. S., Solcz, S., Levine, B., & Moscovitch, M. (2010). Mental space travel: damage to posterior parietal cortex prevents egocentric navigation and reexperiencing of remote spatial memories. *J Exp Psychol Learn Mem Cogn*, *36*(3), 619-634. https://doi.org/10.1037/a0019181

Clark, B. J., Simmons, C. M., Berkowitz, L. E., & Wilber, A. A. (2018). The retrosplenial-parietal network and reference frame coordination for spatial navigation. *Behav Neurosci*, *132*(5), 416-429. https://doi.org/10.1037/bne0000260

Clarke, A., & Tyler, L. K. (2014). Object-specific semantic coding in human perirhinal cortex. *J Neurosci*, *34*(14), 4766-4775. https://doi.org/10.1523/jneurosci.2828-13.2014

Coad, B. M., Craig, E., Louch, R., Aggleton, J. P., Vann, S. D., & Metzler-Baddeley, C. (2020). Precommissural and postcommissural fornix microstructure in healthy aging and cognition. *Brain Neurosci Adv*, *4*, 2398212819899316. https://doi.org/10.1177/2398212819899316

Coad, B. M., Postans, M., Hodgetts, C. J., Muhlert, N., Graham, K. S., & Lawrence, A. D. (2017). Structural connections support emotional connections: Uncinate Fasciculus microstructure is related to the ability to decode facial emotion expressions. *Neuropsychologia*. https://doi.org/10.1016/j.neuropsychologia.2017.11.006

Cohen, A. L., Soussand, L., Corrow, S. L., Martinaud, O., Barton, J. J. S., & Fox, M. D. (2019). Looking beyond the face area: lesion network mapping of prosopagnosia. *Brain*, *142*(12), 3975-3990. https://doi.org/10.1093/brain/awz332

Cohen, M. X. (2008). Assessing transient cross-frequency coupling in EEG data. *J Neurosci Methods*, *168*(2), 494-499. https://doi.org/10.1016/j.jneumeth.2007.10.012

Cohn-Sheehy, B. I., & Ranganath, C. (2017). Time Regained: How the Human Brain Constructs Memory for Time. *Curr Opin Behav Sci*, *17*, 169-177. https://doi.org/10.1016/j.cobeha.2017.08.005

Colclough, G. L., Brookes, M. J., Smith, S. M., & Woolrich, M. W. (2015). A symmetric multivariate leakage correction for MEG connectomes. *Neuroimage*, *117*, 439-448. https://doi.org/10.1016/j.neuroimage.2015.03.071

Colgin, L. L. (2016). Rhythms of the hippocampal network. In *Nat Rev Neurosci* (Vol. 17, pp. 239-249). https://doi.org/10.1038/nrn.2016.21

Colgin, L. L., & Moser, E. I. (2010). Gamma oscillations in the hippocampus. *Physiology (Bethesda)*, *25*(5), 319-329. https://doi.org/10.1152/physiol.00021.2010

Collins, D. R., Pelletier, J. G., & Paré, D. (2001). Slow and fast (gamma) neuronal oscillations in the perirhinal cortex and lateral amygdala. *J Neurophysiol*, *85*(4), 1661-1672. https://doi.org/10.1152/jn.2001.85.4.1661

Collins, J. A., & Dickerson, B. C. (2019). Functional connectivity in category-selective brain networks after encoding predicts subsequent memory. *Hippocampus*, *29*(5), 440-450. https://doi.org/10.1002/hipo.23003

Collins, J. A., & Olson, I. R. (2014). Beyond the FFA: The role of the ventral anterior temporal lobes in face processing. *Neuropsychologia*, *61*, 65-79. https://doi.org/10.1016/j.neuropsychologia.2014.06.005

Colom, L. V., Christie, B. R., & Bland, B. H. (1988). Cingulate cell discharge patterns related to hippocampal EEG and their modulation by muscarinic and nicotinic agents. *Brain Res*, *460*(2), 329-338. https://doi.org/10.1016/0006-8993(88)90377-0

Conner, C. R., Ellmore, T. M., Pieters, T. A., DiSano, M. A., & Tandon, N. (2011). Variability of the relationship between electrophysiology and BOLD-fMRI across cortical regions in humans. *J Neurosci*, *31*(36), 12855-12865. https://doi.org/10.1523/jneurosci.1457-11.2011

Cooper, R. A., & Ritchey, M. (2019). Cortico-hippocampal network connections support the multidimensional quality of episodic memory. *eLife*, *8*, e45591. https://doi.org/10.7554/eLife.45591

Cornwell, B. R., Arkin, N., Overstreet, C., Carver, F. W., & Grillon, C. (2012). Distinct contributions of human hippocampal theta to spatial cognition and anxiety. *Hippocampus*, *22*(9), 1848-1859. https://doi.org/10.1002/hipo.22019

Cornwell, B. R., Johnson, L. L., Holroyd, T., Carver, F. W., & Grillon, C. (2008). Human hippocampal and parahippocampal theta during goal-directed spatial navigation predicts performance on a virtual Morris water maze. *J Neurosci*, *28*(23), 5983-5990. https://doi.org/10.1523/jneurosci.5001-07.2008

Costigan, A. G., Umla-Runge, K., Evans, C. J., Hodgetts, C. J., Lawrence, A. D., & Graham, K. S. (2019). Neurochemical correlates of scene processing in the precuneus/posterior cingulate cortex: A multimodal fMRI and 1H-MRS study. *Human Brain Mapping*, *40*(10), 2884-2898. https://doi.org/10.1002/hbm.24566

Crespo-Garcia, M., Zeiller, M., Leupold, C., Kreiselmeyer, G., Rampp, S., Hamer, H. M., & Dalal, S. S. (2016). Slow-theta power decreases during item-place encoding predict spatial accuracy of subsequent context recall. *Neuroimage*, *142*, 533-543. https://doi.org/10.1016/j.neuroimage.2016.08.021

Cukur, T., Huth, A. G., Nishimoto, S., & Gallant, J. L. (2016). Functional Subdomains within Scene-Selective Cortex: Parahippocampal Place Area, Retrosplenial Complex, and Occipital Place Area. *J Neurosci*, *36*(40), 10257-10273. https://doi.org/10.1523/jneurosci.4033-14.2016

Daducci, A., Canales-Rodriguez, E. J., Zhang, H., Dyrby, T. B., Alexander, D. C., & Thiran, J. P. (2015). Accelerated Microstructure Imaging via Convex Optimization (AMICO) from diffusion MRI data. *Neuroimage*, *105*, 32-44. https://doi.org/10.1016/j.neuroimage.2014.10.026

Dahmani, L., & Bohbot, V. D. (2015). Dissociable contributions of the prefrontal cortex to hippocampus- and caudate nucleus-dependent virtual navigation strategies. *Neurobiol Learn Mem*, *117*, 42-50. https://doi.org/10.1016/j.nlm.2014.07.002

Dakin, S. C., Hess, R. F., Ledgeway, T., & Achtman, R. L. (2002). What causes non-monotonic tuning of fMRI response to noisy images? In *Curr Biol* (Vol. 12, pp. R476-477; author reply R478).

Dalton, M. A., Zeidman, P., McCormick, C., & Maguire, E. A. (2018). Differentiable Processing of Objects, Associations, and Scenes within the Hippocampus. *J Neurosci*, *38*(38), 8146-8159. https://doi.org/10.1523/jneurosci.0263-18.2018

Dash, D., Ferrari, P., Malik, S., Montillo, A., Maldjian, J. A., & Wang, J. (2019). Determining the Optimal Number of MEG Trials: A Machine Learning and Speech Decoding Perspective. *Brain Inform (2018)*, *11309*, 163-172. https://doi.org/10.1007/978-3-030-05587-5_16

Davies, R. R., Graham, K. S., Xuereb, J. H., Williams, G. B., & Hodges, J. R. (2004). The human perirhinal cortex and semantic memory. *Eur J Neurosci*, *20*(9), 2441-2446. https://doi.org/10.1111/j.1460-9568.2004.03710.x

de Dreu, M. J., Schouwenaars, I. T., Rutten, G. M., Ramsey, N. F., & Jansma, J. M. (2019). Brain Activity Associated With Expected Task Difficulty. *Front Hum Neurosci*, *13*, 286. https://doi.org/10.3389/fnhum.2019.00286

De Luca, F., McCormick, C., Mullally, S. L., Intraub, H., Maguire, E. A., & Ciaramelli, E. (2018). Boundary extension is attenuated in patients with ventromedial prefrontal cortex damage. *Cortex*, *108*, 1-12. https://doi.org/10.1016/j.cortex.2018.07.002

De Santis, S., Drakesmith, M., Bells, S., Assaf, Y., & Jones, D. K. (2014). Why diffusion tensor MRI does well only some of the time: variance and covariance of white matter tissue microstructure attributes in the living human brain. *Neuroimage*, *89*, 35-44. https://doi.org/10.1016/j.neuroimage.2013.12.003

De Santis, S., Granberg, T., Ouellette, R., Treaba, C. A., Herranz, E., Fan, Q., Mainero, C., & Toschi, N. (2019). Evidence of early microstructural white matter abnormalities in multiple sclerosis from multi-shell diffusion MRI. *Neuroimage Clin*, *22*, 101699. https://doi.org/10.1016/j.nicl.2019.101699

De Santis, S., Jones, D. K., & Roebroeck, A. (2016). Including diffusion time dependence in the extra-axonal space improves in vivo estimates of axonal diameter and density in human white matter. *Neuroimage*, *130*, 91-103. https://doi.org/10.1016/j.neuroimage.2016.01.047

Dell'acqua, F., Scifo, P., Rizzo, G., Catani, M., Simmons, A., Scotti, G., & Fazio, F. (2010). A modified damped Richardson-Lucy algorithm to reduce isotropic background effects in spherical deconvolution. *Neuroimage*, *49*(2), 1446-1458. https://doi.org/10.1016/j.neuroimage.2009.09.033

Devereux, B. J., Clarke, A., & Tyler, L. K. (2018). Integrated deep visual and semantic attractor neural networks predict fMRI pattern-information along the ventral object processing pathway. *Sci Rep*, *8*(1), 10636. https://doi.org/10.1038/s41598-018-28865-1

Devor, A., Tian, P., Nishimura, N., Teng, I. C., Hillman, E. M., Narayanan, S. N., Ulbert, I., Boas, D. A., Kleinfeld, D., & Dale, A. M. (2007). Suppressed neuronal activity and concurrent arteriolar vasoconstriction may explain negative blood oxygenation level-dependent signal. *J Neurosci*, *27*(16), 4452-4459. https://doi.org/10.1523/jneurosci.0134-07.2007

Diana, R. A., Yonelinas, A. P., & Ranganath, C. (2007). Imaging recollection and familiarity in the medial temporal lobe: a three-component model. *Trends Cogn Sci*, *11*(9), 379-386. https://doi.org/10.1016/j.tics.2007.08.001

Dickinson, C. A., & Intraub, H. (2008). Transsaccadic representation of layout: what is the time course of boundary extension? *J Exp Psychol Hum Percept Perform*, *34*(3), 543-555. https://doi.org/10.1037/0096-1523.34.3.543

Diedenhofen, B., & Musch, J. (2015). cocor: a comprehensive solution for the statistical comparison of correlations. *PLoS One*, *10*(3), e0121945. https://doi.org/10.1371/journal.pone.0121945

Dilks, D. D., Julian, J. B., Paunov, A. M., & Kanwisher, N. (2013). The occipital place area is causally and selectively involved in scene perception. *J Neurosci*, *33*(4), 1331-1336a. https://doi.org/10.1523/jneurosci.4081-12.2013

Dima, D. C., Adams, R., Linden, S. C., Baird, A., Smith, J., Foley, S., Perry, G., Routley, B. C., Magazzini, L., Drakesmith, M., Williams, N., Doherty, J., van den Bree, M. B. M., Owen, M. J., Hall, J., Linden, D. E. J., & Singh, K. D. (2020). Electrophysiological network alterations in adults with copy number variants associated with high neurodevelopmental risk. *Transl Psychiatry*, *10*(1), 324. https://doi.org/10.1038/s41398-020-00998-w

Dobel, C., Junghofer, M., & Gruber, T. (2011). The role of gamma-band activity in the representation of faces: reduced activity in the fusiform face area in congenital prosopagnosia. *PLoS One*, *6*(5), e19550. https://doi.org/10.1371/journal.pone.0019550

Doesburg, S. M., Green, J. J., McDonald, J. J., & Ward, L. M. (2009). From local inhibition to long-range integration: a functional dissociation of alpha-band synchronization across cortical scales in visuospatial attention. *Brain Res*, *1303*, 97-110. https://doi.org/10.1016/j.brainres.2009.09.069

Dragoi, G., & Buzsaki, G. (2006). Temporal encoding of place sequences by hippocampal cell assemblies. *Neuron*, *50*(1), 145-157. https://doi.org/10.1016/j.neuron.2006.02.023

Drieu, C., & Zugaro, M. (2019). Hippocampal Sequences During Exploration: Mechanisms and Functions. *Front Cell Neurosci*, *13*, 232. https://doi.org/10.3389/fncel.2019.00232

Drzezga, A. (2018). The Network Degeneration Hypothesis: Spread of Neurodegenerative Patterns Along Neuronal Brain Networks. *J Nucl Med*, *59*(11), 1645-1648. https://doi.org/10.2967/jnumed.117.206300

Dubois, J., & Adolphs, R. (2016). Building a Science of Individual Differences from fMRI. *Trends Cogn Sci*, *20*(6), 425-443. https://doi.org/10.1016/j.tics.2016.03.014

DuBrow, S., & Davachi, L. (2013). The influence of context boundaries on memory for the sequential order of events. *J Exp Psychol Gen*, *142*(4), 1277-1286. https://doi.org/10.1037/a0034024

Duke, D., Martin, C. B., Bowles, B., McRae, K., & Kohler, S. (2017). Perirhinal cortex tracks degree of recent as well as cumulative lifetime experience with object concepts. *Cortex*, *89*, 61-70. https://doi.org/10.1016/j.cortex.2017.01.015

Dumont, J. R., Amin, E., Wright, N. F., Dillingham, C. M., & Aggleton, J. P. (2015). The impact of fornix lesions in rats on spatial learning tasks sensitive to anterior thalamic and hippocampal damage. *Behav Brain Res*, *278*, 360-374. https://doi.org/10.1016/j.bbr.2014.10.016

Eichenbaum, H. (2017a). On the Integration of Space, Time, and Memory. *Neuron*, *95*(5), 1007-1018. https://doi.org/10.1016/j.neuron.2017.06.036

Eichenbaum, H. (2017b). The role of the hippocampus in navigation is memory. In *J Neurophysiol* (Vol. 117, pp. 1785-1796). https://doi.org/10.1152/jn.00005.2017

Eichenbaum, H., Yonelinas, A. P., & Ranganath, C. (2007). The medial temporal lobe and recognition memory. *Annu Rev Neurosci*, *30*, 123-152. https://doi.org/10.1146/annurev.neuro.30.051606.094328

Ekstrom, A. (2010). How and when the fMRI BOLD signal relates to underlying neural activity: the danger in dissociation. *Brain Res Rev*, *62*(2), 233-244. https://doi.org/10.1016/j.brainresrev.2009.12.004

Ekstrom, A., Suthana, N., Millett, D., Fried, I., & Bookheimer, S. (2009). Correlation between BOLD fMRI and theta-band local field potentials in the human hippocampal area. *J Neurophysiol*, *101*(5), 2668-2678. https://doi.org/10.1152/jn.91252.2008

Ekstrom, A. D., Kahana, M. J., Caplan, J. B., Fields, T. A., Isham, E. A., Newman, E. L., & Fried, I. (2003). Cellular networks underlying human spatial navigation. *Nature*, *425*(6954), 184-188. https://doi.org/10.1038/nature01964

Engell, A. D., & McCarthy, G. (2010). Selective attention modulates face-specific induced gamma oscillations recorded from ventral occipitotemporal cortex. *J Neurosci*, *30*(26), 8780-8786. https://doi.org/10.1523/jneurosci.1575-10.2010

Epstein, R., Graham, K. S., & Downing, P. E. (2003). Viewpoint-specific scene representations in human parahippocampal cortex. *Neuron*, *37*(5), 865-876.

Epstein, R. A. (2008). Parahippocampal and retrosplenial contributions to human spatial navigation. *Trends Cogn Sci*, *12*(10), 388-396. https://doi.org/10.1016/j.tics.2008.07.004

Epstein, R. A., Parker, W. E., & Feiler, A. M. (2007). Where am I now? Distinct roles for parahippocampal and retrosplenial cortices in place recognition. *J Neurosci*, *27*(23), 6141-6149. https://doi.org/10.1523/jneurosci.0799-07.2007

Erickson, M. A., Smith, D., Albrecht, M. A., & Silverstein, S. (2019). Alpha-band desynchronization reflects memory-specific processes during visual change detection. *Psychophysiology*, e13442. https://doi.org/10.1111/psyp.13442

Farquharson, S., Tournier, J. D., Calamante, F., Fabinyi, G., Schneider-Kolsky, M., Jackson, G. D., & Connelly, A. (2013). White matter fiber tractography: why we need to move beyond DTI. *J Neurosurg*, *118*(6), 1367-1377. https://doi.org/10.3171/2013.2.jns121294

Faul, F., Erdfelder, E., Buchner, A., & Lang, A. G. (2009). Statistical power analyses using G*Power 3.1: tests for correlation and regression analyses. *Behav Res Methods*, *41*(4), 1149-1160. https://doi.org/10.3758/brm.41.4.1149

Faul, F., Erdfelder, E., Lang, A. G., & Buchner, A. (2007). G*Power 3: a flexible statistical power analysis program for the social, behavioral, and biomedical sciences. *Behav Res Methods*, *39*(2), 175-191. https://doi.org/10.3758/bf03193146

Fell, J., Ludowig, E., Staresina, B. P., Wagner, T., Kranz, T., Elger, C. E., & Axmacher, N. (2011). Medial temporal theta/alpha power enhancement precedes successful memory encoding: evidence based on intracranial EEG. *J Neurosci*, *31*(14), 5392-5397. https://doi.org/10.1523/jneurosci.3668-10.2011

Fellner, M. C., Volberg, G., Wimber, M., Goldhacker, M., Greenlee, M. W., & Hanslmayr, S. (2016). Spatial Mnemonic Encoding: Theta Power Decreases and Medial Temporal Lobe BOLD Increases Co-Occur during the Usage of the Method of Loci. *eNeuro*, *3*(6). https://doi.org/10.1523/eneuro.0184-16.2016

Fernández, A., Ríos-Lago, M., Abásolo, D., Hornero, R., Alvarez-Linera, J., Paul, N., Maestú, F., & Ortiz, T. (2011). The correlation between white-matter microstructure and the complexity of spontaneous brain activity: a difussion tensor imaging-MEG study. *Neuroimage*, *57*(4), 1300-1307. https://doi.org/10.1016/j.neuroimage.2011.05.079

Fletcher, B. R., Calhoun, M. E., Rapp, P. R., & Shapiro, M. L. (2006). Fornix lesions decouple the induction of hippocampal arc transcription from behavior but not plasticity. *J Neurosci*, *26*(5), 1507-1515. https://doi.org/10.1523/jneurosci.4441-05.2006

Foster, B. L., Dastjerdi, M., & Parvizi, J. (2012). Neural populations in human posteromedial cortex display opposing responses during memory and numerical processing. *Proc Natl Acad Sci U S A*, *109*(38), 15514-15519. https://doi.org/10.1073/pnas.1206580109

Foster, B. L., & Parvizi, J. (2012). Resting oscillations and cross-frequency coupling in the human posteromedial cortex. *Neuroimage*, *60*(1), 384-391. https://doi.org/10.1016/j.neuroimage.2011.12.019

Foster, D. J., & Wilson, M. A. (2007). Hippocampal theta sequences. *Hippocampus*, *17*(11), 1093-1099. https://doi.org/10.1002/hipo.20345

Fox, M. D., & Raichle, M. E. (2007). Spontaneous fluctuations in brain activity observed with functional magnetic resonance imaging. *Nat Rev Neurosci*, *8*(9), 700-711. https://doi.org/10.1038/nrn2201

Fransson, P., & Marrelec, G. (2008). The precuneus/posterior cingulate cortex plays a pivotal role in the default mode network: Evidence from a partial correlation network analysis. *Neuroimage*, *42*(3), 1178-1184. https://doi.org/10.1016/j.neuroimage.2008.05.059

França, A. S., do Nascimento, G. C., Lopes-dos-Santos, V., Muratori, L., Ribeiro, S., Lobão-Soares, B., & Tort, A. B. (2014). Beta2 oscillations (23-30 Hz) in the mouse hippocampus during novel object recognition. *Eur J Neurosci*, *40*(11), 3693-3703. https://doi.org/10.1111/ejn.12739

Fries, P. (2005). A mechanism for cognitive dynamics: neuronal communication through neuronal coherence. *Trends Cogn Sci*, *9*(10), 474-480. https://doi.org/10.1016/j.tics.2005.08.011

Fries, P., Nikolic, D., & Singer, W. (2007). The gamma cycle. *Trends Neurosci*, *30*(7), 309-316. https://doi.org/10.1016/j.tins.2007.05.005

Furtunato, A. M. B., Lobão-Soares, B., Tort, A. B. L., & Belchior, H. (2020). Specific Increase of Hippocampal Delta Oscillations Across Consecutive Treadmill Runs. *Front Behav Neurosci*, *14*, 101. https://doi.org/10.3389/fnbeh.2020.00101

Gaffan, D., & Gaffan, E. A. (1991). Amnesia in man following transection of the fornix. A review. *Brain*, *114 (Pt 6)*, 2611-2618. https://doi.org/10.1093/brain/114.6.2611

Ganzetti, M., & Mantini, D. (2013). Functional connectivity and oscillatory neuronal activity in the resting human brain. *Neuroscience*, *240*, 297-309. https://doi.org/10.1016/j.neuroscience.2013.02.032

Gao, Z., Goldstein, A., Harpaz, Y., Hansel, M., Zion-Golumbic, E., & Bentin, S. (2013). A magnetoencephalographic study of face processing: M170, gamma-band oscillations and source localization. *Hum Brain Mapp*, *34*(8), 1783-1795. https://doi.org/10.1002/hbm.22028

Gardner, J. L., Sun, P., Waggoner, R. A., Ueno, K., Tanaka, K., & Cheng, K. (2005). Contrast adaptation and representation in human early visual cortex. *Neuron*, *47*(4), 607-620. https://doi.org/10.1016/j.neuron.2005.07.016

Gaynor, L. S., Curiel Cid, R. E., Penate, A., Rosselli, M., Burke, S. N., Wicklund, M., Loewenstein, D. A., & Bauer, R. M. (2019). Visual Object Discrimination Impairment as an Early Predictor of Mild Cognitive Impairment and Alzheimer's Disease. *J Int Neuropsychol Soc*, *25*(7), 688-698. https://doi.org/10.1017/s1355617719000316

Geeraert, B. L., Chamberland, M., Lebel, R. M., & Lebel, C. (2020). Multimodal principal component analysis to identify major features of white matter structure and links to reading. *PLoS One*, *15*(8), e0233244. https://doi.org/10.1371/journal.pone.0233244

Ghorashi, S., & Spencer, K. M. (2015). Attentional Load Effects on Beta Oscillations in Healthy and Schizophrenic Individuals. *Front Psychiatry*, *6*, 149. https://doi.org/10.3389/fpsyt.2015.00149

Gilligan, T. M., Sibilia, F., Farrell, D., Lyons, D., Kennelly, S. P., & Bokde, A. L. W. (2019). No relationship between fornix and cingulum degradation and within-network decreases in functional connectivity in prodromal Alzheimer's disease. *PLoS One*, *14*(10), e0222977. https://doi.org/10.1371/journal.pone.0222977

Gilmore, A. W., Nelson, S. M., Chen, H. Y., & McDermott, K. B. (2018). Task-related and resting-state fMRI identify distinct networks that preferentially support remembering the past and imagining the future. *Neuropsychologia*, *110*, 180-189. https://doi.org/10.1016/j.neuropsychologia.2017.06.016

Giulietti, G., Bozzali, M., Figura, V., Spano, B., Perri, R., Marra, C., Lacidogna, G., Giubilei, F., Caltagirone, C., & Cercignani, M. (2012). Quantitative magnetization transfer provides information complementary to grey matter atrophy in Alzheimer's disease brains. *Neuroimage*, *59*(2), 1114-1122. https://doi.org/10.1016/j.neuroimage.2011.09.043

Glover, G. H. (2011). Overview of functional magnetic resonance imaging. *Neurosurg Clin N Am*, *22*(2), 133-139, vii. https://doi.org/10.1016/j.nec.2010.11.001

Godfrey, M., & Singh, K. D. (2020). Measuring robust functional connectivity from resting-state MEG using amplitude and entropy correlation across frequency bands and temporal scales. *Neuroimage*, *226*, 117551. https://doi.org/10.1016/j.neuroimage.2020.117551

Gonsalves, B. D., Kahn, I., Curran, T., Norman, K. A., & Wagner, A. D. (2005). Memory strength and repetition suppression: multimodal imaging of medial temporal cortical contributions to recognition. *Neuron*, *47*(5), 751-761. https://doi.org/10.1016/j.neuron.2005.07.013

Goyal, A., Miller, J., Qasim, S. E., Watrous, A. J., Zhang, H., Stein, J. M., Inman, C. S., Gross, R. E., Willie, J. T., Lega, B., Lin, J. J., Sharan, A., Wu, C., Sperling, M. R., Sheth, S. A., McKhann, G. M., Smith, E. H., Schevon, C., & Jacobs, J. (2020). Functionally distinct high and low theta oscillations in the human hippocampus. *Nat Commun*, *11*(1), 2469. https://doi.org/10.1038/s41467-020-15670-6

Graham, K. S., Barense, M. D., & Lee, A. C. (2010). Going beyond LTM in the MTL: a synthesis of neuropsychological and neuroimaging findings on the role of the medial temporal lobe in memory and perception. *Neuropsychologia*, *48*(4), 831-853. https://doi.org/10.1016/j.neuropsychologia.2010.01.001

Grajski, K. A., & Bressler, S. L. (2019). Differential medial temporal lobe and default-mode network functional connectivity and morphometric changes in Alzheimer's disease. *Neuroimage Clin*, *23*, 101860. https://doi.org/10.1016/j.nicl.2019.101860

Gramann, K., Muller, H. J., Schonebeck, B., & Debus, G. (2006). The neural basis of ego- and allocentric reference frames in spatial navigation: evidence from spatio-temporal coupled current density reconstruction. *Brain Res*, *1118*(1), 116-129. https://doi.org/10.1016/j.brainres.2006.08.005

Green, A. E., Croft, R. J., Maller, J. J., & Fitzgerald, P. B. (2016). White matter correlates of episodic memory encoding and retrieval in schizophrenia. *Psychiatry Res Neuroimaging*, *254*, 188-198. https://doi.org/10.1016/j.pscychresns.2016.07.002

Greicius, M. D., Srivastava, G., Reiss, A. L., & Menon, V. (2004). Default-mode network activity distinguishes Alzheimer's disease from healthy aging: evidence from functional MRI. *Proc Natl Acad Sci U S A*, *101*(13), 4637-4642. https://doi.org/10.1073/pnas.0308627101

Greicius, M. D., Supekar, K., Menon, V., & Dougherty, R. F. (2009). Resting-state functional connectivity reflects structural connectivity in the default mode network. *Cereb Cortex*, *19*(1), 72-78. https://doi.org/10.1093/cercor/bhn059

Gronlund, S. D., Edwards, M. B., & Ohrt, D. D. (1997). Comparison of the retrieval of item versus spatial position information. *J Exp Psychol Learn Mem Cogn*, *23*(5), 1261-1274.

Gross, J., Baillet, S., Barnes, G. R., Henson, R. N., Hillebrand, A., Jensen, O., Jerbi, K., Litvak, V., Maess, B., Oostenveld, R., Parkkonen, L., Taylor, J. R., van Wassenhove, V., Wibral, M., & Schoffelen, J. M. (2013). Good practice for conducting and reporting MEG research. *Neuroimage*, *65*(100), 349-363. https://doi.org/10.1016/j.neuroimage.2012.10.001

Grossi, D., Soricelli, A., Ponari, M., Salvatore, E., Quarantelli, M., Prinster, A., & Trojano, L. (2014). Structural connectivity in a single case of progressive prosopagnosia: the

role of the right inferior longitudinal fasciculus. *Cortex*, *56*, 111-120. https://doi.org/10.1016/j.cortex.2012.09.010

Guitart-Masip, M., Barnes, G. R., Horner, A., Bauer, M., Dolan, R. J., & Duzel, E. (2013). Synchronization of medial temporal lobe and prefrontal rhythms in human decision making. *J Neurosci*, *33*(2), 442-451. https://doi.org/10.1523/jneurosci.2573-12.2013

Hadjipapas, A., Lowet, E., Roberts, M. J., Peter, A., & De Weerd, P. (2015). Parametric variation of gamma frequency and power with luminance contrast: A comparative study of human MEG and monkey LFP and spike responses. *Neuroimage*, *112*, 327-340. https://doi.org/10.1016/j.neuroimage.2015.02.062

Hagmann, P., Cammoun, L., Gigandet, X., Meuli, R., Honey, C. J., Wedeen, V. J., & Sporns, O. (2008). Mapping the structural core of human cerebral cortex. *PLoS Biol*, *6*(7), e159. https://doi.org/10.1371/journal.pbio.0060159

Halgren, E., Raij, T., Marinkovic, K., Jousmäki, V., & Hari, R. (2000). Cognitive response profile of the human fusiform face area as determined by MEG. *Cereb Cortex*, *10*(1), 69-81. https://doi.org/10.1093/cercor/10.1.69

Hanslmayr, S., Staresina, B. P., & Bowman, H. (2016). Oscillations and Episodic Memory: Addressing the Synchronization/Desynchronization Conundrum. *Trends Neurosci*, *39*(1), 16-25. https://doi.org/10.1016/j.tins.2015.11.004

Hanslmayr, S., Staudigl, T., & Fellner, M. C. (2012). Oscillatory power decreases and long-term memory: the information via desynchronization hypothesis. *Front Hum Neurosci*, *6*, 74. https://doi.org/10.3389/fnhum.2012.00074

Harmony, T. (2013). The functional significance of delta oscillations in cognitive processing. *Front Integr Neurosci*, *7*, 83. https://doi.org/10.3389/fnint.2013.00083

Hartopp, N., Wright, P., Ray, N. J., Evans, T. E., Metzler-Baddeley, C., Aggleton, J. P., & O'Sullivan, M. J. (2018). A Key Role for Subiculum-Fornix Connectivity in Recollection in Older Age. *Front Syst Neurosci*, *12*, 70. https://doi.org/10.3389/fnsys.2018.00070

Haskins, A. L., Yonelinas, A. P., Quamme, J. R., & Ranganath, C. (2008). Perirhinal cortex supports encoding and familiarity-based recognition of novel associations. *Neuron*, *59*(4), 554-560. https://doi.org/10.1016/j.neuron.2008.07.035

Hassabis, D., Kumaran, D., Vann, S. D., & Maguire, E. A. (2007). Patients with hippocampal amnesia cannot imagine new experiences. *Proc Natl Acad Sci U S A*, *104*(5), 1726-1731. https://doi.org/10.1073/pnas.0610561104

Hau, J., Sarubbo, S., Houde, J. C., Corsini, F., Girard, G., Deledalle, C., Crivello, F., Zago, L., Mellet, E., Jobard, G., Joliot, M., Mazoyer, B., Tzourio-Mazoyer, N., Descoteaux, M., & Petit, L. (2017). Revisiting the human uncinate fasciculus, its subcomponents and asymmetries with stem-based tractography and microdissection validation. *Brain Struct Funct*, *222*(4), 1645-1662. https://doi.org/10.1007/s00429-016-1298-6

Haxby, J. V., Hoffman, E. A., & Gobbini, M. I. (2000). The distributed human neural system for face perception. *Trends Cogn Sci*, *4*(6), 223-233.

Hayek, D., Thams, F., Flöel, A., & Antonenko, D. (2020). Dentate Gyrus Volume Mediates the Effect of Fornix Microstructure on Memory Formation in Older Adults. *Front Aging Neurosci*, *12*, 79. https://doi.org/10.3389/fnagi.2020.00079

Hellyer, P. J., Clopath, C., Kehagia, A. A., Turkheimer, F. E., & Leech, R. (2017). From homeostasis to behavior: Balanced activity in an exploration of embodied dynamic environmental-neural interaction. *PLoS Comput Biol*, *13*(8), e1005721. https://doi.org/10.1371/journal.pcbi.1005721

Henkelman, R. M., Huang, X., Xiang, Q. S., Stanisz, G. J., Swanson, S. D., & Bronskill, M. J. (1993). Quantitative interpretation of magnetization transfer. *Magn Reson Med*, *29*(6), 759-766. https://doi.org/10.1002/mrm.1910290607

Henkelman, R. M., Stanisz, G. J., & Graham, S. J. (2001). Magnetization transfer in MRI: a review. *NMR Biomed*, *14*(2), 57-64. https://doi.org/10.1002/nbm.683

Herbet, G., Zemmoura, I., & Duffau, H. (2018). Functional Anatomy of the Inferior Longitudinal Fasciculus: From Historical Reports to Current Hypotheses. *Front Neuroanat*, *12*, 77. https://doi.org/10.3389/fnana.2018.00077

Herweg, N. A., Apitz, T., Leicht, G., Mulert, C., Fuentemilla, L., & Bunzeck, N. (2016). Theta-Alpha Oscillations Bind the Hippocampus, Prefrontal Cortex, and Striatum during Recollection: Evidence from Simultaneous EEG-fMRI. *J Neurosci*, *36*(12), 3579-3587. https://doi.org/10.1523/jneurosci.3629-15.2016

Herweg, N. A., Solomon, E. A., & Kahana, M. J. (2020). Theta Oscillations in Human Memory. *Trends Cogn Sci*, *24*(3), 208-227. https://doi.org/10.1016/j.tics.2019.12.006

Heys, J. G., & Dombeck, D. A. (2018). Evidence for a subcircuit in medial entorhinal cortex representing elapsed time during immobility. *Nat Neurosci*, *21*(11), 1574-1582. https://doi.org/10.1038/s41593-018-0252-8

Hildesheim, F. E., Debus, I., Kessler, R., Thome, I., Zimmermann, K. M., Steinsträter, O., Sommer, J., Kamp-Becker, I., Stark, R., & Jansen, A. (2020). The Trajectory of Hemispheric Lateralization in the Core System of Face Processing: A Cross-Sectional Functional Magnetic Resonance Imaging Pilot Study. *Front Psychol*, *11*, 507199. https://doi.org/10.3389/fpsyg.2020.507199

Hill, P. F., Seger, S. E., Yoo, H. B., King, D. R., Lega, B. C., & Rugg, M. D. (2021). Distinct neurophysiological correlates of the fMRI BOLD signal in the hippocampus and neocortex. *bioRxiv*, 2021.2002.2001.429258. https://doi.org/10.1101/2021.02.01.429258

Hillebrand, A., & Barnes, G. R. (2002). A quantitative assessment of the sensitivity of whole-head MEG to activity in the adult human cortex. *Neuroimage*, *16*(3 Pt 1), 638-650. https://doi.org/10.1006/nimg.2002.1102

Hillebrand, A., & Barnes, G. R. (2005). Beamformer analysis of MEG data. *Int Rev Neurobiol*, *68*, 149-171. https://doi.org/10.1016/s0074-7742(05)68006-3

Hillebrand, A., Barnes, G. R., Bosboom, J. L., Berendse, H. W., & Stam, C. J. (2012). Frequency-dependent functional connectivity within resting-state networks: an atlas-based MEG beamformer solution. *Neuroimage*, *59*(4), 3909-3921. https://doi.org/10.1016/j.neuroimage.2011.11.005

Hillebrand, A., Tewarie, P., van Dellen, E., Yu, M., Carbo, E. W., Douw, L., Gouw, A. A., van Straaten, E. C., & Stam, C. J. (2016). Direction of information flow in large-scale resting-state networks is frequency-dependent. *Proc Natl Acad Sci U S A*, *113*(14), 3867-3872. https://doi.org/10.1073/pnas.1515657113

Hillman, E. M. (2014). Coupling mechanism and significance of the BOLD signal: a status report. *Annu Rev Neurosci*, *37*, 161-181. https://doi.org/10.1146/annurev-neuro-071013-014111

Hippocampal Complex. (2009). In M. D. Binder, N. Hirokawa, & U. Windhorst (Eds.), *Encyclopedia of Neuroscience* (pp. 1840-1840). Springer Berlin Heidelberg. https://doi.org/10.1007/978-3-540-29678-2_2211

Hodgetts, C. J., Postans, M., Shine, J. P., Jones, D. K., Lawrence, A. D., & Graham, K. S. (2015). Dissociable roles of the inferior longitudinal fasciculus and fornix in face and place perception. *Elife*, *4*. https://doi.org/10.7554/eLife.07902

Hodgetts, C. J., Postans, M., Warne, N., Varnava, A., Lawrence, A. D., & Graham, K. S. (2017). Distinct contributions of the fornix and inferior longitudinal fasciculus to episodic and semantic autobiographical memory. *Cortex*, *94*, 1-14. https://doi.org/10.1016/j.cortex.2017.05.010

Hodgetts, C. J., Shine, J. P., Lawrence, A. D., Downing, P. E., & Graham, K. S. (2016). Evidencing a place for the hippocampus within the core scene processing network. *Human Brain Mapping*, *37*(11), 3779-3794. https://doi.org/10.1002/hbm.23275

Hodgetts, C. J., Stefani, M., Williams, A. N., Kolarik, B. S., Yonelinas, A. P., Ekstrom, A. D., Lawrence, A. D., Zhang, J., & Graham, K. S. (2020). The role of the fornix in human navigational learning. *Cortex*, *124*, 97-110. https://doi.org/10.1016/j.cortex.2019.10.017

Hodgetts, C. J., Voets, N. L., Thomas, A. G., Clare, S., Lawrence, A. D., & Graham, K. S. (2017). Ultra-High-Field fMRI Reveals a Role for the Subiculum in Scene Perceptual Discrimination. *J Neurosci*, *37*(12), 3150-3159. https://doi.org/10.1523/jneurosci.3225-16.2017

Hoffman, K. L., Dragan, M. C., Leonard, T. K., Micheli, C., Montefusco-Siegmund, R., & Valiante, T. A. (2013). Saccades during visual exploration align hippocampal 3-8 Hz rhythms in human and non-human primates. *Front Syst Neurosci*, *7*, 43. https://doi.org/10.3389/fnsys.2013.00043

Hofstetter, S., Tavor, I., Tzur Moryosef, S., & Assaf, Y. (2013). Short-term learning induces white matter plasticity in the fornix. *J Neurosci*, *33*(31), 12844-12850. https://doi.org/10.1523/jneurosci.4520-12.2013

Horner, A. J., Bisby, J. A., Bush, D., Lin, W. J., & Burgess, N. (2015). Evidence for holistic episodic recollection via hippocampal pattern completion. *Nat Commun*, *6*, 7462. https://doi.org/10.1038/ncomms8462

Hsieh, L. T., Gruber, M. J., Jenkins, L. J., & Ranganath, C. (2014). Hippocampal activity patterns carry information about objects in temporal context. *Neuron*, *81*(5), 1165-1178. https://doi.org/10.1016/j.neuron.2014.01.015

Hsieh, L. T., & Ranganath, C. (2014). Frontal midline theta oscillations during working memory maintenance and episodic encoding and retrieval. *Neuroimage*, *85 Pt 2*, 721-729. https://doi.org/10.1016/j.neuroimage.2013.08.003

Hsieh, L. T., & Ranganath, C. (2015). Cortical and subcortical contributions to sequence retrieval: Schematic coding of temporal context in the neocortical recollection network. *Neuroimage*, *121*, 78-90. https://doi.org/10.1016/j.neuroimage.2015.07.040

Huber, E., Henriques, R. N., Owen, J. P., Rokem, A., & Yeatman, J. D. (2019). Applying microstructural models to understand the role of white matter in cognitive development. *Dev Cogn Neurosci*, *36*, 100624. https://doi.org/10.1016/j.dcn.2019.100624

Huijbers, W., Pennartz, C. M. A., Cabeza, R., & Daselaar, S. M. (2011). The hippocampus is coupled with the default network during memory retrieval but not during memory encoding. *PLOS ONE*, *6*(4), e17463. https://doi.org/10.1371/journal.pone.0017463

Huijbers, W., Vannini, P., Sperling, R. A., C, M. P., Cabeza, R., & Daselaar, S. M. (2012). Explaining the encoding/retrieval flip: memory-related deactivations and activations in the posteromedial cortex. *Neuropsychologia*, *50*(14), 3764-3774. https://doi.org/10.1016/j.neuropsychologia.2012.08.021

Hunsaker, M. R., & Kesner, R. P. (2009). Transecting the dorsal fornix results in novelty detection but not temporal ordering deficits in rats. *Behav Brain Res*, *201*(1), 192-197. https://doi.org/10.1016/j.bbr.2009.02.012

Hutchings, R., Palermo, R., Piguet, O., & Kumfor, F. (2017). Disrupted Face Processing in Frontotemporal Dementia: A Review of the Clinical and Neuroanatomical Evidence. *Neuropsychol Rev*, *27*(1), 18-30. https://doi.org/10.1007/s11065-016-9340-2

Hyde, J. S., Bigler, R. S., Joel, D., Tate, C. C., & van Anders, S. M. (2019). The future of sex and gender in psychology: Five challenges to the gender binary. *Am Psychol*, *74*(2), 171-193. https://doi.org/10.1037/amp0000307

Hyvärinen, A. (1999). Fast and robust fixed-point algorithms for independent component analysis. *IEEE Trans Neural Netw*, *10*(3), 626-634. https://doi.org/10.1109/72.761722

Hämäläinen, M. S., & Ilmoniemi, R. J. (1994). Interpreting magnetic fields of the brain: minimum norm estimates. *Med Biol Eng Comput*, *32*(1), 35-42. https://doi.org/10.1007/bf02512476

Iglói, K., Doeller, C. F., Berthoz, A., Rondi-Reig, L., & Burgess, N. (2010). Lateralized human hippocampal activity predicts navigation based on sequence or place memory. *Proc Natl Acad Sci U S A*, *107*(32), 14466-14471. https://doi.org/10.1073/pnas.1004243107

Intraub, H., & Dickinson, C. A. (2008). False memory 1/20th of a second later: what the early onset of boundary extension reveals about perception. *Psychol Sci*, *19*(10), 1007-1014. https://doi.org/10.1111/j.1467-9280.2008.02192.x

Intraub, H., & Richardson, M. (1989). Wide-angle memories of close-up scenes. *J Exp Psychol Learn Mem Cogn*, *15*(2), 179-187.

Ion Storm. (2000). *Deus Ex*. Dallas, Texas, US.

Irish, M., Halena, S., Kamminga, J., Tu, S., Hornberger, M., & Hodges, J. R. (2015). Scene construction impairments in Alzheimer's disease - A unique role for the posterior cingulate cortex. *Cortex*, *73*, 10-23. https://doi.org/10.1016/j.cortex.2015.08.004

Ishai, A., Ungerleider, L. G., Martin, A., & Haxby, J. V. (2000). The representation of objects in the human occipital and temporal cortex. *J Cogn Neurosci*, *12 Suppl 2*, 35-51. https://doi.org/10.1162/089892900564055

Izen, S. C., Chrastil, E. R., & Stern, C. E. (2018). Resting State Connectivity Between Medial Temporal Lobe Regions and Intrinsic Cortical Networks Predicts Performance in a Path Integration Task. *Front Hum Neurosci*, *12*, 415. https://doi.org/10.3389/fnhum.2018.00415

Jackson, R. L., Hoffman, P., Pobric, G., & Lambon Ralph, M. A. (2016). The Semantic Network at Work and Rest: Differential Connectivity of Anterior Temporal Lobe Subregions. *J Neurosci*, *36*(5), 1490-1501. https://doi.org/10.1523/jneurosci.2999-15.2016

Jacobs, J. (2014). Hippocampal theta oscillations are slower in humans than in rodents: implications for models of spatial navigation and memory. *Philos Trans R Soc Lond B Biol Sci*, *369*(1635), 20130304. https://doi.org/10.1098/rstb.2013.0304

JASP Team. (2020). *JASP (Version 0.14.1)[Computer software]*. URL: https://jasp-stats.org/

Javadi, A. H., Patai, E. Z., Marin-Garcia, E., Margois, A., Tan, H. M., Kumaran, D., Nardini, M., Penny, W., Duzel, E., Dayan, P., & Spiers, H. J. (2019). Backtracking during navigation is correlated with enhanced anterior cingulate activity and suppression of alpha oscillations and the 'default-mode' network. *Proc Biol Sci*, *286*(1908), 20191016. https://doi.org/10.1098/rspb.2019.1016

Jeewajee, A., Lever, C., Burton, S., O'Keefe, J., & Burgess, N. (2008). Environmental novelty is signaled by reduction of the hippocampal theta frequency. *Hippocampus*, *18*(4), 340-348. https://doi.org/10.1002/hipo.20394

Jefferies, E. (2013). The neural basis of semantic cognition: converging evidence from neuropsychology, neuroimaging and TMS. *Cortex*, *49*(3), 611-625. https://doi.org/10.1016/j.cortex.2012.10.008

Jenkins, L. J., & Ranganath, C. (2010). Prefrontal and medial temporal lobe activity at encoding predicts temporal context memory. *J Neurosci*, *30*(46), 15558-15565. https://doi.org/10.1523/jneurosci.1337-10.2010

Jenkins, L. J., & Ranganath, C. (2016). Distinct neural mechanisms for remembering when an event occurred. *Hippocampus*, *26*(5), 554-559. https://doi.org/10.1002/hipo.22571

Jenkinson, M., Beckmann, C. F., Behrens, T. E., Woolrich, M. W., & Smith, S. M. (2012). FSL. *Neuroimage*, *62*(2), 782-790. https://doi.org/10.1016/j.neuroimage.2011.09.015

Jensen, O., & Mazaheri, A. (2010). Shaping functional architecture by oscillatory alpha activity: gating by inhibition. *Front Hum Neurosci*, *4*, 186. https://doi.org/10.3389/fnhum.2010.00186

Jiang, H., van Gerven, M. A., & Jensen, O. (2015). Modality-specific alpha modulations facilitate long-term memory encoding in the presence of distracters. *J Cogn Neurosci*, *27*(3), 583-592. https://doi.org/10.1162/jocn_a_00726

Jones, D. K., Christiansen, K. F., Chapman, R. J., & Aggleton, J. P. (2013). Distinct subdivisions of the cingulum bundle revealed by diffusion MRI fibre tracking: implications for neuropsychological investigations. *Neuropsychologia*, *51*(1), 67-78. https://doi.org/10.1016/j.neuropsychologia.2012.11.018

Jones, D. K., Knosche, T. R., & Turner, R. (2013). White matter integrity, fiber count, and other fallacies: the do's and don'ts of diffusion MRI. *Neuroimage*, *73*, 239-254. https://doi.org/10.1016/j.neuroimage.2012.06.081

Jones, S. R., Pinto, D. J., Kaper, T. J., & Kopell, N. (2000). Alpha-frequency rhythms desynchronize over long cortical distances: a modeling study. *J Comput Neurosci*, *9*(3), 271-291. https://doi.org/10.1023/a:1026539805445

Kafkas, A., & Montaldi, D. (2012). Familiarity and recollection produce distinct eye movement, pupil and medial temporal lobe responses when memory strength is matched. *Neuropsychologia*, *50*(13), 3080-3093. https://doi.org/10.1016/j.neuropsychologia.2012.08.001

Kahn, I., Andrews-Hanna, J. R., Vincent, J. L., Snyder, A. Z., & Buckner, R. L. (2008). Distinct cortical anatomy linked to subregions of the medial temporal lobe revealed by intrinsic functional connectivity. *J Neurophysiol*, *100*(1), 129-139. https://doi.org/10.1152/jn.00077.2008

Kamps, F. S., Julian, J. B., Kubilius, J., Kanwisher, N., & Dilks, D. D. (2016). The occipital place area represents the local elements of scenes. *Neuroimage*, *132*, 417-424. https://doi.org/10.1016/j.neuroimage.2016.02.062

Kantarci, K. (2014). Fractional anisotropy of the fornix and hippocampal atrophy in Alzheimer's disease. *Front Aging Neurosci*, *6*, 316. https://doi.org/10.3389/fnagi.2014.00316

Kanwisher, N., McDermott, J., & Chun, M. M. (1997). The fusiform face area: a module in human extrastriate cortex specialized for face perception. *J Neurosci*, *17*(11), 4302-4311. https://doi.org/10.1523/jneurosci.17-11-04302.1997

Kanwisher, N., & Yovel, G. (2006). The fusiform face area: a cortical region specialized for the perception of faces. *Philos Trans R Soc Lond B Biol Sci*, *361*(1476), 2109-2128. https://doi.org/10.1098/rstb.2006.1934

Kaplan, R., Bush, D., Bisby, J. A., Horner, A. J., Meyer, S. S., & Burgess, N. (2017). Medial Prefrontal-Medial Temporal Theta Phase Coupling in Dynamic Spatial Imagery. *J Cogn Neurosci*, *29*(3), 507-519. https://doi.org/10.1162/jocn_a_01064

Kaplan, R., Bush, D., Bonnefond, M., Bandettini, P. A., Barnes, G. R., Doeller, C. F., & Burgess, N. (2014). Medial prefrontal theta phase coupling during spatial memory retrieval. *Hippocampus*, *24*(6), 656-665. https://doi.org/10.1002/hipo.22255

Karakaş, S. (2020). A review of theta oscillation and its functional correlates. *Int J Psychophysiol*, *157*, 82-99. https://doi.org/10.1016/j.ijpsycho.2020.04.008

Karapanagiotidis, T., Bernhardt, B. C., Jefferies, E., & Smallwood, J. (2017). Tracking thoughts: Exploring the neural architecture of mental time travel during mind-wandering. *Neuroimage*, *147*, 272-281. https://doi.org/10.1016/j.neuroimage.2016.12.031

Karnath, H. O., & Rorden, C. (2012). The anatomy of spatial neglect. *Neuropsychologia*, *50*(6), 1010-1017. https://doi.org/10.1016/j.neuropsychologia.2011.06.027

Kassambara, A. (2019). ggcorrplot: Visualization of a Correlation Matrix using 'ggplot2'. R package version 0.1.1. http://www.sthda.com/english/wiki/ggcorrplot

Kehoe, E. G., Farrell, D., Metzler-Baddeley, C., Lawlor, B. A., Kenny, R. A., Lyons, D., McNulty, J. P., Mullins, P. G., Coyle, D., & Bokde, A. L. (2015). Fornix White Matter is Correlated with Resting-State Functional Connectivity of the Thalamus and Hippocampus in Healthy Aging but Not in Mild Cognitive Impairment - A Preliminary Study. *Front Aging Neurosci*, *7*, 10. https://doi.org/10.3389/fnagi.2015.00010

Ketz, N. A., Jensen, O., & O'Reilly, R. C. (2015). Thalamic pathways underlying prefrontal cortex-medial temporal lobe oscillatory interactions. *Trends Neurosci*, *38*(1), 3-12. https://doi.org/10.1016/j.tins.2014.09.007

Khan, S., Gramfort, A., Shetty, N. R., Kitzbichler, M. G., Ganesan, S., Moran, J. M., Lee, S. M., Gabrieli, J. D., Tager-Flusberg, H. B., Joseph, R. M., Herbert, M. R., Hämäläinen, M. S., & Kenet, T. (2013). Local and long-range functional connectivity is reduced in concert in autism spectrum disorders. *Proc Natl Acad Sci U S A*, *110*(8), 3107-3112. https://doi.org/10.1073/pnas.1214533110

Khanna, P., & Carmena, J. M. (2015). Neural oscillations: beta band activity across motor networks. *Curr Opin Neurobiol*, *32*, 60-67. https://doi.org/10.1016/j.conb.2014.11.010

Kilner, J. M., Mattout, J., Henson, R., & Friston, K. J. (2005). Hemodynamic correlates of EEG: a heuristic. *Neuroimage*, *28*(1), 280-286. https://doi.org/10.1016/j.neuroimage.2005.06.008

Kim, S., Jeneson, A., van der Horst, A. S., Frascino, J. C., Hopkins, R. O., & Squire, L. R. (2011). Memory, visual discrimination performance, and the human hippocampus. *J Neurosci*, *31*(7), 2624-2629. https://doi.org/10.1523/jneurosci.5954-10.2011

Kivisaari, S. L., Tyler, L. K., Monsch, A. U., & Taylor, K. I. (2012). Medial perirhinal cortex disambiguates confusable objects. *Brain*, *135*(Pt 12), 3757-3769. https://doi.org/10.1093/brain/aws277

Klein, S., Staring, M., Murphy, K., Viergever, M. A., & Pluim, J. P. (2010). elastix: a toolbox for intensity-based medical image registration. *IEEE Trans Med Imaging*, *29*(1), 196-205. https://doi.org/10.1109/tmi.2009.2035616

Knutson, A. R., Hopkins, R. O., & Squire, L. R. (2013). A pencil rescues impaired performance on a visual discrimination task in patients with medial temporal lobe lesions. *Learn Mem*, *20*(11), 607-610. https://doi.org/10.1101/lm.032490.113

Kocsis, B., Bragin, A., & Buzsáki, G. (1999). Interdependence of multiple theta generators in the hippocampus: a partial coherence analysis. *J Neurosci*, *19*(14), 6200-6212. https://doi.org/10.1523/jneurosci.19-14-06200.1999

Koelewijn, L., Bompas, A., Tales, A., Brookes, M. J., Muthukumaraswamy, S. D., Bayer, A., & Singh, K. D. (2017). Alzheimer's disease disrupts alpha and beta-band resting-state oscillatory network connectivity. *Clin Neurophysiol*, *128*(11), 2347-2357. https://doi.org/10.1016/j.clinph.2017.04.018

Koelewijn, L., Lancaster, T. M., Linden, D., Dima, D. C., Routley, B. C., Magazzini, L., Barawi, K., Brindley, L., Adams, R., Tansey, K. E., Bompas, A., Tales, A., Bayer, A., & Singh, K. (2019). Oscillatory hyperactivity and hyperconnectivity in young APOE-ε4 carriers and hypoconnectivity in Alzheimer's disease. *Elife*, *8*. https://doi.org/10.7554/eLife.36011

Kong, X. Z., Wang, X., Pu, Y., Huang, L., Hao, X., Zhen, Z., & Liu, J. (2017). Human navigation network: the intrinsic functional organization and behavioral relevance. *Brain Struct Funct*, *222*(2), 749-764. https://doi.org/10.1007/s00429-016-1243-8

Konkle, T., & Caramazza, A. (2017). The Large-Scale Organization of Object-Responsive Cortex Is Reflected in Resting-State Network Architecture. *Cereb Cortex*, *27*(10), 4933-4945. https://doi.org/10.1093/cercor/bhw287

Kramer, M. A., Tort, A. B., & Kopell, N. J. (2008). Sharp edge artifacts and spurious coupling in EEG frequency comodulation measures. *J Neurosci Methods*, *170*(2), 352-357. https://doi.org/10.1016/j.jneumeth.2008.01.020

Kwok, S. C., Mitchell, A. S., & Buckley, M. J. (2015). Adaptability to changes in temporal structure is fornix-dependent. *Learn Mem*, *22*(8), 354-359. https://doi.org/10.1101/lm.038851.115

Lampinen, B., Szczepankiewicz, F., Mårtensson, J., van Westen, D., Sundgren, P. C., & Nilsson, M. (2017). Neurite density imaging versus imaging of microscopic anisotropy in diffusion MRI: A model comparison using spherical tensor encoding. *Neuroimage*, *147*, 517-531. https://doi.org/10.1016/j.neuroimage.2016.11.053

Latini, F. (2015). New insights in the limbic modulation of visual inputs: the role of the inferior longitudinal fasciculus and the Li-Am bundle. *Neurosurg Rev*, *38*(1), 179-189; discussion 189-190. https://doi.org/10.1007/s10143-014-0583-1

Latini, F., Mårtensson, J., Larsson, E. M., Fredrikson, M., Åhs, F., Hjortberg, M., Aldskogius, H., & Ryttlefors, M. (2017). Segmentation of the inferior longitudinal fasciculus in the human brain: A white matter dissection and diffusion tensor tractography study. *Brain Res*, *1675*, 102-115. https://doi.org/10.1016/j.brainres.2017.09.005

Leao, R. N., Targino, Z. H., Colom, L. V., & Fisahn, A. (2015). Interconnection and synchronization of neuronal populations in the mouse medial septum/diagonal band of Broca. *J Neurophysiol*, *113*(3), 971-980. https://doi.org/10.1152/jn.00367.2014

Lee, A. C., Brodersen, K. H., & Rudebeck, S. R. (2013). Disentangling spatial perception and spatial memory in the hippocampus: a univariate and multivariate pattern analysis fMRI study. *J Cogn Neurosci*, *25*(4), 534-546. https://doi.org/10.1162/jocn_a_00301

Lee, A. C., Buckley, M. J., Pegman, S. J., Spiers, H., Scahill, V. L., Gaffan, D., Bussey, T. J., Davies, R. R., Kapur, N., Hodges, J. R., & Graham, K. S. (2005). Specialization in the medial temporal lobe for processing of objects and scenes. *Hippocampus*, *15*(6), 782-797. https://doi.org/10.1002/hipo.20101

Lee, A. C., Bussey, T. J., Murray, E. A., Saksida, L. M., Epstein, R. A., Kapur, N., Hodges, J. R., & Graham, K. S. (2005). Perceptual deficits in amnesia: challenging the medial temporal lobe 'mnemonic' view. *Neuropsychologia*, *43*(1), 1-11. https://doi.org/10.1016/j.neuropsychologia.2004.07.017

Lee, A. C., & Rudebeck, S. R. (2010). Human medial temporal lobe damage can disrupt the perception of single objects. *J Neurosci*, *30*(19), 6588-6594. https://doi.org/10.1523/jneurosci.0116-10.2010

Lee, A. C., Scahill, V. L., & Graham, K. S. (2008). Activating the medial temporal lobe during oddity judgment for faces and scenes. *Cereb Cortex*, *18*(3), 683-696. https://doi.org/10.1093/cercor/bhm104

Lee, B., & Newberg, A. (2005). Neuroimaging in traumatic brain imaging. *NeuroRx*, *2*(2), 372-383. https://doi.org/10.1602/neurorx.2.2.372

Lee, C. H., Ryu, J., Lee, S. H., Kim, H., & Lee, I. (2016). Functional cross-hemispheric shift between object-place paired associate memory and spatial memory in the human hippocampus. *Hippocampus*, *26*(8), 1061-1077. https://doi.org/10.1002/hipo.22587

Lee, K., Lee, Y. M., Park, J. M., Lee, B. D., Moon, E., Jeong, H. J., Kim, S. Y., Chung, Y. I., & Kim, J. H. (2019). Right hippocampus atrophy is independently associated with Alzheimer's disease with psychosis. *Psychogeriatrics*, *19*(2), 105-110. https://doi.org/10.1111/psyg.12369

Lee, P. L., Chou, K. H., Chung, C. P., Lai, T. H., Zhou, J. H., Wang, P. N., & Lin, C. P. (2020). Posterior Cingulate Cortex Network Predicts Alzheimer's Disease Progression. *Front Aging Neurosci*, *12*, 608667. https://doi.org/10.3389/fnagi.2020.608667

Leech, R., & Sharp, D. J. (2014). The role of the posterior cingulate cortex in cognition and disease. *Brain*, *137*(1), 12-32. https://doi.org/10.1093/brain/awt162

Leech, R., & Smallwood, J. (2019). The posterior cingulate cortex: Insights from structure and function. *Handb Clin Neurol*, *166*, 73-85. https://doi.org/10.1016/b978-0-444-64196-0.00005-4

Leemans A, Jeurissen B, Sijbers J, and Jones DK. ExploreDTI: a graphical toolbox for processing, analyzing, and visualizing diffusion MR data. In: 17th Annual Meeting of Intl Soc Mag Reson Med, p. 3537, Hawaii, USA, 2009.

Lega, B., Burke, J., Jacobs, J., & Kahana, M. J. (2016). Slow-Theta-to-Gamma Phase-Amplitude Coupling in Human Hippocampus Supports the Formation of New Episodic Memories. *Cereb Cortex*, *26*(1), 268-278. https://doi.org/10.1093/cercor/bhu232

Lega, B., Germi, J., & Rugg, M. D. (2017). Modulation of oscillatory power and connectivity in the human posterior cingulate cortex supports the encoding and retrieval of episodic memories. *Journal of Cognitive Neuroscience*, *29*(8), 1415-1432. https://doi.org/10.1162/jocn_a_01133

Lescroart, M. D., Stansbury, D. E., & Gallant, J. L. (2015). Fourier power, subjective distance, and object categories all provide plausible models of BOLD responses in scene-selective visual areas. *Front Comput Neurosci*, *9*, 135. https://doi.org/10.3389/fncom.2015.00135

Li, J., Kronemer, S. I., Herman, W. X., Kwon, H., Ryu, J. H., Micek, C., Wu, Y., Gerrard, J., Spencer, D. D., & Blumenfeld, H. (2019). Default mode and visual network activity in an attention task: Direct measurement with intracranial EEG. *Neuroimage*, *201*, 116003. https://doi.org/10.1016/j.neuroimage.2019.07.016

Li, J. Y., Kuo, T. B., Hsieh, S. S., & Yang, C. C. (2008). Changes in electroencephalogram and heart rate during treadmill exercise in the rat. *Neurosci Lett*, *434*(2), 175-178. https://doi.org/10.1016/j.neulet.2008.01.052

Li, S., Bai, W., Liu, T., Yi, H., & Tian, X. (2012). Increases of theta-low gamma coupling in rat medial prefrontal cortex during working memory task. *Brain Res Bull*, *89*(3-4), 115-123. https://doi.org/10.1016/j.brainresbull.2012.07.012

Liang, W. S., Reiman, E. M., Valla, J., Dunckley, T., Beach, T. G., Grover, A., Niedzielko, T. L., Schneider, L. E., Mastroeni, D., Caselli, R., Kukull, W., Morris, J. C., Hulette, C. M., Schmechel, D., Rogers, J., & Stephan, D. A. (2008). Alzheimer's disease is associated with reduced expression of energy metabolism genes in posterior cingulate neurons. *Proc Natl Acad Sci U S A*, *105*(11), 4441-4446. https://doi.org/10.1073/pnas.0709259105

Lin, J. J., Rugg, M. D., Das, S., Stein, J., Rizzuto, D. S., Kahana, M. J., & Lega, B. C. (2017). Theta band power increases in the posterior hippocampus predict successful episodic memory encoding in humans. *Hippocampus*, *27*(10), 1040-1053. https://doi.org/10.1002/hipo.22751

Lisman, J. E., & Jensen, O. (2013). The theta-gamma neural code. *Neuron*, *77*(6), 1002-1016. https://doi.org/10.1016/j.neuron.2013.03.007

Liu, W., & Weiss, S. (2010). *Wideband Beamforming: Concepts and Techniques*. Wiley.

Long, N. M., & Kahana, M. J. (2019). Hippocampal contributions to serial-order memory. *Hippocampus*, *29*(3), 252-259. https://doi.org/10.1002/hipo.23025

Lord, A. R., Li, M., Demenescu, L. R., van den Meer, J., Borchardt, V., Krause, A. L., Heinze, H. J., Breakspear, M., & Walter, M. (2017). Richness in Functional Connectivity Depends on the Neuronal Integrity within the Posterior Cingulate Cortex. *Front Neurosci*, *11*, 184. https://doi.org/10.3389/fnins.2017.00184

Ly, M., Adluru, N., Destiche, D. J., Lu, S. Y., Oh, J. M., Hoscheidt, S. M., Alexander, A. L., Okonkwo, O. C., Rowley, H. A., Sager, M. A., Johnson, S. C., & Bendlin, B. B. (2016). Fornix Microstructure and Memory Performance Is Associated with Altered Neural

Connectivity during Episodic Recognition. *J Int Neuropsychol Soc*, *22*(2), 191-204. https://doi.org/10.1017/s1355617715001216

MacDonald, C. J., Lepage, K. Q., Eden, U. T., & Eichenbaum, H. (2011). Hippocampal "time cells" bridge the gap in memory for discontiguous events. *Neuron*, *71*(4), 737-749. https://doi.org/10.1016/j.neuron.2011.07.012

MacDonald, H. J., Brittain, J. S., Spitzer, B., Hanslmayr, S., & Jenkinson, N. (2019). Memory deficits in Parkinson's disease are associated with reduced beta power modulation. *Brain Commun*, *1*(1), fcz040. https://doi.org/10.1093/braincomms/fcz040

Mackey, W. E., Devinsky, O., Doyle, W. K., Golfinos, J. G., & Curtis, C. E. (2016). Human parietal cortex lesions impact the precision of spatial working memory. *J Neurophysiol*, *116*(3), 1049-1054. https://doi.org/10.1152/jn.00380.2016

Magazzini, L., & Singh, K. D. (2018). Spatial attention modulates visual gamma oscillations across the human ventral stream. *Neuroimage*, *166*, 219-229. https://doi.org/10.1016/j.neuroimage.2017.10.069

Makowski. (2018). The psycho Package: an Efficient and Publishing-Oriented Workflow for Psychological Science. *Journal of Open Source Software*, *3*(420). https://doi.org/https://doi.org/10.21105/joss.00470

Malhotra, P., Coulthard, E. J., & Husain, M. (2009). Role of right posterior parietal cortex in maintaining attention to spatial locations over time. *Brain*, *132*(Pt 3), 645-660. https://doi.org/10.1093/brain/awn350

Malhotra, P., Jäger, H. R., Parton, A., Greenwood, R., Playford, E. D., Brown, M. M., Driver, J., & Husain, M. (2005). Spatial working memory capacity in unilateral neglect. *Brain*, *128*(Pt 2), 424-435. https://doi.org/10.1093/brain/awh372

Marquetand, J., Vannoni, S., Carboni, M., Li Hegner, Y., Stier, C., Braun, C., & Focke, N. K. (2019). Reliability of Magnetoencephalography and High-Density Electroencephalography Resting-State Functional Connectivity Metrics. *Brain Connect*, *9*(7), 539-553. https://doi.org/10.1089/brain.2019.0662

Martin, C. B., Cowell, R. A., Gribble, P. L., Wright, J., & Kohler, S. (2016). Distributed category-specific recognition-memory signals in human perirhinal cortex. *Hippocampus*, *26*(4), 423-436. https://doi.org/10.1002/hipo.22531

MATLAB. (2015). *MATLAB version 8.5.0.197613 (R2015a)*. Natick, Massachusetts: The MathWorks Inc.

Mayhew, S. D., Ostwald, D., Porcaro, C., & Bagshaw, A. P. (2013). Spontaneous EEG alpha oscillation interacts with positive and negative BOLD responses in the visual-auditory cortices and default-mode network. *Neuroimage*, *76*, 362-372. https://doi.org/10.1016/j.neuroimage.2013.02.070

Mayo, C. D., Garcia-Barrera, M. A., Mazerolle, E. L., Ritchie, L. J., Fisk, J. D., & Gawryluk, J. R. (2018). Relationship Between DTI Metrics and Cognitive Function in Alzheimer's Disease. *Front Aging Neurosci*, *10*, 436. https://doi.org/10.3389/fnagi.2018.00436

Mazaheri, A., van Schouwenburg, M. R., Dimitrijevic, A., Denys, D., Cools, R., & Jensen, O. (2014). Region-specific modulations in oscillatory alpha activity serve to facilitate processing in the visual and auditory modalities. *Neuroimage*, *87*, 356-362. https://doi.org/10.1016/j.neuroimage.2013.10.052

McCormick, C., Quraan, M., Cohn, M., Valiante, T. A., & McAndrews, M. P. (2013). Default mode network connectivity indicates episodic memory capacity in mesial temporal lobe epilepsy. *Epilepsia*, *54*(5), 809-818. https://doi.org/10.1111/epi.12098

McCormick, C., Rosenthal, C. R., Miller, T. D., & Maguire, E. A. (2018). Mind-Wandering in People with Hippocampal Damage. *J Neurosci*, *38*(11), 2745-2754. https://doi.org/10.1523/jneurosci.1812-17.2018

McDonald, J. H. (2014). *Handbook of Biological Statistics* (3rd ed. ed.). Sparky House Publishing.

McNab, J. A., Edlow, B. L., Witzel, T., Huang, S. Y., Bhat, H., Heberlein, K., Feiweier, T., Liu, K., Keil, B., Cohen-Adad, J., Tisdall, M. D., Folkerth, R. D., Kinney, H. C., & Wald, L. L. (2013). The Human Connectome Project and beyond: initial applications of 300 mT/m gradients. *Neuroimage*, *80*, 234-245. https://doi.org/10.1016/j.neuroimage.2013.05.074

Meador, K. J., Ray, P. G., Echauz, J. R., Loring, D. W., & Vachtsevanos, G. J. (2002). Gamma coherence and conscious perception. *Neurology*, *59*(6), 847-854. https://doi.org/10.1212/wnl.59.6.847

Messaritaki, E., Foley, S., Schiavi, S., Magazzini, L., Routley, B., Jones, D. K., & Singh, K. D. (2020). Predicting MEG resting-state functional connectivity using microstructural information. *bioRxiv*, 2020.2009.2015.298307. https://doi.org/10.1101/2020.09.15.298307

Metzler-Baddeley, C., Hunt, S., Jones, D. K., Leemans, A., Aggleton, J. P., & O'Sullivan, M. J. (2012). Temporal association tracts and the breakdown of episodic memory in mild cognitive impairment. *Neurology*, *79*(23), 2233-2240. https://doi.org/10.1212/WNL.0b013e31827689e8

Metzler-Baddeley, C., Jones, D. K., Belaroussi, B., Aggleton, J. P., & O'Sullivan, M. J. (2011). Frontotemporal connections in episodic memory and aging: a diffusion MRI tractography study. *J Neurosci*, *31*(37), 13236-13245. https://doi.org/10.1523/jneurosci.2317-11.2011

Metzler-Baddeley, C., Mole, J. P., Sims, R., Fasano, F., Evans, J., Jones, D. K., Aggleton, J. P., & Baddeley, R. J. (2019). Fornix white matter glia damage causes hippocampal gray matter damage during age-dependent limbic decline. *Sci Rep*, *9*(1), 1060. https://doi.org/10.1038/s41598-018-37658-5

Meyer, S. S., Rossiter, H., Brookes, M. J., Woolrich, M. W., Bestmann, S., & Barnes, G. R. (2017). Using generative models to make probabilistic statements about hippocampal engagement in MEG. *Neuroimage*, *149*, 468-482. https://doi.org/10.1016/j.neuroimage.2017.01.029

Michalareas, G., Vezoli, J., van Pelt, S., Schoffelen, J. M., Kennedy, H., & Fries, P. (2016). Alpha-Beta and Gamma Rhythms Subserve Feedback and Feedforward Influences among Human Visual Cortical Areas. *Neuron*, *89*(2), 384-397. https://doi.org/10.1016/j.neuron.2015.12.018

Michalowski, J. M., Weymar, M., & Hamm, A. O. (2014). Remembering the object you fear: brain potentials during recognition of spiders in spider-fearful individuals. *PLoS One*, *9*(10), e109537. https://doi.org/10.1371/journal.pone.0109537

Michel, C. M., & He, B. (2019). EEG source localization. *Handb Clin Neurol*, *160*, 85-101. https://doi.org/10.1016/b978-0-444-64032-1.00006-0

Mielke, M. M., Kozauer, N. A., Chan, K. C., George, M., Toroney, J., Zerrate, M., Bandeen-Roche, K., Wang, M. C., Vanzijl, P., Pekar, J. J., Mori, S., Lyketsos, C. G., & Albert, M. (2009). Regionally-specific diffusion tensor imaging in mild cognitive impairment and Alzheimer's disease. *Neuroimage*, *46*(1), 47-55. https://doi.org/10.1016/j.neuroimage.2009.01.054

Mielke, M. M., Okonkwo, O. C., Oishi, K., Mori, S., Tighe, S., Miller, M. I., Ceritoglu, C., Brown, T., Albert, M., & Lyketsos, C. G. (2012). Fornix integrity and hippocampal volume predict memory decline and progression to Alzheimer's disease. *Alzheimers Dement*, *8*(2), 105-113. https://doi.org/10.1016/j.jalz.2011.05.2416

Miller, J., Watrous, A. J., Tsitsiklis, M., Lee, S. A., Sheth, S. A., Schevon, C. A., Smith, E. H., Sperling, M. R., Sharan, A., Asadi-Pooya, A. A., Worrell, G. A., Meisenhelter, S., Inman, C. S., Davis, K. A., Lega, B., Wanda, P. A., Das, S. R., Stein, J. M., Gorniak, R., & Jacobs, J. (2018). Lateralized hippocampal oscillations underlie distinct aspects of human spatial memory and navigation. *Nat Commun*, *9*(1), 2423. https://doi.org/10.1038/s41467-018-04847-9

Mills, T., Lalancette, M., Moses, S. N., Taylor, M. J., & Quraan, M. A. (2012). Techniques for detection and localization of weak hippocampal and medial frontal sources using beamformers in MEG. *Brain Topogr*, *25*(3), 248-263. https://doi.org/10.1007/s10548-012-0217-2

Minami, S., Oishi, H., Takemura, H., & Amano, K. (2020). Inter-individual Differences in Occipital Alpha Oscillations Correlate with White Matter Tissue Properties of the Optic Radiation. *eNeuro*, *7*(2). https://doi.org/10.1523/eneuro.0224-19.2020

Monk, A. M., Dalton, M. A., Barnes, G. R., & Maguire, E. A. (2020). The role of hippocampal-vmPFC neural dynamics in building mental representations. *bioRxiv*, 2020.2004.2030.069765. https://doi.org/10.1101/2020.04.30.069765

Montaldi, D., Spencer, T. J., Roberts, N., & Mayes, A. R. (2006). The neural system that mediates familiarity memory. *Hippocampus*, *16*(5), 504-520. https://doi.org/10.1002/hipo.20178

Morey, R. D., & Rouder, J. N. (2018). BayesFactor: Computation of Bayes Factors for Common Designs. URL: https://richarddmorey.github.io/BayesFactor/

Morgan, H. M., Muthukumaraswamy, S. D., Hibbs, C. S., Shapiro, K. L., Bracewell, R. M., Singh, K. D., & Linden, D. E. (2011). Feature integration in visual working memory: parietal gamma activity is related to cognitive coordination. *J Neurophysiol*, *106*(6), 3185-3194. https://doi.org/10.1152/jn.00246.2011

Mori, S., & Tournier, J. D. (2013). *Introduction to Diffusion Tensor Imaging: And Higher Order Models*. Elsevier Science.

Mormann, F., Kornblith, S., Cerf, M., Ison, M. J., Kraskov, A., Tran, M., Knieling, S., Quian Quiroga, R., Koch, C., & Fried, I. (2017). Scene-selective coding by single neurons in the human parahippocampal cortex. *Proc Natl Acad Sci U S A*, *114*(5), 1153-1158. https://doi.org/10.1073/pnas.1608159113

Moses, S. N., Ryan, J. D., Bardouille, T., Kovacevic, N., Hanlon, F. M., & McIntosh, A. R. (2009). Semantic information alters neural activation during transverse patterning performance. *Neuroimage*, *46*(3), 863-873. https://doi.org/10.1016/j.neuroimage.2009.02.042

Mosher, J. C., Lewis, P. S., & Leahy, R. M. (1992). Multiple dipole modeling and localization from spatio-temporal MEG data. *IEEE Trans Biomed Eng*, *39*(6), 541-557. https://doi.org/10.1109/10.141192

Mukamel, R., Gelbard, H., Arieli, A., Hasson, U., Fried, I., & Malach, R. (2005). Coupling between neuronal firing, field potentials, and FMRI in human auditory cortex. *Science*, *309*(5736), 951-954. https://doi.org/10.1126/science.1110913

Mukudi, P. B. L., & Hills, P. J. (2019). The combined influence of the own-age, -gender, and -ethnicity biases on face recognition. *Acta Psychol (Amst)*, *194*, 1-6. https://doi.org/10.1016/j.actpsy.2019.01.009

Mullally, S. L., Intraub, H., & Maguire, E. A. (2012). Attenuated boundary extension produces a paradoxical memory advantage in amnesic patients. *Curr Biol*, *22*(4), 261-268. https://doi.org/10.1016/j.cub.2012.01.001

Mundy, M. E., Downing, P. E., & Graham, K. S. (2012). Extrastriate cortex and medial temporal lobe regions respond differentially to visual feature overlap within preferred stimulus category. *Neuropsychologia*, *50*(13), 3053-3061. https://doi.org/10.1016/j.neuropsychologia.2012.07.006

Murray, E. A., & Bussey, T. J. (1999). Perceptual-mnemonic functions of the perirhinal cortex. *Trends Cogn Sci*, *3*(4), 142-151.

Murray, E. A., Bussey, T. J., & Saksida, L. M. (2007). Visual perception and memory: a new view of medial temporal lobe function in primates and rodents. *Annu Rev Neurosci*, *30*, 99-122. https://doi.org/10.1146/annurev.neuro.29.051605.113046

Murray, E. A., Wise, S. P., & Graham, K. S. (2017). *The Evolution of Memory Systems: Ancestors, Anatomy, and Adaptations*. Oxford University Press.

Murray, E. A., Wise, S. P., & Graham, K. S. (2018). Representational specializations of the hippocampus in phylogenetic perspective. *Neurosci Lett*, *680*, 4-12. https://doi.org/10.1016/j.neulet.2017.04.065

Musch, K., Hamame, C. M., Perrone-Bertolotti, M., Minotti, L., Kahane, P., Engel, A. K., Lachaux, J. P., & Schneider, T. R. (2014). Selective attention modulates high-frequency activity in the face-processing network. *Cortex*, *60*, 34-51. https://doi.org/10.1016/j.cortex.2014.06.006

Muthukumaraswamy, S. D. (2013). High-frequency brain activity and muscle artifacts in MEG/EEG: a review and recommendations. *Front Hum Neurosci*, *7*, 138. https://doi.org/10.3389/fnhum.2013.00138

Mårtensson, J., Lätt, J., Åhs, F., Fredrikson, M., Söderlund, H., Schiöth, H. B., Kok, J., Kremer, B., van Westen, D., Larsson, E. M., & Nilsson, M. (2018). Diffusion tensor imaging and tractography of the white matter in normal aging: The rate-of-change differs between segments within tracts. *Magn Reson Imaging*, *45*, 113-119. https://doi.org/10.1016/j.mri.2017.03.007

Nasr, S., Devaney, K. J., & Tootell, R. B. (2013). Spatial encoding and underlying circuitry in scene-selective cortex. *Neuroimage*, *83*, 892-900. https://doi.org/10.1016/j.neuroimage.2013.07.030

Natu, V. S., Lin, J. J., Burks, A., Arora, A., Rugg, M. D., & Lega, B. (2019). Stimulation of the Posterior Cingulate Cortex Impairs Episodic Memory Encoding. *J Neurosci*, *39*(36), 7173-7182. https://doi.org/10.1523/jneurosci.0698-19.2019

Naya, Y., Chen, H., Yang, C., & Suzuki, W. A. (2017). Contributions of primate prefrontal cortex and medial temporal lobe to temporal-order memory. *Proc Natl Acad Sci U S A*, *114*(51), 13555-13560. https://doi.org/10.1073/pnas.1712711114

Nieuwenhuis, S., De Geus, E. J., & Aston-Jones, G. (2011). The anatomical and functional relationship between the P3 and autonomic components of the orienting response. *Psychophysiology*, *48*(2), 162-175. https://doi.org/10.1111/j.1469-8986.2010.01057.x

Nishida, K., Yoshimura, M., Isotani, T., Yoshida, T., Kitaura, Y., Saito, A., Mii, H., Kato, M., Takekita, Y., Suwa, A., Morita, S., & Kinoshita, T. (2011). Differences in quantitative EEG between frontotemporal dementia and Alzheimer's disease as revealed by LORETA. *Clin Neurophysiol*, *122*(9), 1718-1725. https://doi.org/10.1016/j.clinph.2011.02.011

Nolte, G. (2003). The magnetic lead field theorem in the quasi-static approximation and its use for magnetoencephalography forward calculation in realistic volume conductors. *Phys Med Biol*, *48*(22), 3637-3652.

Nolte, G., Bai, O., Wheaton, L., Mari, Z., Vorbach, S., & Hallett, M. (2004). Identifying true brain interaction from EEG data using the imaginary part of coherency. *Clin Neurophysiol*, *115*(10), 2292-2307. https://doi.org/10.1016/j.clinph.2004.04.029

Norris, D. (2017). Short-term memory and long-term memory are still different. *Psychol Bull*, *143*(9), 992-1009. https://doi.org/10.1037/bul0000108

O'Keefe, J., & Dostrovsky, J. (1971). The hippocampus as a spatial map. Preliminary evidence from unit activity in the freely-moving rat. *Brain Res*, *34*(1), 171-175.

O'Keefe, J., & Recce, M. L. (1993). Phase relationship between hippocampal place units and the EEG theta rhythm. *Hippocampus*, *3*(3), 317-330. https://doi.org/10.1002/hipo.450030307

O'Neil, E. B., Barkley, V. A., & Kohler, S. (2013). Representational demands modulate involvement of perirhinal cortex in face processing. *Hippocampus*, *23*(7), 592-605. https://doi.org/10.1002/hipo.22117

O'Neil, E. B., Hutchison, R. M., McLean, D. A., & Kohler, S. (2014). Resting-state fMRI reveals functional connectivity between face-selective perirhinal cortex and the fusiform

face area related to face inversion. *Neuroimage*, *92*, 349-355. https://doi.org/10.1016/j.neuroimage.2014.02.005

Olson, I. R., Ezzyat, Y., Plotzker, A., & Chatterjee, A. (2015). The end point of the ventral visual stream: face and non-face perceptual deficits following unilateral anterior temporal lobe damage. *Neurocase*, *21*(5), 554-562. https://doi.org/10.1080/13554794.2014.959025

Oostenveld, R., Fries, P., Maris, E., & Schoffelen, J. M. (2011). FieldTrip: Open source software for advanced analysis of MEG, EEG, and invasive electrophysiological data. *Comput Intell Neurosci*, *2011*, 156869. https://doi.org/10.1155/2011/156869

Ortibus, E., Verhoeven, J., Sunaert, S., Casteels, I., de Cock, P., & Lagae, L. (2012). Integrity of the inferior longitudinal fasciculus and impaired object recognition in children: a diffusion tensor imaging study. *Dev Med Child Neurol*, *54*(1), 38-43. https://doi.org/10.1111/j.1469-8749.2011.04147.x

Ossandón, T., Jerbi, K., Vidal, J. R., Bayle, D. J., Henaff, M. A., Jung, J., Minotti, L., Bertrand, O., Kahane, P., & Lachaux, J. P. (2011). Transient suppression of broadband gamma power in the default-mode network is correlated with task complexity and subject performance. *J Neurosci*, *31*(41), 14521-14530. https://doi.org/10.1523/jneurosci.2483-11.2011

Ota, M., Noda, T., Sato, N., Hidese, S., Teraishi, T., Setoyama, S., Sone, D., Matsuda, H., & Kunugi, H. (2018). The use of diffusional kurtosis imaging and neurite orientation dispersion and density imaging of the brain in major depressive disorder. *J Psychiatr Res*, *98*, 22-29. https://doi.org/10.1016/j.jpsychires.2017.12.011

Palmer, J., Huk, A. C., & Shadlen, M. N. (2005). The effect of stimulus strength on the speed and accuracy of a perceptual decision. *J Vis*, *5*(5), 376-404. https://doi.org/10.1167/5.5.1

Palop, J. J., Chin, J., & Mucke, L. (2006). A network dysfunction perspective on neurodegenerative diseases. *Nature*, *443*(7113), 768-773. https://doi.org/10.1038/nature05289

Palva, J. M., Palva, S., & Kaila, K. (2005). Phase synchrony among neuronal oscillations in the human cortex. *J Neurosci*, *25*(15), 3962-3972. https://doi.org/10.1523/jneurosci.4250-04.2005

Pan, W. X., & McNaughton, N. (2004). The supramammillary area: its organization, functions and relationship to the hippocampus. *Prog Neurobiol*, *74*(3), 127-166. https://doi.org/10.1016/j.pneurobio.2004.09.003

Papagno, C. (2011). Naming and the role of the uncinate fasciculus in language function. *Curr Neurol Neurosci Rep*, *11*(6), 553-559. https://doi.org/10.1007/s11910-011-0219-6

Park, J., Lee, H., Kim, T., Park, G. Y., Lee, E. M., Baek, S., Ku, J., Kim, I. Y., Kim, S. I., Jang, D. P., & Kang, J. K. (2014). Role of low- and high-frequency oscillations in the human hippocampus for encoding environmental novelty during a spatial navigation task. *Hippocampus*, *24*(11), 1341-1352. https://doi.org/10.1002/hipo.22315

Pastalkova, E., Itskov, V., Amarasingham, A., & Buzsáki, G. (2008). Internally generated cell assembly sequences in the rat hippocampus. *Science*, *321*(5894), 1322-1327. https://doi.org/10.1126/science.1159775

Pasternak, O., Sochen, N., Gur, Y., Intrator, N., & Assaf, Y. (2009). Free water elimination and mapping from diffusion MRI. *Magn Reson Med*, *62*(3), 717-730. https://doi.org/10.1002/mrm.22055

Patil, I. (2021). Visualizations with statistical details: The 'ggstatsplot' approach. Journal of Open Source Software, 6(61), 3167. https://doi.org/10.21105/joss.03167

Pearson, K. (1897). Mathematical contributions to the theory of evolution.—on a form of spurious correlation which may arise when indices are used in the measurement of organs. *Proceedings of the royal society of london*, *60*(359-367), 489-498.

Perry, G. (2016). The visual gamma response to faces reflects the presence of sensory evidence and not awareness of the stimulus. *R Soc Open Sci*, *3*(3), 150593. https://doi.org/10.1098/rsos.150593

Perry, G., Randle, J. M., Koelewijn, L., Routley, B. C., & Singh, K. D. (2015). Linear tuning of gamma amplitude and frequency to luminance contrast: evidence from a continuous mapping paradigm. *PLoS One*, *10*(4), e0124798. https://doi.org/10.1371/journal.pone.0124798

Perry, G., & Singh, K. D. (2014). Localizing evoked and induced responses to faces using magnetoencephalography. *Eur J Neurosci*, *39*(9), 1517-1527. https://doi.org/10.1111/ejn.12520

Pierpaoli, C., Jezzard, P., Basser, P. J., Barnett, A., & Di Chiro, G. (1996). Diffusion tensor MR imaging of the human brain. *Radiology*, *201*(3), 637-648. https://doi.org/10.1148/radiology.201.3.8939209

Pievani, M., Agosta, F., Pagani, E., Canu, E., Sala, S., Absinta, M., Geroldi, C., Ganzola, R., Frisoni, G. B., & Filippi, M. (2010). Assessment of white matter tract damage in mild cognitive impairment and Alzheimer's disease. *Hum Brain Mapp*, *31*(12), 1862-1875. https://doi.org/10.1002/hbm.20978

Pisella, L. (2017). Visual perception is dependent on visuospatial working memory and thus on the posterior parietal cortex. *Ann Phys Rehabil Med*, *60*(3), 141-147. https://doi.org/10.1016/j.rehab.2016.01.002

Pitcher, D., Walsh, V., & Duchaine, B. (2011). The role of the occipital face area in the cortical face perception network. *Exp Brain Res*, *209*(4), 481-493. https://doi.org/10.1007/s00221-011-2579-1

Pizzo, F., Roehri, N., Medina Villalon, S., Trébuchon, A., Chen, S., Lagarde, S., Carron, R., Gavaret, M., Giusiano, B., McGonigal, A., Bartolomei, F., Badier, J. M., & Bénar, C. G. (2019). Deep brain activities can be detected with magnetoencephalography. *Nat Commun*, *10*(1), 971. https://doi.org/10.1038/s41467-019-08665-5

Postans, M., Hodgetts, C. J., Mundy, M. E., Jones, D. K., Lawrence, A. D., & Graham, K. S. (2014). Interindividual variation in fornix microstructure and macrostructure is related to visual discrimination accuracy for scenes but not faces. *J Neurosci*, *34*(36), 12121-12126. https://doi.org/10.1523/jneurosci.0026-14.2014

Pu, M., Heleven, E., Delplanque, J., Gibert, N., Ma, Q., Funghi, G., & Van Overwalle, F. (2020). The posterior cerebellum supports the explicit sequence learning linked to trait attribution. *Cogn Affect Behav Neurosci*, *20*(4), 798-815. https://doi.org/10.3758/s13415-020-00803-7

Pu, Y., Cheyne, D. O., Cornwell, B. R., & Johnson, B. W. (2018). Non-invasive Investigation of Human Hippocampal Rhythms Using Magnetoencephalography: A Review. *Front Neurosci*, *12*, 273. https://doi.org/10.3389/fnins.2018.00273

Pu, Y., Cornwell, B. R., Cheyne, D., & Johnson, B. W. (2017). The functional role of human right hippocampal/parahippocampal theta rhythm in environmental encoding during virtual spatial navigation. *Hum Brain Mapp*, *38*(3), 1347-1361. https://doi.org/10.1002/hbm.23458

Pu, Y., Cornwell, B. R., Cheyne, D., & Johnson, B. W. (2018). High-gamma activity in the human hippocampus and parahippocampus during inter-trial rest periods of a virtual navigation task. *Neuroimage*, *178*, 92-103. https://doi.org/10.1016/j.neuroimage.2018.05.029

Pu, Y., Cornwell, B. R., Cheyne, D., & Johnson, B. W. (2020). Gender differences in navigation performance are associated with differential theta and high-gamma activities in the hippocampus and parahippocampus. *Behav Brain Res*, *391*, 112664. https://doi.org/10.1016/j.bbr.2020.112664

Quental, N. B., Brucki, S. M., & Bueno, O. F. (2013). Visuospatial function in early Alzheimer's disease--the use of the Visual Object and Space Perception (VOSP) battery. *PLoS One*, *8*(7), e68398. https://doi.org/10.1371/journal.pone.0068398

Quraan, M. A., Moses, S. N., Hung, Y., Mills, T., & Taylor, M. J. (2011). Detection and localization of hippocampal activity using beamformers with MEG: a detailed investigation using simulations and empirical data. *Hum Brain Mapp*, *32*(5), 812-827. https://doi.org/10.1002/hbm.21068

R Core Team (2018). R: A language and environment for statistical computing. R Foundation for Statistical Computing, Vienna, Austria. URL http://www.R-project.org/

R Core Team (2019). R: A language and environment for statistical computing. R Foundation for Statistical Computing, Vienna, Austria. URL http://www.R-project.org/

Raftery, A. E. (1995). Bayesian model selection in social research. *Sociological methodology*, 111-163.

Raichle, M. E. (2015). The brain's default mode network. *Annu Rev Neurosci*, *38*, 433-447. https://doi.org/10.1146/annurev-neuro-071013-014030

Ramanan, S., Piguet, O., & Irish, M. (2018). Rethinking the Role of the Angular Gyrus in Remembering the Past and Imagining the Future: The Contextual Integration Model. *Neuroscientist*, *24*(4), 342-352. https://doi.org/10.1177/1073858417735514

Ramani, A., Dalton, C., Miller, D. H., Tofts, P. S., & Barker, G. J. (2002). Precise estimate of fundamental in-vivo MT parameters in human brain in clinically feasible times. *Magn Reson Imaging*, *20*(10), 721-731. https://doi.org/10.1016/s0730-725x(02)00598-2

Ramanoël, S., York, E., Le Petit, M., Lagrené, K., Habas, C., & Arleo, A. (2019). Age-Related Differences in Functional and Structural Connectivity in the Spatial Navigation Brain Network. *Front Neural Circuits*, *13*, 69. https://doi.org/10.3389/fncir.2019.00069

Ranganath, C., & Blumenfeld, R. S. (2005). Doubts about double dissociations between short- and long-term memory. *Trends Cogn Sci*, *9*(8), 374-380. https://doi.org/10.1016/j.tics.2005.06.009

Ranganath, C., & Hsieh, L.-T. (2016). The hippocampus: A special place for time. *Annals of the New York Academy of Sciences*, *1369*(1), 93-110. https://doi.org/10.1111/nyas.13043

Ranganath, C., & Ritchey, M. (2012). Two cortical systems for memory-guided behaviour. *Nat Rev Neurosci*, *13*(10), 713-726. https://doi.org/10.1038/nrn3338

Rawlins, J. N., Feldon, J., & Gray, J. A. (1979). Septo-hippocampal connections and the hippocampal theta rhythm. *Exp Brain Res*, *37*(1), 49-63. https://doi.org/10.1007/bf01474253

Ray, S., & Maunsell, J. H. (2015). Do gamma oscillations play a role in cerebral cortex? *Trends Cogn Sci*, *19*(2), 78-85. https://doi.org/10.1016/j.tics.2014.12.002

Reeders, P. C., Hamm, A. G., Allen, T. A., & Mattfeld, A. T. (2021). Medial prefrontal cortex and hippocampal activity differentially contribute to ordinal and temporal context retrieval during sequence memory. *Learn Mem*, *28*(4), 134-147. https://doi.org/10.1101/lm.052365.120

Reinard, J. C. (2006). *Communication Research Statistics*. SAGE Publications.

Revelle, W. (2020). psych: Procedures for Psychological, Psychometric, and Personality Research. In. Northwestern University.

Riggs, L., Moses, S. N., Bardouille, T., Herdman, A. T., Ross, B., & Ryan, J. D. (2009). A complementary analytic approach to examining medial temporal lobe sources using magnetoencephalography. *Neuroimage*, *45*(2), 627-642. https://doi.org/10.1016/j.neuroimage.2008.11.018

Ripolles, P., Biel, D., Penaloza, C., Kaufmann, J., Marco-Pallares, J., Noesselt, T., & Rodriguez-Fornells, A. (2017). Strength of Temporal White Matter Pathways

Predicts Semantic Learning. *J Neurosci*, *37*(46), 11101-11113. https://doi.org/10.1523/jneurosci.1720-17.2017

Ristori, J., Cocchetti, C., Romani, A., Mazzoli, F., Vignozzi, L., Maggi, M., & Fisher, A. D. (2020). Brain Sex Differences Related to Gender Identity Development: Genes or Hormones? *Int J Mol Sci*, *21*(6). https://doi.org/10.3390/ijms21062123

Ritchey, M., Libby, L. A., & Ranganath, C. (2015). Chapter 3 - Cortico-hippocampal systems involved in memory and cognition: The PMAT framework. In S. O'Mara & M. Tsanov (Eds.), *Progress in Brain Research* (Vol. 219, pp. 45-64). Elsevier.

Rolls, E. T. (2016). Pattern separation, completion, and categorisation in the hippocampus and neocortex. *Neurobiol Learn Mem*, *129*, 4-28. https://doi.org/10.1016/j.nlm.2015.07.008

Rolls, E. T. (2019). The cingulate cortex and limbic systems for emotion, action, and memory. *Brain Struct Funct*, *224*(9), 3001-3018. https://doi.org/10.1007/s00429-019-01945-2

Rolls, E. T., & Mills, P. (2019). The Generation of Time in the Hippocampal Memory System. *Cell Rep*, *28*(7), 1649-1658.e1646. https://doi.org/10.1016/j.celrep.2019.07.042

Ross, R. S., Brown, T. I., & Stern, C. E. (2009). The retrieval of learned sequences engages the hippocampus: Evidence from fMRI. *Hippocampus*, *19*(9), 790-799. https://doi.org/10.1002/hipo.20558

Rottschy, C., Eickhoff, S. B., Schleicher, A., Mohlberg, H., Kujovic, M., Zilles, K., & Amunts, K. (2007). Ventral visual cortex in humans: cytoarchitectonic mapping of two extrastriate areas. *Hum Brain Mapp*, *28*(10), 1045-1059. https://doi.org/10.1002/hbm.20348

Routley, B. C., Singh, K. D., Hamandi, K., & Muthukumaraswamy, S. D. (2017). The effects of AMPA receptor blockade on resting magnetoencephalography recordings. *J Psychopharmacol*, *31*(12), 1527-1536. https://doi.org/10.1177/0269881117736915

Roy, D. S., Kitamura, T., Okuyama, T., Ogawa, S. K., Sun, C., Obata, Y., Yoshiki, A., & Tonegawa, S. (2017). Distinct Neural Circuits for the Formation and Retrieval of Episodic Memories. *Cell*, *170*(5), 1000-1012.e1019. https://doi.org/10.1016/j.cell.2017.07.013

RStudio Team (2015). RStudio: Integrated Development for R. RStudio, PBC, Boston, MA URL http://www.rstudio.com/.

RStudio Team (2020). RStudio: Integrated Development for R. RStudio, PBC, Boston, MA URL http://www.rstudio.com/.

Rudebeck, S. R., Scholz, J., Millington, R., Rohenkohl, G., Johansen-Berg, H., & Lee, A. C. (2009). Fornix microstructure correlates with recollection but not familiarity memory. *J Neurosci*, *29*(47), 14987-14992. https://doi.org/10.1523/jneurosci.4707-09.2009

Rugg, M. D., & Curran, T. (2007). Event-related potentials and recognition memory. *Trends Cogn Sci*, *11*(6), 251-257. https://doi.org/10.1016/j.tics.2007.04.004

Rugg, M. D., Johnson, J. D., Park, H., & Uncapher, M. R. (2008). Encoding-retrieval overlap in human episodic memory: a functional neuroimaging perspective. *Prog Brain Res*, *169*, 339-352. https://doi.org/10.1016/s0079-6123(07)00021-0

Rugg, M. D., & Vilberg, K. L. (2013). Brain networks underlying episodic memory retrieval. *Curr Opin Neurobiol*, *23*(2), 255-260. https://doi.org/10.1016/j.conb.2012.11.005

Rungratsameetaweemana, N., & Squire, L. R. (2018). Preserved capacity for scene construction and shifts in perspective after hippocampal lesions. *Learn Mem*, *25*(8), 347-351. https://doi.org/10.1101/lm.047340.118

Ruzich, E., Crespo-Garcia, M., Dalal, S. S., & Schneiderman, J. F. (2019). Characterizing hippocampal dynamics with MEG: A systematic review and evidence-based guidelines. *Hum Brain Mapp*, *40*(4), 1353-1375. https://doi.org/10.1002/hbm.24445

Sadil, P. S., & Cowell, R. A. (2017). A Computational Model of Perceptual and Mnemonic Deficits in Medial Temporal Lobe Amnesia. *J Cogn Neurosci*, *29*(6), 1075-1088. https://doi.org/10.1162/jocn_a_01106

Salz, D. M., Tiganj, Z., Khasnabish, S., Kohley, A., Sheehan, D., Howard, M. W., & Eichenbaum, H. (2016). Time Cells in Hippocampal Area CA3. *J Neurosci*, *36*(28), 7476-7484. https://doi.org/10.1523/jneurosci.0087-16.2016

Samogin, J., Marino, M., Porcaro, C., Wenderoth, N., Dupont, P., Swinnen, S. P., & Mantini, D. (2020). Frequency-dependent functional connectivity in resting state networks. *Hum Brain Mapp*, *41*(18), 5187-5198. https://doi.org/10.1002/hbm.25184

Sato, K., Kerever, A., Kamagata, K., Tsuruta, K., Irie, R., Tagawa, K., Okazawa, H., Arikawa-Hirasawa, E., Nitta, N., Aoki, I., & Aoki, S. (2017). Understanding microstructure of the brain by comparison of neurite orientation dispersion and density imaging (NODDI) with transparent mouse brain. *Acta Radiol Open*, *6*(4), 2058460117703816. https://doi.org/10.1177/2058460117703816

Sato, N., Nakamura, K., Nakamura, A., Sugiura, M., Ito, K., Fukuda, H., & Kawashima, R. (1999). Different time course between scene processing and face processing: a MEG study. *Neuroreport*, *10*(17), 3633-3637.

Sato, W., Kochiyama, T., Uono, S., Matsuda, K., Usui, K., Inoue, Y., & Toichi, M. (2014). Rapid, high-frequency, and theta-coupled gamma oscillations in the inferior occipital gyrus during face processing. *Cortex*, *60*, 52-68. https://doi.org/10.1016/j.cortex.2014.02.024

Saunders, R. C., & Aggleton, J. P. (2007). Origin and topography of fibers contributing to the fornix in macaque monkeys. *Hippocampus*, *17*(5), 396-411. https://doi.org/10.1002/hipo.20276

Schapiro, A. C., Rogers, T. T., Cordova, N. I., Turk-Browne, N. B., & Botvinick, M. M. (2013). Neural representations of events arise from temporal community structure. *Nat Neurosci*, *16*(4), 486-492. https://doi.org/10.1038/nn.3331

Schapiro, A. C., Turk-Browne, N. B., Norman, K. A., & Botvinick, M. M. (2016). Statistical learning of temporal community structure in the hippocampus. *Hippocampus*, *26*(1), 3-8. https://doi.org/10.1002/hipo.22523

Scheeringa, R., Fries, P., Petersson, K. M., Oostenveld, R., Grothe, I., Norris, D. G., Hagoort, P., & Bastiaansen, M. C. (2011). Neuronal dynamics underlying high- and low-frequency EEG oscillations contribute independently to the human BOLD signal. *Neuron*, *69*(3), 572-583. https://doi.org/10.1016/j.neuron.2010.11.044

Schiller, D., Eichenbaum, H., Buffalo, E. A., Davachi, L., Foster, D. J., Leutgeb, S., & Ranganath, C. (2015). Memory and Space: Towards an Understanding of the Cognitive Map. *J Neurosci*, *35*(41), 13904-13911. https://doi.org/10.1523/jneurosci.2618-15.2015

Schilling, K. G., Petit, L., Rheault, F., Remedios, S., Pierpaoli, C., Anderson, A. W., Landman, B. A., & Descoteaux, M. (2020). Brain connections derived from diffusion MRI tractography can be highly anatomically accurate-if we know where white matter pathways start, where they end, and where they do not go. *Brain Struct Funct*, *225*(8), 2387-2402. https://doi.org/10.1007/s00429-020-02129-z

Schlaffke, L., Leemans, A., Schweizer, L. M., Ocklenburg, S., & Schmidt-Wilcke, T. (2017). Learning Morse Code Alters Microstructural Properties in the Inferior Longitudinal Fasciculus: A DTI Study. *Front Hum Neurosci*, *11*, 383. https://doi.org/10.3389/fnhum.2017.00383

Schmitt, M., & Blum, G. S. (2020). State/Trait Interactions. In V. Zeigler-Hill & T. K. Shackelford (Eds.), *Encyclopedia of Personality and Individual Differences* (pp. 5206-5209). Springer International Publishing. https://doi.org/10.1007/978-3-319-24612-3_1922

Schultheiss, N. W., Schlecht, M., Jayachandran, M., Brooks, D. R., McGlothan, J. L., Guilarte, T. R., & Allen, T. A. (2019). 'Awake delta' and theta-rhythmic hippocampal network modes during intermittent locomotor behaviors in the rat. *bioRxiv*, 866962. https://doi.org/10.1101/866962

Scoville, W. B., & Milner, B. (1957). Loss of recent memory after bilateral hippocampal lesions. *J Neurol Neurosurg Psychiatry*, *20*(1), 11-21.

Seehaus, A., Roebroeck, A., Bastiani, M., Fonseca, L., Bratzke, H., Lori, N., Vilanova, A., Goebel, R., & Galuske, R. (2015). Histological validation of high-resolution DTI in human post mortem tissue. *Front Neuroanat*, *9*, 98. https://doi.org/10.3389/fnana.2015.00098

Seghier, M. L. (2013). The angular gyrus: multiple functions and multiple subdivisions. *Neuroscientist*, *19*(1), 43-61. https://doi.org/10.1177/1073858412440596

Sergent, J., Ohta, S., & MacDonald, B. (1992). Functional neuroanatomy of face and object processing. A positron emission tomography study. *Brain*, *115 Pt 1*, 15-36. https://doi.org/10.1093/brain/115.1.15

Seymour, R. A., Rippon, G., & Kessler, K. (2017). The Detection of Phase Amplitude Coupling during Sensory Processing. *Front Neurosci*, *11*, 487. https://doi.org/10.3389/fnins.2017.00487

Sheldon, S., Farb, N., Palombo, D. J., & Levine, B. (2016). Intrinsic medial temporal lobe connectivity relates to individual differences in episodic autobiographical remembering. *Cortex*, *74*, 206-216. https://doi.org/10.1016/j.cortex.2015.11.005

Shin, J., Rowley, J., Chowdhury, R., Jolicoeur, P., Klein, D., Grova, C., Rosa-Neto, P., & Kobayashi, E. (2019). Inferior Longitudinal Fasciculus' Role in Visual Processing and Language Comprehension: A Combined MEG-DTI Study. *Front Neurosci*, *13*, 875. https://doi.org/10.3389/fnins.2019.00875

Shine, J. P., Hodgetts, C. J., Postans, M., Lawrence, A. D., & Graham, K. S. (2015). APOE-ε4 selectively modulates posteromedial cortex activity during scene perception and short-term memory in young healthy adults. *Scientific Reports*, *5*, 1-12. https://doi.org/10.1038/srep16322

Shulman, G. L., Fiez, J. A., Corbetta, M., Buckner, R. L., Miezin, F. M., Raichle, M. E., & Petersen, S. E. (1997). Common Blood Flow Changes across Visual Tasks: II. Decreases in Cerebral Cortex. *J Cogn Neurosci*, *9*(5), 648-663. https://doi.org/10.1162/jocn.1997.9.5.648

Shumbayawonda, E., López-Sanz, D., Bruña, R., Serrano, N., Fernández, A., Maestú, F., & Abasolo, D. (2020). Complexity changes in preclinical Alzheimer's disease: An MEG study of subjective cognitive decline and mild cognitive impairment. *Clin Neurophysiol*, *131*(2), 437-445. https://doi.org/10.1016/j.clinph.2019.11.023

Singh, K. D. (2012). Which "neural activity" do you mean? fMRI, MEG, oscillations and neurotransmitters. *Neuroimage*, *62*(2), 1121-1130. https://doi.org/10.1016/j.neuroimage.2012.01.028

Singh, S. P. (2014). Magnetoencephalography: Basic principles. *Ann Indian Acad Neurol*, *17*(Suppl 1), S107-112. https://doi.org/10.4103/0972-2327.128676

Singular Inversions. (1998). *Facegen.* URL: https://facegen.com/

Sirota, A., Montgomery, S., Fujisawa, S., Isomura, Y., Zugaro, M., & Buzsaki, G. (2008). Entrainment of neocortical neurons and gamma oscillations by the hippocampal theta rhythm. *Neuron*, *60*(4), 683-697. https://doi.org/10.1016/j.neuron.2008.09.014

Soares, J. M., Marques, P., Alves, V., & Sousa, N. (2013). A hitchhiker's guide to diffusion tensor imaging. *Front Neurosci*, *7*, 31. https://doi.org/10.3389/fnins.2013.00031

Song, S. K., Sun, S. W., Ju, W. K., Lin, S. J., Cross, A. H., & Neufeld, A. H. (2003). Diffusion tensor imaging detects and differentiates axon and myelin degeneration in mouse

optic nerve after retinal ischemia. *Neuroimage*, *20*(3), 1714-1722. https://doi.org/10.1016/j.neuroimage.2003.07.005

Sosa, M., Gillespie, A. K., & Frank, L. M. (2018). Neural Activity Patterns Underlying Spatial Coding in the Hippocampus. *Curr Top Behav Neurosci*, *37*, 43-100. https://doi.org/10.1007/7854_2016_462

Squire, L. R., Shrager, Y., & Levy, D. A. (2006). Lack of evidence for a role of medial temporal lobe structures in visual perception. *Learn Mem*, *13*(2), 106-107. https://doi.org/10.1101/lm.178406

Stark, C. E., & Squire, L. R. (2000). Intact visual perceptual discrimination in humans in the absence of perirhinal cortex. *Learn Mem*, *7*(5), 273-278.

Stefanacci, L., Suzuki, W. A., & Amaral, D. G. (1996). Organization of connections between the amygdaloid complex and the perirhinal and parahippocampal cortices in macaque monkeys. *J Comp Neurol*, *375*(4), 552-582. https://doi.org/10.1002/(sici)1096-9861(19961125)375:4<552::aid-cne2>3.0.co;2-0

Stephen, J. M., Ranken, D. M., Aine, C. J., Weisend, M. P., & Shih, J. J. (2005). Differentiability of simulated MEG hippocampal, medial temporal and neocortical temporal epileptic spike activity. *J Clin Neurophysiol*, *22*(6), 388-401. https://doi.org/?10.1097/01.wnp.0000172141.26081.78

Sulpizio, V., Boccia, M., Guariglia, C., & Galati, G. (2016). Functional connectivity between posterior hippocampus and retrosplenial complex predicts individual differences in navigational ability. *Hippocampus*, *26*(7), 841-847. https://doi.org/10.1002/hipo.22592

Summerfield, J. J., Hassabis, D., & Maguire, E. A. (2010). Differential engagement of brain regions within a 'core' network during scene construction. *Neuropsychologia*, *48*(5), 1501-1509. https://doi.org/10.1016/j.neuropsychologia.2010.01.022

Sundqvist, M., Routier, A., Dubois, B., Colliot, O., & Teichmann, M. (2020). The White Matter Module-Hub Network of Semantics Revealed by Semantic Dementia. *J Cogn Neurosci*, *32*(7), 1330-1347. https://doi.org/10.1162/jocn_a_01549

Suzuki, W. A. (2009). Perception and the medial temporal lobe: evaluating the current evidence. *Neuron*, *61*(5), 657-666. https://doi.org/10.1016/j.neuron.2009.02.008

Suzuki, W. A., & Amaral, D. G. (1994). Topographic organization of the reciprocal connections between the monkey entorhinal cortex and the perirhinal and parahippocampal cortices. *J Neurosci*, *14*(3 Pt 2), 1856-1877.

Swanson, L. W., & Cowan, W. M. (1979). The connections of the septal region in the rat. *J Comp Neurol*, *186*(4), 621-655. https://doi.org/10.1002/cne.901860408

Sweeney-Reed, C. M., Zaehle, T., Voges, J., Schmitt, F. C., Buentjen, L., Kopitzki, K., Richardson-Klavehn, A., Hinrichs, H., Heinze, H. J., Knight, R. T., & Rugg, M. D. (2016). Pre-stimulus thalamic theta power predicts human memory formation. *Neuroimage*, *138*, 100-108. https://doi.org/10.1016/j.neuroimage.2016.05.042

Talk, A., Kang, E., & Gabriel, M. (2004). Independent generation of theta rhythm in the hippocampus and posterior cingulate cortex. *Brain Res*, *1015*(1-2), 15-24. https://doi.org/10.1016/j.brainres.2004.04.051

Thomas, D. G., Grice, J. W., Najm-Briscoe, R. G., & Miller, J. W. (2004). The influence of unequal numbers of trials on comparisons of average event-related potentials. *Dev Neuropsychol*, *26*(3), 753-774. https://doi.org/10.1207/s15326942dn2603_6

Tiganj, Z., Jung, M. W., Kim, J., & Howard, M. W. (2017). Sequential Firing Codes for Time in Rodent Medial Prefrontal Cortex. *Cereb Cortex*, *27*(12), 5663-5671. https://doi.org/10.1093/cercor/bhw336

Torralba, A., & Oliva, A. (2003). Statistics of natural image categories. *Network*, *14*(3), 391-412.

Tournier, J. D., Calamante, F., Gadian, D. G., & Connelly, A. (2004). Direct estimation of the fiber orientation density function from diffusion-weighted MRI data using spherical

deconvolution. *Neuroimage*, *23*(3), 1176-1185. https://doi.org/10.1016/j.neuroimage.2004.07.037

Townsend, J. T., & Ashby, F. G. (1978). Methods of modeling capacity in simple processing systems. *Cognitive theory*, *3*, 199-139.

Tsanov, M., Wright, N., Vann, S. D., Erichsen, J. T., Aggleton, J. P., & O'Mara, S. M. (2011). Hippocampal inputs mediate theta-related plasticity in anterior thalamus. *Neuroscience*, *187*, 52-62. https://doi.org/10.1016/j.neuroscience.2011.03.055

Tuch, D. S. (2004). Q-ball imaging. *Magn Reson Med*, *52*(6), 1358-1372. https://doi.org/10.1002/mrm.20279

Tuch, D. S., Reese, T. G., Wiegell, M. R., Makris, N., Belliveau, J. W., & Wedeen, V. J. (2002). High angular resolution diffusion imaging reveals intravoxel white matter fiber heterogeneity. *Magn Reson Med*, *48*(4), 577-582. https://doi.org/10.1002/mrm.10268

Turati, L., Moscatelli, M., Mastropietro, A., Dowell, N. G., Zucca, I., Erbetta, A., Cordiglieri, C., Brenna, G., Bianchi, B., Mantegazza, R., Cercignani, M., Baggi, F., & Minati, L. (2015). In vivo quantitative magnetization transfer imaging correlates with histology during de- and remyelination in cuprizone-treated mice. *NMR Biomed*, *28*(3), 327-337. https://doi.org/10.1002/nbm.3253

Tzourio-Mazoyer, N., Landeau, B., Papathanassiou, D., Crivello, F., Etard, O., Delcroix, N., Mazoyer, B., & Joliot, M. (2002). Automated anatomical labeling of activations in SPM using a macroscopic anatomical parcellation of the MNI MRI single-subject brain. *Neuroimage*, *15*(1), 273-289. https://doi.org/10.1006/nimg.2001.0978

Umesh, P. (2012). Image processing in python. *CSI Communications*, *23*, 2.

Unger, A., Alm, K. H., Collins, J. A., O'Leary, J. M., & Olson, I. R. (2016). Variation in White Matter Connectivity Predicts the Ability to Remember Faces and Discriminate Their Emotions. *J Int Neuropsychol Soc*, *22*(2), 180-190. https://doi.org/10.1017/s1355617715001009

Uono, S., Sato, W., Kochiyama, T., Kubota, Y., Sawada, R., Yoshimura, S., & Toichi, M. (2017). Time course of gamma-band oscillation associated with face processing in the inferior occipital gyrus and fusiform gyrus: A combined fMRI and MEG study. *Hum Brain Mapp*, *38*(4), 2067-2079. https://doi.org/10.1002/hbm.23505

Urgolites, Z. J., Levy, D. A., Hopkins, R. O., & Squire, L. R. (2018). Spared perception of object geometry and object components after hippocampal damage. *Learn Mem*, *25*(7), 330-334. https://doi.org/10.1101/lm.047464.118

van Assche, M., Kebets, V., Vuilleumier, P., & Assal, F. (2016). Functional Dissociations Within Posterior Parietal Cortex During Scene Integration and Viewpoint Changes. *Cereb Cortex*, *26*(2), 586-598. https://doi.org/10.1093/cercor/bhu215

van der Schaaf, A. (1998). *Natural image statistics and visual processing* University of Groningen]. Groningen.

van Diessen, E., Numan, T., van Dellen, E., van der Kooi, A. W., Boersma, M., Hofman, D., van Lutterveld, R., van Dijk, B. W., van Straaten, E. C., Hillebrand, A., & Stam, C. J. (2015). Opportunities and methodological challenges in EEG and MEG resting state functional brain network research. *Clin Neurophysiol*, *126*(8), 1468-1481. https://doi.org/10.1016/j.clinph.2014.11.018

Van Hoesen, G. W. (1995). Anatomy of the medial temporal lobe. *Magn Reson Imaging*, *13*(8), 1047-1055. https://doi.org/10.1016/0730-725x(95)02012-i

Van Veen, B. D., & Buckley, K. M. (1988). Beamforming: A versatile approach to spatial filtering. *IEEE assp magazine*, *5*(2), 4-24.

Van Veen, B. D., Van Drongelen, W., Yuchtman, M., & Suzuki, A. (1997). Localization of brain electrical activity via linearly constrained minimum variance spatial filtering. *IEEE Transactions on biomedical engineering*, *44*(9), 867-880.

Vann, S. D., & Aggleton, J. P. (2002). Extensive cytotoxic lesions of the rat retrosplenial cortex reveal consistent deficits on tasks that tax allocentric spatial memory. *Behav Neurosci*, *116*(1), 85-94.

Vaz, A. P., Yaffe, R. B., Wittig, J. H., Jr., Inati, S. K., & Zaghloul, K. A. (2017). Dual origins of measured phase-amplitude coupling reveal distinct neural mechanisms underlying episodic memory in the human cortex. *Neuroimage*, *148*, 148-159. https://doi.org/10.1016/j.neuroimage.2017.01.001

Vinck, M., Bos, J. J., Van Mourik-Donga, L. A., Oplaat, K. T., Klein, G. A., Jackson, J. C., Gentet, L. J., & Pennartz, C. M. (2015). Cell-Type and State-Dependent Synchronization among Rodent Somatosensory, Visual, Perirhinal Cortex, and Hippocampus CA1. *Front Syst Neurosci*, *9*, 187. https://doi.org/10.3389/fnsys.2015.00187

Vlcek, K., Fajnerova, I., Nekovarova, T., Hejtmanek, L., Janca, R., Jezdik, P., Kalina, A., Tomasek, M., Krsek, P., Hammer, J., & Marusic, P. (2020). Mapping the Scene and Object Processing Networks by Intracranial EEG. *Front Hum Neurosci*, *14*, 561399. https://doi.org/10.3389/fnhum.2020.561399

von Stein, A., & Sarnthein, J. (2000). Different frequencies for different scales of cortical integration: from local gamma to long range alpha/theta synchronization. *Int J Psychophysiol*, *38*(3), 301-313.

Voss, J. L., & Cohen, N. J. (2017). Hippocampal-cortical contributions to strategic exploration during perceptual discrimination. *Hippocampus*, *27*(6), 642-652. https://doi.org/10.1002/hipo.22719

Wagner, A. D., Schacter, D. L., Rotte, M., Koutstaal, W., Maril, A., Dale, A. M., Rosen, B. R., & Buckner, R. L. (1998). Building memories: remembering and forgetting of verbal experiences as predicted by brain activity. *Science*, *281*(5380), 1188-1191.

Wakana, S., Caprihan, A., Panzenboeck, M. M., Fallon, J. H., Perry, M., Gollub, R. L., Hua, K., Zhang, J., Jiang, H., Dubey, P., Blitz, A., van Zijl, P., & Mori, S. (2007). Reproducibility of quantitative tractography methods applied to cerebral white matter. *Neuroimage*, *36*(3), 630-644. https://doi.org/10.1016/j.neuroimage.2007.02.049

Wang, N., Zhang, J., Cofer, G., Qi, Y., Anderson, R. J., White, L. E., & Allan Johnson, G. (2019). Neurite orientation dispersion and density imaging of mouse brain microstructure. *Brain Struct Funct*, *224*(5), 1797-1813. https://doi.org/10.1007/s00429-019-01877-x

Wang, P., Zhou, B., Yao, H., Xie, S., Feng, F., Zhang, Z., Guo, Y., An, N., Zhou, Y., Zhang, X., & Liu, Y. (2020). Aberrant Hippocampal Functional Connectivity Is Associated with Fornix White Matter Integrity in Alzheimer's Disease and Mild Cognitive Impairment. *J Alzheimers Dis*, *75*(4), 1153-1168. https://doi.org/10.3233/jad-200066

Wang, X., Casadio, M., Weber, K. A., 2nd, Mussa-Ivaldi, F. A., & Parrish, T. B. (2014). White matter microstructure changes induced by motor skill learning utilizing a body machine interface. *Neuroimage*, *88*, 32-40. https://doi.org/10.1016/j.neuroimage.2013.10.066

Wang, Y., Romani, S., Lustig, B., Leonardo, A., & Pastalkova, E. (2015). Theta sequences are essential for internally generated hippocampal firing fields. *Nat Neurosci*, *18*(2), 282-288. https://doi.org/10.1038/nn.3904

Wang, Z., Bovik, A. C., Sheikh, H. R., & Simoncelli, E. P. (2004). Image quality assessment: from error visibility to structural similarity. *IEEE Trans Image Process*, *13*(4), 600-612. https://doi.org/10.1109/tip.2003.819861

Wang, Z., Liang, P., Zhao, Z., Han, Y., Song, H., Xu, J., Lu, J., & Li, K. (2014). Acupuncture modulates resting state hippocampal functional connectivity in Alzheimer disease. *PLoS One*, *9*(3), e91160. https://doi.org/10.1371/journal.pone.0091160

Warren, D. E., Duff, M. C., Jensen, U., Tranel, D., & Cohen, N. J. (2012). Hiding in plain view: lesions of the medial temporal lobe impair online representation. *Hippocampus*, *22*(7), 1577-1588. https://doi.org/10.1002/hipo.21000

Watrous, A. J., Fried, I., & Ekstrom, A. D. (2011). Behavioral correlates of human hippocampal delta and theta oscillations during navigation. *J Neurophysiol*, *105*(4), 1747-1755. https://doi.org/10.1152/jn.00921.2010

Watrous, A. J., Lee, D. J., Izadi, A., Gurkoff, G. G., Shahlaie, K., & Ekstrom, A. D. (2013). A comparative study of human and rat hippocampal low-frequency oscillations during spatial navigation. *Hippocampus*, *23*(8), 656-661. https://doi.org/10.1002/hipo.22124

Waxman, S. G. (1980). Determinants of conduction velocity in myelinated nerve fibers. *Muscle Nerve*, *3*(2), 141-150. https://doi.org/10.1002/mus.880030207

Wedeen, V. J., Hagmann, P., Tseng, W. Y., Reese, T. G., & Weisskoff, R. M. (2005). Mapping complex tissue architecture with diffusion spectrum magnetic resonance imaging. *Magn Reson Med*, *54*(6), 1377-1386. https://doi.org/10.1002/mrm.20642

Wegman, J., & Janzen, G. (2011). Neural encoding of objects relevant for navigation and resting state correlations with navigational ability. *J Cogn Neurosci*, *23*(12), 3841-3854. https://doi.org/10.1162/jocn_a_00081

Weigelt, S., Koldewyn, K., & Kanwisher, N. (2012). Face identity recognition in autism spectrum disorders: a review of behavioral studies. *Neurosci Biobehav Rev*, *36*(3), 1060-1084. https://doi.org/10.1016/j.neubiorev.2011.12.008

Weiner, K. S., & Zilles, K. (2016). The anatomical and functional specialization of the fusiform gyrus. *Neuropsychologia*, *83*, 48-62. https://doi.org/10.1016/j.neuropsychologia.2015.06.033

Wen, Q., Mustafi, S. M., Li, J., Risacher, S. L., Tallman, E., Brown, S. A., West, J. D., Harezlak, J., Farlow, M. R., Unverzagt, F. W., Gao, S., Apostolova, L. G., Saykin, A. J., & Wu, Y. C. (2019). White matter alterations in early-stage Alzheimer's disease: A tract-specific study. *Alzheimers Dement (Amst)*, *11*, 576-587. https://doi.org/10.1016/j.dadm.2019.06.003

Wens, V., Bourguignon, M., Goldman, S., Marty, B., Op de Beeck, M., Clumeck, C., Mary, A., Peigneux, P., Van Bogaert, P., Brookes, M. J., & De Tiège, X. (2014). Inter- and intra-subject variability of neuromagnetic resting state networks. *Brain Topogr*, *27*(5), 620-634. https://doi.org/10.1007/s10548-014-0364-8

Whishaw, I. Q., & Jarrard, L. E. (1995). Similarities vs. differences in place learning and circadian activity in rats after fimbria-fornix section or ibotenate removal of hippocampal cells. *Hippocampus*, *5*(6), 595-604. https://doi.org/10.1002/hipo.450050610

Whittington, M. A., Cunningham, M. O., LeBeau, F. E., Racca, C., & Traub, R. D. (2011). Multiple origins of the cortical gamma rhythm. *Dev Neurobiol*, *71*(1), 92-106. https://doi.org/10.1002/dneu.20814

Wickham, H. (2016). ggplot2: Elegant Graphics for Data Analysis. In: Springer-Verlag New York.

Willenbockel, V., Sadr, J., Fiset, D., Horne, G. O., Gosselin, F., & Tanaka, J. W. (2010). Controlling low-level image properties: the SHINE toolbox. *Behav Res Methods*, *42*(3), 671-684. https://doi.org/10.3758/brm.42.3.671

Wolff, M., Gibb, S. J., & Dalrymple-Alford, J. C. (2006). Beyond spatial memory: the anterior thalamus and memory for the temporal order of a sequence of odor cues. *J Neurosci*, *26*(11), 2907-2913. https://doi.org/10.1523/jneurosci.5481-05.2006

Wu, S. Z., Masurkar, A. V., & Balcer, L. J. (2020). Afferent and Efferent Visual Markers of Alzheimer's Disease: A Review and Update in Early Stage Disease. *Front Aging Neurosci*, *12*, 572337. https://doi.org/10.3389/fnagi.2020.572337

Wu, Y., Sun, D., Wang, Y., & Ou, S. (2016). Segmentation of the Cingulum Bundle in the Human Brain: A New Perspective Based on DSI Tractography and Fiber Dissection Study. *Front Neuroanat*, *10*, 84. https://doi.org/10.3389/fnana.2016.00084

Xue, J., Guo, H., Gao, Y., Wang, X., Cui, H., Chen, Z., Wang, B., & Xiang, J. (2019). Altered Directed Functional Connectivity of the Hippocampus in Mild Cognitive Impairment and Alzheimer's Disease: A Resting-State fMRI Study. *Front Aging Neurosci*, *11*, 326. https://doi.org/10.3389/fnagi.2019.00326

Yasuno, F., Hirata, M., Takimoto, H., Taniguchi, M., Nakagawa, Y., Ikejiri, Y., Nishikawa, T., Shinozaki, K., Tanabe, H., Sugita, Y., & Takeda, M. (1999). Retrograde temporal order amnesia resulting from damage to the fornix. *J Neurol Neurosurg Psychiatry*, *67*(1), 102-105. https://doi.org/10.1136/jnnp.67.1.102

Yee, L. T. S. (2014). The hippocampus uses information just encountered to guide efficient ongoing behavior. *24*(2), 154-164. https://doi.org/10.1002/hipo.22211

Yokoi, T., Watanabe, H., Yamaguchi, H., Bagarinao, E., Masuda, M., Imai, K., Ogura, A., Ohdake, R., Kawabata, K., Hara, K., Riku, Y., Ishigaki, S., Katsuno, M., Miyao, S., Kato, K., Naganawa, S., Harada, R., Okamura, N., Yanai, K., Yoshida, M., & Sobue, G. (2018). Involvement of the Precuneus/Posterior Cingulate Cortex Is Significant for the Development of Alzheimer's Disease: A PET (THK5351, PiB) and Resting fMRI Study. *Front Aging Neurosci*, *10*, 304. https://doi.org/10.3389/fnagi.2018.00304

Yonelinas, A. P. (1994). Receiver-operating characteristics in recognition memory: evidence for a dual-process model. *J Exp Psychol Learn Mem Cogn*, *20*(6), 1341-1354.

Yu, M., Engels, M. M. A., Hillebrand, A., van Straaten, E. C. W., Gouw, A. A., Teunissen, C., van der Flier, W. M., Scheltens, P., & Stam, C. J. (2017). Selective impairment of hippocampus and posterior hub areas in Alzheimer's disease: an MEG-based multiplex network study. *Brain*, *140*(5), 1466-1485. https://doi.org/10.1093/brain/awx050

Yu, M., Gouw, A. A., Hillebrand, A., Tijms, B. M., Stam, C. J., van Straaten, E. C., & Pijnenburg, Y. A. (2016). Different functional connectivity and network topology in behavioral variant of frontotemporal dementia and Alzheimer's disease: an EEG study. *Neurobiol Aging*, *42*, 150-162. https://doi.org/10.1016/j.neurobiolaging.2016.03.018

Zeidman, P., & Maguire, E. A. (2016). Anterior hippocampus: the anatomy of perception, imagination and episodic memory. In *Nat Rev Neurosci* (Vol. 17, pp. 173-182). https://doi.org/10.1038/nrn.2015.24

Zeithamova, D., Dominick, A. L., & Preston, A. R. (2012). Hippocampal and ventral medial prefrontal activation during retrieval-mediated learning supports novel inference. *Neuron*, *75*(1), 168-179. https://doi.org/10.1016/j.neuron.2012.05.010

Zhang, H., Schneider, T., Wheeler-Kingshott, C. A., & Alexander, D. C. (2012). NODDI: practical in vivo neurite orientation dispersion and density imaging of the human brain. *Neuroimage*, *61*(4), 1000-1016. https://doi.org/10.1016/j.neuroimage.2012.03.072

Zhu, Q., Zhang, J., Luo, Y. L., Dilks, D. D., & Liu, J. (2011). Resting-state neural activity across face-selective cortical regions is behaviorally relevant. *J Neurosci*, *31*(28), 10323-10330. https://doi.org/10.1523/jneurosci.0873-11.2011

Zielinski, M. C., Shin, J. D., & Jadhav, S. P. (2019). Coherent Coding of Spatial Position Mediated by Theta Oscillations in the Hippocampus and Prefrontal Cortex. *J Neurosci*, *39*(23), 4550-4565. https://doi.org/10.1523/jneurosci.0106-19.2019